University of Zagreb

FACULTY OF CHEMICAL ENGINEERING AND TECHNOLOGY

Ivana Šoić

RESEARCH AND DEVELOPMENT OF A SYSTEM FOR *IN SITU* IMPEDANCE MEASUREMENTS OF CORROSION RESISTANCE

DOCTORAL THESIS

Zagreb, 2025

University of Zagreb

FACULTY OF CHEMICAL ENGINEERING AND TECHNOLOGY

Ivana Šoić

RESEARCH AND DEVELOPMENT OF A SYSTEM FOR *IN SITU* IMPEDANCE MEASUREMENTS OF CORROSION RESISTANCE

DOCTORAL THESIS

Supervisor:
Prof. Sanja Martinez, Ph.D.

Zagreb, 2025

Sveučilište u Zagrebu

FAKULTET KEMIJSKOG INŽENJERSTVA I TEHNOLOGIJE

Ivana Šoić

ISTRAŽIVANJE I RAZVOJ SUSTAVA ZA IMPEDANCIJSKA MJERENJA KOROZIJSKE OTPORNOSTI *IN SITU*

DOKTORSKI RAD

Mentor:
Prof. dr. sc. Sanja Martinez

Zagreb, 2025

Bibliographic page

UDK: 621.317.73:620.193(043.3)=111
Scientific area: Tehnical sciences
Scientific field: Chemical Engineering
Scientific branch: Chemical Engineering in Materials Development
Institution: University of Zagreb, Faculty of Chemical Engineering and Technology, Department of Electrochemistry
Supervisor: Prof. Sanja Martinez, Ph.D.
Number of pages: 110
Numbers of figures: 3
Numbers of tables: 5
Number of appendices: 4
Number of references:
Date of defence:
Defence Committee:

Dissertation topic was accepted on regular session of Council of the Faculty of Chemical Engineering and Technology, University of Zagreb, held on September 20th 2021., and approved at 11th session of the Senate of the University of Zagreb in 353th academic year (2021./2022.) held on March 29th 2022.

Information about supervisor

Prof. Sanja Martinez, Ph.D.

Prof. Sanja Martinez, Ph.D., is a Full Professor with a permanent tenure at the Faculty of Chemical Engineering and Technology (FCET), University of Zagreb, where she has been working since 1994. She graduated in Engineering Physics from the Faculty of Science (PMF), and completed her Master's and Doctoral degrees in Electrochemistry at FCET, under the mentorship of Prof. Ivica Štern, Ph.D.

She is the author of more than 60 papers indexed in WoSCC, cited over 2600 times, with an h-index of 21. She has led or participated in numerous projects, and is currently a collaborator on the HORIZON-EIC Pathfinder (Aelectra) and EU NextGenerationEU (AntiBacHip) projects. She has supervised five doctoral dissertations, co-supervised three others, and is currently mentoring new doctoral candidates. She is particularly dedicated to the development of young researchers, the transfer of knowledge, and the integration of experimental and digital approaches in electrochemical research.

Other information is available at the link: https://www.fkit.unizg.hr/sanja.martinez

This PhD thesis was financially supported by the project Development of new solutions for characterization and protection of bronze cultural heritage exposed to outdoor environment (Croatian Science Foundation, IP-2019-04-5030). The material presented in the published paper, I. Šoić, I. Šoljić, M. Eškinja, A. Mujezinović, S. Martinez, The novel paste electrolyte measuring cell for EIS testing of the commonly used surface protection on bronze, Prog. Org. Coat. 177 (2023) 107442. DOI: 10.1016/j.porgcoat.2023.107442., was developed with financial support from the same project.

Zahvala…

Abstract

Electrochemical impedance spectroscopy (EIS) has long been recognized as a powerful technique for quantitatively evaluating the corrosion resistance of coatings and metals in both laboratory and field environments. Yet, despite decades of research, EIS has not become a routine tool in engineering practice, mainly due to the complexity of conventional immersion cells, sensitivity to environmental noise, and the lack of portable, reproducible systems for on-site measurements.

The aim of this doctoral research was to develop an experimental setup, measurement regime, and data interpretation protocol that enable reliable impedance measurements directly on coated and metallic surfaces. The distinctive feature of the developed system is the use of paste electrolyte and flexible conductive rubber electrodes that allow stable and reproducible measurements without spillage or surface damage.

The research integrates results from four peer-reviewed papers published between 2019 and 2023, which together represent a continuous development cycle from concept to implementation. The initial work introduced a gel-electrolyte configuration that demonstrated the feasibility quasi solid state electrolyte impedance measurements. Subsequent studies established a unified equivalent-circuit model applicable to both dielectric and porous coatings, defined accuracy limits and interference tolerance, and culminated in the construction and validation of portable paste-electrolyte cells suitable for use in both laboratory and field conditions.

The accompanying software provides automated data acquisition and signal-quality control, ensuring reproducibility and traceability of measurements, and incorporates simplified quantitative criteria for evaluating the protective performance of coatings based on an improved model interpretation of impedance data.

The unified analysis of these studies demonstrates that the combination of paste electrolyte, suitable cell construction, and optimized measurement regime enables reliable and reproducible assessment of corrosion resistance over a broad range of materials, while preserving the sensitivity of laboratory EIS in practical *in situ* use. This work bridges the gap between experimental EIS research and its application in engineering practice by providing a fully validated methodology for portable, non-destructive impedance evaluation. The resulting system establishes a foundation for the wider use of impedance-based corrosion diagnostics and for the future integration of *in situ* monitoring with data-driven analysis and digital corrosion-management approaches.

Keywords: electrochemical impedance spectroscopy, corrosion resistance, coatings, paste electrolyte, *in situ* measurement, equivalent circuit model, reproducibility, field diagnostics.

Sažetak

Elektrokemijska impedancijska spektroskopija (EIS) već je desetljećima prepoznata kao snažna metoda za kvantitativnu procjenu otpornosti premaza i metala na koroziju, kako u laboratorijskim tako i u terenskim uvjetima. Ipak, unatoč dugogodišnjem istraživanju, EIS se još uvijek nije afirmirala kao rutinski alat u inženjerskoj praksi, ponajprije zbog složenosti konvencionalnih ćelija s tekućim elektrolitom, osjetljivosti na šumove iz okoline te nedostatka prijenosnih i reproducibilnih sustava za mjerenja na terenu.

Cilj ovog doktorskog istraživanja bio je razviti eksperimentalni sklop, režim mjerenja i protokol interpretacije podataka koji omogućuju pouzdana impedancijska mjerenja izravno na premazanim i metalnim površinama. Posebnost razvijenog sustava jest uporaba elektrolita u obliku paste i fleksibilnih vodljivih gumenih elektroda, koji omogućuju stabilna i ponovljiva mjerenja bez prolijevanja elektrolita i oštećenja površine.

Istraživanje objedinjuje rezultate četiri rada objavljena u časopisima s recenzijom u razdoblju od 2019. do 2023. godine, koji zajedno čine kontinuirani razvojni ciklus od koncepta do primjene. Početno istraživanje uvelo je konfiguraciju s gel-elektrolitom kojom je dokazana izvedivost impedancijskih mjerenja s kvazi-krutim elektrolitom. Naknadna su istraživanja uspostavila jedinstveni ekvivalentni električni krug primjenjiv na dielektrične i porozne premaze, definirala granice točnosti i otpornost na smetnje te rezultirala konstrukcijom i validacijom prijenosnih ćelija s elektrolitom u pasti, pogodnih za uporabu u laboratorijskim i terenskim uvjetima.

Prateći softver omogućuje automatizirano prikupljanje podataka i kontrolu kvalitete signala, čime se osigurava reproducibilnost i sljedivost mjerenja, te uključuje pojednostavljene kvantitativne kriterije za procjenu zaštitnih svojstava premaza, temeljene na poboljšanom modelu interpretacije impedancijskih podataka.

Jedinstvena analiza ovih istraživanja pokazuje da kombinacija elektrolita u obliku paste, prikladne konstrukcije ćelije i optimiziranog režima mjerenja omogućuje pouzdanu i reproducibilnu procjenu otpornosti na koroziju širokog spektra materijala, uz očuvanje osjetljivosti laboratorijske EIS metode u praktičnoj *in situ* primjeni. Ovim se radom premošćuje jaz između eksperimentalnih EIS istraživanja i njihove inženjerske primjene, pružajući potpuno validiranu metodologiju za prijenosno, nedestruktivno impedancijsko ispitivanje. Razvijeni sustav postavlja temelj za širu primjenu impedancijski utemeljenih dijagnostičkih metoda korozije te za buduću integraciju *in situ* praćenja s analitikom temeljnom na podacima i digitalnim pristupima upravljanja korozijom.

Ključne riječi: elektrokemijska impedancijska spektroskopija, otpornost na koroziju, premazi, pasta-elektrolit, *in situ* mjerenje, ekvivalentni krug, ponovljivost, terenska dijagnostika.

Table of Contents

1. INTRODUCTION

Electrochemical impedance spectroscopy (EIS) is one of the most informative electrochemical techniques for assessing the corrosion resistance of metals and protective coatings. Although the method has been extensively validated in laboratory environments, its use in engineering practice remains limited. Conventional EIS measurements require liquid electrolyte cells, rigid electrode configurations, and stable laboratory conditions, which restrict the method's applicability for *in situ* or field assessment of coatings and metallic surfaces.

International standards such as ISO 16773 (Parts 1–4) [1–4], ASTM D8370-22 [5], and AMPP TM21449-2021[6] provide formalized procedures for electrochemical impedance spectroscopy (EIS) on metallic and coated substrates. The ISO 16773 series, published between 2016 and 2017, defines the methodology for both coated and uncoated metallic specimens, encompassing terminology, laboratory measurement principles, data acquisition, verification using dummy cells, and representative examples of data interpretation. Together, these four parts form the primary international framework for EIS measurements in liquid-electrolyte configurations. Building upon this foundation, ASTM D8370-22 extends standardized EIS methodology to field applications, specifying procedures for non-destructive testing of coatings and linings directly on in-service structures. More recently, AMPP TM21449-2021 has addressed continuous monitoring of protective coatings, particularly in aerospace applications, reflecting growing interest in real-time impedance-based performance assessment. Collectively, these documents illustrate the evolution of EIS from laboratory-based characterization toward field and condition-monitoring methodologies, establishing the technical background against which the present work is positioned.

Both ISO 16773 and ASTM D8370-22 rely on conventional liquid-electrolyte cells, which are impractical for field or *in situ* use because they require controlled cell geometries, stable electrolyte containment, and flat surfaces. Consequently, ASTM D8370-22, despite being specifically developed for field measurements, has not yet achieved broad industrial acceptance due to the inherent difficulties of handling liquid electrolytes outside laboratory conditions. In contrast, AMPP TM21449-2021 introduces an embedded electrode system designed for continuous impedance monitoring of protective coatings, primarily in aerospace applications. However, such embedded configurations are restricted to dedicated design integrations and are not adaptable for general *in situ* surface evaluation. Other experimental efforts to translate EIS into the field remain diverse in design and purpose, yet many still lack the simplicity required for routine practical use and clear evidence of reproducibility and robustness. The present doctoral research was therefore motivated by the need to develop and validate a universally applicable *in situ* EIS methodology that preserves the sensitivity and

diagnostic precision of laboratory measurements while enabling reliable, non-destructive testing on real surfaces.

To ensure that the research followed a clear and verifiable framework, both hypotheses and expected scientific contributions were defined at the beginning of the doctoral study. The hypotheses guided the experimental development and testing of the *in situ* EIS system, while the expected contributions defined the broader scientific and methodological advances to be achieved through this work.

Each hypothesis and contribution was systematically verified through the studies published between 2019 and 2023, which together constitute the doctoral thesis. Table 1, with the legend below, provides an integrated overview showing how individual hypotheses and expected scientific contributions were fulfilled and validated through the included publications.

Table 1. Overview of how the defined research hypotheses and the expected scientific contributions from the DrSc01 plan were verified and fulfilled through the included peer-reviewed publications (2019 – 2023).

No.	Hypothesis / Expected scientific contribution	Verification / Achieved through	Publication(s)
H1	Use of a two-electrode cell and conductive paste electrolyte enables accurate impedance measurements of coatings across 10^3–10^{11} Ω cm².	Demonstrated by gel- and paste-electrolyte configurations tested on high-resistance coatings and metallic substrates.	P1, P4
H2	Measurement and adjustment of AC interference amplitude ensure sufficient precision and accuracy under simulated interference.	Quantified interference thresholds, optimized signal amplitude, validated algorithm for noise control.	P3
H3	Conductive paste electrolyte with suitable conductivity, wetting, and consistency enables accurate measurements without damaging coatings or substrates.	Comparative evaluation on high- and low-impedance systems; verified harmlessness for conservation coatings.	P4
H4	The developed method distinguishes small changes in coating impedance reflecting protective performance.	Continuous-exposure studies and model interpretation reveal sensitivity to minor degradation changes.	P2, P4
H5 / C4	Simplified quantitative criteria based on improved model interpretation facilitate	Unified equivalent-circuit model and evaluation criteria implemented in custom software.	P2, P4

	practical evaluation of coating condition.		
C1	Application of a system with polymer electrodes and conductive paste electrolyte for coating evaluation across full impedance range.	Developed flexible polymer electrodes and paste-electrolyte cells validated on industrial and conservation coatings.	P1, P4
C2	Systematic study of AC interference effects on precision and accuracy of EIS measurements.	Reproducibility confirmed via dummy cells, calibration foils, and interference simulations.	P3
C3	Examination of conductive paste electrolyte effects on low-resistance conservation systems (bronze patina, coatings).	Verified harmlessness and measurement stability on conservation coatings.	P4

Legend 1 – Research hypotheses

H1. The application of a two electrode system and conductive paste electrolyte for EIS measurements will enable precise and accurate impedance measurements in the wide range over several orders of magnitude (10^3 to 10^{11} Ω cm^2).

H2. Measuring AC interferences amplitudes and adjusting the signal amplitude can ensure sufficient accuracy and precision of the result obtained under simulated AC interferences found in practice.

H3. A solid electrolyte with appropriate characteristics (conductivity, surface wetting, consistency) will enable accurate measurements in a wide range of impedance and on various protective systems without damaging impact on coating or on metal substrate.

H4. By using developed method, it will be possible to distinguish very small differences and changes in impedance of the coatings that reflects its protective properties.

H5. The proposed simplified criteria based on the improved model of the results interpretation will facilitate the practical assessment of the condition of protective coatings.

Legend 2 – Expected scientific contributions

C1. For the first time, the applicability of system with polymer electrodes and conductive paste electrolyte on impedance measurements and evaluation of coating protective properties will be tested. The tests will be conducted in whole range of impedances that have practical significance.

C2. For the first time, systematic testing of the influence of AC interferences on the precision and accuracy of EIS measurements will be performed on dummy cells, calibration foils and high resistance coatings.

C3. For the first time, systematic testing of application and influence of conductive paste electrolyte on low resistance conservator coating protection systems will be performed

C4. New, simplified criteria for quantitative coating quality assessment, based on the improved model for interpretation of results, will be proposed.

Legend 3 – PhD qualifying papers

P1. I. Šoić, I., S. Martinez, M. Dubravić, Gel-electrolyte EIS setup used for probing of IR dried/cured industrial coatings, Prog. Org. Coat. 137 (2019) 105331. DOI: 10.1016/j.porgcoat.2019.105331. [7]

P2. S. Martinez, I. Šoić, V. Špada, Unified equivalent circuit of dielectric permittivity and porous coating formalisms for EIS probing of thick industrial grade coatings, Prog. Org. Coat. 153 (2021) 106155. DOI: 10.1016/j.porgcoat.2021.106155. [8]

P3. I. Šoljić, I. Šoić, L. Kostelac, S. Martinez, AC interference impact on EIS assessment of organic coatings using dummy cells, calibration foils and field exposed coated samples, Prog. Org. Coat. 165 (2022) 106767. DOI: 10.1016/j.porgcoat.2022.106767 [9]

P4. I. Šoić, I. Šoljić, M. Eškinja, A. Mujezinović, S. Martinez, The novel paste electrolyte measuring cell for EIS testing of the commonly used surface protection on bronze, Prog. Org. Coat. 177 (2023) 107442. DOI: 10.1016/j.porgcoat.2023.107442. [10]

This doctoral research focuses on the verification and validation of a novel *in situ* electrochemical impedance spectroscopy (EIS) methodology employing a semisolid electrolyte cell. The study addresses the entire measurement chain — from data acquisition and signal quality to processing and interpretation — with the objective of ensuring accurate, reproducible, and meaningful impedance data across the full range from metallic to insulating surfaces. The developed methodology provides immediate, quantitative criteria for assessing coating integrity and barrier performance, enabling reliable *in situ* diagnostics, but does not extend to predictive modelling of coating lifetime or failure.

The foundational nature of this work is demonstrated in the subsequent chapters, beginning with a comprehensive literature review covering relevant scientific studies and technical standards. This is followed by a concise overview of the papers that compose this thesis and

their integration within the overall research framework. The combined analysis synthesizes these findings into a unified methodology, highlighting a merged scientific contribution that surpasses the scope of the individual publications. Finally, the thesis concludes with a forward-looking discussion outlining the potential for further development of the *in situ* impedance system, including its integration with automated data analysis and digital corrosion-management concepts.

2. LITERATURE REVIEW

2.1. Overview of EIS

From the mid 90-ties, a steady yearly number of studies (Table 2) have explored the possibility of transferring electrochemical impedance spectroscopy (EIS) from controlled laboratory conditions to *in situ* or on-site applications for coatings and metallic substrates. A bibliometric search of the Web of Science Core Collection using the keywords “coating” AND (“corrosion” OR “degradation”) AND (“electrochemical impedance spectroscopy” OR “EIS”) AND (“sensor” OR “monitoring”) returned approximately 740 records, of which only 81 were directly relevant to the topic. From these, the subset of publications listed in table 2 represents the examples pertinent to the development of portable EIS configurations, gel electrolytes cells, embedded electrode systems, and related theoretical or practical approaches aimed at adapting EIS for field or non-destructive evaluation of coatings and metallic substrates.

Table 2. Representative studies illustrating the evolution of EIS methods and sensing concepts for coated metals

Period / Subtitle (corresponds to literature-review section)	**Characteristic developments and technical focus**	**Representative studies**
1989-1995: Early developments: atmospheric and *in situ* EIS studies	Establishment of EIS as a diagnostic tool for organic-coated metals; identification of time-dependent water uptake and coating capacitance; definition of barrier versus interfacial responses.	Lecuyer et al. 1991 [11]; van Westing et al. 1993[12]; Amirudin & Thierry 1995[13,14]
2000-2009: First topically applied and embedded sensors	Transition from conventional immersion cells to localized or embedded configurations; development of topically applied sensors and internal reference electrodes for in situ monitoring.	Davis et al. 2002 [15]; Qi et al. 2009 [16]; Allahar et al. 2009 [17]; Bierwagen et al. 2009 [18]
2010-2018: Expansion to multi-sensor and real-time corrosion monitoring	Implementation of embedded and wireless EIS systems; humidity- and temperature-dependent impedance monitoring; early use of gel/solid electrolytes and networked data acquisition.	Yu et al. 2013 [19]; Upadhyay et al. 2014 [20]; Cai et al. 2018 [21]; Ramírez Barat et al. 2018 [22]

2018-2022: Portable and compact impedance detectors	Emergence of compact, low-power, field-ready EIS devices; introduction of CID-type instruments and paste/gel electrolytes enabling on-site measurements.	Kuo et al. 2018 [23] Friedersdorf et al. 2019 [24]; Merten et al. 2019 [25]; Monrrabal et al. 2019 [26]
2022-2025: Recent directions: non-invasive, model-driven and AI-assisted systems	Integration of impedance sensing with digital-twin concepts, ML-based classification and threshold-triggered maintenance schemes; progress toward autonomous diagnostic platforms.	Rondinella et al. 2023 [27]; Popova et al. 2024 [28]; Ji et al. 2025 [29]; Hein et al. 2025 [30]; Dong et al. 2025 [31]; Jiryaeisharahi et al. 2025 [32]

The 81 papers identified as directly relevant to the transfer of electrochemical impedance spectroscopy (EIS) into *in situ* or field applications are distributed across more than twenty international journals (table 3). The largest share (≈20%) appears in *Progress in Organic Coatings*, confirming its central role in advancing EIS methodologies for coating degradation, atmospheric corrosion, and sensor-based studies. Notably, four of the papers forming this doctoral thesis were published in the same journal, underscoring both thematic alignment and methodological continuity with the leading body of work in the field. Additional key contributions were published in *Corrosion*, *Corrosion Science*, *Measurement*, and the *Journal of Coatings Technology*, addressing embedded electrode systems, portable EIS configurations, and field monitoring protocols. More recent publications in *Sensors and Actuators B: Chemical* and *Corrosion Materials and Degradation* illustrate the growing integration of modeling, data-driven interpretation, and field-ready diagnostic devices.

Table 3. Distribution of publications addressing the transfer of electrochemical impedance spectroscopy (EIS) from laboratory to *in situ* or sensor-based applications for coatings and metallic substrates across major journals.

Journal / Source	**Abbreviation**	**Number of Papers**	**Focus / Relevance**
Progress in Organic Coatings	Prog. Org. Coat.	15	Core journal for EIS studies of coatings, equivalent-circuit models, and sensor validation.
Corrosion	Corrosion	8	Publishes embedded-sensor and applied

			corrosion monitoring studies (NACE/AMPP).
Corrosion Science	Corros. Sci.	4	High-impact journal covering mechanistic and modeling aspects of coating degradation.
Measurement	Measurement	3	Focus on EIS hardware, portable detectors, and metrological validation.
IEEE Access	IEEE Access	3	Features modern, electronics- and AI-based EIS developments.
Sensors	Sensors	3	Open-access venue for EIS-based sensing, monitoring, and smart diagnostic systems.
Materials Science Forum	Mater. Sci. Forum	2	Early venue for environmental EIS and mechanical effects on coatings.
Journal of Solid State Electrochemistry	J. Solid State Electrochem.	2	Studies on adhesion, coating interlayers, and EIS of stressed coatings.
Electrochimica Acta	Electrochim. Acta	2	Fundamental electrochemistry and EIS parameterization of coatings.
Anti-Corrosion Methods and Materials	Anti-Corros. Methods Mater.	2	Field-oriented EIS applications on rubber and metal coatings.
IEEE Transactions on Instrumentation and Measurement	IEEE Trans. Instrum. Meas.	2	Low-cost and logarithmic amplifier EIS systems.
Materials Performance	Mater. Perform.	2	Industry-focused corrosion monitoring and sensor application studies.
Sensors and Actuators B: Chemical	Sens. Actuators B Chem.	2	Gel-based and embedded-electrode EIS sensors.
Journal of Food Engineering	J. Food Eng.	2	EIS of protective food-contact coatings and can corrosion.
Journal of Adhesion Science and Technology	J. Adhes. Sci. Technol.	2	EIS for sealant and adhesion evaluation in coating and bonding systems.

2.2. From laboratory electrochemical impedance to in-service monitoring

Electrochemical Impedance Spectroscopy (EIS) has long been established as a powerful diagnostic tool for investigating corrosion mechanisms, coating barrier properties, and electrochemical kinetics at electrochemical interfaces. However, its conventional implementation, requiring immersion in liquid electrolytes and a direct electrical connection to the substrate, has constrained its use to controlled laboratory environments. This limitation has motivated a series of innovations aiming to bring EIS closer to real-time, non-destructive, or in-service evaluation of metals and protective coatings. The overall trajectory of this research, spanning three decades, shows a clear evolution from early embedded sensors and accelerated laboratory methods toward miniaturized, portable, and data-driven systems capable of non-invasive field deployment.

The present PhD builds upon this trend by introducing paste-electrolyte cell designed for rapid, *in situ*, repeatable, and spatially resolved impedance measurements on coated and bare metallic surfaces. This approach addresses the enduring challenge of bridging laboratory-grade spectral quality with field practicality. To position this development among existing research, the following sections trace the main conceptual and technological advances that have defined the field.

2.3. Early developments: Atmospheric and *in situ* EIS studies (1989–1995)

The concept of using electrochemical impedance spectroscopy (EIS) for *in situ* or atmospheric corrosion monitoring of coated metals originated in the early 1990s through pioneering work by Lecuyer, Barreau, and Thierry [11], van Westing et al. [12], and Amirudin and Thierry [13]. Lecuyer's group at the Institut de la Corrosion introduced an electrochemical sensor placed on coated metallic surfaces under atmospheric conditions [11], demonstrating that reliable impedance spectra could be obtained without immersion by maintaining a thin electrolyte film on the coating surface. This was the first study to frame EIS as a *surface-contact monitoring technique* rather than a laboratory immersion test. Shortly afterwards, van Westing et al. applied EIS to epoxy coatings on steel, correlating constant-phase-element behaviour with early loss of adhesion and localized corrosion initiation [12]. Their comparison between coated steel panels and a dielectric sensor coated with the same system showed that impedance variations could detect subsurface de-adhesion even when the coating appeared visually intact, establishing the mechanistic basis for EIS as a diagnostic of interfacial failure.

Building on these findings, Amirudin and Thierry published a comprehensive review and experimental synthesis of EIS for polymer-coated metals [13], consolidating knowledge of pigment effects, water uptake, and atmospheric degradation mechanisms. Their work integrated earlier laboratory and field studies and effectively defined the methodological framework for coating-impedance analysis still referenced today. Together, these studies laid the experimental and conceptual foundation for the subsequent evolution of EIS-based corrosion sensors, introducing the idea that impedance spectra, interpreted through dielectric or interfacial models, could serve as quantitative indicators of coating integrity and early corrosion activity under realistic atmospheric exposure.

During the second half of the decade, EIS matured from a laboratory characterization method into an operational diagnostic and monitoring tool. Mansfeld (1995) formalized the quantitative relationship between impedance parameters, coating porosity, and disbonded area, introducing the breakpoint-frequency method for rapid evaluation of corrosion protection [33]. In parallel, Amirudin and Thierry (1995) developed a gold-grid electrode deposited on top of organic coatings to perform EIS during alternating wet/dry exposure [13], representing one of the first topical sensors capable of atmospheric impedance monitoring.

Around the same time, Xiao et al. (1997) demonstrated that impedance spectra could also be gathered remotely under marine exposure using multiplexed probes and data transmission via modem [34]. Their work provided the first proof that EIS could be implemented as an autonomous field-monitoring system, directly linking laboratory-derived electrochemical parameters with in-service coating performance. van der Weijde, van Westing, and de Wit (1998) extended EIS methodology toward *controlled-humidity environments*, demonstrating that coating capacitance and dielectric response could be quantitatively correlated with atmospheric water uptake [35]. By maintaining defined relative humidity rather than liquid immersion, they captured Arrhenius-type behavior of diffusion and solubility parameters, illustrating that atmospheric exposure could be simulated electrochemically without the need for full immersion. This approach further blurred the line between laboratory testing and *in situ* field monitoring and complemented the development of topical and remote EIS sensors later in the decade.

A major technological advance followed with the work of Mansfeld and co-workers (1997–1998), who combined EIS and electrochemical-noise analysis for remote marine corrosion monitoring of polymer-coated steels. Using multiplexed data acquisition and modem communication between field sites and the laboratory, they demonstrated that impedance measurements could be obtained automatically under natural and artificial seawater exposure

[36–38]. These studies established the first remote EIS surveillance systems, showing that impedance-derived polarization resistance reliably tracked coating degradation in service environments.

Concurrently, González, Otero, Bautista, Morcillo, and Almeida (1998–1999) developed specialized lap-joint sensors for EIS and noise analysis of coated galvanized steel sheets [39,40]. Their custom geometries enabled detection of corrosion processes within overlapped regions, emphasizing the roles of under-film contamination, humidity, and crevice geometry in the loss of protection.

Collectively, the research of the 1990s defined this decade as the period of methodological consolidation in coating-impedance studies. It introduced topical and geometry-specific electrodes, remote data transmission, and quantitative impedance criteria that transformed EIS from a laboratory diagnostic into a practical tool for *in situ* and field corrosion monitoring. These developments provided the direct technological and conceptual basis for the embedded, gel-based, and portable impedance sensors that emerged in the following decades and underpin the present research.

2.4. First topically applied and embedded sensors (2000–2010)

The earliest systematic attempts to extend electrochemical impedance spectroscopy (EIS) beyond conventional immersion testing were led by Guy D. Davis and co-workers in the early 2000s. They pioneered the first topically applied EIS corrosion sensors, capable of measuring impedance directly on coated surfaces without the need for immersion in electrolyte solutions [15,41]. Their work introduced the concept of *in situ* corrosion sensors for coatings and adhesive systems, enabling impedance-based assessment of degradation under service-relevant conditions. Unlike later embedded or integrated electrodes, these early sensors operated externally and required only a thin electrolyte film to establish ionic conduction, yet they successfully detected coating defects, tracked barrier deterioration, and correlated accelerated laboratory exposures with natural field degradation.

In a seminal *Materials Performance* article, Davis et al. [41] demonstrated an electrochemical impedance corrosion sensor that could detect coating deterioration during salt fog, humidity, and Florida beach exposures—representing the first true attempt to use EIS as a prognostic tool under realistic environmental conditions. Their follow-up study [15] further validated these *in situ* measurements by demonstrating close correspondence between cyclic corrosion tests and natural marine exposure, showing that the test duration could be reduced

by up to 40 % without loss of discriminatory power. Together, these studies marked the transition from purely diagnostic to predictive EIS applications.

Concurrently, Davis and co-workers applied EIS to adhesive bond monitoring, a concept that foreshadowed modern structural-health-monitoring approaches. Using external electrodes attached to opposite sides of bonded joints, they demonstrated that changes in circuit parameters — especially capacitance and constant-phase-element (*CPE*) magnitude — quantitatively reflected moisture ingress, bond integrity, and interfacial degradation [42–45]. Equivalent-circuit modeling revealed distinct stages of moisture uptake and delamination, and the impedance response was found to correlate with both wedge and lap-shear mechanical tests. These investigations demonstrated that EIS could identify early-stage bondline weakening—well before visible or mechanical failure occurred—laying the conceptual foundation for condition-based maintenance and *in situ* bond evaluation.

The methodology was later extended to sealants and polymer interfaces [46]. By combining EIS with adhesion strength testing, the authors differentiated non-conductive sealants according to moisture absorption, interfacial breakdown, and internal corrosion activity—parameters previously inaccessible through visual inspection alone. This broadened the scope of *in situ* EIS to multiphase polymer–metal junctions, where coatings, adhesives, and environmental factors interact simultaneously.

In parallel, other researchers developed complementary electrochemical sensing concepts for coated and confined interfaces. Otero et al. [47] employed multilaminar electrochemical sensors to measure potential differences in underfilm differential-aeration and contamination cells, directly quantifying the driving forces for localized corrosion beneath coatings. Bautista et al. [48] and Krakowiak et al. [49] used impedance and noise methods to study crevice and lap-joint corrosion or water penetration in rubber linings, demonstrating that EIS could quantify degradation in geometrically complex or thick barrier systems. Simultaneously, Bordzilowski et al. [50] demonstrated on-site impedance monitoring of bridge coating systems, providing one of the first examples of field-deployed EIS instrumentation for thick organic linings under industrial conditions.

Instrumental advances also appeared at this time. Carullo et al. [51] designed a low-cost portable EIS system based on a digital-signal-processor architecture for corrosion monitoring of metallic cultural heritage objects, showing that simplified electronics could deliver reliable impedance alerts—an important step toward later handheld or embedded corrosion sensors.

From the mid-2000s onward, EIS was increasingly used *in situ* to interrogate coatings under mechanical, photochemical, and electrochemical stress. Darowicki et al. [52]

demonstrated that cyclic mechanical loading of coatings causes characteristic impedance changes, while Miszczyk et al. [53] developed a multilayer interfacial-adhesion sensor that detected delamination between coating layers through EIS signals. Le Thu et al. [54] introduced localized EIS measurements around artificial coating flaws under cathodic protection, and Strunz et al. [55] refined time-dependent impedance evaluation using the Z-HIT algorithm to distinguish true dielectric changes from non-stationary effects during initial immersion. Klüppel et al. [56] advanced these ideas further with an *in situ* microcapillary EIS cell capable of tracking defect formation during uniaxial deformation of coated galvanized steel, one of the earliest demonstrations of real-time electrochemical–mechanical coupling in coatings research.

Qi et al. [16,57] demonstrated the feasibility of a two-electrode EIS configuration capable of distinguishing coating degradation on conductive and non-conductive substrates, providing the immediate methodological basis for later embedded systems developed by Bierwagen's group.

Between 2008 and 2010, Bierwagen and co-workers at North Dakota State University established embedded electrodes as a new paradigm for *in situ* coating monitoring [18,58–60]. These sensors were incorporated between primer and topcoat layers, allowing impedance and electrochemical-noise measurements to be obtained continuously during AC–DC–AC cycling, thermal cycling, and QUV/Prohesion weathering. The embedded-sensor configuration eliminated the need for external electrolyte contact and provided time-resolved insight into barrier degradation, ionic transport, and relaxation phenomena within multilayer coatings. Equivalent-circuit analyses enabled separation of bulk-primer and metal/coating-interface properties, clarifying the protective roles of chromate primers versus polyurethane topcoats.

Their subsequent studies further advanced this concept by systematically investigating the behavior of multilayer coating systems under realistic environmental exposures. Allahar et al. [61] and Su et al. [62] demonstrated real-time *in situ* monitoring of polyurethane topcoats over chromate-epoxy and Mg-rich primers under controlled humidity and thermal conditions, confirming that embedded sensors can capture dielectric and barrier-property changes within the primer layer. Allahar et al. [17] and Wang et al. [63] extended this approach to Prohesion exposure, correlating impedance evolution with coating degradation under cyclic salt and humidity. Allahar, Su, and Bierwagen [64] further introduced a non-substrate, two-electrode configuration in which embedded electrodes between primer and topcoat functioned as both working and reference electrodes, broadening EIS applicability to non-conductive substrates. These studies collectively established the methodological foundation for embedded-electrode EIS, directly inspiring subsequent field-adaptable and paste-electrolyte approaches.

The concept of embedding electrochemical sensing elements within coating systems was subsequently expanded toward wireless and autonomous data-acquisition architectures. Yu et al. [19] proposed an impedance-based wireless sensor network for monitoring the degradation of metal-protective coatings in both static and flowing media. Their system integrated miniaturized impedance analyzers (AD5933) and RF transceivers to transmit data from multiple coated panels in real time. This work marked an early attempt to decentralize EIS measurements and demonstrated the feasibility of continuous, untethered coating evaluation — a technological precursor to later developments in portable, on-site impedance instruments.

Together, these pioneering studies reframed EIS from a laboratory characterization tool into an operational monitoring technique capable of capturing the dynamics of coating degradation, adhesive debonding, and moisture transport under realistic exposure conditions. They also exposed enduring challenges, signal stability, spatial representativeness, and physical interpretation of impedance obtained through non-traditional electrode configurations. The paste-electrolyte concept developed in this PhD research directly addresses these same challenges by achieving controlled, reproducible ionic contact without immersion or destructive access to the substrate, thereby combining the accessibility of Davis's surface-applied sensors with the continuity of Bierwagen's embedded systems.

2.5. Expansion to multi-sensor and real-time corrosion monitoring (2011–2018)

Following the pioneering embedded-sensor studies of the 2000s, the next phase of development focused on automation, miniaturization, and real-time monitoring of coating degradation under realistic exposure. This period marked the gradual transition of electrochemical impedance spectroscopy (EIS) from a laboratory technique to an operational diagnostic tool integrated within sensor networks and portable instruments.

Upadhyay et al. [20] extended this concept by examining the effect of environmental humidity on polyurethane/Mg-rich primer systems with embedded electrodes, confirming that moisture fluctuations directly alter impedance response and coating protection levels.

A transitional milestone was reached around 2010 with the commercialization of wireless EIS monitoring. The Coating Health Monitor (CHM) developed by ElectraWatch, Inc. and Virginia Technologies, Inc. represented one of the first battery-powered, autonomous impedance-based corrosion sensors for coated structures [65]. The CHM system, based on the earlier concepts of Davis and co-workers, enabled non-destructive, wireless assessment of coating integrity through the periodic acquisition of impedance spectra that reflected

progressive coating degradation. This development signified the first practical realization of a field-deployable EIS platform, anticipating subsequent efforts toward distributed sensor networks and condition-based maintenance.

Building on this concept, researchers in the early 2010s sought to scale and automate EIS sensing for extended environmental exposures. Shi et al. [66] developed one of the first EIS-based wireless sensor networks consisting of compact nodes that communicated with a base station, acquiring impedance data within seconds. The system achieved strong correlation with potentiostat-based measurements and demonstrated the feasibility of rapid, in-field impedance screening for coating evaluation.

In parallel, Xia et al. [67], Zheng et al. [68], and Wang et al. [69] extended EIS and electrochemical noise (EN) sensing to metal-can packaging, using embedded probes to monitor internal corrosion and metal release during long-term storage. These studies provided direct quantitative links between EIS parameters, such as coating resistance and charge-transfer resistance, and the chemical evidence of corrosion obtained by inductively coupled plasma mass spectrometry (ICP-MS). The results established a model for correlating impedance-based degradation indicators with analytical measurements of corrosion products.

Meanwhile, the miniaturization and cost reduction of impedance instrumentation gained momentum. Angelini and Grassini [70,71] introduced Arduino- and microcontroller-based EIS systems using logarithmic amplifiers, capable of measuring impedances over 0,01 Hz–100 kHz at a cost below $100. These portable instruments enabled corrosion and coating assessments on cultural-heritage objects where compact, low-power equipment was essential. Around the same time, Tokutake et al. [72] applied *in situ* EIS diagnostics to oil-storage-tank coatings, using equivalent-circuit models with dual constant-phase elements (*CPEs*) to distinguish intact from deteriorated coating regions and predict residual service life.

In the mid 2010s, sensor networks combining multiple measurement principles began to appear. Integrated EIS, electrical resistance (ER), and EN sensors were designed to operate continuously during cyclic environmental exposures for infrastructure and defense applications [6,12,73]. Zajec et al. [73], for example, deployed combined impedance- and resistance-based sensors on coated bridge components over nine months of exposure, proving that real-time field monitoring was achievable with robust sensor encapsulation and semi-solid electrolytes. Cai et al. [21] proposed an impedance-based sensor for early failure diagnosis of organic coatings, showing that characteristic phase-angle shifts at mid frequencies can serve as predictive indicators of coating breakdown.

Simultaneously, researchers addressed the practical limitations of immersion-based electrochemical cells, seeking alternatives suitable for vertical, irregular, or heritage surfaces. Ramírez Barat et al. [22] optimized gel-polymer-electrolyte (GPE) cells for *in situ* EIS on metallic monuments, minimizing parasitic impedances and enabling reliable interpretation of coating and corrosion behavior without liquid handling. Hosbein et al. [74] developed co-planar hydrogel EIS cells capable of measuring both coating capacitance and surface sheet resistance on painted sculptures. Their design required only surface contact and provided early warning of paint degradation unavailable from conventional immersion cells.

Other advances targeted specific industrial or marine systems. Hayashibara et al. [75] used EIS to monitor the early degradation of epoxy coatings in ballast tanks, correlating time-dependent changes in coating resistance and capacitance with water uptake and microstructural aging. Nazir et al. [76] presented a non-destructive magnetic-aluminum electrode system for on-site Tafel and EIS testing on large, coated infrastructures, demonstrating the potential of ruggedized, reusable field sensors.

Parallel exploration of non-electrochemical diagnostic methods further emphasized the growing demand for non-invasive assessment. For example, Welp et al. [77] compared optical coherence tomography (OCT) and EIS for detecting coating defects and monitoring transparent protective layers on industrial monuments, underscoring EIS's continued relevance as a benchmark electrochemical technique.

Collectively, the studies between 2010 and 2018 redefined coating-monitoring technology. EIS evolved from a laboratory analytical tool to a field-capable, multi-sensor diagnostic platform. Systems became portable, self-powered, and adaptable to complex geometries, employing solid or gel electrolytes to ensure stable contact. The progression from Davis's surface sensors to Bierwagen's embedded electrodes, then to Larsen's wireless CHM, and finally to gel- and hydrogel-based cells such as those of Barat and Hosbein, established the design logic that informs the paste-electrolyte cell developed in this PhD. The present approach continues this trajectory by providing a controllable, viscoelastic ionic interface that ensures reproducible contact and high-quality EIS data under both laboratory and *in situ* conditions.

2.6. Portable and compact impedance detectors (2018–2022)

As electrochemical impedance spectroscopy (EIS) sensing matured, emphasis shifted toward portability, low-cost instrumentation, and real-time field applicability. Friedersdorf et al. [24] described multi-sensor corrosion-monitoring panels designed for atmospheric exposure testing of coated structures. These panels integrated impedance, galvanic

and environmental sensors within a single self-contained unit, capable of continuous, autonomous data collection under natural conditions. This development represented the transition of EIS sensing from embedded laboratory prototypes to networked, field-ready diagnostic systems.

Building upon this evolution, Kuo and Lee introduced the first compact coating impedance detector (CID) — a miniaturized circuit providing rapid, single-frequency impedance measurements up to 10^9 Ω cm², with strong correlation to potentiostat data [23]. Their later designs culminated in CID 2.0, a field programmable gate array (FPGA)-based version offering wider dynamic range and automated signal generation [78], and CID 3.0, featuring improved analog circuitry, oversampling, and reduced power consumption for stable measurement of high-impedance coatings [79]. Collectively, these detectors established the foundation for compact and portable EIS hardware that could be deployed on-site for coating health evaluation.

In parallel, several groups adapted electrochemical sensing to industrial and packaging applications. Wang et al. [80] developed a portable sensor to estimate the shelf life of lacquered tinplate cans, using open-circuit potential (OCP), potentiostatic step tests, and EIS to track coating resistance and charge transfer kinetics over time. Xia et al. [81] demonstrated that electrochemical noise (EN) recorded in single-cell configuration could discriminate defect levels in organic coatings, offering a fast diagnostic complementary to EIS.

Zajec et al. [82] further combined impedance and electrical resistance (ER) sensors in encapsulated corrosion kits for monitoring coating degradation on steel structures under aggressive atmospheric exposures.

Merten et al. [25] validated field EIS measurements on real infrastructure, establishing practical procedures and repeatability metrics for coatings at the end of service life.

At the same time, flexible and adaptive sensing media were explored to improve surface contact and measurement robustness.

Chowdhury et al. [83,84] fabricated ZnO–PVDF nanocomposite fiber textiles that functioned both as embedded sensors and protective layers. These non-conductive meshes provided *in situ* impedance feedback under immersion or thermal cycling, effectively acting as early-warning corrosion sensors.

Monrrabal et al. [26] introduced gel electrolytes based on glycerol–agar matrices with chloride conductivity optimized for portable cells, allowing EIS and polarization measurements on carbon and galvanized steel without crevice corrosion or liquid leakage. Such

gel and fiber-based sensors bridged the gap between traditional electrochemical cells and modern flexible electronics.

In the field of cultural-heritage conservation, Valentini [85] summarized portable EIS and biosensor technologies for *in situ* diagnosis of metal and organic layers on artworks, emphasizing analytical optimization of miniaturized cell geometries.

Large-scale collaborations such as the EIS round-robin by Ritter et al. [86] confirmed that modern portable instruments achieve reproducible data across laboratories, while Laschuk et al. [87] provided a comprehensive guide encouraging wider adoption of EIS for material characterization beyond corrosion science.

Looking toward the future, Frias-Cacho et al. [88] reviewed in-service coating health monitoring technologies within the context of Industry 4.0 and IoT-connected neural-like sensor networks, envisioning autonomous, condition-based maintenance driven by embedded EIS sensing and data analytics.

Collectively, these developments mark a decisive transition from multi instrument laboratory setups to compact, self contained diagnostic devices. EIS has evolved into a portable, intelligent sensing method capable of quantifying coating performance in real time and under realistic service conditions.

The paste-electrolyte EIS cell developed in this PhD research continues this trajectory by coupling the analytical precision of laboratory impedance measurements with the simplicity and versatility of portable instruments. Unlike purely electronic detectors, it preserves a genuine electrochemical interface, ensuring mechanistic interpretability of impedance spectra while enabling reproducible measurements under both laboratory and field conditions.

2.7. Recent directions: Non-invasive, model-driven, and AI-assisted systems (2022–2025)

In the past few years, the field has diversified into two complementary directions:

(i) the development of non-invasive and flexible EIS-based sensors, and
(ii) the integration of data-driven models for predictive coating-health assessment and lifetime prediction.

As previously mentioned, Frias-Cacho et al. [88] reviewed the emerging landscape of in-service coating-health monitoring technologies, highlighting a convergence between embedded electrochemical sensing, wireless communication, and neural-like architectures for condition-based maintenance. Their review emphasized the growing industrial demand for

autonomous, connected systems capable of detecting coating failure in non-accessible locations and anticipating corrosion long before visual degradation becomes evident.

Building on this vision, Rondinella et al. [27] developed a warning system for defect onset in organic coatings on large surfaces, demonstrating that impedance thresholds derived from normalized $|Z|$ values can serve as early indicators for coating maintenance scheduling. Their system was validated over two years of immersion monitoring using a portable potentiostat, confirming the practical viability of compact EIS devices for long-term field diagnostics.

Parallel advances have extended EIS to realistic and high-temperature industrial environments.

Tieu et al. [89] performed *in situ* EIS under retort conditions (121 °C, pressurized saline) to evaluate non-BPA food contact coatings, establishing correlations between coating glass-transition temperature (T_g), pore resistance (R_{pore}), and long-term storage stability. Similarly, Filippas et al. [90] implemented a continuous EIS platform for monitoring aluminum beverage can lids directly in beverages, demonstrating reliable reproduction of multi-month degradation trends within a compact chamber mimicking packaging conditions. These examples illustrate the growing use of EIS for accelerated, realistic-life assessments of industrial coating systems.

Further research has moved toward integrating physics-based and statistical models for degradation prediction.

Ji et al. [29] proposed a hybrid framework that combines kinetic modeling with a three-phase Wiener process, coupling EIS-derived coating resistance and capacitance features to probabilistically describe degradation evolution and remaining life. This approach bridges mechanistic understanding with reliability analysis and supports digital-twin development for coatings.

Hein et al. [30] provided a broad comparative review of monitoring methods for coated steel structures, situating EIS among other non-destructive techniques and evaluating their accuracy and cost-effectiveness. Their holistic view reinforced EIS's role as a cornerstone diagnostic for both coating condition and underfilm corrosion monitoring.

The field is also seeing rapid progress in non-contact and solid-electrolyte EIS sensors. Recent work by Dong et al. [31] introduced a dual-compartment agar-based solid electrolyte that enables indirect impedance measurements without electrical contact to the substrate, achieving spectra of comparable quality to conventional three-electrode setups. This demonstrated that non-invasive EIS can yield quantitative information on coating thickness

and interfacial conduction paths which is critical for applications on heritage objects and painted surfaces.

Meanwhile, Popova et al. [28] integrated resistometric and EIS sensors for continuous monitoring under variable humidity and immersion, providing comparative validation between ER and electrochemical responses which is an important step toward multi-modal sensing integration.

Jiryaeisharahi et al. [32] further advanced this direction by developing a hybrid EIS–machine learning framework for corrosion monitoring, combining physics-based feature extraction with data-driven prediction of degradation states. Their approach exemplifies how intelligent signal processing can extend EIS beyond conventional frequency-domain analysis toward real-time condition assessment, reinforcing the trend toward autonomous diagnostic systems.

Together, these studies illustrate the ongoing transition from descriptive, case-based EIS analyses toward mechanistic and data-integrated frameworks.

The paste-electrolyte EIS cell developed in this PhD aligns closely with these contemporary trends by ensuring reproducible *in situ* impedance acquisition through a controlled viscoelastic interface, combined with automated data reduction, clustering, and interpretation. This integrated approach responds directly to the field's demand for expert-independent, predictive and portable assessment tools that connect fundamental electrochemistry with real-world performance monitoring.

2.8. Synthesis and position of the present research

Reviewing this progression reveals a coherent technological and methodological trajectory. Early works established the diagnostic potential of EIS for detecting subsurface changes in coatings long before failure. Embedded electrode configurations then allowed continuous *in situ* monitoring during environmental exposure, while solid and gel electrolytes removed the dependence on liquid immersion. The following generation of portable and textile-based sensors achieved practical deployment but often sacrificed spectral resolution or mechanistic interpretability.

Current research, including this PhD, seeks to unify these achievements — maintaining laboratory-grade impedance fidelity while achieving the robustness and adaptability required for field use. The paste-electrolyte cell enables conformal, stable electrode contact across diverse surfaces, while preserving a defined electrochemical interface suitable for frequency-domain analysis. This design is conceptually related to the sensors of Dong [31] and gel-based

cells of Molina [91], but introduces a tunable viscoelastic electrolyte phase optimized for reproducibility and minimal self-impedance.

Beyond hardware innovation, the analytical framework employed in this research — principal component analysis, clustering, and neural-network classification — responds to the emerging need for automated interpretation highlighted by Ji et al. [29] and Frias-Cacho et al. [88]. The combined approach transforms impedance spectra from complex expert-dependent datasets into structured inputs for data-driven degradation assessment.

By integrating these elements, this PhD occupies a unique position within the literature. It bridges the non-invasive, field-applicable designs of recent sensor developments with the interpretive rigor of classical EIS, providing a pathway toward high-throughput, expert-free assessment of coating wear. Furthermore, the methodology proposed here can be generalized to other passive materials, such as oxide-forming metals and biomaterials, where reliable evaluation of passivity remains challenging.

2.9. Concluding remarks

Over the past three decades, research on EIS-based corrosion and coating sensors has advanced from immersion-based laboratory measurements to autonomous, non-contact, and data-interpreted systems. Early embedded sensors proved the feasibility of *in situ* impedance monitoring, gel and hydrogel cells introduced flexible electrolyte interfaces, and miniaturized impedance detectors brought EIS into the realm of portable diagnostics. The newest generation of model-based and wireless sensors points toward fully integrated digital corrosion monitoring infrastructures.

Within this trajectory, the paste-electrolyte EIS cell developed in this doctoral work represents a pragmatic synthesis of electrochemical precision and field practicality. It builds upon the methodological heritage of the embedded sensor community while addressing the long-standing obstacles of surface adaptability, measurement repeatability, and expert-independent interpretation. In doing so, it contributes both conceptually and instrumentally to the ongoing transformation of electrochemical impedance spectroscopy from a laboratory technique into a universal, deployable tool for monitoring the integrity of protective coatings and other passive surfaces.

3. DISCUSSION

3.1. Overview of EIS Measurement Geometries

ISO 16773 Cell

Electrochemical impedance spectroscopy for coated and metallic materials is conventionally performed using electrochemical cells defined by international standards such as ISO 16773-2 [2] and ASTM D8370-22 [5], and further detailed in ISO/TR 16208:2014 [92]. These standards collectively define how electrodes, electrolytes, and measurement geometries should be arranged to ensure reproducible and interpretable impedance data.

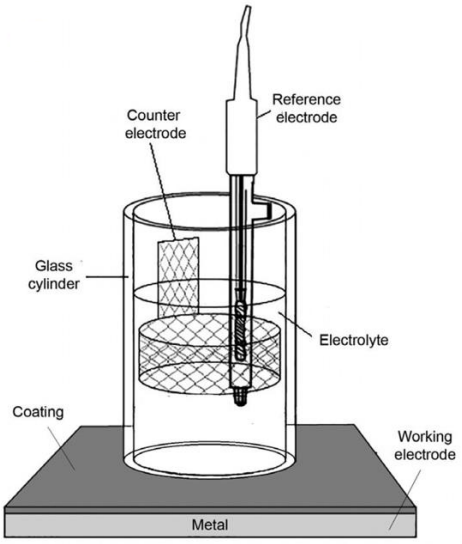

Figure 1. Schematic representation [93] of the ISO 16773 laboratory cell employing a three-electrode geometry.

In the ISO 16773-2 [2] configuration, a three-electrode cell is employed consisting of a working electrode (the coated or metallic specimen), a reference electrode, and a counter electrode immersed in a liquid electrolyte (schematically shown in Figure 1). The working electrode is sealed at the base of the cell—typically by an O-ring—to expose a well-defined circular area, while the counter electrode (often a platinum mesh or rod) ensures homogeneous current distribution. The reference electrode (Ag/AgCl or calomel) is positioned close to the coated surface to minimize potential drop.

This arrangement, described in detail in ISO 16773-1– 4 [1–4] and further elaborated in the technical report ISO/TR 16208 [92], allows accurate control of potential and current, providing high-precision impedance data across a broad frequency range. However, the geometry requires stable electrolyte containment and flat, horizontal surfaces. It is ideally suited to laboratory testing of small panels but not easily applicable to large, curved, or field-installed components.

Recent large-scale interlaboratory studies have highlighted the challenges of ensuring reliable and reproducible impedance measurements across different laboratories and instrument types. The 2nd international round-robin test on EIS measurements of organic coatings, reported by Bakalli et al. [94], systematically assessed 30 laboratories using a uniform epoxy-based electrodeposition coating and a well-defined dummy cell configuration. Despite standardized sample preparation and measurement protocols based on ISO 16773-2 [2], the study revealed significant scatter in both high-impedance coating and dummy-cell data, with total variances in low-frequency impedance exceeding 80 %.

The authors attributed these discrepancies primarily to instrument limitations at very high impedance levels (>10^9 Ω cm^2), inadequate shielding, inconsistent grounding and cable connections, and user-related factors such as insufficient calibration and poor interpretation of raw data. Importantly, the study demonstrated that even when using identical coatings and electrolytes, differences in potentiostat design, input impedance, and software filtering can produce orders-of-magnitude deviations in measured impedance values. The accompanying corrigendum [95] corrected numerical units but did not alter the overall conclusion: that reproducibility of high-impedance EIS data remains a fundamental limitation of conventional liquid-electrolyte systems.

These findings underscore the need for simpler, well-sealed, and low-noise cell designs that reduce operator dependency and environmental sensitivity. The approach developed in the present doctoral research directly responds to these issues by eliminating the open liquid electrolyte and adopting a semisolid (paste or gel) electrolyte with a two-electrode configuration. This geometry minimizes leakage currents, stabilizes contact impedance, and provides consistent performance on both flat and curved surfaces and thereby addressing the reproducibility gap identified in the international round-robin exercise.

ASTM D8370-22 Cell

ASTM D8370-22 [5] defines a simplified two-electrode arrangement specifically for field measurements of coating impedance (Figure 2). Two non-conductive cells are temporarily attached to the coating surface, each containing a liquid electrolyte and an inert electrode (platinum, stainless steel, or graphite). The substrate itself serves as the common return path, meaning that an electrical connection to the metal beneath the coating is unnecessary. The impedance is measured between the two electrolyte cells placed a few centimeters apart on the coating surface.

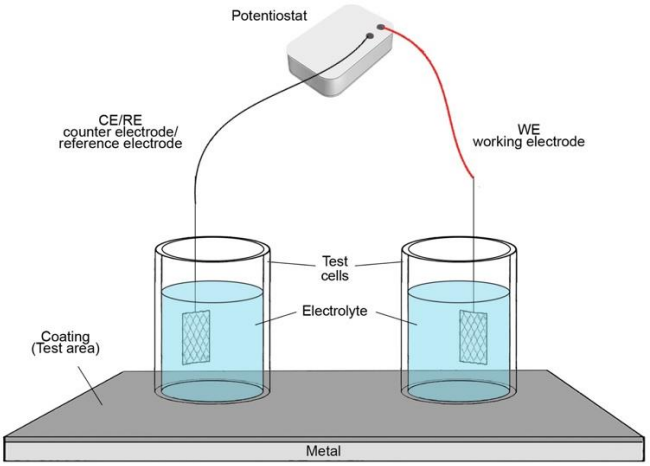

Figure 2. Schematic representation of the two-electrode field cell configuration according to ASTM D8370-22.

This configuration avoids the need for direct substrate connection and enables non-destructive testing on intact coatings, while maintaining the basic EIS measurement principle. The geometry is versatile and suitable for various orientations, although careful sealing and electrolyte retention remain essential for measurement reliability. ASTM D8370 also allows the use of conductive gels as electrolytes, provided they ensure adequate wetting and low solution resistance.

Paste-Electrolyte Cell (This Work)

Two paste-electrolyte cell configurations were developed to enable impedance measurements across a wide range of materials, from highly resistive industrial coatings to bare metals and thin lacquer films (Figure 3). Both use the same semisolid conductive paste-electrolyte, formulated to provide stable ionic conduction (electrolyte resistance ≤ 250 Ω) without leakage, evaporation, or surface alteration.

a)

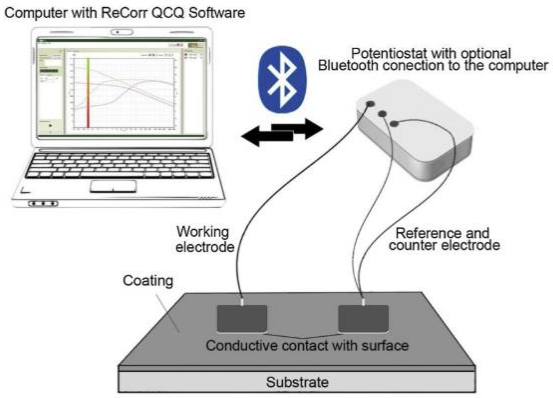

b) c)

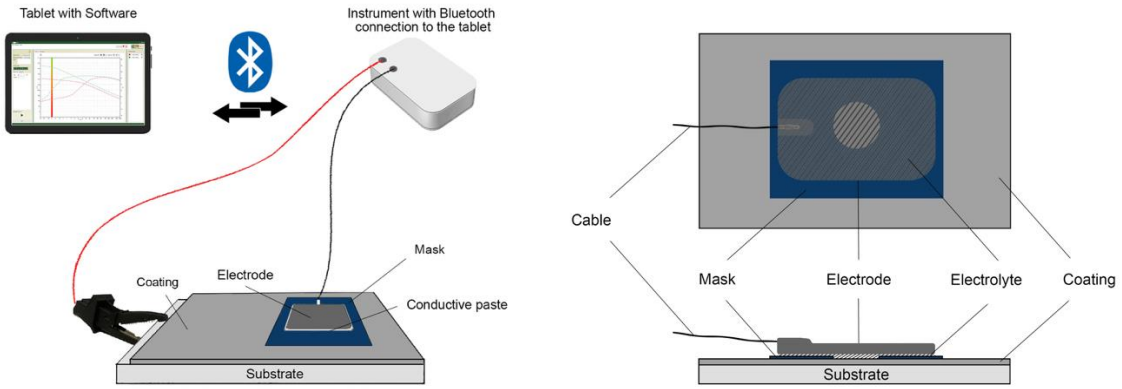

Figure 3. Schematic representation of the two-electrode paste-electrolyte cell configurations, where (a) represents the configuration for high-impedance coatings (functionally analogous to ASTM D8370-22 [5]), (b) represents the configuration for low-impedance coatings and bare metals, with (c) providing a closer look at the electrode setup.

The upper configuration (a) represents a two-electrode geometry designed for high-impedance industrial barrier coatings. The coated or metallic substrate acts as the working electrode, while two flexible conductive-rubber electrodes are placed directly on the surface and remain in position through the self-adhesive consistency of the paste electrolyte. Each conductive electrode has an active area of approximately 25,96 cm^2, and the exposed coating area corresponds to the total region wetted by the electrolyte layer. The paste forms a uniform 0,3–0,5 mm thick film that ensures complete ionic contact without external pressure, mechanical spacing, or sealing. In this configuration, the alternating current passes twice through the coating layer—from one conductive-rubber electrode to the substrate and back through the other — thus closing the circuit without any direct metallic connection. This setup is functionally analogous to the two-cell arrangement described in ASTM D8370-22 [5], but the semisolid electrolyte eliminates the need for O-rings or liquid containment and maintains stable, spill-free contact even on vertical or curved surfaces.

The lower (b) configuration is a two-electrode design optimized for bare metals and thin or conductive coatings, where direct contact between the conductive-rubber electrode and the substrate would otherwise produce a short circuit. A non-conductive mask defines the electrolyte layer and provides insulation between electrodes. The exposed working-electrode area is 2,67 cm^2, to which a paste electrolyte volume of 1,13 cm^3 is applied and covered by the counter/reference electrode. A single conductive-rubber counter/reference electrode is

positioned above the paste. The metallic surface functions as the working electrode. This configuration prevents short-circuiting, while maintaining the same semisolid, non-destructive operation and enabling accurate measurements on low-impedance substrates

Both geometries employ the same electrode material and electrolyte composition described in Šoljić et al., *Progress in Organic Coatings* 165 (2022) 106767 [9], and Šoić et al., *Progress in Organic Coatings* 177 (2023) 107442 [10], differing only in electrode arrangement and mechanical adaptation to the surface conductivity and morphology of the tested specimens.

Summary Cell Constructions

The comparison of electrochemical cell geometries used for impedance measurements is summarized in table 4. The table outlines key characteristics of representative systems based on the ISO 16773 [1–4] laboratory standard, the ASTM D8370-22 [5] field configuration, and the semisolid paste-electrolyte cells developed in this doctoral research. While ISO and ASTM approaches rely on liquid or gel electrolytes requiring controlled geometries and sealing, the present system replaces the liquid phase with a stable semisolid paste and employs flexible conductive-rubber electrodes. This design enables reproducible impedance measurements on both coated and uncoated metallic surfaces across a wide impedance range, while allowing operation on vertical, curved, or irregular geometries without leakage or surface alteration. The table summarizes their key constructional and operational features, such as electrode configuration, electrolyte type, sealing, applicable surface geometries, and impedance range, highlighting how the paste-electrolyte design achieves reproducible, spill-free, and field-ready performance across both high- and low-impedance systems.

Table 4. Comparison of electrochemical cell geometries used for impedance measurements of coated and metallic substrates, including the standardized ISO 16773 laboratory cell, the ASTM D8370-22 two-electrode field configuration, and the semisolid paste-electrolyte cells developed in this doctoral research.

Feature	**ISO 16773**	**ASTM D8370-22**	**Paste-Electrolyte Cell (this work)**
Configuration	3-electrode (WE–RE–CE)	2-electrode (WE–CE/RE combined)	Two-electrode (25,96 cm² each) for high-impedance coatings; two-electrode with mask and direct contact with the substrate for

			bare metals and thin coatings
Electrolyte	Liquid (immersion)	Liquid or gel	Semisolid conductive paste (R_{el} ≤ 250 Ω, thickness 0,3–0,5 mm)
Sealing	O-ring, fixed area	Adhesive or magnetic seal	Self-adhering paste, no seal
Surface type	Flat, horizontal	Flat or slightly curved	Any geometry, vertical or curved
Field applicability	Laboratory only	Field-portable	Fully portable and reusable
Impedance range	up to at least 10^{10} Ω cm² at 0,1 Hz	up to 10^{8}–10^{9} Ω cm²	10^{3}–10^{12} Ω cm²
Reproducibility	High, fixed geometry	Moderate, field dependent	High, stable contact geometry

3.2. Šoić et al. (2019): Gel-Electrolyte EIS Probing of IR-Cured Industrial Coatings

The first paper of this doctoral research, Šoić et al. (2019) [7], introduced a gel-electrolyte electrochemical impedance spectroscopy (EIS) setup designed for the non-destructive evaluation of industrial coatings dried or cured using infrared (IR) radiation. The work addressed a long-standing limitation in high-impedance EIS measurements — namely, the disturbance and leakage risks inherent in conventional liquid-electrolyte cells and demonstrated that accurate measurements could be achieved using a self-contained two-electrode system with flexible, self-adhesive gel electrodes.

The developed system employed commercial ELYSAID self-adhesive silicon electrodes, which contain a conductive polymer layer and a conductive gel electrolyte that conform to the surface without mechanical sealing. In the two-electrode configuration, both electrodes were placed on the coating surface, eliminating the need for electrical contact with the metallic substrate. The method thus allowed impedance characterization of high-resistance coatings exceeding 10^{9} Ω cm², with negligible interference from external electrolyte resistance or evaporation. The experiments were carried out using a custom-built ReCorr QCQ instrument with an input impedance of 1 TΩ and current sensitivity in the pA range. Spectra were recorded over a frequency range from 100 kHz to 10 mHz using a ± 50 mV sinusoidal signal.

The study proposed a new analytical approach for early detection of non-visible coating degradation by introducing the first derivative of the phase angle ($d\theta/d \log f$) as a diagnostic parameter. This derivative highlights subtle distortions in the Bode phase curve that precede the appearance of an additional time constant associated with substrate corrosion. Since highly

efficient barrier coatings often maintain phase angles above -80° across most of the frequency range, the traditional breakpoint-frequency method (based on the -45° criterion) was inapplicable. By contrast, the derivative analysis sensitively revealed incipient dielectric deterioration and the onset of low-frequency relaxation even after a short, one-week neutral salt spray (NSS) exposure, during which no visible damage occurred.

A qualitative four-level rating system (A–D) was established based on the number and position of extrema in the $d\theta/d\ log\ f$ curve:

- A – purely capacitive response with no extrema (intact coating, θ > -80°),
- B – single maximum (early dielectric decline),
- C – one maximum and one minimum (appearance of corrosion-related time constant), and
- D – fully developed concave/convex phase shape with two zeros (advanced delamination).

This diagnostic tool provided a rapid, reproducible means of assessing early coating degradation in the absence of visible defects.

In parallel, quantitative parameters were extracted from the impedance spectra:

- Coating resistance (R_p) was obtained at 0,01 Hz, while $|Z|$ at 0,1 Hz was used for ranking relative barrier performance.
- Coating capacitance (C_p) was determined at $10^{4,6}$ Hz, where the impedance slope equaled −1, using $C = 1/(\omega \mid Z \mid)$.
- Water uptake (φ) was calculated by the Brasher–Kingsbury equation,

$$\phi = log\ \frac{C_t}{C_0} / log\ \varepsilon_e,$$

  assuming $\varepsilon_e = 80$ for water.
- Relative dielectric constant (ε_r) was derived from $C = \varepsilon_r \varepsilon_0 / d$, taking the dry-film thickness d as constant.

Complementary FTIR and DSC analyses confirmed that IR curing did not alter coating chemistry, while *pull-off* adhesion testing revealed a minor (~10 %) decrease in adhesion, attributable to internal stresses from rapid solvent release. Despite this, IR curing substantially improved the barrier performance of epoxy and polyurethane coatings, yielding higher impedance, lower water uptake, and 10–30 % lower dielectric constants compared to ambient-cured analogues.

From a process standpoint, the study highlighted that IR curing reduces production time and energy consumption, enables selective heating of coated components, and allows "wet-on-wet" application without intermediate drying, thereby enhancing coating productivity without compromising protection.

Overall, this work demonstrated that gel-electrolyte EIS enables reliable, high-impedance measurements on intact coatings, while the phase-derivative method provides a sensitive criterion for early-stage degradation. These findings established both the methodological and analytical foundations for the subsequent development of the paste-electrolyte cell, extending the concept toward in-situ and field measurements.

Significance for the Doctoral Framework

This study established the experimental and conceptual foundation of the doctoral work by demonstrating that EIS measurements can be successfully performed using a gel (semisolid) electrolyte and a two-electrode configuration on high-impedance coatings. It proved that non-liquid electrolytes can yield reliable spectra and introduced an analytical approach (first derivative of phase angle) for detecting early-stage degradation. These findings directly motivated the development of the subsequent paste-electrolyte cell, forming the methodological starting point of the doctoral research.

3.3. Martinez et al. (2021): EIS Assessment of Industrial Coating Barrier Properties

The second paper forming part of this doctoral research, Martinez et al. (2021) [8], expanded upon the gel-electrolyte concept by introducing and validating a paste-electrolyte EIS cell suitable for reproducible laboratory assessment of thick industrial coatings. The new configuration combined semisolid electrolyte contact with flexible conductive rubber electrodes, maintaining stable ionic coupling without the need for a liquid reservoir, sealing rings, or cell containment. This innovation preserved the high-impedance measurement capability demonstrated in the 2019 work, while improving control of the electrode geometry and eliminating artefacts associated with surface wetting and electrolyte leakage. The setup was specifically designed for coatings with impedance values up to 10^9 Ω cm², enabling quantitative evaluation of barrier performance and its evolution during environmental exposure.

Experimental and Analytical Approach

EIS measurements were carried out over a frequency range of 100 kHz to 10 mHz at a sinusoidal amplitude of ± 50 mV using the paste-electrolyte cell placed directly on the coating

surface. The active electrode area was defined by the cell geometry (≈ 27 cm²) and the paste-electrolyte layer thickness of 0,3–0,5 mm. The cell provided a highly reproducible electrolyte resistance (≤ 250 Ω) and allowed long-term testing of the same surface area without mechanical damage.

Four commercial coating systems—two water-based and two solvent-based—were exposed to 3,5 % NaCl immersion and neutral salt spray (NSS) conditions to simulate industrial service environments. The resulting impedance spectra typically displayed two relaxation domains, corresponding to polymer dielectric behavior at high frequencies and ionic or electrochemical processes at low frequencies.

This paper advanced the interpretation of electrochemical impedance spectroscopy (EIS) data for thick industrial coatings by introducing a unified equivalent-circuit model, $R_e\ (Q_1\ [R_1\ (Q_2 R_2)])$, which consolidates the dielectric-permittivity and porous-coating formalisms into a single physically meaningful framework. This model was validated on four representative commercial coating systems—two water-based and two solvent-based—exposed to 3,5 % NaCl solution and accelerated salt-cabinet conditions, thereby encompassing both diffusion-controlled and corrosion-related degradation regimes.

EIS measurements were performed over a broad frequency window (100 kHz–10 mHz) at ± 50 mV amplitude. The impedance spectra exhibited two distinguishable relaxation regions, prompting the adoption of the nested-circuit configuration above. The high-frequency loop corresponded to the intrinsic polymer response (dipole relaxation and dielectric loss), while the low-frequency loop represented ionic conduction and, where applicable, interfacial corrosion processes.

The model components were assigned unambiguous physical meanings as given in table 5.

Table 5. Physical interpretation of equivalent circuit model elements

Model element	**Dielectric interpretation**	**Porous-film interpretation**
R_e	Electrolyte resistance	Solution resistance
Q_1 (CPE_1)	High-frequency capacitance limit $C\infty$	Coating capacitance C_c
R_1	Resistance to dipole movement / polymer relaxation	Pore resistance R_p
Q_2 (CPE_2)	Low-frequency capacitance limit C_s	Double-layer capacitance C_{dl}
R_2	Film resistance linked to ionic conduction	Charge-transfer resistance R_{ct}

The fittings achieved $\chi^2 < 0{,}001$ across all systems, confirming the model's robustness and ability to describe both intact and partially degraded coatings with a single mechanistic scheme.

Water and Ion-Transport Effects

The study analyzed how water absorption and ionic mobility govern the evolution of impedance spectra. Water acts as a plasticizer, lowering the coating's T_g by ≈ 20–30 °C, which increases polymer-chain mobility and shortens dipole relaxation times. Consequently, high-frequency capacitance rises and R_1 decreases. At lower frequencies, absorbed water enhances ionic hopping and percolation, decreasing R_2 and producing conduction plateaus characteristic of Maxwell–Wagner–Sillars (MWS) interfacial polarization. These coupled mechanisms were quantitatively captured by the evolution of the model parameters over immersion time.

New Quantitative Criteria

To complement conventional indicators such as the impedance modulus at 0,1 Hz, the work introduced two diagnostic quantities that substantially improve predictive capability: Dielectric loss tangent, *tan δ(ω)* – defined as the resistive-to-capacitive current ratio:

$$tan\ \delta = \epsilon''/\epsilon' = 1/tan\ (-\theta).$$

- High-frequency *tan δ* peaks identify polymer dipole relaxation and thus reflect intrinsic coating quality.
- Low-frequency peaks reveal MWS polarization or active substrate areas, signaling the onset of corrosion or wet adhesion loss.

Polarized impedance response – EIS spectra were acquired under various cathodic DC offsets (0 to −5 V) to differentiate polymeric from electrochemical contributions. A rise in the low-frequency *tan δ* maximum during polarization, accompanied by blister formation, confirmed substrate activity and loss of wet adhesion.

Together, these criteria allowed discrimination between mere water saturation and genuine corrosion initiation—an ambiguity often unsolved by impedance-modulus trends alone.

Predictive and Diagnostic Outcomes

The model successfully ranked coating performance and mechanistic stability:

- System A (water-based) showed a continuous decline of R_2 and a growing low-frequency *tan δ* peak under polarization, indicating increasing porosity and hydrogen-induced blistering. Adhesion strength dropped by ≈ 50 %.

- Systems B–D attained stable R_2 values, reflecting water saturation without structural failure; their impedance and *tan δ* responses remained unchanged upon polarization, corroborating durable barrier function.

Significance for the Doctoral Framework

This paper provided the interpretative and theoretical framework of the dissertation by unifying dielectric and porous coating models into a single equivalent circuit applicable across coating systems. It introduced the dielectric loss tangent (*tanδ*) and its response to polarization as new diagnostic parameters, linking EIS spectra to physical degradation mechanisms. These concepts underpin all subsequent analyses and define the core data interpretation protocol used throughout the doctoral research.

3.4. Šoljić et al. (2022): AC Interference Impact on Coating EIS Assessment

The study by Šoljić et al. (2022) [9] represents a key step in validating the measurement reliability of electrochemical impedance spectroscopy for high-impedance coatings under realistic, field-relevant conditions. While the earlier studies focused on improving coating interpretation (Šoić et al., 2019 [7]) and unifying model formalisms (Martinez et al., 2021 [8]), this paper addresses a fundamental practical obstacle in transferring EIS to *in situ* use—the influence of external AC interference on the precision and accuracy of impedance measurements.

The authors systematically investigated how electromagnetic interferences, such as those originating from nearby AC power lines or railway systems, affect the quality of EIS data obtained for high-performance coatings and simulated systems with extremely high impedance values. A combination of dummy cells, calibration foils, and field-exposed coated samples was employed to decouple instrument imprecision from external signal disturbances and to quantify the limits of precision achievable under different excitation amplitudes and interference levels.

The experiments demonstrated that AC interference primarily affects the phase angle, causing stochastic variations that become pronounced when measuring highly capacitive, intact coatings with total impedance in the GΩ range. The magnitude of interference-induced variation decreased with coating degradation, confirming that the problem is most critical for undamaged barrier systems. Under low excitation signals (10–50 mV), measurement currents fall into the picoampere range, where the synergistic influence of interference and instrument precision leads to a notable loss of repeatability—manifesting as relative standard deviation (RSD) values up to 5–6%.

A major contribution of this study is the quantitative definition of the excitation amplitude threshold required to overcome interference. By progressively increasing the signal amplitude from 10 mV to 250 mV, the authors established that at amplitudes ≥150 mV, both precision (>99%) and accuracy (>97%) could be maintained even in the presence of interference voltages up to 250 mV. The results confirmed that higher excitation amplitudes improve the signal-to-noise ratio without inducing measurable nonlinearity or distortion in the impedance response.

For highly intact coatings ($log|Z| > 9\ \Omega\ cm^2$), this finding is of critical importance. It demonstrates that by optimizing signal amplitude, reliable impedance measurements can be achieved outside shielded laboratory conditions, thereby validating the robustness of the methodology for field use. The study also reported excellent repeatability for calibration foils (RSD < 1% for 150–250 mV signals) and confirmed that even under AC railway interference environments, precision remained within acceptable limits when using the maximum excitation amplitude.

These findings were interpreted within the framework of equivalent circuit theory, where interference acts as a superimposed voltage that modifies the effective potential drop across the cell. By maintaining a sufficiently high impressed AC voltage, the measurement system ensures dominance of the controlled signal over the induced interference, thus preserving the integrity of the impedance response.

The paste-electrolyte measurement cell developed within this doctoral research also benefited from these findings. Although not the primary focus of this paper, the results directly supported subsequent optimization of signal amplitude and data acquisition protocols for portable EIS systems. The confirmation that linear EIS responses can be obtained up to 250 mV AC amplitude under interference-prone conditions provided the necessary experimental validation for reliable high-impedance measurement using compact, unshielded, *in situ* cells.

In summary, Šoljić et al. (2022) [9] established a crucial foundation for extending EIS beyond laboratory environments by quantifying the relationship between interference amplitude, signal strength, and achievable precision. This work strengthened the methodological framework of the doctoral research by ensuring that the semisolid-electrolyte and flexible-electrode configurations operate within verified precision limits even when environmental disturbances are unavoidable. Together with the unified modeling approach and prior gel- and paste-electrolyte developments, this study confirmed the feasibility of accurate, reproducible EIS diagnostics directly on real surfaces.

Significance for the Doctoral Framework

This study contributed to the validation and metrological reliability of the developed methodology. By quantifying the influence of external AC interference on EIS precision and accuracy, it defined practical criteria for stable and reproducible *in situ* measurements. The findings guided the design of the portable measurement system and ensured data integrity under real-field conditions, making the EIS methodology robust beyond laboratory environments.

3.5. Šoić et al. (2023): EIS Testing of Bronze Coatings Using a Novel Paste Electrolyte Cell

The paper by Šoić et al. (2023) [10] presents the culmination of the experimental development in this doctoral research—introducing and validating a novel paste-electrolyte cell for non-destructive *in situ* Electrochemical Impedance Spectroscopy (EIS) testing of coated metallic surfaces. This work extends the methodology initially established for industrial coatings to the domain of cultural heritage conservation, using bronze coins coated with Paraloid B-72 as representative systems.

The cell geometry, optimized in previous developmental work, allows reliable measurement of both high- and low-impedance systems across a broad frequency range without spillage, evaporation, or surface alteration.

Experimental Focus and Methodology

The study investigated the protective performance of Paraloid B-72 coatings of different thicknesses (one, two, and three layers) applied over sulfide patinas on two bronze alloys ($CuSn_6$ and $CuSn_{12}$). The experimental setup employed the two-electrode paste-electrolyte configuration, where the paste ensured ionic contact while preserving the underlying surface integrity.

EIS spectra were recorded over the frequency range from 10 kHz to 0,1 Hz, with full measurement stabilization achieved in under three minutes enabling rapid, on-site applicability. The impedance data were analyzed in terms of both magnitude ($log|Z|$) and phase angle, complemented by equivalent circuit modeling to quantify the coating and patina responses.

Key Findings

The paste-electrolyte EIS cell proved capable of resolving distinct responses from the coating, patina and substrate, thereby offering a mechanistic insight into protective performance:

- Barrier performance: The low-frequency impedance ($log|Z|$ at 0,1 Hz) increased systematically with the number of coating layers, ranging from 10^4 Ω cm^2 for bare/patinated bronze to above 10^8 Ω cm^2 for triple-layer Paraloid coatings.
- Condensation resistance: After 24 h exposure to 100% RH, only the three-layer coatings retained high resistance (~10^8 Ω cm^2), confirming superior water-barrier performance, while single- and double-layer coatings exhibited marked impedance drops (~10^6 Ω cm^2).
- Patina quality differentiation: The medium-frequency capacitance (1,1 μF cm^{-2} to 2,3 nF cm^{-2}) reflected coating penetration into the patina pores, enabling discrimination between compact ($CuSn_{12}$) and porous ($CuSn_6$) patinas.
- All spectra passed the Kramers–Kronig (K–K) consistency test, confirming that the EIS data obtained with the paste cell were free of artifacts and linearly valid, with residuals within ± 0,5%.

Significance for the Doctoral Framework

This paper represents the implementation and generalization stage of the doctoral research. It introduced the final version of the paste-electrolyte cell and demonstrated its universal applicability to irregular surfaces and cultural heritage materials. By establishing quantitative assessment criteria ($|Z|_{0,1}$Hz and phase angle thresholds) and confirming data validity via Kramers–Kronig testing, it validated the complete methodology as a portable, non-destructive diagnostic tool ready for field deployment.

4. CONCLUSION

This doctoral dissertation, prepared in accordance with the Scandinavian model, integrates four peer-reviewed scientific papers that together form a complete developmental cycle — from the conceptualization and experimental demonstration of electrochemical impedance spectroscopy measurements in semisolid electrolytes, through the unification of the interpretation model, to the verification of measurement accuracy and the demonstration of applicability across different materials and surface geometries.

The collective contribution of these studies exceeds their individual results, as they are synergistically interconnected through:

1. The development of an experimental configuration (from gel to paste-electrolyte with flexible electrodes) that ensures stable contact and reproducible measurements;
2. The unification of data-interpretation models, providing consistent physical meaning for impedance spectra of both dielectric and porous coatings;
3. The quantification of noise sensitivity and measurement accuracy, thereby establishing metrological reliability even outside controlled laboratory conditions; and
4. The demonstration of universal applicability of the developed methodology to both industrial and conservation systems, confirming its robustness and transferability.

Together, these advances achieved the central goal of the research—the establishment of a reproducible, portable, and methodologically validated EIS methodology that preserves laboratory-grade precision while enabling *in situ* measurements directly on real surfaces.

The integrated contribution of this dissertation is reflected in:

1. Methodological integration – measurement, modeling, data analysis, and interpretation combined into a single coherent framework;
2. Scientific novelty – demonstration of reliable EIS measurement over the full impedance range from 10^3 to 10^{11} Ω cm^2 without liquid electrolytes; and
3. Technological applicability – a system suitable for field and conservation testing, with clear potential for automated and data-driven diagnostics.

As a whole, this dissertation demonstrates that the combination of a semisolid electrolyte, flexible electrodes, and an optimized measurement regime bridges the gap between experimental electrochemistry and engineering practice. The results establish a foundation for the future development of digitally assisted, predictive monitoring of passive materials and protective coatings.

5. BIBLIOGRAPHY

[1] ISO 16773-1:2016. Paints and varnishes — Electrochemical impedance spectroscopy (EIS) on coated and uncoated metallic specimens — Part 1: Terms and definitions. International Organization for Standardization, Geneva, Switzerland, 2016..

[2] ISO 16773-2:2016. Paints and varnishes — Electrochemical impedance spectroscopy (EIS) on coated and uncoated metallic specimens — Part 2: Collection of data. International Organization for Standardization, Geneva, Switzerland, 2016.

[3] ISO 16773-3:2016. Paints and varnishes — Electrochemical impedance spectroscopy (EIS) on coated and uncoated metallic specimens — Part 3: Processing and analysis of data from dummy cells. International Organization for Standardization, Geneva, Switzerland, 2016.

[4] ISO 16773-4:2017. Paints and varnishes — Electrochemical impedance spectroscopy (EIS) on coated and uncoated metallic specimens — Part 4: Examples of spectra for polymer-coated and uncoated specimens. International Organization for Standardization, Geneva, Switzerland, 2017.

[5] ASTM D8370-22. Standard Test Method for Field Measurement of Electrochemical Impedance on Coatings and Linings. ASTM International, West Conshohocken, PA, USA, 2022.

[6] AMPP TM21449-2021. Continuous Measurements for Determination of Aerospace Coating Protective Properties. AMPP (Association for Materials Protection and Performance), Houston, TX, USA, 2021

[7] I. Šoić, S. Martinez, M. Dubravić, Gel-Electrolyte EIS setup used for probing of IR Dried/Cured industrial coatings, Prog Org Coat 137 (2019) 105331. https://doi.org/10.1016/j.porgcoat.2019.105331.

[8] S. Martinez, I. Šoić, V. Špada, Unified equivalent circuit of dielectric permittivity and porous coating formalisms for EIS probing of thick industrial grade coatings, Prog Org Coat 153 (2021) 106155. https://doi.org/10.1016/j.porgcoat.2021.106155.

[9] I. Šoljić, I. Šoić, L. Kostelac, S. Martinez, AC interference impact on EIS assessment of organic coatings using dummy cells, calibration foils and field exposed coated samples, Prog Org Coat 165 (2022) 106767. https://doi.org/10.1016/j.porgcoat.2022.106767.

[10] I. Šoić, I. Šoljić, M. Eškinja, A. Mujezinović, S. Martinez, The novel paste electrolyte measuring cell for EIS testing of the commonly used surface protection on bronze, Prog Org Coat 177 (2023) 107442. https://doi.org/10.1016/j.porgcoat.2023.107442.

[11] C. Lecuyer, C. Barreau, D. Thierry, Electrochemical sensor for in-situ monitoring of coated metals degradation under atmospheric conditions, 88 (1991) 691–701.

[12] E.P.M. van Westing, G.M. Ferrari, F.M. Geenen, J.H.W. de Wit, In situ determination of the loss of adhesion of barrier epoxy coatings using electrochemical impedance spectroscopy, Prog Org Coat 23 (1993) 89–103. https://doi.org/10.1016/0033-0655(93)80006-V.

[13] A. AMIRUDIN, D. THIERRY, Electrochemical sensor for monitoring atmospheric corrosion of polymer coated metal, British Corrosion Journal 30 (1995) 214–220. https://doi.org/10.1179/000705995798113871.

[14] A. Amirudin, D. Thieny, Application of electrochemical impedance spectroscopy to study the degradation of polymer-coated metals, Prog Org Coat 26 (1995) 1–28. https://doi.org/10.1016/0300-9440(95)00581-1.

[15] G.D. Davis, L.A. Krebs, C.M. Dacres, Coating evaluation and validation of accelerated test conditions using an in-situ corrosion sensor, Journal of Coatings Technology 74 (2002) 69–74. https://doi.org/10.1007/BF02697959.

[16] X. Qi, B. Hinderliter, V.J. Gelling, Two-Electrode Electrochemical Impedance Sensor: Part 1—Response to Coating Degradation on Conductive Substrates, Corrosion 65 (2009) 343–349. https://doi.org/10.5006/1.3319139.

[17] K.N. Allahar, V. Upadhyay, G.P. Bierwagen, V.J. Gelling, Monitoring of a military vehicle coating under Prohesion exposure by embedded sensors, Prog Org Coat 65 (2009) 142–151. https://doi.org/10.1016/j.porgcoat.2008.10.011.

[18] G.P. Bierwagen, K.N. Allahar, Q. Su, V.J. Gelling, Electrochemically characterizing the ac–dc–ac accelerated test method using embedded electrodes, Corros Sci 51 (2009) 95–101. https://doi.org/10.1016/j.corsci.2008.09.023.

[19] R. Yu, Q. Zhou, Y. Wang, C. You, Impedance-Based Wireless Sensor Network for Metal-Protective Coating Evaluation, in: Advanced Instrument Engineering, IGI Global, 2013: pp. 177–192. https://doi.org/10.4018/978-1-4666-4165-5.ch014.

[20] V. Upadhyay, K.N. Allahar, G.P. Bierwagen, Environmental humidity influence on a topcoat/Mg-rich primer system with embedded electrodes, Sens Actuators B Chem 193 (2014) 522–529. https://doi.org/10.1016/j.snb.2013.11.084.

[21] G. Cai, H. Wang, D. Jiang, Z. Dong, Impedance sensor for the early failure diagnosis of organic coatings, J Coat Technol Res 15 (2018) 1259–1272. https://doi.org/10.1007/s11998-018-0072-5.

[22] B. Ramírez Barat, E. Cano, P. Letardi, Advances in the design of a gel-cell electrochemical sensor for corrosion measurements on metallic cultural heritage, Sens Actuators B Chem 261 (2018) 572–580. https://doi.org/10.1016/j.snb.2018.01.180.

[23] Y.-T. Kuo, C.-Y. Lee, Y.-L. Lee, Compact coating impedance detector for fast evaluation of coating degradation, Measurement 124 (2018) 303–308. https://doi.org/10.1016/j.measurement.2018.04.041.

[24] F.J. Friedersdorf, J.C. Demo, N.K. Brown, P.C. Kramer, Electrochemical Sensors for Continuous Measurement of Corrosion and Coating System Performance in Outdoor and Accelerated Atmospheric Tests, in: Advances in Electrochemical Techniques for Corrosion Monitoring and Laboratory Corrosion Measurements, ASTM International100 Barr Harbor Drive, PO Box C700, West Conshohocken, PA 19428-2959, 2019: pp. 91–113. https://doi.org/10.1520/STP160920170222.

[25] B.J.E. Merten, M.T. Walsh, J.D. Torrey, Validation of Coated Infrastructure Examination by Electrochemical Impedance Spectroscopy, in: Advances in Electrochemical Techniques for Corrosion Monitoring and Laboratory Corrosion Measurements, ASTM International100 Barr Harbor Drive, PO Box C700, West Conshohocken, PA 19428-2959, 2019: pp. 137–159. https://doi.org/10.1520/STP160920170223.

[26] G. Monrrabal, A. Bautista, F. Velasco, Use of Innovative Gel Electrolytes for Electrochemical Corrosion Measurements on Carbon and Galvanized Steel Surfaces, Corrosion 75 (2019) 1502–1512. https://doi.org/10.5006/3309.

[27] A. Rondinella, R. Offoiach, F. Andreatta, G. Capurso, L. Calabrese, E. Proverbio, L. Fedrizzi, Development of a warning system for defects onset in organic coatings on large surfaces, Prog Org Coat 179 (2023) 107528. https://doi.org/10.1016/j.porgcoat.2023.107528.

[28] K. Popova, M.F. Montemor, T. Prošek, Application of Resistometric Sensors for Real-Time Corrosion Monitoring of Coated Materials, Corrosion and Materials Degradation 5 (2024) 573–593. https://doi.org/10.3390/cmd5040026.

[29] H. Ji, Y. Liu, X. Ma, H. Wang, Y. Cai, S. Jiao, Electrochemical performance monitoring and degradation modeling method for organic coating systems: Integrating three-phase Wiener process and kinetic models, Measurement 240 (2025) 115532. https://doi.org/10.1016/j.measurement.2024.115532.

[30] K.S. Hein, Y. Wang, Y. Li, Q. Liu, K. Chen, Y. Chen, J. Chen, W.-L. Jin, R. Wu, J. Xia, A holistic approach to evaluating techniques for monitoring coated steel degradation: Integrating techniques and applications, Prog Org Coat 200 (2025) 109067. https://doi.org/10.1016/j.porgcoat.2025.109067.

[31] Z. Dong, B. Ter-Ovanessian, H. Abe, N. Mary, Y. Watanabe, B. Normand, Design of an EIS-based sensor for indirect non-invasive corrosion inspection, Corros Sci 254 (2025) 113029. https://doi.org/10.1016/j.corsci.2025.113029.

[32] Z. Jiryaeisharahi, D. De Keukeleere, Y. Desmet, B. Wouters, N. Madelat, H. Terryn, A. Hubin, Exploring transport properties and onset of corrosion in organic coated metals using an innovation sensor-based methodology supported by ORP-EIS, Prog Org Coat 207 (2025) 109388. https://doi.org/10.1016/j.porgcoat.2025.109388.

[33] F. Mansfeld, Use of electrochemical impedance spectroscopy for the study of corrosion protection by polymer coatings, J Appl Electrochem 25 (1995). https://doi.org/10.1007/BF00262955.

[34] H. Xiao, L.T. Han, C.C. Lee, F. Mansfeld, Collection of Electrochemical Impedance and Noise Data for Polymer-Coated Steel from Remote Test Sites, Corrosion 53 (1997) 412–422. https://doi.org/10.5006/1.3280484.

[35] D.H. van der Weijde, E.P.M. van Westing, J.H.W. de Wit, Monitoring the Effect of Environmental Changes on Coating Properties with EIS, Materials Science Forum 289–292 (1998) 237–246. https://doi.org/10.4028/www.scientific.net/MSF.289-292.237.

[36] F. Mansfeld, H. Xiao, L.T. Han, C.C. Lee, Electrochemical impedance and noise data for polymer coated steel exposed at remote marine test sites, Prog Org Coat 30 (1997) 89–100. https://doi.org/10.1016/S0300-9440(96)00675-3.

[37] F. Mansfeld, C.C. Lee, G. Zhang, Comparison of Electrochemical Impedance and Noise Data for Polymer Coated Steel in the Frequency Domain, Materials Science Forum 289–292 (1998) 93–106. https://doi.org/10.4028/www.scientific.net/MSF.289-292.93.

[38] F. Mansfeld, L.T. Han, C.C. Lee, G. Zhang, Evaluation of corrosion protection by polymer coatings using electrochemical impedance spectroscopy and noise analysis, Electrochim Acta 43 (1998) 2933–2945. https://doi.org/10.1016/S0013-4686(98)00034-6.

[39] J.A. González, E. Otero, A. Bautista, E. Almeida, M. Morcillo, Use of electrochemical impedance spectroscopy for studying corrosion at overlapped joints, Prog Org Coat 33 (1998) 61–67. https://doi.org/10.1016/S0300-9440(98)00009-5.

[40] A. Bautista, J.A. González, E. Otero, M. Morcillo, E. Almeida, Discrimination by EIS of degradation mechanisms in lap joints of coated metal sheet, Journal of Coatings Technology 71 (1999) 61–68. https://doi.org/10.1007/BF02697907.

[41] G. Davis, C.M. Dacres, L.A. Krebs, In-situ corrosion sensor for coating, testing and screening, Mater Perform 39 (2000).

[42] G.D. Davis, L.A. Krebs, L.T. Drzal, M.J. Rich, P. Askeland, Electrochemical Sensors for Nondestructive Evaluation of Adhesive Bonds, J Adhes 72 (2000) 335–358. https://doi.org/10.1080/00218460008029289.

[43] G.D. Davis, K. Thayer, M.J. Rich, L.T. Drzal, Inspection of composite and metal adhesive bonds with an electrochemical sensor, J Adhes Sci Technol 16 (2002) 1307–1326. https://doi.org/10.1163/156856102320252822.

[44] G.D. Davis, B.J. Harkless, Use of an electrochemical probe for predictive assessment of bonded repair, Int J Adhes Adhes 22 (2002) 323–329. https://doi.org/10.1016/S0143-7496(02)00011-8.

[45] G.D. Davis, M.J. Rich, L.T. Drzal, Monitoring Moisture Uptake and Delamination in CFRP-Reinforced Concrete Structures with Electrochemical Impedance Sensors, J Nondestr Eval 23 (2004) 1–9. https://doi.org/10.1023/B:JONE.0000045216.94094.f5.

[46] G.D. Davis, J.G. Dillard, Development of an electrochemical impedance spectroscopy sealant test: I. Nonconductive sealants, J Adhes Sci Technol 20 (2006) 1215–1233. https://doi.org/10.1163/156856106777920848.

[47] E. Otero, J.A. González, B. Chico, M. Morcillo, Measure of the driving forces of underfilm differential contamination cells and differential aeration cells, Prog Org Coat 45 (2002) 441–447. https://doi.org/10.1016/S0300-9440(02)00148-0.

[48] A. Bautista, J.A. González, E. Otero, M. Morcillo, Electrochemical study of lap-joint corrosion of steel with metallic coatings, Journal of Coatings Technology 73 (2001) 73–79. https://doi.org/10.1007/BF02698378.

[49] S. Krakowiak, K. Darowicki, J. Bordzilowski, The impedance method of monitoring the degradation of rubber linings in applications where progressive deterioration is the predominant failure mechanism, Anti-Corrosion Methods and Materials 48 (2001) 358–363. https://doi.org/10.1108/00035590110410218.

[50] J. Bordziłowski, K. Darowicki, S. Krakowiak, A. Królikowska, Impedance measurements of coating properties on bridge structures, Prog Org Coat 46 (2003) 216–219. https://doi.org/10.1016/S0300-9440(02)00193-5.

[51] A. Carullo, F. Ferraris, M. Parvis, A. Vallan, E. Angelini, P. Spinelli, Low-cost electrochemical impedance spectroscopy system for corrosion monitoring of metallic antiquities and works of art, IEEE Trans Instrum Meas 49 (2000) 371–375. https://doi.org/10.1109/19.843080.

[52] K. Darowicki, M. Szocinski, Evaluating the performance of organic coatings under mechanical stress using electrochemical impedance spectroscopy, Journal of Solid State Electrochemistry 8 (2004) 346–351. https://doi.org/10.1007/s10008-003-0451-3.

[53] A. Miszczyk, K. Darowicki, T. Schauer, Impedance-based sensing of the interlayer adhesion loss in organic coating systems, Journal of Solid State Electrochemistry 9 (2005) 909–913. https://doi.org/10.1007/s10008-005-0050-6.

[54] Q. Le Thu, H. Takenouti, S. Touzain, EIS characterization of thick flawed organic coatings aged under cathodic protection in seawater, Electrochim Acta 51 (2006) 2491–2502. https://doi.org/10.1016/j.electacta.2005.07.049.

[55] W. Strunz, C.A. Schiller, J. Vogelsang, The change of dielectric properties of barrier coatings during the initial state of immersion, Materials and Corrosion 59 (2008) 159–166. https://doi.org/10.1002/maco.200804156.

[56] I. Klüppel, B. Schinkinger, G. Grundmeier, In situ electrochemical studies of forming-induced defects of organic coatings on galvanised steel, Electrochim Acta 54 (2009) 3553–3560. https://doi.org/10.1016/j.electacta.2009.01.003.

[57] X. Qi, B. Hinderliter, V.J. Gelling, Two-Electrode Electrochemical Impedance Sensor: Part 2—Impedance Measurement and Simulation of Coatings on Nonmetal Substrates, Corrosion 66 (2010) 025002-1-025002–10. https://doi.org/10.5006/1.3319659.

[58] K.N. Allahar, Q. Su, G.P. Bierwagen, In Situ Monitoring of Organic Coatings Under QUV/Prohesion Exposure by Embedded Sensors, Corrosion 64 (2008) 860–870. https://doi.org/10.5006/1.3279920.

[59] K.N. Allahar, Q. Su, G.P. Bierwagen, D.-H. Lee, Monitoring of the AC-DC-AC Degradation of Organic Coatings Using Embedded Electrodes, Corrosion 64 (2008) 773–787. https://doi.org/10.5006/1.3278445.

[60] Q. Su, K.N. Allahar, G.P. Bierwagen, Application of embedded sensors in the thermal cycling of organic coatings, Corros Sci 50 (2008) 2381–2389. https://doi.org/10.1016/j.corsci.2008.06.010.

[61] K.N. Allahar, D. Wang, D. Battocchi, G.P. Bierwagen, S. Balbyshev, Real-Time Monitoring of a United States Air Force Topcoat/Mg-Rich Primer System in ASTM

B117 Exposure by Embedded Electrodes, Corrosion 66 (2010) 075003-1-075003–11. https://doi.org/10.5006/1.3462975.

[62] Q. Su, K.N. Allahar, G.P. Bierwagen, In Situ Embedded Sensor Monitoring of a United States Air Force Primer Beneath a Topcoat Exposed to Atmospheric Humidity and Thermal Conditions, Corrosion 66 (2010) 066001-1-066001–12. https://doi.org/10.5006/1.3452403.

[63] D. Wang, D. Battocchi, K.N. Allahar, S. Balbyshev, G.P. Bierwagen, In situ monitoring of a Mg-rich primer beneath a topcoat exposed to Prohesion conditions, Corros Sci 52 (2010) 441–448. https://doi.org/10.1016/j.corsci.2009.10.001.

[64] K. Allahar, Q. Su, G. Bierwagen, Non-substrate EIS monitoring of organic coatings with embedded electrodes, Prog Org Coat 67 (2010) 180–187. https://doi.org/10.1016/j.porgcoat.2009.10.001.

[65] K.R. Larsen, Corrosion monitor senses coating health using EIS technology, Mater Perform 49 (2010) 15–16. https://doi.org/10.5006/MP2010_49_10-15.

[66] Y. Shi, D. Wang, C. You, Electrochemical Impedance Spectroscope-Based Sensor System Designed for Detecting Corrosion Resistance Level of a Coating, Sens Lett 9 (2011) 464–471. https://doi.org/10.1166/sl.2011.1499.

[67] D. Xia, S. Song, W. Gong, Y. Jiang, Z. Gao, J. Wang, Detection of corrosion-induced metal release from tinplate cans using a novel electrochemical sensor and inductively coupled plasma mass spectrometer, J Food Eng 113 (2012) 11–18. https://doi.org/10.1016/j.jfoodeng.2012.05.035.

[68] X. Zheng, D. Xia, H. Wang, C. Fu, Detection of the corrosion degree of beverage cans using a novel electrochemical sensor, Anti-Corrosion Methods and Materials 60 (2013) 153–159. https://doi.org/10.1108/00035591311315382.

[69] K. Wang, J. Wang, H. Wang, C. Fu, D. Xia, X. Zheng, L. Dang, J. Shi, Corrosion detection of tinplate cans containing coffee using EIS/EN sensor, J Cent South Univ 21 (2014) 76–82. https://doi.org/10.1007/s11771-014-1918-3.

[70] S. Grassini, S. Corbellini, E. Angelini, F. Ferraris, M. Parvis, Low-Cost Impedance Spectroscopy System Based on a Logarithmic Amplifier, IEEE Trans Instrum Meas 64 (2015) 1110–1117. https://doi.org/10.1109/TIM.2014.2371191.

[71] E. Angelini, S. Corbellini, M. Parvis, F. Ferraris, S. Grassini, An Arduino-based EIS with a logarithmic amplifier for corrosion monitoring, in: 2014 IEEE International Instrumentation and Measurement Technology Conference (I2MTC) Proceedings, 2014: pp. 905–910. https://doi.org/10.1109/I2MTC.2014.6860873.

[72] K. Tokutake, H. Nishi, D. Ito, S. Okazaki, Y. Serizawa, Relationship between degradation characteristics of organic coating on internal bottom plate of oil storage tank and constant-phase element parameter values, Prog Org Coat 87 (2015) 69–74. https://doi.org/10.1016/j.porgcoat.2015.05.004.

[73] B. Zajec, M. Bajt Leban, S. Lenart, K. Gavin, A. Legat, Electrochemical impedance and electrical resistance sensors for the evaluation of anticorrosive coating degradation, Corrosion Reviews 35 (2017) 65–74. https://doi.org/10.1515/corrrev-2016-0055.

[74] K.N. Hosbein, A.H. England, C.A. Price, T.L. Clare, Measuring Sheet Resistances of Dielectrics Using Co-Planar Hydrogel Electrochemical Cells with Practical Applications to Characterize the Protective Quality of Paints on Sculptures, Electroanalysis 29 (2017) 1377–1387. https://doi.org/10.1002/elan.201600765.

[75] H. Hayashibara, E. Tada, A. Nishikata, Monitoring the Early Stage of Degradation of Epoxy-Coated Steel for Ballast Tank by Electrochemical Impedance Spectroscopy, Mater Trans 58 (2017) 1687–1694. https://doi.org/10.2320/matertrans.M2017243.

[76] M.H. Nazir, Z.A. Khan, A. Saeed, A Novel Non-Destructive Sensing Technology for On-Site Corrosion Failure Evaluation of Coatings, IEEE Access 6 (2018) 1042–1054. https://doi.org/10.1109/ACCESS.2017.2777532.

[77] H. Welp, M. Lenz, C. Mazzon, C. Dillmann, N.C. Gerhardt, M. Prange, M.R. Hofmann, Nondestructive evaluation of protective coatings for the conservation of industrial monuments, in: L. Pezzati, P. Targowski (Eds.), 2017: p. 1033109. https://doi.org/10.1117/12.2270170.

[78] Y.-L. Lee, Y.-T. Kuo, H.-H. Chen, Y.-A. Hsieh, Field-Programmable Gate Array-Based Coating Impedance Detector for Rapid Evaluation of Early Degradation of Protective Coatings, IEEE Access 7 (2019) 20472–20478. https://doi.org/10.1109/ACCESS.2019.2896996.

[79] H.-C. Liao, Z.-H. Cai, H.-H. Chen, C.-H. Chung, I.-C. Cheng, Y.-L. Lee, Degradation Observations of Protective Coatings: An Improved Version of Coating Impedance Detector, IEEE Access 10 (2022) 18074–18080. https://doi.org/10.1109/ACCESS.2022.3151100.

[80] Y.-C. Wang, M. Su, D.-H. Xia, Z. Wu, Z. Qin, L. Xu, H.-Q. Fan, W. Hu, Development of an electrochemical sensor and measuring the shelf life of tinplate cans, Measurement 134 (2019) 500–508. https://doi.org/10.1016/j.measurement.2018.10.096.

[81] D.-H. Xia, Y. Song, S. Song, Y. Behnamian, L. Xu, Z. Wu, Z. Qin, Z. Gao, W. Hu, Identifying defect levels in organic coatings with electrochemical noise (EN) measured in Single Cell (SC) mode, Prog Org Coat 126 (2019) 53–61. https://doi.org/10.1016/j.porgcoat.2018.10.027.

[82] Corrosion Monitoring of Steel Structure Coating Degradation, Tehnicki Vjesnik - Technical Gazette 25 (2018). https://doi.org/10.17559/TV-20170206004112.

[83] T. Chowdhury, N. D'Souza, N. Dahotre, Low-Cost Reliable Corrosion Sensors Using ZnO-PVDF Nanocomposite Textiles, Sensors 21 (2021) 4147. https://doi.org/10.3390/s21124147.

[84] T. Chowdhury, N. D'Souza, Y.H. Ho, N. Dahotre, I. Mahbub, Embedded Corrosion Sensing with ZnO-PVDF Sensor Textiles, Sensors 20 (2020) 3053. https://doi.org/10.3390/s20113053.

[85] F. Valentini, Smart Electrochemical Portable Tools for Cultural Heritage Analysis: A Review, Sensors 19 (2019) 4303. https://doi.org/10.3390/s19194303.

[86] S. Ritter, R.-W. Bosch, F. Huet, K. Ngo, R.A. Cottis, M. Bakalli, M. Curioni, M. Herbst, A. Heyn, J. Macak, R. Novotny, J. Öijerholm, T. Saario, J.M. Sanchez-Amaya, H. Takenouti, B. Zajec, W. Zhang, Results of an international round-robin exercise on electrochemical impedance spectroscopy, Corrosion Engineering, Science and Technology 56 (2021) 254–268. https://doi.org/10.1080/1478422X.2020.1850070.

[87] N.O. Laschuk, E.B. Easton, O. V. Zenkina, Reducing the resistance for the use of electrochemical impedance spectroscopy analysis in materials chemistry, RSC Adv 11 (2021) 27925–27936. https://doi.org/10.1039/D1RA03785D.

[88] X. Frias-Cacho, M. Castro, D.-D. Nguyen, A.-M. Grolleau, J.-F. Feller, A Review of In-Service Coating Health Monitoring Technologies: Towards "Smart" Neural-Like Networks for Condition-Based Preventive Maintenance, Coatings 12 (2022) 565. https://doi.org/10.3390/coatings12050565.

[89] S.T. Tieu, E. Sikora, A.T. Ozyilmaz, L.A. Wolfe, H. Hopfer, G.R. Ziegler, In situ electrochemical impedance spectroscopy of non-BPA food contact coatings on electrolytic tinplate under retort conditions, J Food Eng 395 (2025) 112541. https://doi.org/10.1016/j.jfoodeng.2025.112541.

[90] A. Filippas, L. Onua, A. Manavbasi, J. Liska, N. Liu, A platform for continuous monitoring of the degradation of aluminum beverage can lids in realistic conditions through electrochemical impedance spectroscopy, Food Packag Shelf Life 44 (2024) 101321. https://doi.org/10.1016/j.fpsl.2024.101321.

[91] M.T. Molina, E. Cano, B. Ramírez-Barat, Testing protective coatings for metal conservation: the influence of the application method, Herit Sci 11 (2023) 94. https://doi.org/10.1186/s40494-023-00937-0.

[92] Corrosion of metals and alloys-Test method for corrosion of materials by electrochemical impedance measurements Corrosion des métaux et alliages-Méthode d'essai pour la corrosion des matériaux par des mesures électrochimiques d'impédance COPYRIGHT PROTECTED DOCUMENT, 2014.

[93] M.M. Lalic, S. Martinez, A Novel Application of EIS for Quantitative Coating Quality Assessment During Neutral Salt Spray Testing of High-Durability Coatings, Acta Chim Slov (2019) 913–922. https://doi.org/10.17344/acsi.2019.5113.

[94] M. Bakalli, P. Keil, W. Strunz, T. Broeker, R. Herrmann, J. Vogelsang, Critical view of the results of the 2nd international round-robin test on EIS measurements of organic coatings, Prog Org Coat 180 (2023) 107565. https://doi.org/10.1016/j.porgcoat.2023.107565.

[95] M. Bakalli, P. Keil, W. Strunz, T. Broeker, R. Herrmann, J. Vogelsang, Corrigendum to "Critical view of the results of the 2nd international round-robin test on EIS measurements of organic coatings" [Prog. Org. Coatings 180 (2023) 107565], Prog Org Coat 182 (2023) 107639. https://doi.org/10.1016/j.porgcoat.2023.107639.

APPENDIX I

I. Šoić, S. Martinez, M. Dubravić, Gel-Electrolyte EIS setup used for probing of IR Dried/Cured industrial coatings, Prog. Org. Coat. 137 (2019) 105331

https://doi.org/10.1016/j.porgcoat.2019.105331

Ivana Šoić: validation, formal analysis, investigation, data curation, writing−original draft preparation, writing−review & editing
Sanja Martinez: conceptualization, methodology, validation, resources, writing−original draft preparation, writing−review & editing, supervision
Mia Dubravić: formal analysis, investigation, data curation

Progress in Organic Coatings 137 (2019) 105331

Contents lists available at ScienceDirect

Progress in Organic Coatings

journal homepage: www.elsevier.com/locate/porgcoat

Gel-Electrolyte EIS setup used for probing of IR Dried/Cured industrial coatings

Ivana Šoić*, Sanja Martinez, Mia Dubravić

Research Laboratory for Corrosion Engineering and Surface Protection – ReCorr, Department of Electrochemistry, Faculty of Chemical Engineering and Technology, University of Zagreb, Marulicev trg 19, 10000, Zagreb, Croatia

ARTICLE INFO

Keywords:
EIS
IR curing
Coating
Corrosion
Resistance

ABSTRACT

Probing of IR dried/cured solvent based industrial coatings has been done by employing a two-electrode, gel-electrolyte electrochemical impedance spectroscopy setup that has enabled measurement of the coating electrical characteristics without the influence of the liquid electrolyte. In the present study, along with the coating impedance at 0.1 Hz, we suggest the use of the first derivative of the phase angle as a sensitive tool to detect the influence of the corrosion related low frequency RC circle appearance on the coating performance in the early stages of exposure. The conclusions of the EIS analysis are that the IR curing improves barrier properties of common industrial coatings and decreases the coating capacitance and dielectric constant, with respect to the laboratory ambient dried/cured referent systems. FTIR and DSC show no indications of permanent coating degradation, while the pull-off strength shows a slight, ≤ 10% decay of coating adhesion/cohesion characteristics. The water uptake calculated from the EIS data compared to the FTIR and DSC results, indicates various modes of water adsorption into the coating. It has been demonstrated that EIS may be used for obtaining quick information about the early-stage, non-visible coating degradation in the case of IR drying/curing as a time saving production process alteration that may bring significant benefit to the manufacturer of coated metallic products.

1. Introduction

Scientific literature is replete with the examples demonstrating one of the most successful applications of electrochemical impedance spectroscopy (EIS) [1] by which protective properties of polymer coatings on metals and their changes during exposure to natural and artificial corrosive environments are quantitatively evaluated. A sound theoretical basis for the interpretation of the coating EIS spectra has been set from the 70 s to 90 s of the last century [1–10]. There is a general agreement that EIS spectrum of an efficient protective coating can be fitted by a simple model of capacitance shorted by a resistance [1]. Water uptake causes an increase of the coating capacitance reflecting an alteration of the polymer dielectric behaviour and lowering of the coating resistance reflecting formation of the pores with ion conductive pathways [2]. With the further weakening of the coating barrier properties, the second time constant appears at frequencies below 10^0 Hz that reflects substrate behaviour at the bottom of the pores and below the delaminated coating. In the case of rapid charge transfer reaction, the low-frequency nested equivalent circuit is comprised of a double layer capacitance and a polarization resistance. In the case of a slow charge transfer reaction, Warburg element is added in series with the charge transfer resistance.

The early researchers have readily recognized the practical potential of EIS for optimizing coating formulation [11] and coating quality assurance [12,13] and had therefore broadened their research to methodologies for coating lifetime prediction from the EIS measurements of unexposed specimen and specimen in the early stages of exposure [2,4,6,14–16]. The need for highly resistive coatings with extended service life and reduced maintenance costs has prompted this research ever since [17–25].

Despite the diagnostic and predictive capabilities of EIS which have been proven through decades of scientific research, and the fact that method has been standardized by EN ISO 17663, it has not found widespread use in engineering practice for the in-situ coating quality control and the routine coating testing in laboratories. Paradoxically, EIS has found most appreciation in the area of metal conservation [26–29] where more serious obstacles for its application exist when compared to probing of industrial coating systems. EIS is applied on surfaces of art and heritage objects that are either clean metal surfaces protected by thin layers of wax, thermoplastic resin or clear lacquer

* Corresponding author.
E-mail address: ivana.soic@fkit.hr (I. Šoić).

https://doi.org/10.1016/j.porgcoat.2019.105331
Received 5 March 2019; Received in revised form 9 August 2019; Accepted 10 September 2019

[30,31], surfaces covered with porous layer of corrosion products such as patina on copper and bronze [32] or rust on iron artefacts and Corten [33,34]. The difficulties encountered are: a concern of damaging the surface coating layer and/or unsightly alteration of surface appearance at the place of EIS cell contact [35], inability of measuring low impedances due to the comparably high impedance of the EIS cell electrolyte [32,35] and inability of the non-liquid electrolyte of the EIS cell to follow pores of the substrate [36]. Nevertheless, significant advancements have been made by the conservation scientists in transferring the EIS from the laboratory to the field [32], in developing the flexible gel EIS cells [32,35,36], in overcoming the influence of substrate porosity [37] and in the construction of portable low-cost instruments [37,38].

Following this trend, a recent report describes the development of a prototype miniaturized impedance measurement instrument for a quick estimate of the protective capacity of coatings [39]. However, nowadays, laboratory and field measurements on high-impedance industrial coating systems should be facilitated by the availability of affordable portable lightweight hi-end potentiostats with variable gain amplifiers and variable filters input front-ends [38], a floating ground [29], high input impedance of 1 TΩ, and a pA measurement range. The measurement procedure may further be significantly simplified by adopting a two-electrode EIS measuring approach that cancels the need for the electric contact with the metallic substrate [37,38] and by the use of commercial flexible gel electrodes that were found suitable form measurements on high-impedance coatings [28]. These electrodes can adhere to and conform to the surface [35] and eliminate the possible influence of aggressive liquid electrolyte on the results [28] thereby recording the state of the coating attained solely by natural or artificial weathering.

A sufficient number of measurements at each frequency and data averaging have been used historically to reduce the scatter of the experimental data [1]. The scatter is observed due to noise when low currents in the pA range are measured [38]. In our experience, the use of Faraday cage in the laboratory and well shielded instrument and cables in the field significantly reduce the measurement error and eliminate the need for data averaging or filtering. Calibration of the instrument may be done on dummy cells mimicking high-impedance coatings and compared to the interlaboratory test results in EN ISO 16773-3. Limitation of the instrument with respect to the highest impedance that may be measured can be checked in an open lead experiment. With the use of the instrument having measurement capabilities compatible with the coating characteristics, highly repeatable and reproducible results are obtained.

It is also reasonable to assume that simplification of the EIS data analysis would likely increase the use of EIS in engineering and laboratory practice [40]. To avoid fitting of the data to equivalent circuits, various strategies have been proposed [9,40–46].

In the present study, the influence of the IR accelerated drying/curing on the protective properties of commercial high-durability coating systems, has been investigated by EIS. It is reasonable to assume that IR facilitates both, physical drying by evaporation of the coating solvent and chemical curing reactions between the base and the hardener. This topic is of significant technical importance because the IR drying/curing provides the reduction in production time and it can be applied to the entire product, or to selected parts only, without heating the surroundings which leads to lower cost with respect to the air convection drying [47]. IR curing has the ability to transfer energy faster into the wet film which lets the drying/curing to happen from the bottom to the top of the film reducing product deterioration and excessive evaporation of volatile components from solvent based coatings [47,48]. With further industrial improvements, IR drying/curing allows using *"wet on wet"* coating technology where top coat is applied without fully drying the basecoat. The short time between applications, the so called flash-off time, typically leads to a solid content over 90% in the film. Time of coating processing is significantly shortened with drying/curing primer and top coat together, but heating optimization and coating compatibility are necessary for the successfully completed process [48]. This kind of drying/curing can be especially useful in stripe coating where sufficient corrosion resistivity is very important.

The measurements in the present study were aimed towards observing the fine distinctions among the intact coatings obtained without and with the IR accelerated drying/curing and their degradation after the one-week exposure in the salt chamber according to EN ISO 9227 that inflicted no visible damage. We have used the first derivative of the phase angle with respect to the logarithm of frequency to resolve between the overlapping time constants that are due to the high-frequency response of the polymer and the low-frequency response of the substrate. Furthermore, qualitative rating based on the functional dependency of the first derivative on the logarithm of frequency has been compared to the quantitate characteristics deduced from the impedance spectra, such as coating resistance at 0.01 Hz, coating capacitance at high frequencies, the volume of the absorbed water and the coating dielectric constant. The EIS results were correlated to those of the differential scanning calorimetry and the pull-off adhesion tests. The investigation yielded interesting conclusions about the influence of IR accelerated drying/curing on the conventional industrial coating systems that have not been not previously reported in the literature.

2. Experimental

2.1. Coated samples preparation

Cold rolled steel samples having dimensions of 15 cm × 10 cm × 0.6 cm were prepared by shot blasting. Before applying the coating, sample preparation grade of Sa 2 ½ was checked in accordance with EN ISO 8501-1, surface roughness according to EN ISO 8503-1, cleanness with respect to dust according to EN ISO 8502-3, surface water-soluble by the Bresle method given in EN ISO 8502- 6 and by conductometric method according to EN ISO 8502- 9.

Samples were coated per instructions of the paint manufacturer. The commercial solvent based coating system comprised of a zinc rich base coat, an epoxy mastic intermediate coat and a polyurethane topcoat. The system has been chosen in conformance with system C.5.08 (very high durability) in Table C.5 of EN ISO 12944-6 and system for CX (offshore) corrosivity category in Table 3 of EN ISO 12944-9. Wet and dry film thicknesses were measured according to EN ISO 2808 and ISO 19840 and the measured dry film thickness (DFT) conformed to the 80/20 rule.

Besides the complete system, denoted by EP + EP + PUR, the samples with only two layers of epoxy applied dry-on-dry, denoted by EP + EP, and wet-on-wet, denoted by EP + EP WOW, have been tested in order to simulate two types of the stripe coating procedure. For the first two systems, a comparison is made between samples cured under atmospheric conditions and the IR dried/cured samples, denoted by EP + EP + PUR IR and EP + EP IR, respectively. In the case of wet-on-wet system, only the IR dried/cured sample has been tested and denoted by EP + EP IR WOW. In some of the experiments, the distance between the IR source and the samples was varied, the shortest distance being 40 cm and the longest being 100 cm. The curing time was increased from 10 to 90 min, to account approximately proportionally for the paint layer thickness increase and the distance from the source increase.

Details of the tested systems and preparation methods along with the coating systems abbreviations that are used in the rest of the text are given in Table 1.

Infrared heating emitter from Heraeus Noblelight powered by natural gas was used for coating drying/curing. The dimension of the emitter was 60 cm × 60 cm. The sample rack was placed in front of the IR emitter at different distances of 40, 60, 80 and 100 cm. The used IR emitter had a power of 6 kW and provides a range of wavelengths from 2 to 10 μm.

Table 1
Details of the tested systems and preparation methods.

Coating system		Min. NDFT µm	Drying/ curing conditions	Coating system abbreviation
Coating system				
Basecoat	zinc rich epoxy	70	Dried/cured under laboratory ambient conditions.	EP + EP + PUR
Intermediate layer	Epoxy mastic	125	Dried/cured 40 cm from IR for 10, 25 and 25 min per layer, respectively.	EP + EP + PUR IR
Top coat	polyurethane	125		
Stripe coats				
Basecoat	epoxy mastic	150	Dried/cured under laboratory ambient conditions.	EP + EP
			Each layer dried/cured at 40, 60, 80 and 100 cm from IR for 17.5, 25, 32.5 and 45 min, respectively.	
			"Wet on wet" with 15 min of drying under laboratory ambient conditions between layers.	EP + EP IR
Top coat	epoxy mastic	150	Final layer dried/cured at 40, 60, 80 and 100 cm from IR for 35, 50, 65 and 90 min, respectively.	EP + EP IR WOW

2.2. Neutral salt spray (NSS) test

The neutral salt spray test was conducted in the CW Specialist Equipment model SF/100 salt cabinet according to the EN ISO 9227 and had lasted 168 h. Before conducting further experiments, the samples were left to dry for 60 days under laboratory ambient conditions. The term exposure in the following text refers to subjecting samples to the above described procedure. Thereby, only the irreversible changes to the coatings that remain even after 60 days of drying have been captured by the measurements.

2.3. Electrochemical impedance spectroscopy (EIS)

EIS of coating systems that were laboratory ambient dried/cured and those dried/cured by IR were tested before and after exposure. EIS measurements were carried out by a customized ReCorr QCQ experimental setup developed in our laboratory. It consists of a potentiostat/frequency response analyser with a high input impedance of 1 TΩ, a pA measurement range and two flexible electrodes with the conductive polymer surface and conductive gel electrolyte, each with the surface area of 13.32 cm^2. The setup is electrically shielded from the external electromagnetic influences. Frequency range used in measurements was between 100 kHz and 10 mHz with sinusoidal amplitude of ± 50 mV. Calibration of the setup was done on a high-impedance dummy cell mimicking the coating according to EN ISO 16773-3.

Commercial ELYSAID, 4 cm × 4 cm self-adhesive silicon electrodes were used. Schematic view of the substrate, coating, positioning of the electrodes and the EIS equivalent circuits is given in Fig. 1. The current path through the coating is easily verified by recording the impedance using a single electrode with respect to the substrate whereby identical results are obtained since the current path through the coating is shortened twice, while at the same time the electrode surface is also halved. The two electrode method is however preferred because it requires no contact with the substrate, which may be significant if EIS is measured on a coated structure with no exposed metallic parts. Surface conduction between the electrodes is avoided by performing measurements on a clean and dry surface.

The results are highly repeatable and reproducible. The error estimate of the impedance at 0.1 Hz based on the 10 repetitive measurements is 1.51%. The validity of the measurements is also supported by the following behaviour typical of organic coatings:

- The impedance of an efficient intact coating is of the expected order of magnitude > 10^9 Ω cm^2.
- The capacitance of the intact coating is of the expected order of magnitude of pF cm^{-2}.
- The impedance of the intact coating shows a single time constant comprised of a coating capacitance and a resistance.
- The second time constant at lower frequencies appears after exposure to humid environments.

2.4. Attenuated total reflectance Fourier-transform infrared spectroscopy (ATR-FTIR)

ATR-FTIR of coating systems that were laboratory ambient dried/cured and those dried/cured by IR was tested before and after exposure by using a PerkinElmer spectrometer Spectrum One. Spectra were obtained in the range from 650 to 4000 cm^{-1} and each spectrum was an average of ten scans with a resolution of 4 cm^{-1}.

2.5. Differential scanning calorimetry (DSC)

In order to determine the glass transition temperature (T_g), DSC curves of coating systems that were laboratory ambient dried/cured and those dried/cured by IR were measured before and after exposure. The measurements were carried out on Mettler Toledo DSC 823 instrument in accordance with EN ISO 11357. The scanning rate was 20 °C/min and the temperature ranged from 0 to 90 °C in two heating cycles. The experiments were done under a nitrogen atmosphere with a constant flow of nitrogen equal to 60 mL/min. All samples (10 mg ± 3 mg) were weighed and sealed in a hermetic aluminium pan with lids.

2.6. Pull off test

Adhesion of coating systems that were laboratory ambient dried/cured and those dried/cured by IR was tested after exposure according to ISO 12944-6 with the Elcometer 108 pull off tester. Separation occurs with tensile stress necessary to break the weakest part of the system, either at the interface (adhesive failure) or within the layer (cohesive failure). Mixed failures may also occur. The operating range of the used device is 0–25 MPa.

3. Results and discussion

3.1. IR accelerated Drying/curing and the low-frequency EIS behaviour

It is well known that EIS is highly sensitive to alteration of coating barrier properties and it can detect initiation of coating failure long before visible damage has become apparent [11,12,35]. Kendig [49] states that EIS is best suited for evaluating the deviation from purely capacitive behaviour of organic coatings on steel which is, alongside the drop in the pore resistance, the main phenomenon observed at early stages of coating failure. However, the coating resistance of high-performance coatings may retain high during the first stage or even after several months of exposure [50]. For very efficient barrier coatings, detection of the second time constant at low frequencies is difficult [3,9]. The widely accepted breakpoint frequency method, based on the analysis of the frequency at the phase angle of -45°, cannot be applied as the phase angle of the intact or high-performance coating in the early stages never reaches this value [1,51].

The first derivative of the impedance modulus has previously been suggested as the means to resolve better the low-frequency behaviour of

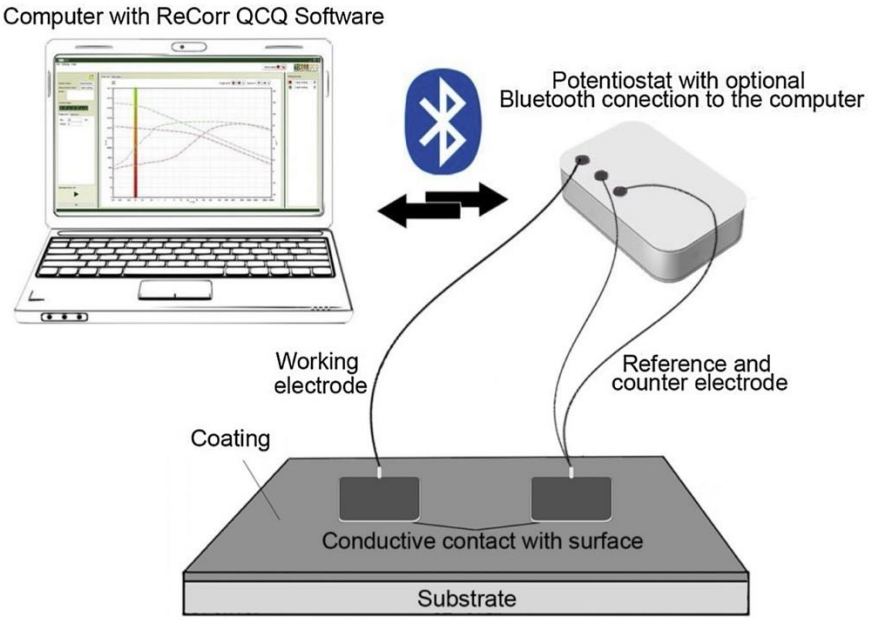

(a)

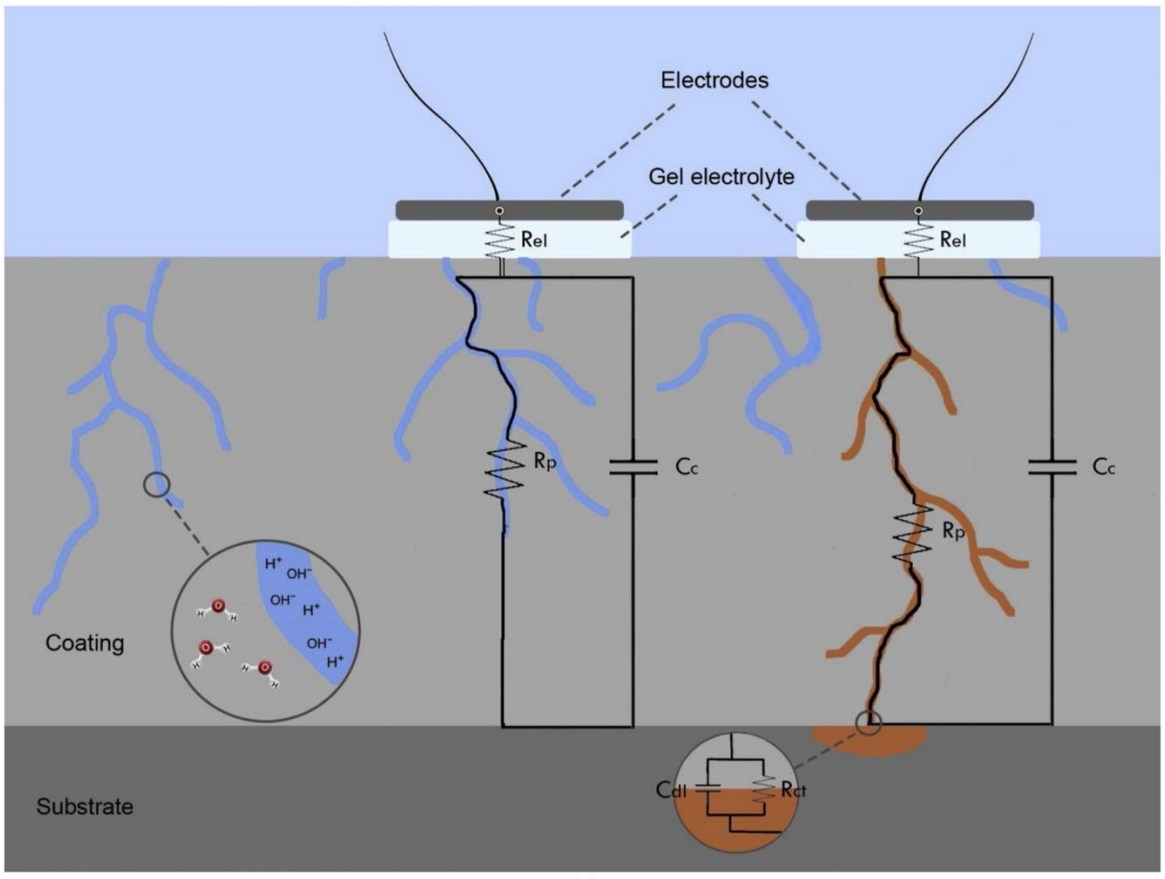

(b)

Fig. 1. Schematic view of the: (a) new EIS experimental setup, (b) EIS equivalent circuits of the measured system.

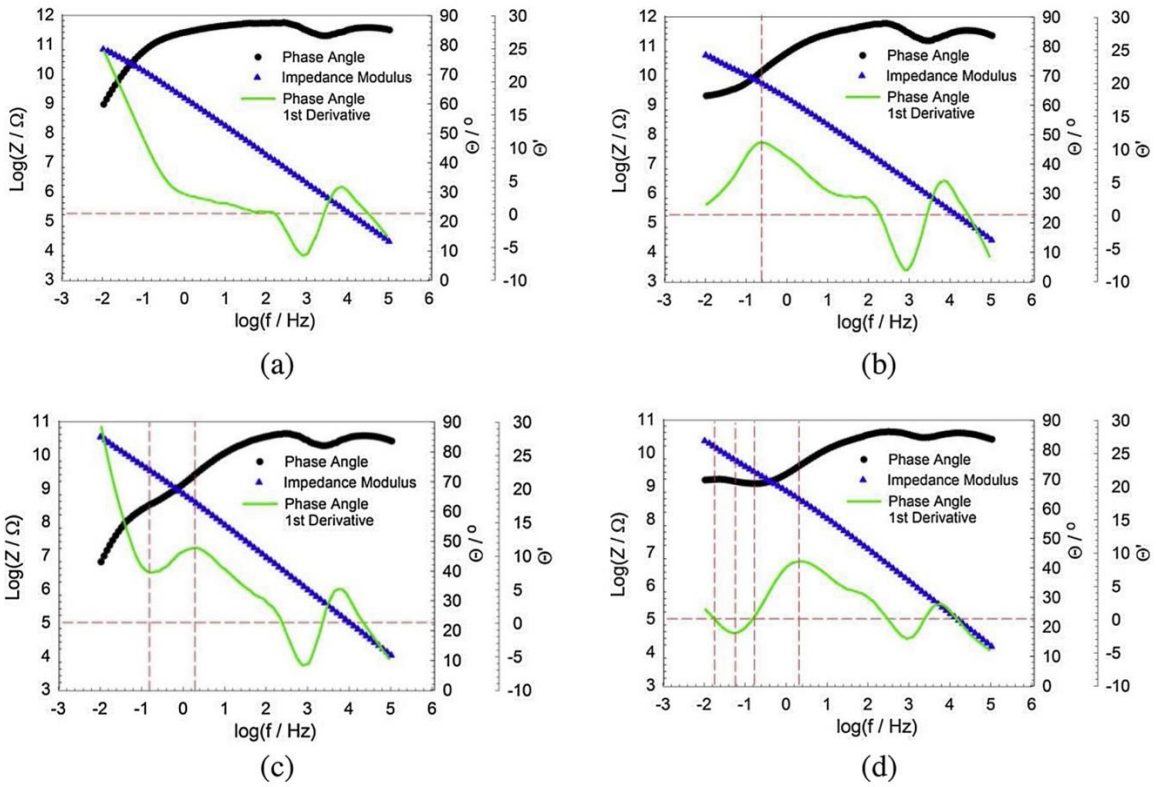

Fig. 2. Four typical EIS responses in Bode representation along with the first derivatives of the phase angle.

the coatings reflecting the processes at the interface between the coating and the metal [40,43,52–56]. In the present study we suggest the use of the first derivative of the phase angle as a sensitive tool to detect the influence of the corrosion related low frequency RC circle appearance on the coating performance in the early stages of exposure. Fig. 2 shows four typical EIS responses in Bode representation along with the first derivatives of the phase angle. The maxima and minima of the first derivative correspond to the inflexion points of the phase angle and the zeroes of the first derivative denote maxima and minima of the phase angle. The frequency below 1 Hz is analysed to exclusively account for the corrosion phenomenon [2]. The coating state rating system applied is based on the following observations:

- The highest rating denoted by A is assigned to the first derivative curve in Fig. 2 (a) that shows no minima or maxima. This corresponds to the coating with predominantly capacitive behaviour ($\theta > 80°$) in a wide frequency range (down to approximately 10^{-1} Hz) indicating that the coating is a good dielectric.
- The second highest rating B is assigned to the first derivative curve in Fig. 2 (b) that shows a single maximum corresponding to the phase angle inflexion point signifying the change from concave to convex phase angle shape. The capacitance-like behaviour is shifted to higher frequencies (above 10^{0} Hz) indicating a decline of the dielectric coating property.
- The third highest rating C is assigned to the first derivative curve in Fig. 2 (c) that shows one maximum and one minimum corresponding to the onsets of the convex and concave shape of the phase angle curve, respectively, with no minima and maxima. The concave shape at lower frequencies may unequivocally be ascribed to the appearance of the second time constant corresponding to the substrate corrosion process [7,9,11]. The capacitance-like behaviour of the coating is shifted to even higher frequencies (above 10^{1} Hz) indicating a further decline of the dielectric coating property.
- The worse rating D is assigned to the first derivative curve in Fig. 2 (d) that shows two zeros, a minimum and a maximum, indicating fully convex and concave shapes of the phase angle, respectively. The better resolution of the two time constants could be interpreted as an increase in the delaminated coating area at the coating substrate interface [7,9,11]. The capacitance-like coating behaviour region remained unchanged with respect to C rated coating.

Fig. 3 (a) and (b) show EIS coating rating based on the shape of the low frequency phase angle and the impedance modulus at 0.1 Hz. It is apparent from Fig. 3 (a) that various coatings are differently rated based on the low-frequency phase angle appearance. All the coatings before exposure, except the EP + EP system, are A rated meaning that initially there is no indication of corrosion within the coating pores and below the coatings.

All the EP + EP based samples, laboratory ambient or IR dried/cured are D rated in the final state. All the other samples are either B or C rated and show a better rating in the case of IR drying/curing. The EP + EP IR based samples are somewhat better rated if the impedance modulus at 0.1 Hz shown in Fig. 3 (b) is analysed. The overall trend for the other coatings is similar to the one deduced from the low-frequency segments of the Bode plots.

However, it should be noted that the first rating primarily reflects the increasingly pronounced low-frequency RC circle due to substrate corrosion while the second rating refers to the drop of the overall ohmic resistance of the system, both phenomena occurring with coating deterioration.

Unexposed three-layer system EP + EP + PUR, has higher impedance than the two-layer EP + EP system, while the IR cured samples show various impedances that are on average also lower for the EP + EP system. The conclusion is that IR drying/curing either retains the barrier properties of the laboratory ambient dried/cured coatings or even improves them.

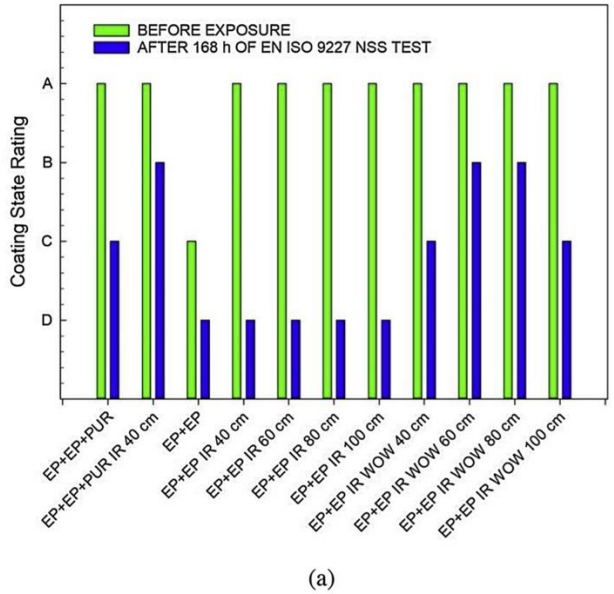

(a)

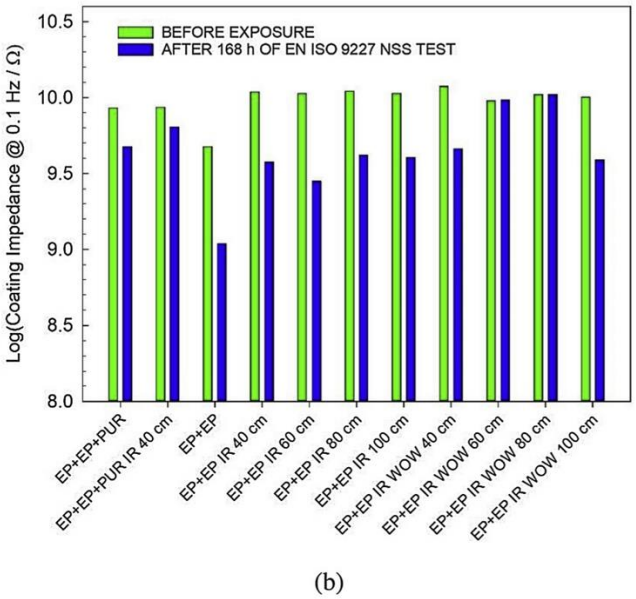

(b)

Fig. 3. EIS coating rating based on the (a) shape of the low frequency phase angle and (b) impedance modulus at 0.1 Hz before and after exposure of 168 h to NSS and subsequent drying/curing on air under laboratory ambient conditions for 60 days.

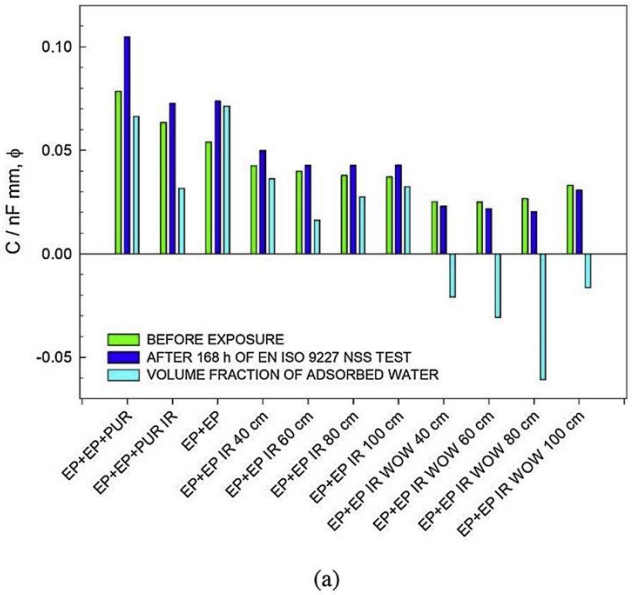

(a)

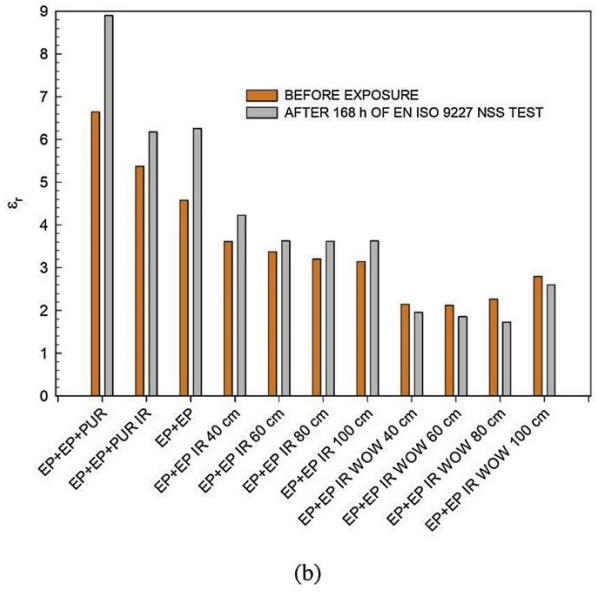

(b)

Fig. 4. (a) reduced capacitances and (b) dielectric constants of the coatings before and after exposure of 168 h to NSS and subsequent drying/curing on air under laboratory ambient conditions for 60 days.

3.2. IR accelerated Drying/curing, coating dielectric properties and water uptake

Fig. 4 (a) shows the capacitance of the coatings normalized by the coating thickness. The capacitances were determined at the frequency of $10^{4.6}$ that has been identified as optimal for all systems with respect to the requirement of impedance modulus Z having a slope of -1 due to the purely capacitive behaviour of the coating. In that case, the coating capacitance may be calculated from the equation, $Z = -1/\omega C$ [11,13]. For all coatings the normalized capacitances are of the order of 10 pF mm.

The coating characteristics prior to and after the exposure were compared.

For all the coating systems, except for the EP + EP + WOW system, the capacitance is higher after the exposure to NSS due to the electrolyte uptake. The Brasher and Kingsbury [57] equation:

$$\phi = \log\frac{C_t}{C_0} / \log\varepsilon_e$$

is used for calculating a fraction of electrolyte, φ, absorbed by the coating, where C_0 is the capacitance prior to absorption, C_t is the capacitance after the absorption and ε_e is the dielectric constant of the electrolyte within the coating. It is often argued that coating capacitance is very sensitive to water uptake since the dielectric constant of water equal to 80 is much higher than the dielectric constant of the coating [1,13].

For the purpose of easy comparison with the results of similar studies, the water uptake in the present study was calculated with $\varepsilon_e = 80$. The water volume fractions in Fig. 4 (a) show no particular pattern among the samples of the same kind but it is clearly visible that the IR cured samples have smaller water uptake than the samples cured at laboratory ambient conditions and that the wet-on-wet applied coatings show negative water uptake.

The unit surface area capacitance is related to the relative dielectric constant ε_r, vacuum dielectric constant ε_0 and thickness d of the coating and is given by the equation [6]:

$$c = \frac{\varepsilon_0 \varepsilon_r}{d} \quad (2)$$

The increase in d, which would lead to decrease in c has been excluded from further discussion in the present study as it would have to cause a measurable increase in the coating thickness that has not been observed. The coating relative dielectric constants have therefore been calculated assuming constant d. The dielectric constants shown in Fig. 4 (b) are between 3 and 9 which is in concordance with the literature data [58]. The dielectric constants vary among the samples of the same kind showing no particular pattern but are by approximately 10, 15 and 30% lower for the EP + EP + PU, EP + EP and EP + EP IR WOW dried/cured samples with respect to the reference samples, respectively.

Besides from the loss of water from the coating, the decrease in the coating capacitance and therefore of the apparent dielectric constant may be due to (i) accumulation of water within the delaminated area at the coating/metal interface [59], (ii) leaching of polar substances from the coating [60] (iii) ingress of electrolyte ions into the coating [61,62] and (iv) reduced water dielectric constant [63].

The accumulation of water at the coating/metal interface has been eliminated as a cause of capacitance decrease based on the pull off adhesion results given in chapter 3.4. Typically, complete loss of adhesion is observed in the case of coating/metal interface water accumulation that is not the case in the present study [59].

Leaching effect has been observed for marine epoxy coatings during immersion in NaCl solution [60]. Leaching is attributed to the dissolution of ionic soluble species from the polymers that are being replaced by the Na^+ and Cl^- ions from the solution. Leaching causes polymer density loss and a decrease of the polymer specimen mass after the immersion experiments when the effect of leaching overpowers the effect of water uptake. However, the decrease of coating capacitance leading to apparently negative water uptake has not been obtained previously. It was assumed that the mass loss phenomenon detected by gravimetric measurements involved low dielectric constant species in small quantities, therefore, their leaching not affecting the coating capacitance.

Krauklis [64] reports leaching of unreacted bisphenol A or epichlorohydrin due to the diffusion gradient of epichlorohydrin between the resin and its environment. Epichlorohydrin has a dielectric constant equal to 20.8 at 21.5 °C which is relatively high for an organic substance but cannot readily be accounted for the decrease of the EP + EP IR WOW coating capacitance after exposure.

A lower dielectric constant of about 60 can be assumed for the water within the polymer if the Na^+ and Cl^- ions are also present [61]. Na^+ and Cl^- ions within the coating originate from the percolation of water and the diffusion of ions into the coating, although the concentration may not be exactly equal to that of the electrolyte from the surroundings [62]. Also, Woo et al [63] found that water within the polymer does not behave as free water and that decrease of the effective dielectric constant of water is about 55–77% in the case of water clustering.

It is apparent that the effect of ionic ingress and water clustering could account for a significant decrease in the coating capacitance. It is, however, hard to speculate about the exact dielectric constant of the electrolyte within the coating and the Brasher and Kingsbury that assumes only the consequences of the high dielectric constant electrolyte ingress, is not likely to give the correct volume of the absorbed water.

To further elucidate the water uptake effect, FTIR measurements have been done and the representative curves of the EP + EP IR and EP + EP IR WOW epoxy systems before and after exposure are shown in Fig. 5 (a) and (b). The spectra were normalized to the peak at 1509 cm^{-1} in order to avoid the influence of the contact area size

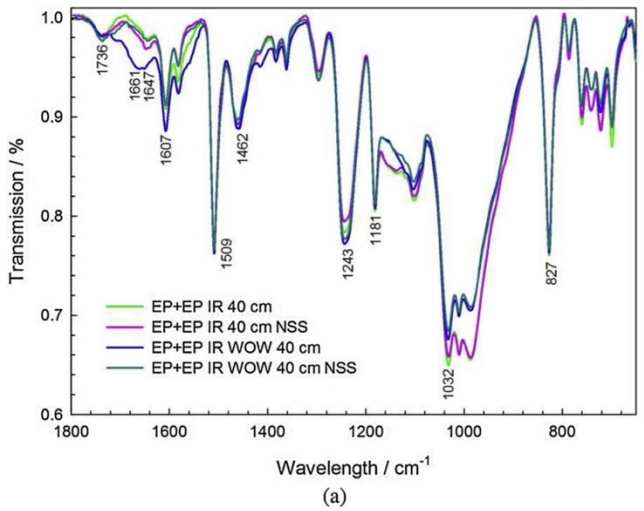

Fig. 5. Representative ATR-FTIR spectra of EP + EP IR and EP + EP IR WOW systems before and after exposure of the 168 h to NSS and subsequent drying in under laboratory ambient conditions for 60 days.

during ATR-FTIR measurements. Amine cured bisphenol A epoxy resin can be identified from the peaks around 827, 1032, 1181, 1243, 1462, 1509, 1607, 1647, 2852, 2925 and 3337 cm^{-1} [65]. The most prominent changes are in FTIR spectra are visible in the 1650-1590 cm^{-1} range that corresponds to water O—H bending in a liquid state and at ≈ 3300 cm^{-1} due to O—H stretching of water forming hydrogen bonds with the polymer [66]. The additional shoulder is observed for the EP + EP WOW sample at 3203 cm^{-1}. The band corresponds to the OH stretch of highly-orientated, multiple hydrogen-bonded species, corresponding to clustered water [67]. Weak bands of O—H stretching of water in a liquid state at 3800-3600 cm^{-1} are also observed. It appears that the water within the polymer is mostly bound by hydrogen bonds. Indeed, by observing the intensity of the band ≈ 3300 cm^{-1} more water is observed for the EP + EP IR WOW before then after the exposure. This explains the negative water uptake calculated from EIS coating capacitances. Contrarily, for the EP + EP IR system, the sample after exposure has more absorbed water than prior to exposure confirming positive water uptake.

However, according to ATR-FTIR, the EP + EP IR WOW system has more water absorbed than the EP + EP IR system, but this water appears to be more tightly hydrogen-bonded leading to overall lower relative dielectric constant and capacitance of the EP + EP IR WOW

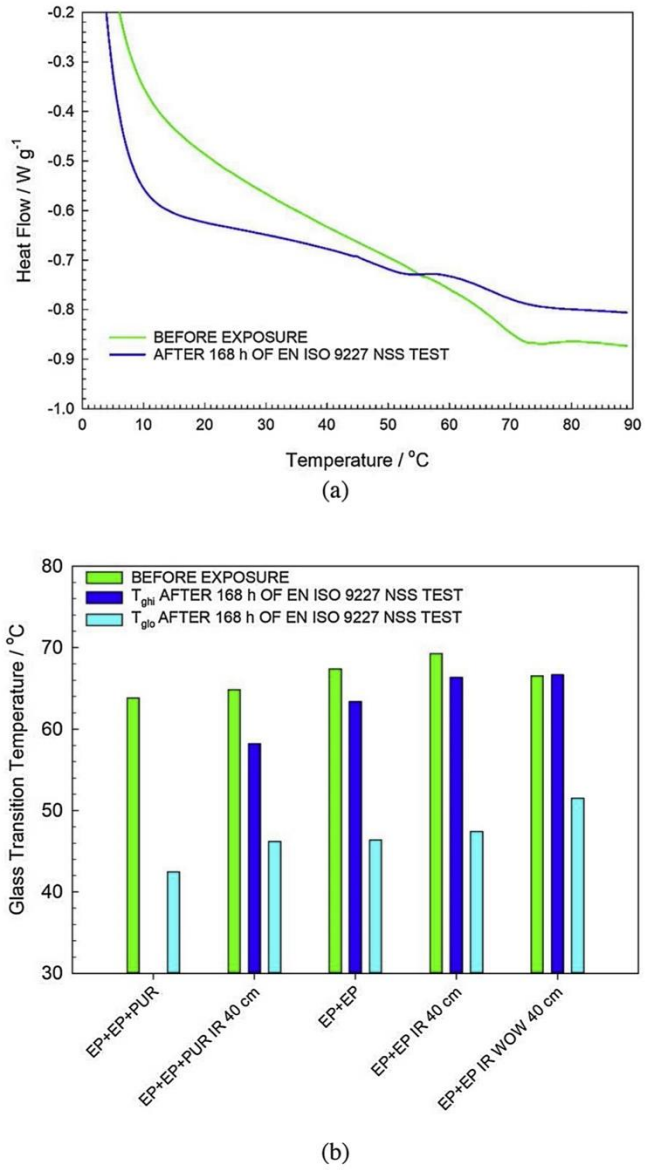

Fig. 6. Representative (a) DSC curves and (b) glass transition temperatures of the investigated coating systems before and after the exposure of the 168 h to NSS and subsequent drying/curing on air under laboratory ambient conditions for 60 days.

system. Water uptake is further discussed based on DSC measurements.

3.3. IR accelerated Drying/curing and glass transition temperature

Fig. 6 (a) shows a typical shape of DSC heating curves obtained for the intact coatings and for the coatings after exposure. All the coatings before exposure and only the EP + EP + PU system after exposure show one T_g. All the other systems after exposure show two T_g values denoted as T_{glo} and T_{ghi}.

The decrease in T_g as a consequence of exposure, shown in Fig. 6 (b), is consistent with the literature mentions of T_g drop of about 20 °C [68,69] or down to one half of the original value [59]. The phenomenon is ascribed to the plasticization effect of water. Water is considered to occupy the free volume of the coating and/or to infiltrate the polymer structure. Water molecules can form single hydrogen bonds or multiple hydrogen bonds with the polymer network. Plasticization effect is attained when single hydrogen bonds that increase the chain flexibility are formed in the low cross-linking zones. Hence, the water contained in the apparent free volume of these low cross-linking zones is associated with the depression of T_g [70]. Water entering high cross-linking zones is likely to form multiple hydrogen bonds and induce secondary cross-linking, hardening of the polymer and increase in T_g [59].

Initially, only one T_g value denoted as T_{g0} is observed which would implicate homogeneity of the coating [70]. The appearance of two glass transition temperatures after the exposure indicates heterogeneous solution distribution in the coating [59].

Fig. 6 (b) shows similar T_g values among specimen of each of the coating systems, EP + EP + PUR and EP + EP, almost within the standard uncertainty for T_g of about 3 °C. In the case of the EP + EP + PUR system dried/cured under laboratory ambient conditions, the lowest T_{g0} before the exposure and a single T_{glo} after the exposure implicates homogeneous coating of the lowest cross-linking density. Interestingly, T_{ghi} is slightly higher than T_{g0} for the EP + EP IR WOW system that could indicate that one of the phases is highly cross-linked and supports single hydrogen bonds while the second phase is highly cross-linked and supports secondary cross-linking trough formation of multiple hydrogen bonds. The other coatings would within the same interpretation contain two phases after exposure, one of smaller and one of larger free volume.

Due to the complexity of the system, a very general correlation can be found between the Tg and the EIS water absorption data. Both, the trend of *Tg* increase and EIS capacitance decrease in the order EP + EP + PUR > EP + EP > EP + EP WOW indicate also the trend of adsorbed water decrease.

Heterogeneous solution distribution of electrolyte in the coating causes long-range internal stresses and alters the mechanical properties of the coating. In particular, upon drying, the free volume will probably relax internal stresses but a cross-linked network being more restrained with respect to internal motion may not be able to relax completely [26]. In the present study, the mechanical properties of the well-adhered coatings are revealed through the pull-off adhesion test.

3.4. IR accelerated Drying/curing and coating pull-off strength

Fig. 7 shows pull-off strength after exposure. Fig. 8 depicts the representative appearance of the pull-off circles after exposure. The EP + EP + PU system shows a cohesion type failure between the

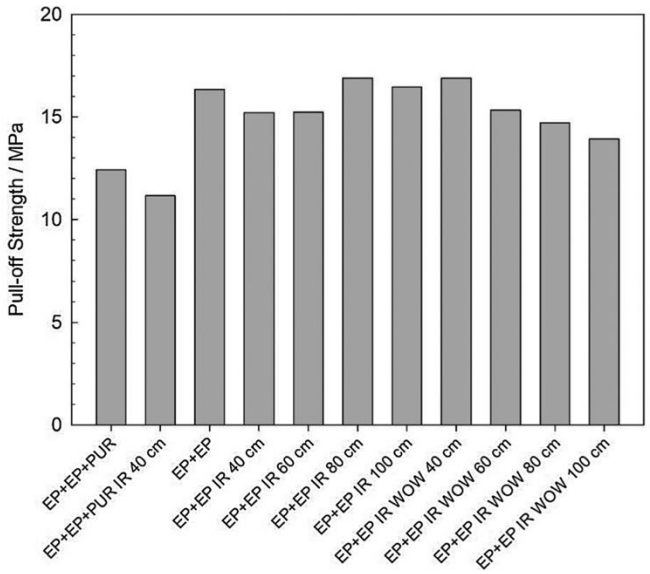

Fig. 7. Pull –off adhesion/cohesion strength after the exposure of 168 h to NSS and subsequent drying/curing on air under laboratory ambient conditions for 60 days.

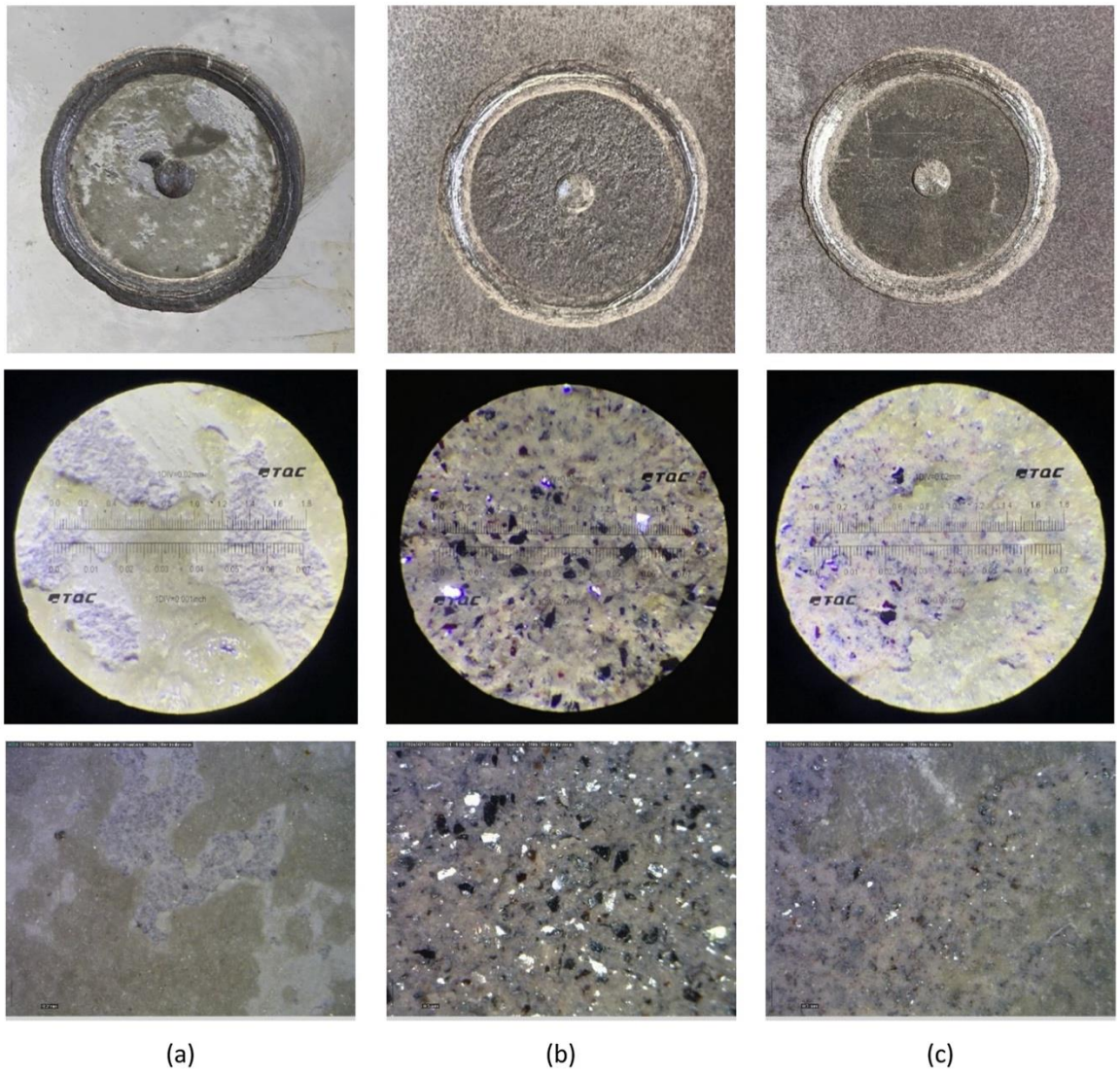

Fig. 8. Representative appearance of the pull –off circles for (a) EP + EP + PU system, (b) EP + EP system and (c) EP + EP IR WOW system, without magnification and magnified 50 and 200 × .

topcoat and the intermediate coat which along with the high strength shows that adhesion between coating and steel is outstanding [71]. For the EP + EP and EP + EP IR WOW systems, the cohesive failure protrudes throughout the entire thickness and at micro locations reaches the substrate indicating a minute amount of adhesion type failure. The cohesion type failure is more pronounced for the EP + EP system. These results may be compared to Fig. 2 which predominantly reflects the influence of the corrosion at the base of the coating pores that could account for the observed cohesion/adhesion behaviour.

On average, the cohesion strength value is lower by about 2.5% for the EP + EP IR systems and by about 7.5% for the EP + EP IR WOW systems with respect to the referent EP + EP system. For the EP + EP + PUR IR system, the value of cohesion strength is lower by 10% with respect to the referent EP + EP + PUR system.

4. Conclusions

In the present study, we have used a custom made EIS electrochemical setup with two flexible gel electrodes that enabled capturing of the coating electrical properties without the influence of the cell electrolyte on the measurements. This allowed us to detect distinctive barrier and dielectric properties of the laboratory ambient and IR dried/cured samples before and after short, one-week NSS exposure according to EN ISO 9227 standard.

The conclusions of the EIS analysis are that the IR drying/curing improves barrier properties of common industrial coatings with respect to the laboratory ambient dried/cured referent systems, or at least introduces no harmful influence. Samples of each system positioned at increasing distances from the IR source that were dried/cured for a proportionally longer time, show similar behaviour, characteristic of the system tested. However, a clear distinction is observed between the laboratory ambient and IR dried/cured coatings, the latter being characterized by the higher impedance moduli, lower capacitances and lower dielectric constants.

FTIR and DSC, that primarily reflect the effect of the IR drying/curing and the water uptake on the coating polymer structure show no indications of permanent coating degradation induced by accelerated drying/curing or short-term weathering.

Pull-off strength shows a slightly negative influence of the IR accelerated drying/curing process on the coating adhesion/cohesion characteristics.

It has been demonstrated that EIS may be used for reaching a quick, informed decision on a coating practice alteration that may speed up the production process.

Declaration

The raw/processed data required to reproduce these findings cannot be shared at this time as the data also forms part of an ongoing study.

References

[1] F. Mansfeld, Use of electrochemical impedance spectroscopy for the study of corrosion protection by polymer coatings, J. Appl. Electrochem. 25 (3) (1995) 187–202.
[2] F. Mansfeld, M.W. Kendig, S. Tsai, Evaluation of corrosion behavior of coated metals with ac impedance measurements, Corrosion 38 (9) (1982) 478–485.
[3] F. Mansfeld, S.L. Jeanjaquet, M.W. Kendig, An electrochemical impedance spectroscopy study of reactions at the metal/coating interface, Corros. Sci. 26 (9) (1986) 735–742.
[4] J.R. Scully, Electrochemical impedance of organic coated steel: correlation of impedance parameters with long-term coating deterioration, J. Electrochem. Soc. 136 (4) (1989) 979–989.
[5] F. Mansfeld, Electrochemical Impedance Spectroscopy (EIS) as a new tool for investigating methods of corrosion protection, Electrochim. Acta 35 (10) (1990) 1533–1544.
[6] M. Kendig, J. Scully, Basic aspects of electrochemical impedance application for the life prediction of organic coatings on metals, Corrosion 46 (1) (1990) 22–29.
[7] J. Titz, G.H. Wagner, H. Spáhn, M. Ebert, K. Jüttner, W.J. Lorenz, Characterization of organic coatings on metal substrates by electrochemical impedance spectroscopy, Corrosion 46 (3) (1990) 221–229.
[8] H.P. Hack, J.R. Scully, Defect area determination of organic coated steels in seawater using the breakpoint frequency method, J. Electrochem. Soc. 138 (1) (1991) 33–40.
[9] F. Mansfeld, C.H. Tsai, Determination of coating deterioration with EIS I. Basic relationships, Corrosion 47 (12) (1991) 958–963.
[10] P.L. Bonora, F. Deflorian, L. Fedrizzi, Electrochemical impedance spectroscopy as a tool for investigating underpaint corrosion, Electrochim. Acta 41 (l/8) (1996) 1073–1082.
[11] J.M. McIntyre, H.Q. Pham, Electrochemical impedance spectroscopy; A coatings optimizations, Prog. Org. Coat. 27 (1-4) (1996) 201–207.
[12] J.N. Murray, H.P. Hack, Long-term testing of epoxy-coated steel in ASTM seawater using electrochemical impedance spectroscopy, Corrosion 47 (6) (1991) 480–489.
[13] F. Mansfeld, M.W. Kendig, Electrochemical impedance spectroscopy of protective coatings, Werkst. Und Korrosion 36 (11) (1985) 473–483.
[14] R.E. Touhsaent, H. Leidheiser, A capacitance-resistance study of polybutadiene coatings on steel, Corrosion 28 (12) (1972) 435–440.
[15] J.R. Scully, S.T. Hensley, Lifetime prediction for organic coatings on steel and a magnesium, alloy using electrochemical impedance methods, Corros. Sci. 50 (9) (1994) 705–716.
[16] C.H. Tsai, F. Mansfeld, Determination of coating deterioration with EIS: part II. Development of a method for field testing of protective coatings, Corros. Sci. 49 (9) (1993) 726–737.
[17] G. Bierwagen, D. Tallman, J. Li, L. Hea, C. Jeffcoate, EIS studies of coated metals in accelerated exposure, Prog. Org. Coat. 46 (2) (2003) 148–157.
[18] F.L. Floyd, S. Avudaiappan, J. Gibsonb, B. Mehta, P. Smith, T. Provder, J. Escarsega, Using electrochemical impedance spectroscopy to predict the corrosion resistance of unexposed coated metal panels, Prog. Org. Coat. 66 (1) (2009) 8–34.
[19] F.X. Perrin, C. Merlatti, E. Aragon, A. Margaillan, Degradation study of polymer coating: improvement in coating weatherability testing and coating failure prediction, Prog. Org. Coat. 64 (4) (2009) 466–473.
[20] S. Shreepathi, A.K. Guin, S.M. Naik, M.R. Vattipalli, Service life prediction of organic coatings: electrochemical impedance spectroscopy vs actual service life, J. Coat. Technol. Res. 8 (2) (2011) 191–200.
[21] F.E. Bedoya, Á. Bermúdez, J.G. Castaño, F. Echeverría, J.A. Calderón, Electrochemical impedance study for modeling the anticorrosive performance of coatings based on accelerated tests and outdoor exposures, J. Coat. Technol. Res. 13 (5) (2016) 895–904.
[22] W. Tian, F. Meng, L. Liu, Y. Li, F. Wang, Lifetime prediction for organic coating under alternating hydrostatic pressure by artificial neural network, Sci. Rep. 7 (40827) (2017) 1–12.
[23] J. Ran, Y. Xu, Y. Tong, The EIS-based Kohonen neural network for high strength steel coating degradation assessment, J. Chemom. 31 (11) (2017) 1–15.
[24] Z. Chen, C. He, F. Yu, Y. Wang, Study and application of electrochemical impedance spectroscopy for quickly evaluating the performance of coatings and predicting the failure time in the development of waterborne epoxy micaceous iron oxide coatings, Int. J. Electrochem. Sci. 12 (4) (2017) 2798–2812.
[25] D.P. Allerton, I.T. Greszler, B.S. Skerry, Testing of coatings for offshore service, NACE-2018-10886, Corrosion (2018) 1–8.
[26] S.G. Croll, Electrolyte transport in polymer barrier coatings: perspectives from other disciplines, Prog. Org. Coat. 124 (2018) 41–48.
[27] E. Cano, D. Lafuente, D.M. Bastidas, Use of EIS for the evaluation of the protective properties of coatings for metallic cultural heritage: a Review, J. Solid State Electrochem. 14 (3) (2010) 381–391.
[28] S. Corbellini, M. Parvis, S. Grassini, Noninvasive solution for electrochemical impedance spectroscopy on metallic works of art, IEEE Trans. Instrum. Meas. 61 (5) (2012) 1193–1200.
[29] B. Ramírez Barat, E. Cano, In situ electrochemical impedance spectroscopy measurements and their interpretation for the diagnostic of metallic cultural heritage: a review, ChemElectroChem 5 (19) (2018) 2698–2716.
[30] L.A. Ellingson, T.J. Shedlosky, G.P. Bierwagen, E.R. de la Rie, L.B. Brostoff, The use of electrochemical impedance spectroscopy in the evaluation of coatings for outdoor bronze, Stud. Conserv. 49 (1) (2004) 53–62.
[31] A.H. England, K.N. Hosbein, C.A. Price, M.K. Wylder, K.S. Miller, T.L. Clare, Assessing the protective quality of wax coatings on bronze sculptures using hydrogel patches in impedance measurements, Coatings 6 (45) (2016) 1–13.
[32] B. Ramírez Barat, E. Cano, P. Letardi, Advances in the design of a gel-cell electrochemical sensor for corrosion measurements on metallic cultural heritage, Sens. Actuators B Chem. 261 (2018) 572–580.
[33] E. Angelini, D. Assante, S. Grassini, M. Parvis, In-situ electrochemical impedance spectroscopy measurements on immovable cultural heritage, Recent Res. Applied Eco Manage.- Volume II (2013) 223–227.
[34] E. Angelini, S. Grassini, M. Parvis, F. Zucchi, An in situ investigation of the corrosion behaviour of a weathering steel work of art, Surf. Interface Anal. 44 (8) (2012) 942–946.
[35] A.H. England, T.L. Clare, Synthesis and characterization of flexible hydrogel electrodes for electrochemical impedance measurements of protective coatings on metal sculptures, Electroanalysis 26 (5) (2014) 1059–1067.
[36] S. Corbellini, M. Parvis, S. Grassini, Development and characterization of flexible electrodes for protective painting monitoring, 2011 IEEE International Instrumentation and Measurement Technology Conference (2011) 1–6.
[37] S. Grassini, Electrochemical impedance spectroscopy (EIS) for the in-situ analysis of metallic heritage artefacts, European Federation of Corrosion (EFC) Series 2013, Woodhead Publishing Limited, 2013, pp. 347–367.
[38] S. Grassini, S. Corbellini, M. Parvis, E. Angelini, F. Zucchi, A simple arduino-based eis system for in situ corrosion monitoring of metallic works of art, Measurement 114 (2018) 508–514.
[39] Y.T. Kuo, C.Y. Lee, Y.L. Lee, Compact coating impedance detector for fast evaluation of coating degradation, Measurement 124 (2018) 303–308.
[40] K.N. Hosbein, The Application of Electrochemical Impedance Spectroscopy to Immediately Diagnose the Protective Quality of Coatings on Artistic and Architectural Metalwork (Master's Thesis), Portland State University, 2016 (accessed 15 February 2019), https://pdfs.semanticscholar.org/e995/579a6a9bb7da573a46aad7ca141e2ab854cb.pdf.
[41] S. Haruyama, M. Asari, T. Tsuru, Impedance characteristics during degradation of coated steel, Proc. Symposium Corrosion Protection Organic Coatings Electrochemical Soc. 87 (2) (1987) 197.
[42] M. Mahdavian, M.M. Attar, Another approach in analysis of paint coatings with EIS measurement: phase angle at high frequencies, Corros. Sci. 48 (12) (2006) 4152–4157.
[43] E. Akbarinezhad, H.R. Faridi, Different approaches in evaluating organic paint coatings with electrochemical impedance spectroscopy, Surf. Eng. 24 (4) (2008) 280–286.
[44] E. Akbarinezhad, M. Bahremandi, H.R. Faridi, F. Rezaei, Another approach for ranking and evaluating organic paint coatings via electrochemical impedance spectroscopy, Corros. Sci. 51 (2) (2009) 356–363.
[45] A. Xu, F. Zhang, F. Jin, R. Zhang, B. Luo, T. Zhang, The evaluation of coating performance by analyzing the intersection of bode plots, Int. J. Electrochem. Sci. 9 (9) (2014) 5116–5125.
[46] A. Razin, B. Ramezanzadeh, H. Yaria, Detecting and estimating the extent of automotive coating delamination and damage indexes after stone chipping using electrochemical impedance spectroscopy, Prog. Org. Coat. 92 (2016) 95–109.
[47] A.S. Mujumdar, Handbook of Industrial Drying, fourth ed., Taylor & Francis Group, LLC, Boca Raton, 2015.
[48] H.J. Streitberger, K.F. Dössel, Automotive Paints and Coatings, second ed., Wiley-VCH, Weinheim, 2008.
[49] M. Kendig, J. Scully, Basic aspects of electrochemical impedance application for the life prediction of organic coatings on metals, Corros. Sci. 46 (1) (1990) 22–29.
[50] M. Del Grosso Destreria, J. Vogelsangb, L. Fedrizzi, F. Deflorian, Water up-take evaluation of new waterborne and high solid epoxy coatings. Part II: electrochemical impedance spectroscopy, Prog. Org. Coat. 37 (1999) 69–81.
[51] J.A. Calderón-Gutierrez, F.E. Bedoya-Lora, Barrier property determination and lifetime prediction by electrochemical impedance spectroscopy of a high performance organic coating, Dyna 81 (183) (2014) 97–106.
[52] X. Zhao, J. Wang, Y. Wang, T. Kong, L. Zhong, W. Zhang, Analysis of deterioration process of organic protective coating using EIS assisted by SOM network, Electrochem. commun. 9 (6) (2007) 1394–1399.
[53] L. Bing, A. Xu, Y. Liang, Z. Huang, Z. Qiao, D. Xia, S. Zhang, Z. Li, F. Zhang, P. Chen, Evaluation on protective performance of organic coatings by analyzing the change rate of phase angle at high frequency, Int. J. Electrochem. Sci. 7 (9) (2012) 8859–8868.
[54] A. Xu, F. Zhang, B. Luo, F. Jin, T. Zhang, Investigation the deterioration process of organic coating using changing rate of phase angle at high frequency united to neural network, Int. J. Electrochem. Sci. 8 (1) (2013) 773–779.
[55] X. Zhao, J. Wang, W. Li, B. Hou, Research on coating deterioration process under fully immersing condition by using multi-parameters, Mater. Corros. 62 (5) (2011) 431–435.
[56] X. Dahai, S. Shizhe, W. Jihui, B. Huichao, H. Zhewen, Fast evaluation of degradation degree of organic coatings by analyzing electrochemical impedance spectroscopy data, Trans. Tianjin Univ. 18 (1) (2012) 15–20.
[57] D.M. Brasher, A.H. Kingsbury, Electrical measurements in the study of immersed paint coatings on metal. I. Comparison between capacitance and gravimetric methods of estimating water uptake, J. Appl. Chem. 4 (2) (1954) 62–72.
[58] A.S. Castela, A.M. Simões, Assessment of water uptake in coil coatings by capacitance measurements, Prog. Org. Coat. 46 (2003) 55–61.

[59] F. Deflorian, L. Fedrizzi, S. Rossi, P.L. Bonora, Organic coating capacitance measurement by EIS: ideal and actual trends, Electrochim. Acta 44 (24) (1999) 4243–4249.
[60] N. Fredj, S. Cohendoz, X. Feaugas, S. Touzain, Some consequences of saline solution immersion on mechanical behavior of two marine epoxy-based coatings, Prog. Org. Coat. 69 (2010) 82–91.
[61] J.M. Mollerup, M.P. Breil, Modeling the permittivity of electrolyte solutions, Aiche J. 61 (9) (2015) 2854–2860.
[62] Q. Zhou, Y. Wang, G.P. Bierwagen, Influence of the composition of working fluids on flow-accelerated organic coating degradation: deionized water versus electrolyte solution, Corros. Sci. 55 (2011) 97–106.
[63] M. Woo, M.R. Piggott, Water-absorption of Resin and Composites. 1. Epoxy Homopolymers and Copolymers, J. Compos. Technol. Res. 9 (3) (1987) 101–107.
[64] A.E. Krauklis, A.T. Echtermeyer, Mechanism of yellowing: carbonyl formation during hygrothermal aging in a common amine epoxy IR accelerated curing and adhesion, Polymers 10 (9) (2018) 1017.
[65] F. Delor-Jestin, D. Drouin, P.Y. Cheval, J. Lacoste, Thermal and photochemical ageing of epoxy resin-Influence of curing agents, Polym. Degrad. Stab. 91 (6) (2006) 1247–1255.
[66] M. González, J.C. Cabanelas, J. Baselga, Applications of FTIR on epoxy resins-identification, monitoring the curing process, phase separation and water uptake, in: T. Theophile (Ed.), Infrared Spectroscopy-Materials Science, Engineering and Technology, InTech, 2012, pp. 261–268.
[67] S. Morsch, S. Lyon, P. Greensmith, S.D. Smith, S.R. Gibbon, Mapping water uptake in organic coatings using AFM-IR, Faraday Discuss. 180 (2015) 527–542.
[68] J. Li, C.S. Jeffcoate, G.P. Bierwagen, D.J. Mills, D.E. Tallman, Thermal transition effects and electrochemical properties in organic coatings: part 1 — initial studies on corrosion protective organic coatings, Corrosion 54 (10) (1998) 763–771.
[69] F. Deflorian, S. Rossi, P.L. Bonora, L. Fedrizzi, Advanced testing procedures for high performance coatings, J. Coat. Technol. 72 (908) (2000) 81–87.
[70] M.Y.M. Chiang, M. Fernandez-Garcia, Relation of swelling and Tg depression to the apparent free volume of a particle-filled, epoxy-based adhesive, J. Appl. Polym. Sci. 87 (9) (2003) 1436–1444.
[71] W. Tian, F. Meng, L. Liu, Y. Li, F. Wang, The failure behaviour of a commercial highly pigmented epoxy coating under marine alternating hydrostatic pressure, Prog. Org. Coat. 82 (2015) 101–112.

APPENDIX II

S. Martinez, I. Šoić, V. Špada, Unified equivalent circuit of dielectric permittivity and porous coating formalisms for EIS probing of thick industrial grade coatings, Prog. Org. Coat. 153 (2021) 106155

https://doi.org/10.1016/j.porgcoat.2021.106155

Sanja Martinez: conceptualization, methodology, writing – original draft, writing - review & editing
Ivana Šoić: investigation, visualization, methodology
Vedrana Špada: resources, validation

Progress in Organic Coatings 153 (2021) 106155

Contents lists available at ScienceDirect

Progress in Organic Coatings

journal homepage: www.elsevier.com/locate/porgcoat

Unified equivalent circuit of dielectric permittivity and porous coating formalisms for EIS probing of thick industrial grade coatings

Sanja Martinez [a], Ivana Šoić [a,*], Vedrana Špada [b]

[a] Research Laboratory for Corrosion Engineering and Surface Protection – ReCorr, Department of Electrochemistry, Faculty of Chemical Engineering and Technology, University of Zagreb, Marulicev trg 19, 10000, Zagreb, Croatia
[b] Research Centre for Metal Industry in Istrian County - MET.R.IS, Zagrebačka 30, 52100, Pula, Croatia

ARTICLE INFO

Keywords:
Polymeric coatings
EIS
Dielectric permittivity
Dielectric loss
Wet adhesion

ABSTRACT

The equivalent circuit $R_e(Q_1[R_1(Q_2R_2)])$ was fitted to the impedance spectra of the two water based and the two solvent based industrial coating systems measured during long term exposure to 3.5 % NaCl. The initial states of the samples were the intact state and the salt cabinet aged state. The elements of $R_e(Q_1[R_1(Q_2R_2)])$ were ascribed physical meaning within the dielectric permittivity and EIS porous coating formalisms. A real capacitor behavior of a coating was simulated by a lossless capacitor in series with a resistance and the distributed time-constant behavior was simulated by a set of parallel circuits representing either space related or frequency related heterogeneity of the system. The equivalent circuit parameters and the impedance modulus at 0.1 Hz reflected various degrees of coatings sensitivity to environmental conditions that correlated with the harshness and length of exposure. The additional parameters suggested for rating of the coating barrier properties were $\tan[f_0]\delta$, equal to the resistive to capacitive current ratio, and its response to various cathodic offset potentials indicating the retention or loss of wet adhesion. The compromised barrier property of one of the water based coatings was deduced from a continuously decreasing low-frequency impedance and the appearance of the low frequency $\tan[f_0]\delta$ peak that increased upon cathodic polarization. These observations were linked to blistering, adhesion strength decrease, corrosion of the substrate revealed after the adhesion test, cratering defects at the coating surface and pronounced rust leaching at the sample edges and welds that were lacking the stripe coats.

1. Introduction

Quantitative coating quality assessment is of paramount importance for advancing the application and quality control of coatings that act as means of corrosion protection. Barrier action of organic coatings that provides high resistance to movement of water and ions is, alongside the coating adhesion, regarded a key to good coating performance [1,2]. Electrochemical Impedance Spectroscopy (EIS) is a method that yields an explicit quantitative result in the form of a coating impedance spectrum. The impedance spectrum is linked to a particular physical model, enabling explanation and rating of the coating response to the adverse environmental circumstances i.e. its barrier property [3]. Despite decades of research, that offer compelling evidence of EIS versatility and usefulness, the method has not gained a strong foothold in routine coating testing and field engineering practice [4].

Maturing of the EIS method towards practical engineering application includes intensive exploring of increasingly complex physical and equivalent circuit models [5–9] as well as significant instrumental improvements [10–14]. Recently, we have reported on an experimental setup schematically shown in ref. [15]. It is comprised of a high-end potentiostat/FRA, flexible conductive polymer electrodes and a wax-based conductive paste that enable simple and fast EIS measurements on coatings in the intact/dry state or during exposure to natural or artificial moist corrosive environments. A 1 TB input impedance, current resolution of 5 fA in the 100 pA range, the accuracy $\geq$ 99 % for impedances $\leq$ 10 GΩ and purely ohmic resistance of the electrode/conductive paste/coating contact equal to 150 Ω per 24 cm^2 of electrode area, are sufficient for high precision EIS measurements on thick industrial coatings, e.g. those defined in EN ISO 12944−5.

Paradoxically, high-performance EIS instruments introduce an additional ambiguity into the EIS spectrum interpretation, even amplifying the old controversies that have yet to be settled beyond doubt [16]. In particular, this refers to interpreting the early indicators of coating degradation, e.g. the low-frequency coating impedance modulus [3] and

* Corresponding author.
E-mail address: ivana.soic@fkit.hr (I. Šoić).

https://doi.org/10.1016/j.porgcoat.2021.106155
Received 9 October 2020; Received in revised form 8 January 2021; Accepted 18 January 2021
Available online 6 February 2021

the capacitive-resistive transition often embodied in the breakpoint frequency as an indicator of the coating delamination [17].

Extension of the EIS measurement ability into the teraohm range makes EIS sensitive to the intrinsic polymer response, i.e. the relaxation of polymer dipoles and the migration of polymer ionic impurities [18–20]. The polymer chain mobility and ionic space charge movement may be facilitated by the increase of the polymer water content at a constant temperature or by the increase of temperature at constant water content [21]. The absorbed water that eases the polymer chain movements trough plasticizing effect, may significantly enhance the coating dipolar relaxation response at high frequencies. At low frequencies, the coating response is enhanced by the hopping movement and/or propagation of ions along percolation paths that may extend over macroscopic distances [22,23]. Additionally, the low frequency coating response may be enhanced by the Maxwell–Wagner–Sillars (MWS) polarization [23–31] that is characteristic of composite or otherwise heterogeneous polymer systems. The inhomogeneity originates from internal interfaces between the polymer and other coating components (such as fillers or pigments) [24], the adhesion loss zones at the metal/polymer interface such as microblisters [25] and interfaces of various polymer defects with surface water [22] that may store mobile positive and negative ionic charge and may act as macrodipoles [19].

In conclusion, the polymer matrix dipole relaxations are responsible for the high-frequency coating response while the space charge movement is responsible for the low-frequency coating response [28]. As a result, a complex EIS spectrum may be obtained even for the intact/dry coatings, and coatings at the early stages of exposure, when there are no through-pores in the coating and no corrosion reaction at the metal substrate. More specifically, dipolar relaxations (both of the polymer dipoles or interfacial) may manifest themselves in the EIS spectrum equivalent to the two electrode processes having distinct time constants, as graphically shown by Roggero et al. [20]. Also, ionic polarization may cause a predominantly resistive behavior of the coating at low frequencies and a significant decrease in the low frequency impedance modulus [19]. Hence, when EIS is applied to organic coatings, especially the thick industrial grade coating systems, there is a concern that a loss of coating barrier properties and substrate corrosion may be falsely indicated.

On the other hand, a rapid loss of barrier properties may indeed occur on coatings with non-stoichiometric polymer composition [32], low-molecular-weight or low cross-linked polymers [22] and polymers containing a network of nanopores, especially if they contain hydrophilic polar groups, as in the case of epoxies.

Apparently, there is a definite need to distinguish between the intrinsic polymer response and the substrate corrosion response in the EIS spectra of protective coatings. However, there are only a few papers [18–20,25] applying dielectric spectroscopy concepts alongside the conventional EIS approach, to interpret the EIS spectra of a polymer coating. In the present study, we propose an equivalent circuit model that unifies dielectric permittivity (dipole relaxation and disordered solids conduction) and EIS porous coating formalisms. As a result of applying the unified model to the four coating systems of various barrier performance, we suggest the additional criteria for rating thick industrial grade coatings, besides the frequently used low-frequency coating impedance. Those criteria rely upon the shape of the tangent loss angle curve and an additional polarization routine. Polarized impedance response proves or disproves the existence of reactive areas [16] of the substrate as well as retention or loss of wet coating adhesion.

2. Experimental

2.1. Coated samples preparation

Cold rolled steel samples having dimensions of 15 cm × 10 cm × 0.3 cm and 15 cm × 10 cm × 1 cm, with and without rebars welded longitudinally on one side, were prepared for painting by shot blasting to Sa 2 ½. Samples were coated per instructions of the paint manufacturer. The samples were not stripe coated at the edges and the welds. Table 1 list the data of the four commercial coating system investigated.

2.2. EN ISO 9227 neutral salt spray (NSS) test

The neutral salt spray test was conducted in the CW Specialist Equipment model SF/100 salt cabinet according to the EN ISO 9227 and had lasted 720 h.

2.3. Electrochemical impedance spectroscopy (EIS)

EIS measurements on the intact specimen and the specimen after 720 h of NSS were carried out by the ReCorr QCQ device [15]. It consists of a potentiostat/frequency response analyser, a flexible electrode with the conductive polymer surface and conductive paste electrolyte, with the surface area of 24 cm^2. The coated samples were used as working electrode, while the flexible polymer electrode was used as both, a counter and a reference electrode. Calibration of the instrument was done on a high-impedance dummy cell mimicking the coating according to EN ISO 16773−3. Exposure to 3.5 % NaCl was done in a hollow cylinder cell attached to the coating surface. EIS measurements were done using of a three-electrode cell comprised of the coated sample as a working electrode, a stainless steel mesh as a counter electrode, and a SCHOTT B3510+ calomel reference electrode, constructed according to EN ISO 16773−2, also using ReCorr QCQ device and software. The frequency range used in measurements was from 10 kHz to 100 mHz a sinusoidal amplitude of ±50 mV.

2.4. Differential scanning calorimetry

The measurement was conducted according to the EN ISO 11357 on Mettler Toledo DSC 823 controller at a scan rate of 20 °C min^{-1} over the temperature range from 0 to 90 °C in two heating cycles under a nitrogen atmosphere with a constant flow of 60 mL min^{-1}.

2.5. Microscopic examination

Microphotographs of the coating surface were obtained by Dino-Lite High Magnification microscope, model AM7515MT8A. SEM and EDX analysis was done in high vacuum, using Tescan Vega III, SBU EasyProbe scanning electron microscope with 15 kV accelerating voltage of the electron beam at various magnifications.

Table 1
Details of the tested systems. (1.5 column fitting).

System annotation	Basecoat (NDFT/ µm)	Intermediate layers (NDFT/ µm)	Top coat (NDFT/ µm)	No. of layers (Measured DFT/µm)
A	zinc rich epoxy (70–80)	waterborne acrylic with zinc phosphate pigment (100–125)	waterborne acrylic (60–70)	3 (259 ± 5)
B	zinc rich epoxy (80–100)	waterborne acrylic with zinc phosphate pigment (2 × 60)	waterborne acrylic with iron flakes (80)	4 (344 ± 14)
C	zinc rich epoxy (70)	epoxy with iron flakes (100)	polyurethane with unspecified barrier pigments (70)	3 (250 ± 26)
D	zinc rich epoxy (70–80)	epoxy with zinc phosphate (2 × 55–70)	acrylic polyurethane (60–70)	4 (291 ± 7)

2.6. Pull off test

Adhesion of the coating systems was tested according to EN ISO 4624 with the Pull-Off Adhesion Tester - PosiTest AT. Separation occurred with tensile stress necessary to break the weakest part of the system, either at the interface (adhesive failure) or within the layer (cohesive failure). The operating range of the device is 0–25 MPa.

3. Results

3.1. EIS spectra and modelling

A set of coated samples denoted by A, B, C and D and described in detail in the experimental part, has been investigated. The EIS results include impedance spectra of (i) a set of intact coatings, (ii) a set of the same coatings exposed to 3.5 % NaCl for up to 1440 h, (iii) a set of aged coatings after 720 h in NSS in the wet state and (iv) a set of the same aged coatings that were subsequently exposed to 3.5 % NaCl for 1440 h. Representative Bode plots of each of the categories (i) to (iv) and for each coating type, are shown in Fig. 1. The equivalent circuit model denoted by $R_e(Q_1[R_1(Q_2R_2)])$ shown in Fig. 1 d was used. CPE1 is related to Q_1 and α_1 and CPE2 is related to Q_2 and α_2. The model fits very well to the data with $\chi^2 < 0.001$ and the fits are shown by full lines in the same Fig. 1. The $R_e(Q_1[R_1(Q_2R_2)])$ model was used because two time constants could be observed in the phase angle plots. EIS modelling with the simplest possible equivalent circuits is preferable because the increase in the number of parameters of the EIS multi-parametric model increases the inherent uncertainty of the calculated parameters [33].

Fig. 2 presents the evolution of the fitted parameters of the $R_e(Q_1[R_1(Q_2R_2)])$ equivalent circuit with the duration of exposure to 3.5 % NaCl, first for the intact and then for the NSS aged samples. C values have been calculated from the Q, R and α values by the equation: $C = Q^{1/\alpha}R^{(1-\alpha)/\alpha}$ [34]. For the coating system A, both capacitances increase and both resistances decrease with the time of exposure of the intact coatings to 3.5 % NaCl and even more so for the NSS aged coatings. After drying of the coatings that have been exposed to 720 h of NSS, the parameters return to near original value of the intact coating (not shown). Upon subsequent exposure to 3.5 % NaCl, parameters of the coatings A and B, do not follow the pattern of the intact coating but quickly acquire the values of the NSS aged coating in the wet state. This shows that NSS inflicts permanent coating damage to coatings A and B. Also, for coating A, NSS, i.e. 5% NaCl fog at 35 °C, appears to be a harsher environment than the liquid 3.5 % NaCl solution at ambient temperature. R_2 of the aged wet coating is significantly lower than that of the intact coating for the same exposure time. This may be explained by an influence of the coatings T_g [4]. Majority of technologically important dry coatings are formulated to be in a glassy state under normal service conditions and have a glass transition temperature in the vicinity of 50 °C [20]. T_g decrease by water saturation, e.g. of epoxy industrial coatings, is 20–30 °C [4,35–37]. Coating impedance measurements are usually done at the room temperature, EN ISO 16773 prescribes the temperature of 23 ± 2 °C. Hence, water absorption may pull T_g towards the measurement temperature. If the measurement or service temperature is above the water-plasticized T_g, macromolecular chains acquire mobility, large enough to cause the formation of ionic paths through the coating [18, 29]. The consequences may be fast Fickian water diffusion into the coating [38], a sharp decrease of the low-frequency impedance [39], irreversible coating damage, e.g. in a form of adhesion loss and cracks [40] and shortening of the coating lifetime [29]. T_g of the coating A in the dry state equaled 37.1 °C and for the coatings B, C and D, equaled 43.64, 42.94 and 41.04 °C, respectively, hence the influence of the wet T_g on the observed coating performance is feasible.

The change of parameters observed for the system A is progressively less pronounced for systems B, C and D. CPE coefficients α_1 and α_2 (not shown), are similar within pairs of coatings A and B and C and D. For A and B, α_1 and α_2 decrease monotonously from 1 to 0.8 and from 0.6 to

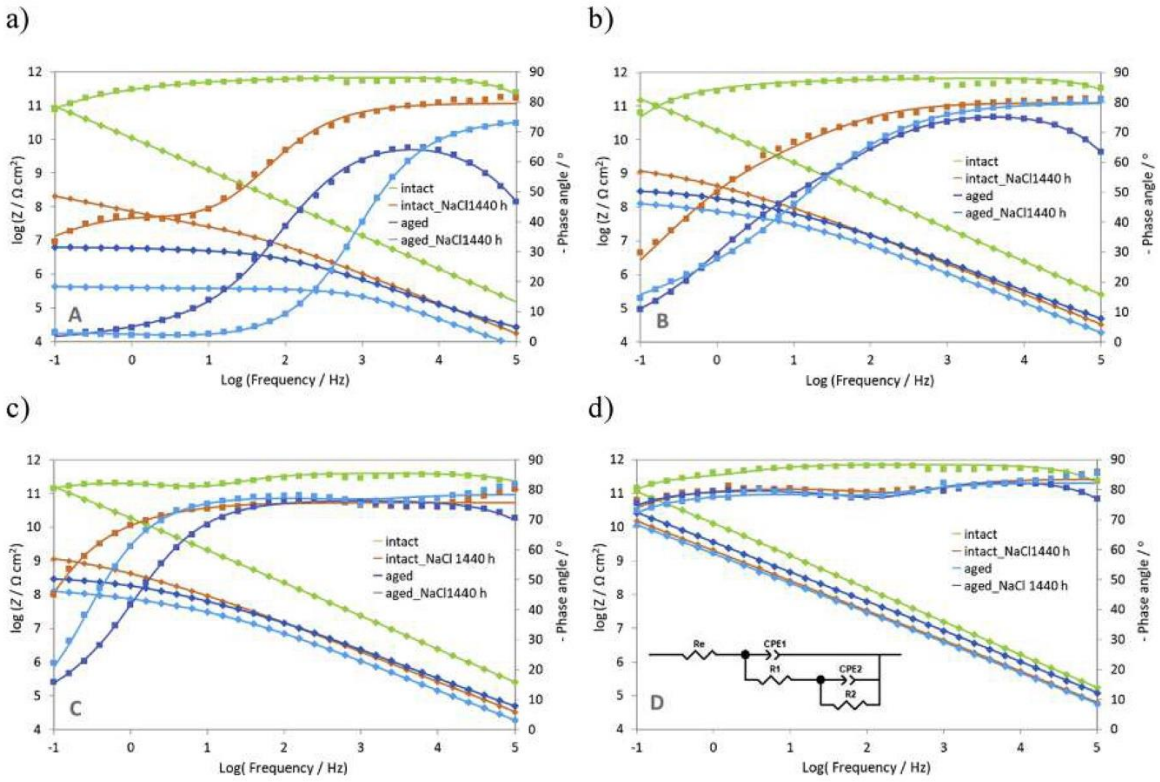

Fig. 1. Bode plots (log Z - ◆ and Phase angle -■) of the coating systems A to D obtained for the intact coatings, coatings after 1440 h of immersion in 3.5 % NaCl, NSS aged coatings in the wet state and NSS aged coatings after 1440 h of immersion in 3.5 % NaCl. Full lines denote fits of the $R_e(Q_1[R_1(Q_2R_2)])$ equivalent circuit. (double column fitting).

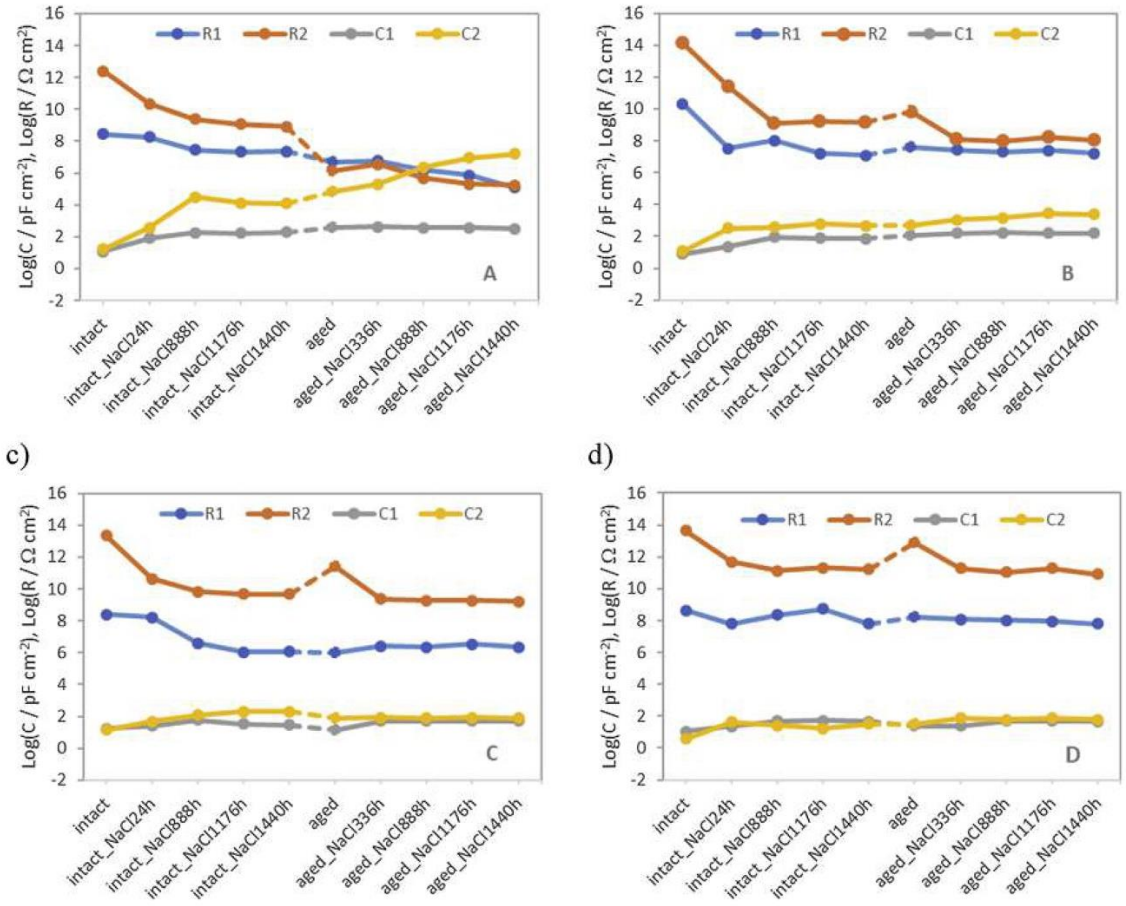

Fig. 2. Capacitances and resistances derived from fitting the $R_e(Q_1[R_1(Q_2R_2)])$ equivalent circuit to the experimental data, for various times and types of exposure. (double column fitting).

0.4, respectively. For coatings C and D, α_1 decreases from 1 to 0.9 but α_2 shows an increase from 0.6 to 0.8.

Impedance modulus Z at 0.1 Hz, shown in Fig. 3, may be taken as an indicator of thick organic coating barrier properties [41–43]. The behavior of Z at 0.1 Hz is in concordance with the trends of coating behavior observed from equivalent circuit modelling of the EIS data. Z at 0.1 Hz indicates that coating D is the least sensitive to exposure to 3.5 % NaCl and NSS ageing while coating A is the most sensitive. It should also be noted that the thicker coatings within each type, water and solvent based, have shown higher impedance than the thinner ones, but overall, the water based coatings performed less good than the solvent based coatings.

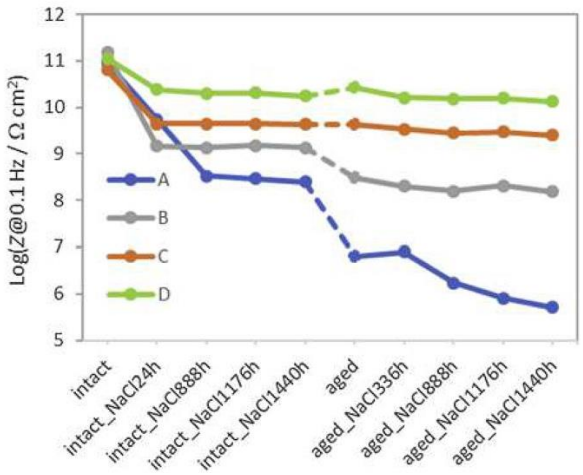

Fig. 3. Impedance modulus at 0.1 Hz for the tested coating systems after various times and types of exposure. (single column fitting).

3.2. Derivation and application of the unified model

Fig. 4 shows the two equivalent circuits [20], the left one related to the dielectric relaxation, and the disordered solids conduction of a non-porous polymer coating, and the right one related to the behavior of a porous polymer coating.

The elements of the $R_e(Q_1[R_1(Q_2R_2)])$ equivalent circuit and the data in Fig. 2 are ascribed a physical meaning trough comparison to the equivalent circuits in Fig. 4, as follows:

(i) In the dielectric permittivity model and the porous coating model, C_1 related to Q_1, has the meaning of the coating's high-frequency capacitance limit [20] and corresponds to C_∞ and C_c from Fig. 4. We propose that the dissipation of time constant leading to a high-frequency CPE behavior expressed through Q_1 and α_1 is attributable to the heterogeneous surface distribution of the electrolyte resistance, R_e.

The model of Hirschorn et. al. [44] is used, stating that spatial heterogeneity of R_x in an equivalent circuit $R_x(QR_y)$, may be modeled by a set of parallel circuits $R_{xi}(C_iR_{yi})$ shown in Fig. 5.

The effective value of C_y and the effective time constant τ_y are given by:

$$C_y = Q^{1/\alpha}\left(\frac{R_xR_y}{R_x+R_y}\right)^{(1-\alpha)/\alpha} \quad (1)$$

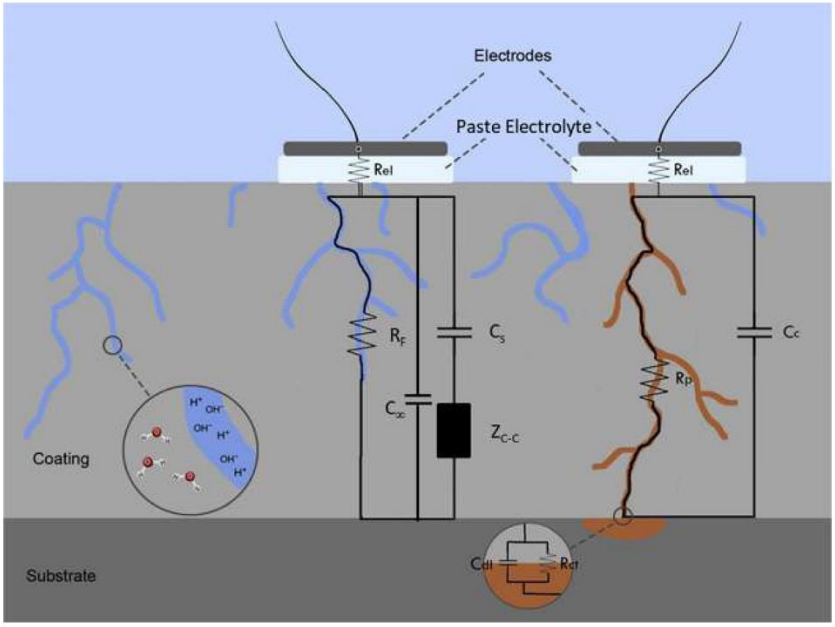

Fig. 4. Equivalent circuit models of a polymeric coating in a dielectric permittivity (left) and a porous coating (right) formalisms. (1.5 column fitting).

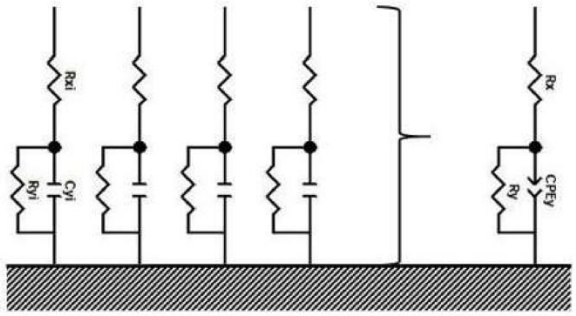

Fig. 5. Schematic representation of a surface distribution of time constants that may be expressed through a CPE. (single column fitting).

$$\tau_y = C_y\left(\frac{R_x R_y}{R_x + R_y}\right) \tag{2}$$

$R_x = R_e$ is obtained from the fitting procedure and had a value of 158 ± 34 Ω, in the case of the paste electrolyte. In the case of the 3.5 % NaCl solution R_e equalled 16 Ω, and was close to the value assumed in the literature, equal to 15 Ω [16]. Since, in the present study, the resistance $R_y = R_1$ is in all cases much higher than R_e, Eq.s (1) and (2) reduce to:

$$C_1 = Q_1^{1/\alpha_1}(R_e)^{(1-\alpha_1)/\alpha_1} \tag{3}$$

$$\tau_1 = C_1 R_e \tag{4}$$

The effective high-frequency capacitance may be calculated from Q_1, α_1 and R_e, independent of the nested circuit $R_1(Q_2R_2)$.

(ii) In the case of a porous coating model, the rest of the circuit is interpreted by assigning R_1 the meaning of the pore resistance R_p, C_2 the meaning of the double-layer capacitance C_{dl}, and R_2 the meaning of the charge transfer resistance, R_{ct}. On bare metal electrodes, CPE2 behavior is justified by the distribution of reactivities of a Faradaic system [44]. In the present case, turning again to the Hirchorn model, we can ascribe distribution of time constants of CPE2 to the spatial distribution of pore resistivities. In that case C_2 equal to C_{dl}, and the appending time constant τ_2, equal:

$$C_2 = Q_2^{1/\alpha_2}\left(\frac{R_1 R_2}{R_1 + R_2}\right)^{(1-\alpha_2)/\alpha_2} \tag{5}$$

$$\tau_2 = C_2\left(\frac{R_1 R_2}{R_1 + R_2}\right) \tag{6}$$

(iii) When the coating is nonporous, the overall capacitance derived for the equivalent circuit of the dielectric permittivity model shown in Fig. 4 equals [18]:

$$C(\omega) = C_\infty + \frac{C_s}{1 + (j\omega\tau_{cc})^{1-\alpha_{cc}}} + \frac{1}{R_f(j\omega)^\gamma} \tag{7}$$

$C_s = \Delta\varepsilon C_v$ is the difference between the low and the high frequency limits of capacitance and $\Delta\varepsilon$ is the dispersion strength of dipolar relaxation. τ_{cc} denotes the dipole relaxation time constant. The Cole-Cole impedance equals [20]:

$$Z_{cc} = \frac{\tau_{cc}}{C_s(j\omega\tau_{cc})^{\alpha_{cc}}} \tag{8}$$

Cole-Cole distribution is symmetric and yields a depressed semicircle in ε'- ε'' plane, with the angle between the real axis and its center equal to $\alpha_{cc}\pi/2$. The series combination of C_s and Z_{cc} shown in Fig. 4 yields the middle term in Eq. (7). Ionic conduction through the coating, by the hopping mechanism or thought the percolation paths, causes the appearance of the resistance R_f [18]. It should be noted that R_f appears in parallel to the Cole-Cole impedance.

We propose that the $[C_sZ_{cc}]R_f$ circuit is equivalent to the nested $R_1(Q_2R_2)$. By once more applying the Hirchorn model [44], $R_1(Q_2R_2)$ may be substituted by a parallel combination of $R_{1i}(C_{2i}R_{2i})$ circuits that yield the effective parameters R_1, R_2 and Q_2. In concordance with the fact that a real capacitor can be treated as a lossless capacitor in series with a resistor [28], the resistance R_1 is given a physical meaning related to the energy dissipated during the dielectric relaxation and disordered solid ionic conduction. When there is no ionic conduction, $R_2 \to \infty$, R_1 acquires the meaning of resistance to the movement of polymer dipoles, and Eq. (5) reduces to:

$$C_2 = Q_2^{1/\alpha_2}(R_1)^{(1-\alpha_2)/\alpha_2} \tag{9}$$

Fusion of the Eq. (8) with the assumed expression for the Cole-Cole

time constant, $\tau_{cc} = C_s R_1$ gives:

$$Z_{cc} = \frac{1}{(j\omega)^{\alpha_{cc}} C_s^{\alpha_{cc}} R_1^{\alpha_{cc}-1}} \quad (10)$$

When the Cole-Cole impedance given by the Eq. (9) is compared to the general expression for Z_{CPE}:

$$Z_{CPE} = 1/(j\omega)^{\alpha} Q \quad (11)$$

a relation equivalent to Eq. (8) is obtained:

$$C_s = Q_2^{1/\alpha_{cc}} (R_1)^{(1-\alpha_{cc})/\alpha_{cc}} \quad (12)$$

It is apparent from the Eq.s (9) and (12) that $\alpha_2 = \alpha_{cc}$, $C_2 = C_s$. Equating C_2 and C_s sets the maximum capacitance change with frequency, i.e. the low-frequency limit of the capacitance, in the present model.

When the influence of the ionic conduction is present, R_f is put in parallel to Z_{cc} and corresponds to R_2 in the $R_1(Q_2R_2)$ equivalent circuit. The resistance $R_1 = \tau_{cc}/C_s = \tau_{cc}/\Delta\varepsilon C_v$ appears in series with the resistance R_f. As stressed by Duval et. al. [18], this point contrasts to the classical approach considering a parallel connection of the film resistance R_f to the capacitance hereby denoted as C_∞.

To further clarify relation of the $R_1(Q_2R_2)$ equivalent circuit shown in the inset of Fig. 6 a, to the $[C_sZ_{cc}]R_f$ equivalent circuit shown in the inset of Fig. 6 b, $\alpha_2 = 1$ case that corresponds to the lack of dispersion of C_2, is first explored. Real, imaginary and absolute impedance spectra of the $R_1(Q_2R_2)$ circuit, with $R_1 = 10\ \Omega$, $R_2 = 1000\ \Omega$, $Q_2 = C_2 = 0.001$ F and $\alpha_2 = 1$ is shown in Fig. 6 a. In the porous coating framework the previously mentioned equation $C_2 = Q_2^{1/\alpha_2} R_2^{(1-\alpha)/\alpha}$, derived by Hsu and Mansfeld [34], should be used. This equation is equivalent to $C_2 = Q_2(\omega_2'')^{\alpha_2-1}$, for a (R_2Q_2) circuit under the assumption that ω_2'' is the frequency at which the imaginary part of the impedance, Z'', has a maximum. Fig. 6 a, indeed, shows a spectrum with Z'' maximum at the characteristic frequency $\omega_2'' = 1/C_2R_2 = 1$.

In the dielectric permittivity framework, the respective real and imaginary components of the capacitance C, C' and C'' can be calculated from the dielectric spectra by the equations [20]:

$$C'(\omega) = \varepsilon'(\omega)C_v = \frac{-Z''(\omega)}{\omega(Z'(\omega)^2 + Z''(\omega)^2)} \quad (13)$$

$$C''(\omega) = \varepsilon''(\omega)C_v = \frac{Z'(\omega)}{\omega(Z'(\omega)^2 + Z''(\omega)^2)} \quad (14)$$

Joining the equation for the characteristic frequency of dipolar relaxation $\omega_{cc}'' = 1/2\pi\tau_d$ and Eq. (12), relates ω_{cc}'' to Q_2 and C_2 through $C_2 = Q(\omega_{cc}'')^{\alpha_2-1}$. The effective characteristic frequency in the dielectric permittivity framework, for $R_f >>$ and $\alpha_{cc} = 0$, corresponds to the frequency of the C'' maximum and to the frequency of the inflexion point of C' (Fig. 6 b), or equivalently the inflexion point of ε' [18,29]. The imaginary component of capacitance, C'', or equivalently ε'', is related to the dielectric loss of energy and the real component of capacitance, C', or equivalently ε', is associated with conservative phenomena.

As previously discussed, the movement of dipoles may be eased by polymer plasticizing by water, causing R_1, and therefore, τ_{cc} to decrease i.e. ω_{cc} to increase. Also the change in the number of dipoles will influence C_2 and therefore also τ_{cc}. The impact of changing R_1 and C_2 on capacitance is shown in Fig. 7 a and b, respectively. Fig. 7 c shows modification of the capacitance spectra when ionic conduction appears, and Fig. 7 d shows the influence of dispersion, when $\alpha_2 \neq 1$.

When the dipolar relaxation prevails, $\alpha_2 \rightarrow \alpha_{cc}$ and when ionic conduction influence prevails, R_1 is related to the energy loss due to ionic charge movement and $\alpha_2 \rightarrow \gamma$. This is concordant with the fact that γ corresponds to the Q exponent of the (QR) circuit that may be used as an equivalent circuit reflecting the Jonscher's law [20]:

$$\sigma'(\omega) = \sigma_{dc} + k\omega^{\gamma} \quad (15)$$

Which describes the conductivity of disordered solids. σ_{dc} is the dc conductivity, k is a constant.

Characteristic frequency ω_2'' of the circuit that includes both, R_1 and R_2, i.e. the influence of ionic conductivity and dipole relaxation, is calculated from τ_2 given by the Eq. (6). For a lossless polymer relaxation process, $R_1 = 0$, the real part of capacitance becomes constant and equal to C_2. For $R_1 = 0$ and without ionic conduction contribution, i.e. for $R_2 \rightarrow \infty$, capacitance becomes constant and equal to C_2.

It has been mentioned by Duval et al. [18] that the high and low-frequency capacitances that result from the Cole-Cole model regression calculation are close to those determined from fitting the $(C_1[R_1(C_2R_2)])$ circuit to dielectric impedance data. When the $R_eQ_1[R_1(Q_2R_2)])$ equivalent circuit is used, based on the presented model, the equality of these parameters may be claimed.

To summarize, during exposure to aqueous or moist environments at constant temperature, the EIS response of the polymer may change due to: (i) shortening of the polymer chains relaxation time τ_{cc} through plasticizing by water [18], (ii) appearance of interfacial polarization [24], (iii) increased mobility of ionic impurities due to water presence [28] and (iv) appearance of the coating porosity and active surface area of the substrate. As long as there is no Faradaic reaction occurring at the surface of the metal, the dielectric permittivity model is valid. Movement of ionic charges in alternating electric field yields an apparent dc current at low frequencies but the coating retains its blocking nature. As soon as the current starts flowing through the coating/metal phase boundary, the current leakage occurs through the coating and the coating pores and the resultant circuit is a parallel combination of

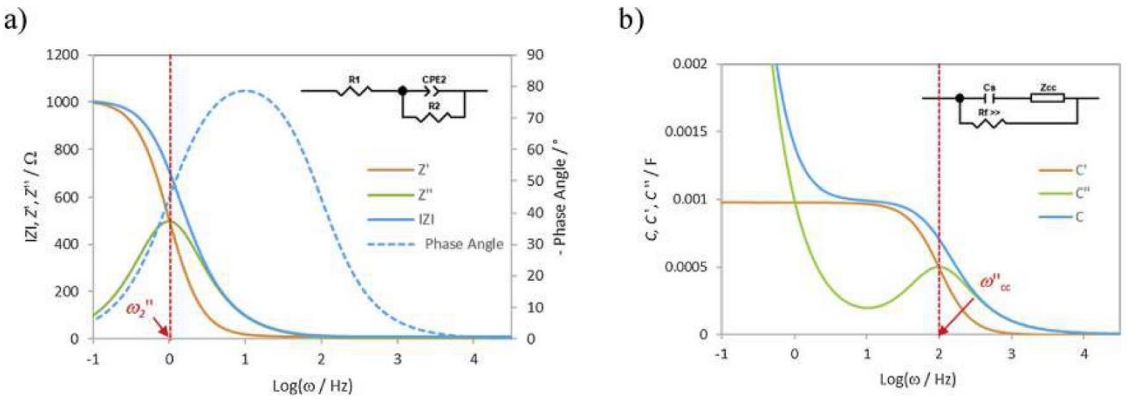

Fig. 6. a) impedance spectra of the (QR) circuit, with $R_1 = 10\ \Omega$, $R_2 = 1000\ \Omega$, $Q_2 = C_2 = 0.001$ F and $\alpha_2 = 1$ and b) the corresponding dielectric capacitance spectra. (double column fitting).

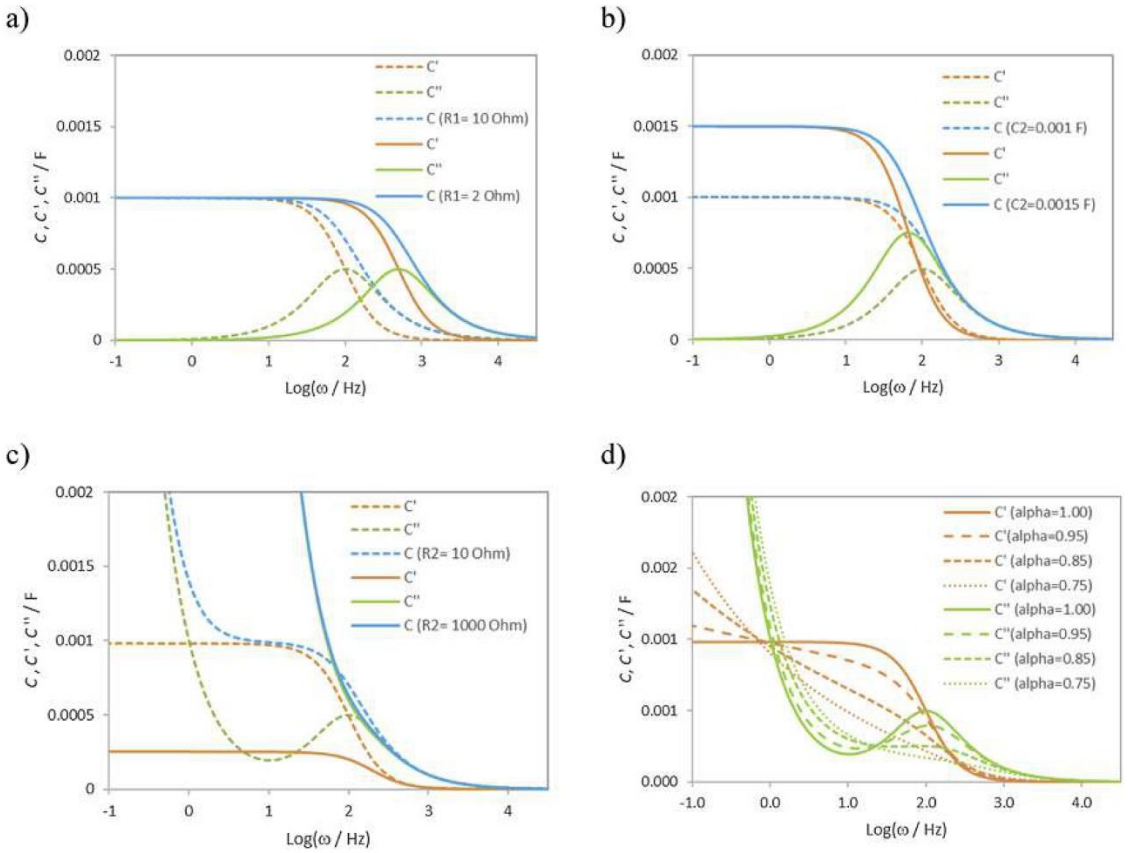

Fig. 7. Dielectric capacitance spectra of the $R_1(Q_2R_2)$ circuits, with $R_1 = 10\ \Omega$, $R_2 = 10^7\ \Omega$, $C_2 = 0.001$ F and the modified spectra when: a) R_1 is changed to 2 Ω, b) C_2 is changed to 0.0015 F c) R_2 is changed to 1000 Ω and 10 Ω and d) α_2 is changed between 1 and 0.75, shown by solid lines. (double column fitting).

polymer conduction and pore conduction paths. Due to the coating degradation, pore conduction paths may prevail as a mean of current transport through the coating.

Applicability of the $R_e(Q_1[R_1(Q_2R_2)])$ model for all the investigated coatings confirms the presence of dipole relaxation impedance response since for dry or shortly exposed coatings metal/electrolyte interface contribution is not expected. For coating systems B, C and D, the low-frequency resistance R_2 (Fig. 2), decreases and then levels off with prolongation of exposure to 3.5 % NaCl. In the dielectric permittivity model, the decrease of R_2 can be associated with the absorbed water that increases the ionic mobility and makes the film resistance smaller [28]. It appears that for B, C and D systems the minimum low-frequency resistance R_2, attained at the end of exposure and respectively equal to 2.10×10^8, 3.00×10^9 and $1.57 \times 10^{11}\ \Omega\ cm^2$ is determined by the water saturation level and availability and mobility of ionic impurities. However, for coating system A, R_2 decreases continuously with no indication of saturation. This would suggest that either water is being continuously absorbed and ionic impurities are being continuously released from the polymer network during exposure, or that the coating is becoming more porous.

The following discussion is aimed at discerning between low-frequency manifestation of the ionic conduction, interfacial polarization and substrate Faradaic reaction appearance, by further exploring the physical model of the coating.

3.3. Characteristic frequencies of the dielectric permittivity and porous coating models

The effective time constant τ_d of the left circuit from Fig. 4, is calculated by adding the high-frequency capacitance to the low frequency capacitance, and making use of Eq. (2):

$$\tau_d = (C_1 + C_2)\frac{R_1R_2}{R_1 + R_2} \tag{16}$$

For the coating system A, Fig. 8 compares the characteristic frequencies $f_d^{''}$, calculated from τ_d in Eq. (15) with the characteristic frequencies of the high-frequency $f_{HF}^{''} = R_1C_1$ and low-frequency $f_{LF}^{''} = R_2C_2$ circuits of the porous coating model.

For coatings B, C and D, $f_d^{''}$ closely follows $f_{HF}^{''}$ and levels off with exposure. In the case of the coating A, $f_{HF}^{''}$ of is continuously pushed towards higher values as the exposure to aqueous environment proceeds. For the investigated exposure times > 24 h, $f_d^{''}$ continuously declines from $f_d^{''} \approx f_{HF}^{''}$ to $f_d^{''} \approx f_{LF}^{''}$. $f_{LF}^{''}$ of the aged coating A is much higher than that of the intact coatings and closely follows $f_d^{''}$. In Fig. 2 a, it is apparent that $f_d^{''}$ decreases, while the resistance R_1 and R_2 decrease and the capacitance C_2 increases, confirming that the capacitance term C_2 has a major influence on $f_d^{''}$ and on the $f_{LF}^{''}$ of the aged coating A. A jump in $f_{LF}^{''}$ between the intact and aged coating A is due to a decline in R_2, observed in Fig. 2 a, again confirming the harshness of NSS exposure.

3.4. Dielectric loss tangent

Phase lag of the polymer dipoles and collisions of charge carriers travelling through the material under the applied electric field are sources of dielectric loss in the form of heat [22,28,36]. Dissipation factor, loss factor, dielectric loss tangent or $\tan\delta(\omega)$ may be calculated from the measured impedance curves, according to the equation:

$$\tan\delta(\omega) = \frac{\varepsilon''(\omega)}{\varepsilon'(\omega)} \tag{17}$$

and conductivity $\sigma'(\omega)$ is calculated from:

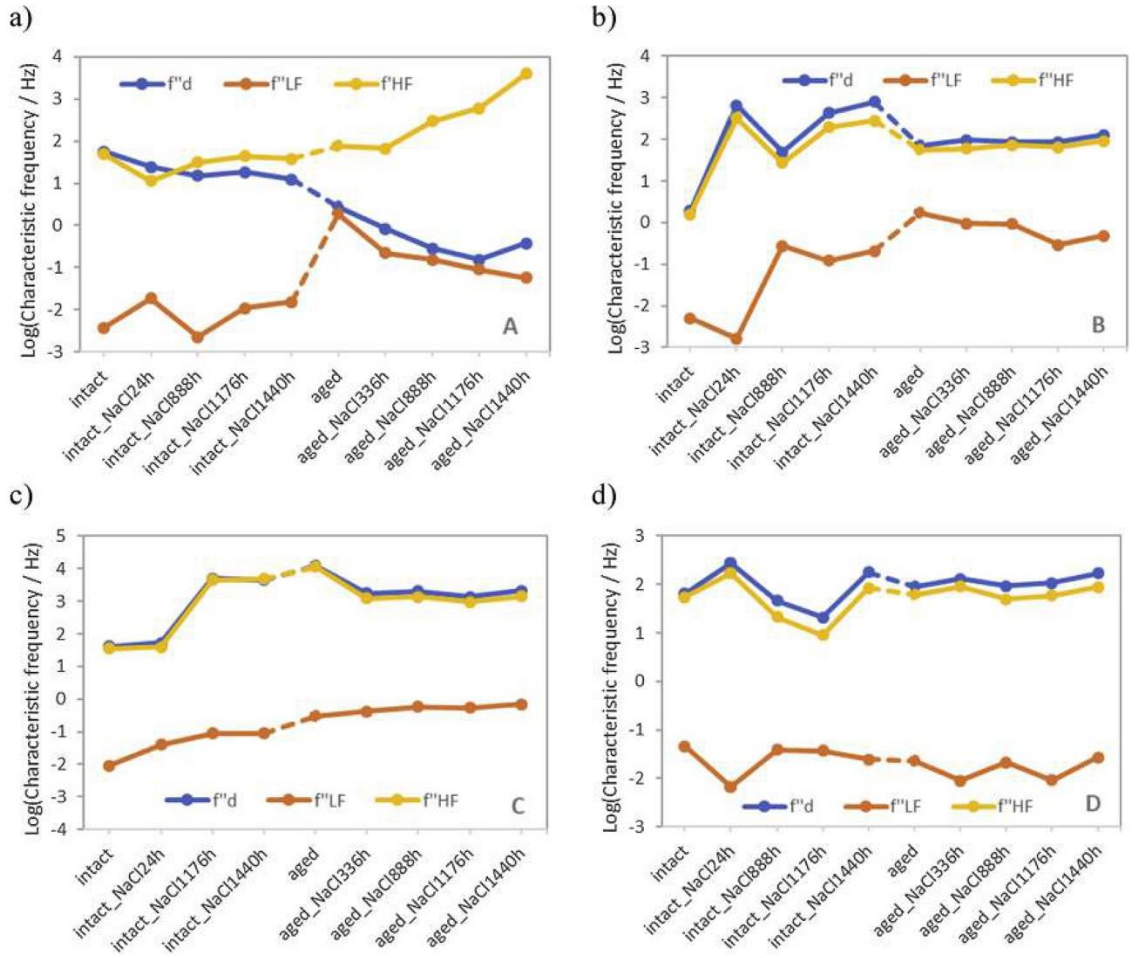

Fig. 8. Characteristic frequencies of the dielectric permittivity equivalent circuit and the porous coating equivalent circuit. (double column fitting).

$$\sigma^{'}(\omega) = \omega\varepsilon_{v}\varepsilon^{''}(\omega) \tag{18}$$

In the dielectric permittivity formalism and the porous coating formalism, tanδ equals to the resistive to capacitive current ratio.

Fig. 9 shows the phase angle, tanδ and capacitance plots simulated for the parameters shown in Table 2. Circuit 1 is representative of investigated industrial coatings in the dry state or the coatings at the early stages of exposure and Circuit 2 is representative of the coating A in the wet state.

In the framework of dielectric permittivity, tanδ peaks indicate either polymer dipole relaxation or the aforementioned Maxwell-Wagner-Sillars interfacial polarization. tanδ peak, observed for Circuit 1, originates from the dipole movement and is related to the inflexion point of C'. The low frequency tan delta peak of Circuit 2 results from the specific shape of ionic conductivity part of C' which is consistent with the fact that interfacial polarization arises from the local accumulation of charges and their drifting through the material [28].

By combining Eqs. (13), (14) and (17), it may be seen that tanδ corresponds to $1/\tan(-\text{Phase Angle})$ and that tanδ peak corresponds to the minimum in the phase angle curve (Fig. 9 a). Hence, for a porous coating, tanδ peak indicates onset of the low-frequency time constant that is due to the polarization resistance/double layer capacitance

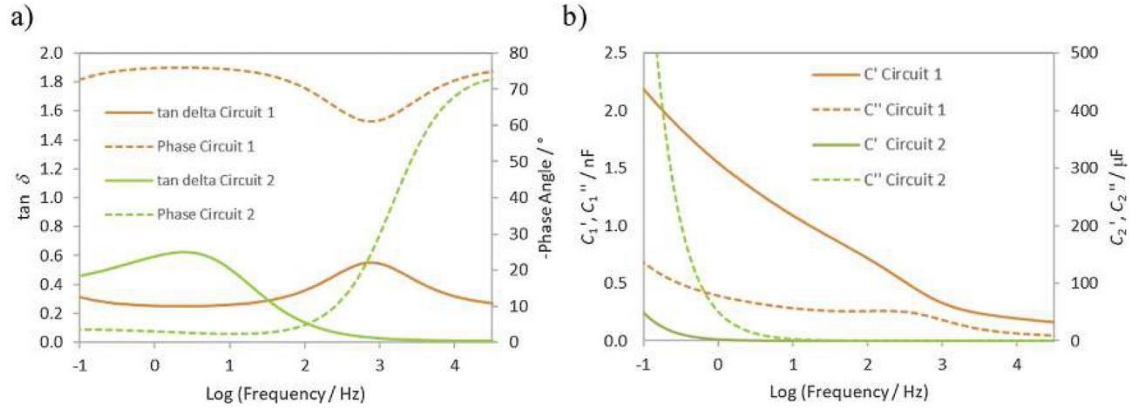

Fig. 9. Spectra of Circuits 1 and 2 from Table 2, showing a) phase angle and tan δ and b) real and imaginary capacitance. (double column fitting).

Table 2
Parameters of the circuits used for simulating impedance of the dry coatings or the coatings at the early stages of exposure (Circuit 1) and the wet (Circuit 2) coatings. (single column fitting).

Parameter	Unit	Circuit 1	Circuit 2
Equivalent Circuit		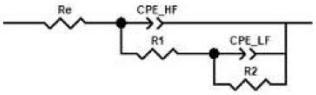	
R_e	Ω	15	15
R_1	Ω	10^5	1.5×10^4
R_2	Ω	10^9	10^4
Q_1	Ω^{-1} s^{-n}	5×10^{-9}	5×10^{-8}
Q_2	Ω^{-1} s^{-n}	5×10^{-9}	3×10^{-4}
α_1	–	0.85	0.85
α_2	–	0.85	0.30
log $f_1^{''}$	Hz	3.09	2.88
log $f_2^{''}$	Hz	−1.62	−2.39
Equivalent Circuit		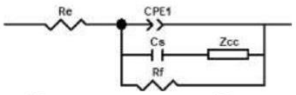	
$R_eR_1/(R_e+R_1)$	Ω	15	15
$R_1R_2/(R_1+R_2)$	Ω	10^5	6×10^3
C_1	F	2.76×10^{-10}	4.15×10^{-9}
C_2	F	1.31×10^{-9}	1.18×10^{-3}
log $f_d^{''}$	Hz	3.00	−1.65
log (f tan δ_{max}) log (f -Phase angle$_{min}$)	–	2.89	0.40

equivalent circuit at the active area of the substrate. Minimum of the phase angle curve is barely visible in the phase angle plots while the tan delta peak is well emphasized in the tanδ plots [31]. Therefore, calculating tanδ, is of particular importance for detecting the appearance of the low frequency time constant, i.e. active substrate area, in the case of the porous coating.

tan$\delta(f)$ and $\sigma^{'}(f)$ have been calculated and are shown in Fig. 10 a to h. Figures a, c, e and g show the respective results for the intact coatings A, B, C and D exposed to 3.5 % NaCl. Figures b, d, f and h show the respective results for the NSS aged coatings, A, B, C and D, exposed to 3.5 % NaCl.

For the coating system D, after 24 h of exposure, maximum off tanδ is not observed (Fig. 10 g and h). For longer exposure times, maxima of tanδ (0.21 ± 0.01) are observable in Fig. 10 g and h, at frequencies 46.16 ± 16.30 Hz, with no specific trend in intensity or peak frequency variation with exposure time. tanδ probably reflects α-mode dipolar relaxation appearing as a consequence of polymer plasticizing [20]. No dc current plateaus are observed at the $\sigma^{'}$ graph. dc conductivity decreases by approximately an order of magnitude during the exposure, but still remains low ($< 10^{-13}$ S cm^{-1}), showing that the coating system D retains its excellent insulating properties.

Maxima of tanδ equal to $0.287 \pm 1 \times 10^3$ are observed for coating C in Fig. 10 e and f at 2692 ± 756 Hz, for exposure times ≥ 336 h. The intensity of tanδ peaks approximately equals that for the coating D, probably pointing to the same nature of the phenomenon. For coatings C and D, the difference in the width and the maximum frequency of tanδ, may be explained by different structure and inter- and intramolecular interactions that determine the ease of dipole orientation over a wide range of frequencies [45]. Again, there is no specific trend in intensity and peak frequency variation with exposure time, probably indicating water saturation has been reached before 336 h of exposure.

No peaks are discerned on the tanδ graphs of the coating system B (Fig. 10 c and d). The shape of tanδ curves indicates ionic conductance, reflecting the Jonscher's power law. The absence of the relaxation peak in all graphs of the coating system B may be due to ionic conductivity effect masking the relaxation behavior of polymer [21,25]. Conductivity of systems B and C exerts a low-frequency plateau in the region between 10^{-10} and 10^{-9} S m^{-1} and between 10^{-12} and 10^{-10} S m^{-1}, respectively.

For the coating system A (Fig. 10 a and b), well defined maxima of the NSS aged specimens lay at 2.40 ± 1.13 Hz. These maxima gain intensity with exposure. Pronounced dc plateaus are observed between 10^{-8} and 10^{-6} S m^{-1}.

In order to discriminate between interfacial polarization and the response of the active substrate area, sample A has been subjected to EIS measurements performed at dc offset potentials ranging from 0 to −5 V. The impedance spectra are shown in Fig. 11 a, and the corresponding tanδ curves are shown in Fig. 11 b. Only the segment of the curve below the tanδ peak frequency, and the corresponding part of the phase angle curve, are affected by polarization which is concordant with the decrease of R_2. This observation indicates that the high-frequency EIS response, reflecting behavior of the polymeric film, is unaffected by the dc offset. The low-frequency EIS response, is affected by the dc offset probably due to the decreased polarization resistance at progressively more cathodic potentials of the underlying steel. For this reason, cathodic polarization has been chosen as a method of wet adhesion evaluation [2,46].

Furthermore, the NSS exposed samples were kept in 3.5 % NaCl for additional 1440 h after performing the experiments that yielded data shown in Fig. 10. Fig. 12 a to d, shows loss tangent of those specimen obtained for various dc offset potentials ranging from 0 to −2 V. The measurements were done in sequence, from 0 to −2 V, each scan lasting for 85 s. tanδ peak of sample A in Fig. 12 a has shifted to higher frequencies and gained intensity with prolongation of the exposure i.e. with respect to the tanδ shown in Fig. 10 a. This is consistent with the higher delamination degree of the coating from the substrate. tanδ graphs of other coating systems have not changed significantly with exposure.

Coatings A and B show a rise of tanδ and conductivity for dc offsets negative of –650 mV$_{SCE}$. –650 mV$_{SCE}$ approximately corresponds to the substrate corrosion potential measured in 3.5 % NaCl.

A rise of tanδ is observed at the dc offset of −2 V, in the whole frequency range, indicating porosity of the polymer film and the leakage of current through the coating. Blistering was observed at the surface of the coating A, with a single blister of 5 mm in diameter and a dense population of blisters of 1 mm in diameter. After cathodic polarization had ended, the 5 mm blister became deflated, confirming that hydrogen had evolved from the substrate surface. It should also be noted that small blisters have spontaneously appeared on coating A, around the circular hole after NSS exposure. Blistering of coating A gives firm evidence that the tanδ maximum may be linked to the porous coating model and the onset of cathodic reaction at the substrate active area [16]. Blistering has not been observed at the surface of the coatings B, C and D.

Current plateaus, like those observed in conductivity plots of coating A, in Fig. 12 a and b, may originate from the dependent dipole behavior [26]. This behavior is due to the interfacial polarization in the form of the intra-cluster motion of charges. It is expected that, for polymer composites, the plateau appears at low frequencies and for temperatures below T_g. Longer range, inter-cluster charge movement is known to cause a low-frequency, quasi continuous conduction plateaus at temperatures above T_g. However, this plateaus may also be due to the current leakage through the coating and the electrochemical reactions at the substrate active area [16]. The argument in favor of the latter hypothesis is that after the occurrence of delamination on coatings A and B, at −2 V of polarization. The plateau current is significantly increased, even deflecting to higher values at frequencies below, approximately, 3 Hz, indicating delamination in progress.

3.5. Pull off adhesion

The adhesion test was carried out by the pull-off method after two weeks of drying under laboratory conditions at the area of the coating that had been exposed to the electrolyte. The results of the tests are

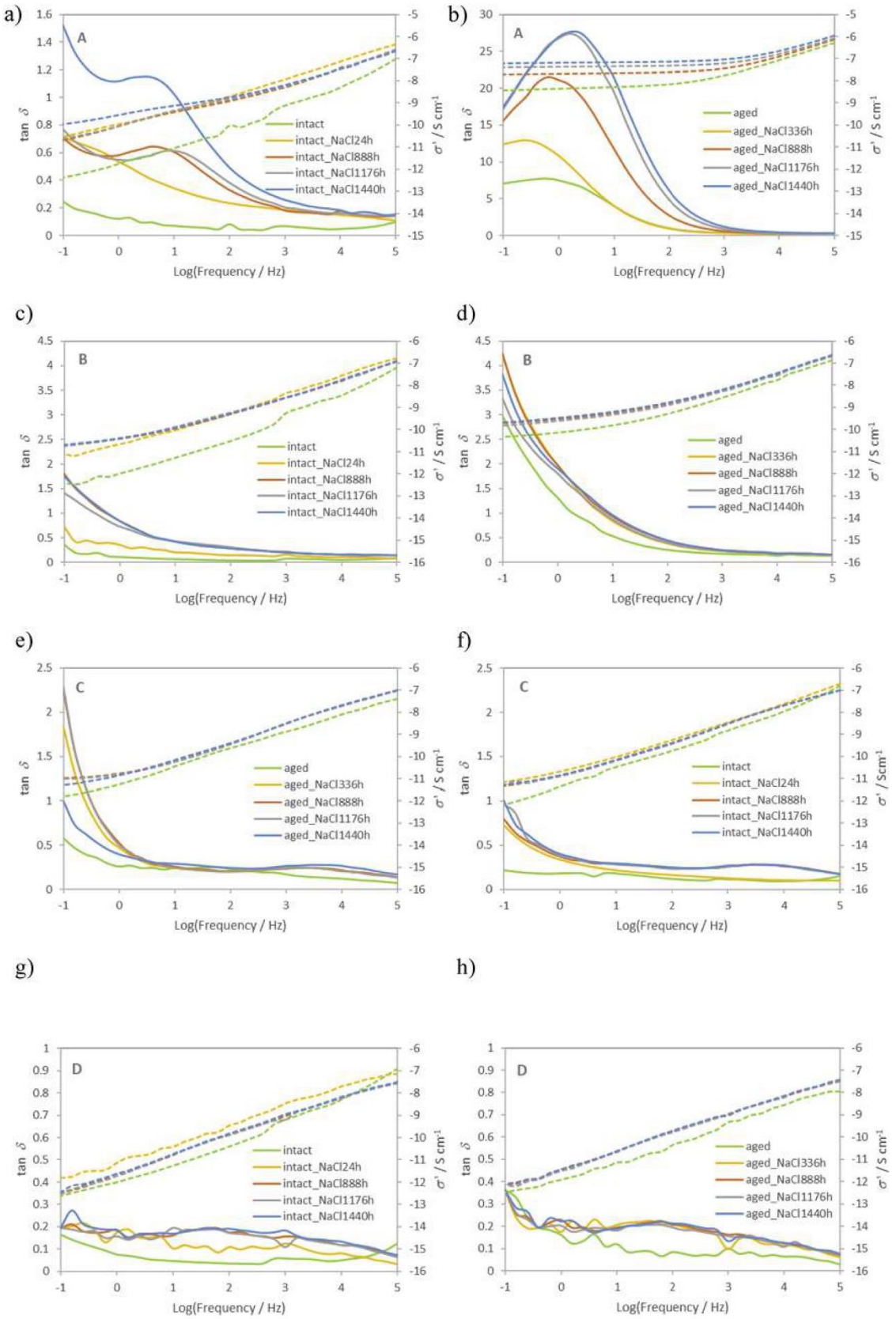

Fig. 10. tan δ and conductivity for the intact and aged coatings exposed to 3.5 % NaCl solution for 1440 h. (double column fitting).

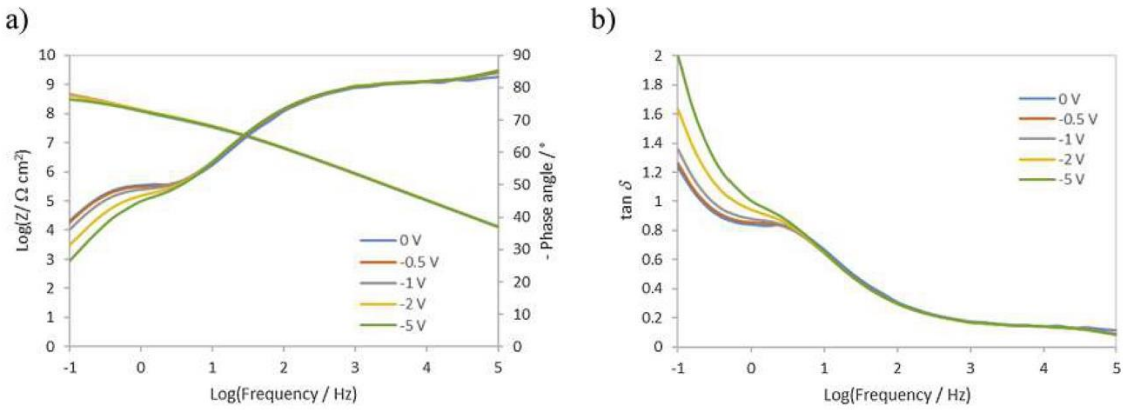

Fig. 11. EIS spectra and tan δ of the intact coating A after 1440 h of immersion in 3.5 % NaCl obtained at dc offset potentials ranging from 0 to −5 V on. (double column fitting).

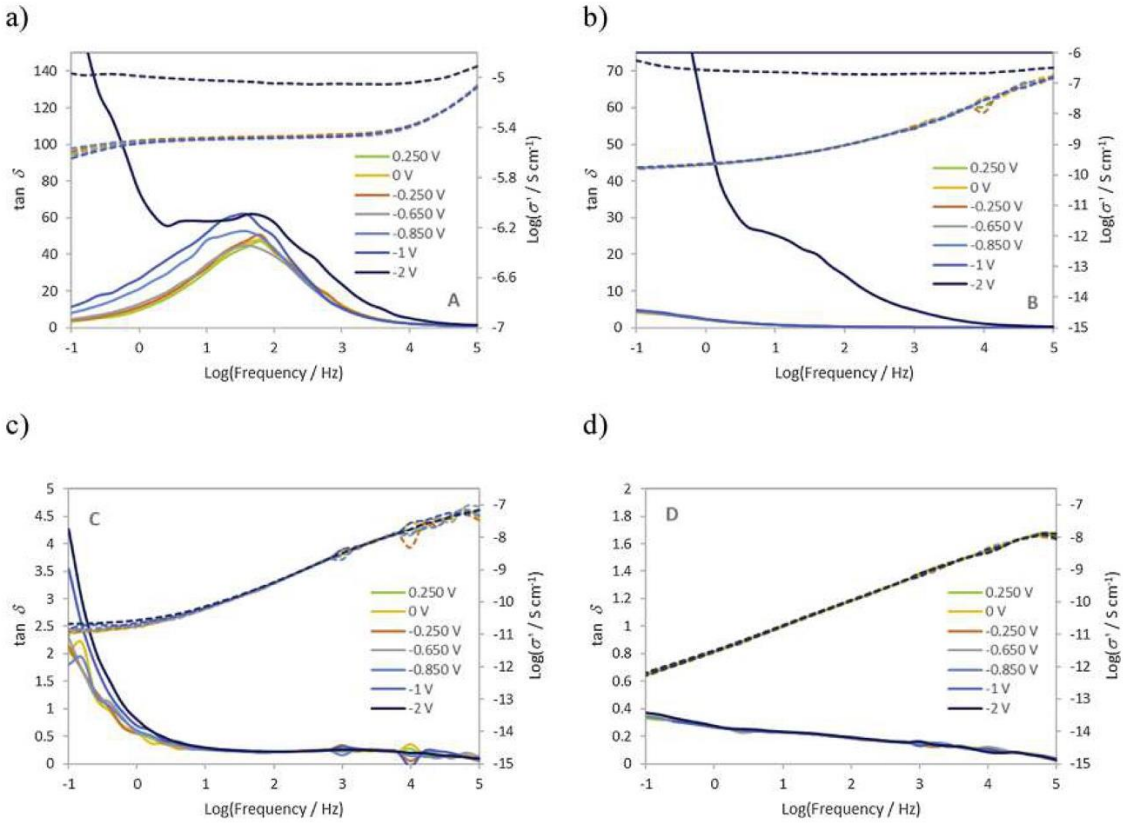

Fig. 12. tan δ at dc offset potentials ranging from 0 to −2 V on the aged coatings after 2880 h of immersion in 3.5 % NaCl. (double column fitting).

shown in Fig. 13. For all the coatings, except the coating A, the adhesion strength before and after exposure was within the estimated extended measurement uncertainty. Only in the case of coating A, the adhesion strength decreased by half, due to exposure. Also, the mode of failure of the coating A is adhesive. In the intact state the adhesion failed between the topcoat and the intermediate coat while for the exposed coating, the location of adhesive failure was the coating/substrate interface. Within the pull off test area, corrosion spots were visible at the substrate, surrounded by areas of bright metal. The adhesion strength of 9.10 MPa is still well above the of 5 MPa requested by the standards [7,47]. It confirms common knowledge that coating adhesion opposes negative effects of barrier property loss [46]. Coating porosity does not solely determine the coating performance. The most important additional factors are corrosion containment in defect areas and adhesion [2]. This is visible in the case of the pull-off result for the coating A, that shows relatively high adhesion strength along with the spot-like corrosion of the substrate. Therefore, EIS should be treated as a complementary method to the other methods of coating assessment, particularly the pull off adhesion testing.

3.6. *Visual appearance*

Examined under the optical microscope (Fig. 14), the surface of the intact coating A reveals cratering defects of approximately 40 μm in diameter. Rare cratering defects are also found on coating B. Coatings C and D show no coating defects. Surfaces of coatings from A to D, show an increasingly smoother appearance. The craters on coating A that were not visible by the naked eye, were further examined by SEM/EDS.

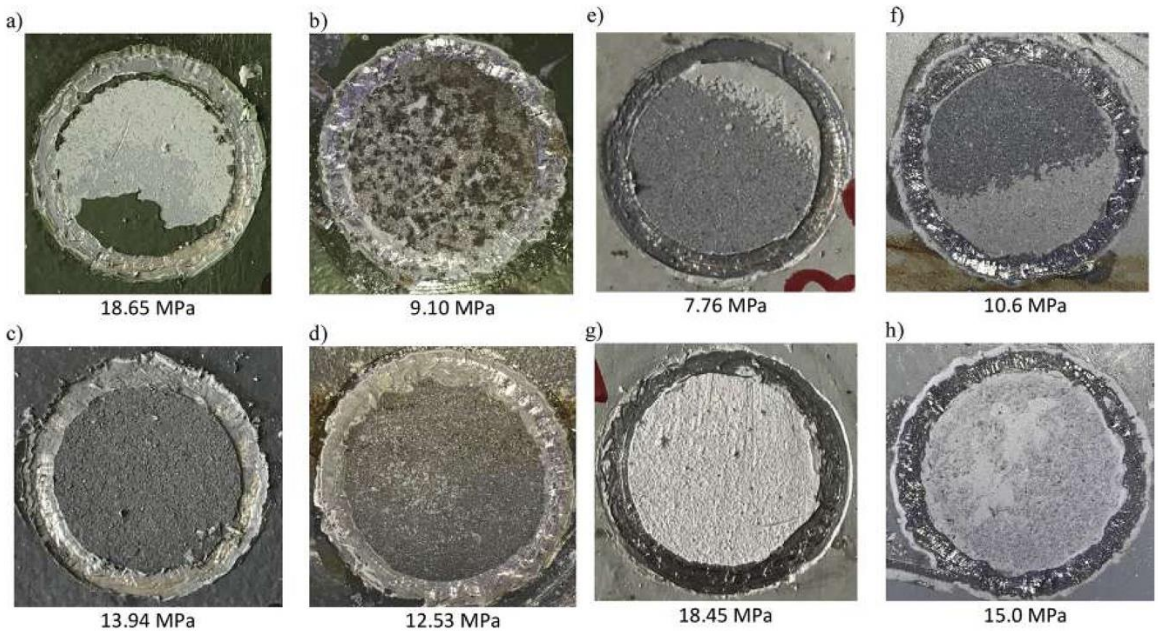

Fig. 13. Results of the pull off adhesion test on the unexposed, intact coatings (left) and on the aged coatings (right) after the exposure to 3.5 % NaCl 2280 h. (single column fitting).

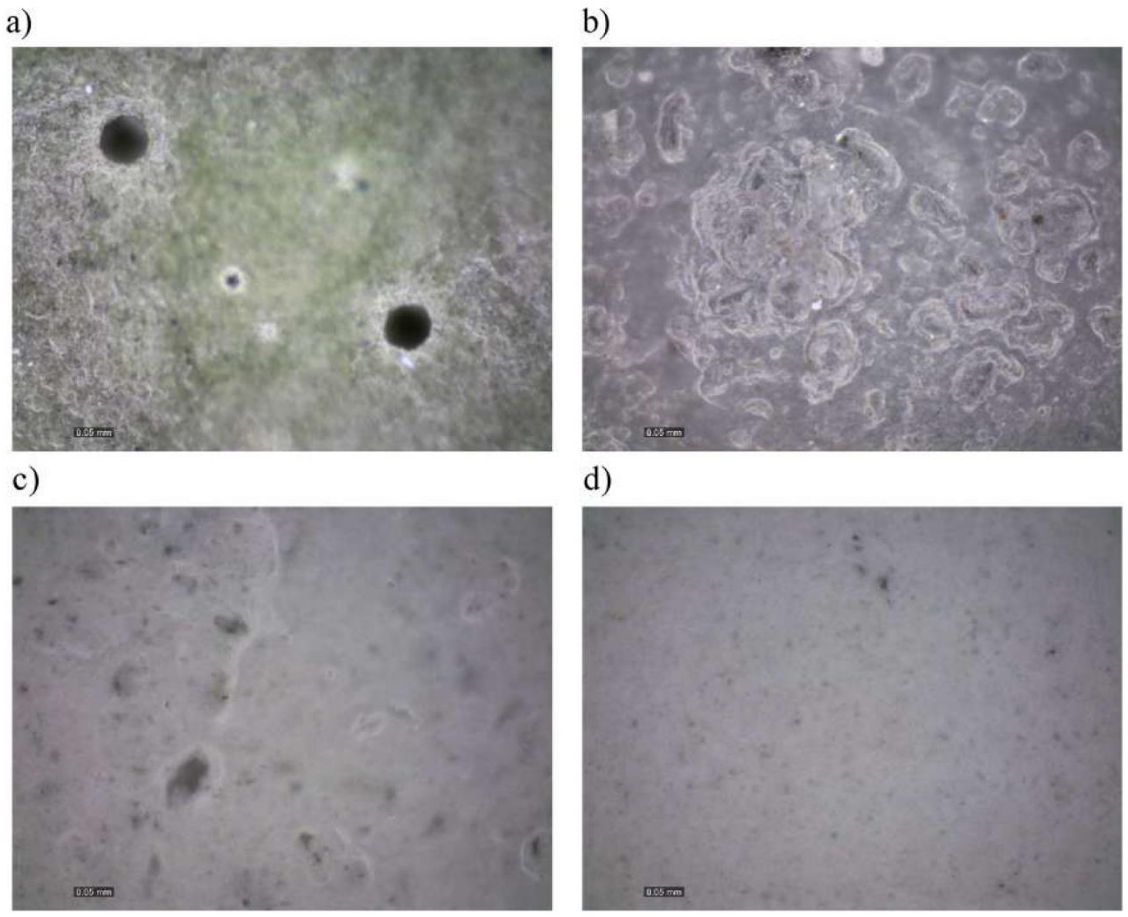

Fig. 14. Micrographs of the surface of the intact coatings, enlarged 745 × .

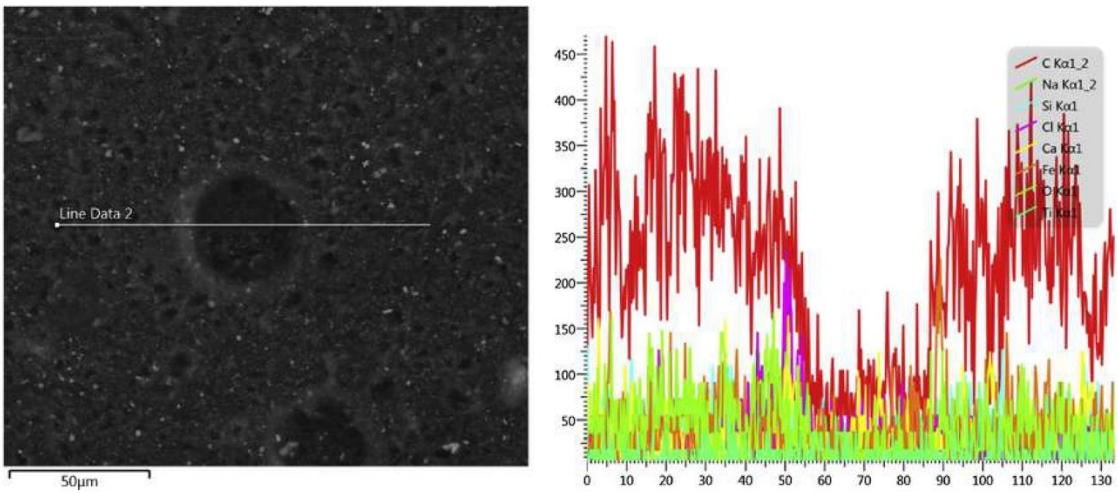

Fig. 15. SEM/EDX analysis of a crater defect on the coating A. (1.5 column fitting).

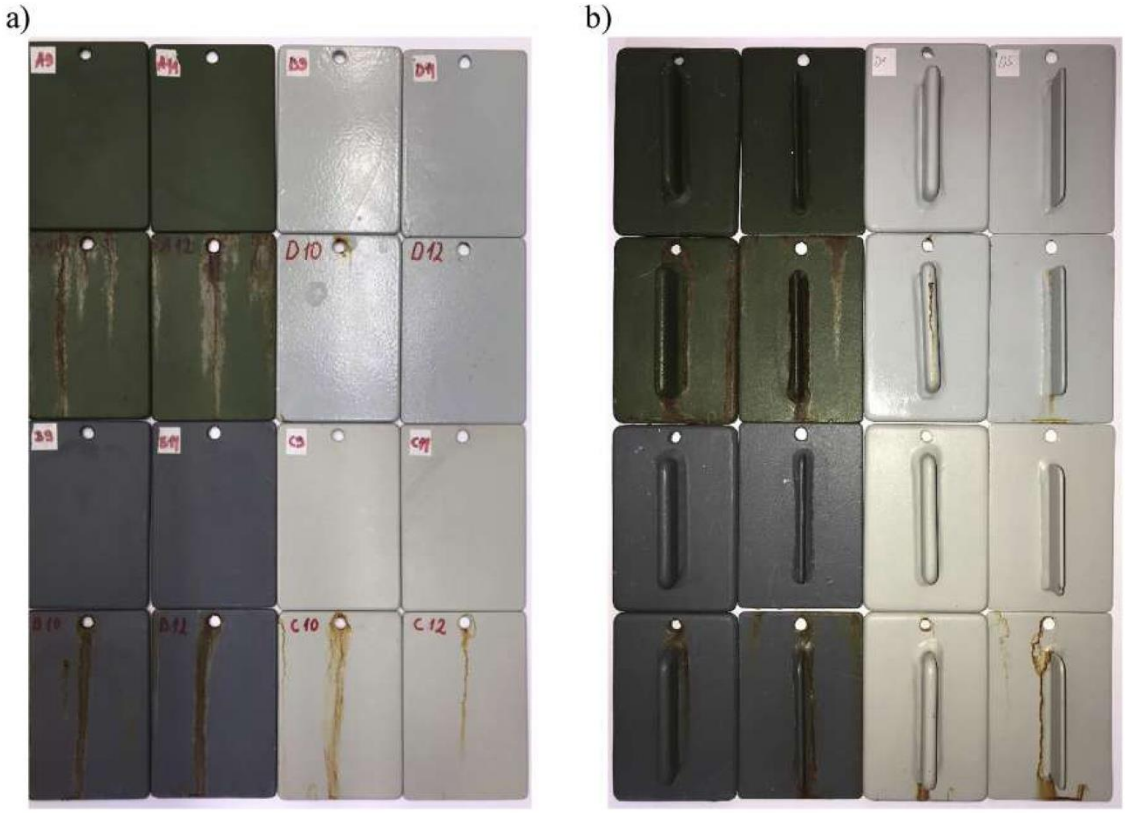

Fig. 16. Visual appearance of the flat and T-welded samples after 720 h of the EN ISO 9227 NSS test. (double column fitting).

Analysis in Fig. 15, has shown the presence of various coating components as well as the substrate signal. The most intensive signal belonged to carbon that was weakened within the area of the crater. This indicates a significant thinning of the coating that could have contributed to the compromised performance of coating A in impedance tests.

Fig. 16 a and b show four flat and four T-welded specimens of each coating type after 720 h of the EN ISO 9227 NSS test, placed counterclockwise, starting from coating A in the upper left corner to coating D in the upper right corner. For each coating type, the upper pair of specimens were unexposed and the lower pair of specimens were NSS exposed. The left pair of specimens of each coating type was made of 1 cm thick steel plates and the right pair of specimens of 3 mm thick steel plates. Samples edges and welds were lacking stripe coats, so that rust leaking was observed for all the coatings. However, the extent of rust leakage is most pronounced for coating A and getting less visible for coatings in a sequence from B to D.

3.7. Conclusion

$Re(Q_1[R_1(Q_2R_2)])$ equivalent circuit was found to yield an excellent fit to the impedance spectra of the tested industrial coating systems. Elements of the $R_e(Q_1[R_1(Q_2R_2)])$ equivalent circuit may be given the physical meaning within the dielectric permittivity and porous coating formalisms. The equivalent circuit parameters, as well as the impedance modulus at 0.1 Hz, show two types of behavior: (i) attainment of stable values after prolonged exposure, probably corresponding to the

maximum water saturation and maximum amount and mobility of ionic impurities released within the coating and (ii) a continuous decline with exposure, probably corresponding to the appearance of the coating porosity. Maximum of tanδ, that equals a resistive to the capacitive current ratio in both formalisms, shows the dipole relaxation response for excellent barrier coatings and/or for short exposure times. For the longer exposures, tanδ maximum of high intensity may appear at low frequencies indicating a highly dispersive phenomenon of interfacial polarization or the substrate active area. Significant increase in tanδ with cathodic polarization as well as the visible formation of blisters may help distinguish between the two aforementioned phenomena. The coating that has shown a continuous decline of impedance with exposure to corrosive environments to the level below 10^6 Ω cm^2, has also shown cratering defects in the intact state, a decline in the pull-off adhesion by 50 % after exposure, the appearance of corrosion spots at the substrate exposed by the pull-off test, the appearance of blisters in the vicinity of the edges and the most pronounced rust leaching from the edges and welds lacking stripe coats. The other coatings have shown only the rust leaching to the extent that correlated with the order of their barrier quality predicted by EIS.

CRediT authorship contribution statement

Sanja Martinez: Conceptualization, Methodology, Writing - original DRAFT, Writing - review & editing. **Ivana Šoić:** Investigation, Visualization, Methodology. **Vedrana Špada:** Resources, Validation.

Declaration of Competing Interest

The authors report no declarations of interest.

Acknowledgements

This work was performed with the support of the Zagreb Innovation Centre, within Startup Factory BATCH 2019 Programme.

References

[1] S.B. Lyon, R. Bingham, D.J. Mills, Advances in corrosion protection by organic coatings: what we know and what we would like to know, Prog. Org. Coat. 102 (2017) 2–7.
[2] I.C.P. Margarit-Mattos, EIS and organic coatings performance: revisiting some key points, Electrochim. Acta 354 (2020), 136725.
[3] G. Bierwagen, D. Tallman, J. Li, L. Hea, C. Jeffcoate, EIS studies of coated metals in accelerated exposure, Prog. Org. Coat. 46 (2003) 148–157.
[4] B.J. Merten, M.T. Walsh, J.D. Torrey, Validation of coated infrastructure examination by electrochemical impedance spectroscopy, in: S. Papavinasam, R. Rebak, L. Yang, N. Berke (Eds.), Advances in Electrochemical Techniques for Corrosion Monitoring and Laboratory Corrosion Measurements, ASTM International, West Conshohocken, 2019, pp. 137–159.
[5] B.R. Hinderliter, S.G. Croll, D.E. Tallman, Q. Su, G.P. Bierwagen, Interpretation of EIS data from accelerated exposure of coated metals based on modeling of coating physical properties, Electrochim. Acta 51 (2006) 4505–4515.
[6] G. Bouvet, D.D. Nguyen, S. Mallarino, S. Touzain, Analysis of the non-ideal capacitive behavior for high impedance organic coatings, Prog. Org. Coat. 77 (2014) 2045–2053.
[7] H. Hayashibara, E. Tada, A. Nishikata, Monitoring the early stage of degradation of epoxy-coated steel for ballast tank by electrochemical impedance spectroscopy, Mater. Trans. 58 (2017) 1687–1694.
[8] D. Wang, E. Sikora, B. Shaw, A study of the effects of filler particles on the degradation mechanisms of powder epoxy novolac coating systems under corrosion and erosion, Prog. Org. Coat. 121 (2018) 97–104.
[9] J. Niu, J.I. Barraza-Fierro, H. Castaneda, Quantification of protective properties of the coating/corrosion product/steel interface by integration of transmission line model with EIS results, J. Coat. Technol. Res. 12 (2015) 393–405.
[10] G. Cai, H. Wang, D. Jiang, Z. Dong, Impedance sensor for the early failure diagnosis of organic coatings, J. Coat. Technol. Res. 15 (6) (2018) 1259–1272.
[11] Y. Lee, Y.T. Kuo, H.H. Chen, Y.A. Hsieh, Field-Programmable Gate Array-Based Coating Impedance Detector for Rapid Evaluation of Early Degradation of Protective Coatings, IEEE Access 7 (2019) 2047–20478.
[12] M.H. Nazir, Z.A. Khan, A. Saeed, A Novel Non-Destructive Sensing Technology for On-Site Corrosion Failure Evaluation of Coatings, IEEE Access 6 (2018) 1042–1054.
[13] K. Tokutake, H. Nishi, D. Ito, S. Okazaki, Y. Serizawa, Prog. Org. Coat. 87 (2015) 69–74.
[14] B. Zajec, M. Bajt Leban, S. Lenart, K. Gavin, A. Legat, Electrochemical impedance and electrical resistance sensors for the evaluation of anticorrosive coating degradation, Corros. Rev. 35 (2017) 1348–1355.
[15] I. Šoić, S. Martinez, M. Dubravić, Gel-Electrolyte EIS setup used for probing of IR Dried/Cured industrial coatings, Prog. Org. Coat. 137 (2019) 105331.
[16] A. Amirudin, D. Thierry, Application of electrochemical impedance spectroscopy to study the degradation of polymer-coated metals, Prog. Org. Coat. 26 (1995) 1–28.
[17] S. Haruyama, M. Asari, T. Tsuru, Mass transport in blistering of coating steel, in: M. W. Kendig, H. Leidheiser (Eds.), Proc. Symp. Corrosion Protection by Organic Coatings, The Electrochemical Society. USA, 1987, p. 197.
[18] S. Duval, M. Keddam, M. Sfaira, A. Srhiri, H. Takenouti, Electrochemical impedance spectroscopy of epoxy-vinyl coating in aqueous medium analyzed by dipolar relaxation of polymer, J. Electrochem. Soc. 149 (2002) B520–B529.
[19] A. Roggero, N. Causs, E. Dantras, L. Villareal, A. Santos, N. Pebere, Thermal activation of impedance measurements on an epoxy coating for the corrosion protection: 1. Dielectric spectroscopy response in the dry state, Electrochim. Acta 303 (2019) 239–245.
[20] A. Roggero, N. Causs, E. Dantras, L. Villareal, A. Santos, N. Pebere, Thermal activation of impedance measurements on an epoxy coating for the corrosion protection: 2. electrochemical impedance spectroscopy study, Electrochim. Acta 305 (2019) 116–124.
[21] P. Pissis, A. Kyritsis, Electrical conductivity studies in hydrogels, Solid State Ion. 97 (1997) 105–113.
[22] R. Raihan, F. Rabbi, V. Vadlamudi, K. Reifsnider, Composite Materials Damage Modeling Based on Dielectric Properties, Mater. Sci. Appl. Chem. 6 (2015) 1033–1053.
[23] F. Kremer, A. Schönhals (Eds.), Broadband Dielectric Spectroscopy, Springer-Verlag, Berlin Heidelberg, 2003, p. 61.
[24] A. Fukuda, H. Mitsui, Y. Inoue, K. Goto, The influence of Water absorption on dielectric properties of cycloaliphatic epoxy resin, in: Proceedings of the 5" International Conference on Properties and Applications of Dielectric Materials, Seoul, Korea,, 1997, pp. 58–61.
[25] A.A. Korzhenko, M. Tabellout, J.R. Emery, Dielectric relaxation properties of the polymer coating during its exposition to water, Mater. Chem. Phys. 65 (2000) 253–260.
[26] M.A. Omri, M.R. Sanjay, A. Triki, B. Yogesha, A. Kallel, Dielectric properties and interfacial adhesion of jute, Kenaf and E-Glass fabrics reinforcing epoxy composites, Polym. Compos. 40 (2019) 2142–2153.
[27] M.R.P. Elenchezhian, V. Vadlamudi, P.K. Banerjee, C. Dave, A. Mahmood, R. Raihan, K. Reifsnider, Quality assessment of adhesive bond based on dielectric properties, in: SAMPE Conference Proceedings, Seattle, WA, 2017, pp. 1–14.
[28] D. Quiang, Dielectric Properties of Epoxy Based Nanocomposites Filled With Nano SiO2 and BN and Moisture Effects, PhD Thesis, University of Southampton, 2017.
[29] M. Samet, V. Levchenko, G. Boiteux, G. Seytre, A. Kallel, A. Serghei, Electrode polarization vs. Maxwell-Wagner-Sillars interfacial polarization in dielectric spectra of materials: characteristic frequencies and scaling laws, J. Chem. Phys. 42 (2015) 194703.
[30] A. Korzhenko, M. Tabellout, J.R. Emery, Influence of a metal–polymer interfacial interaction on dielectric relaxation properties of polyurethane, Polymer 40 (1999) 7187–7195.
[31] A. Korzhenko, M. Tabellout, J.R. Emery, Application of dielectric relaxation spectroscopy to study metal/polymer interfacial interaction, Ferroelectrics 228 (1999) 249–256.
[32] S. Duval, Y. Camberlin, M. Glotin, M. Keddam, F. Ropital, H. Takenouti, Characterisation of organic coatings in sour media and influence of polymer structure on corrosion performance, Prog. Org. Coat. 39 (2000) 15–22.
[33] D.I. Abouelamaiem, G. He, T.P. Neville, D. Patel, S. Ji, R. Wang, I.P. Parkin, A. B. Jorge, M.-M. Titirici, P.R. Shearing, D.J.L. Brett, Correlating electrochemical impedance with hierarchical structure for porous carbon-based supercapacitors using a truncated transmission line model, Electrochim. Acta, Volume 284 (2018) 597–608.
[34] C.H. Hsu, F. Mansfeld, Technical Note: Concerning the Conversion of the Constant Phase Element Parameter Y0 into a Capacitance, Corrosion 57 (2001) 747–748.
[35] Chen Zou, J.C. Fothergill, S.W. Rowe, The effect of water absorption on the dielectric properties of epoxy nanocomposites, IEEE Trans. Dielectr. Electr. Insul. 15 (2008) 106–116.
[36] D. Vaishampayan, Dielectric Spectroscopy of Bisphenol A Epoxy Resin Aged in Wet and Dry Conditions, Master Thesis, Norwegian University of Science and Technology, 2009.
[37] S. Touzain, Q. Le Thu, G. Bonnet, Evaluation of thick organic coatings degradation in seawater using cathodic protection and thermally accelerated tests, Prog. Org. Coat. 52 (2005) 311–319.
[38] F.E. Bedoya, F. Echeverría, J.A. Calderón, Effectiveness of non-Fickian diffusion model on the water uptake determination of different organic coatings, Prog. Org. Coat. 136 (2019) 105206.
[39] H.M. Ha, A. Alfantazi, On the role of water, temperature, and glass transition in the corrosion protection behavior of epoxy coatings for underground pipelines, J. Coat. Technol. Res. 12 (2015) 1095–1110.
[40] T.C. da Silva, S. Mallarino, S. Touzain, I.C.P. Margarit-Mattos, DMA, EIS and thermal fatigue of organic coatings, Electrochim. Acta 318 (2019) 989–999.
[41] N. Fredj, S. Cohendoz, X. Feaugas, S. Touzain, Effect of mechanical stresses on marine organic coating ageing approached by EIS measurements, Prog. Org. Coat. 72 (2011) 260–268.

[42] N. Fredj, S. Cohendoz, X. Feaugas, S. Touzain, Effect of mechanical stress on kinetics of degradation of marine coatings, Prog. Org. Coat. 63 (2008) 316–322.
[43] S. Touzain, Q. Le Thua, G. Bonnet, Evaluation of thick organic coatings degradation in seawater using cathodic protection and thermally accelerated tests, Prog. Org. Coat. 52 (2005) 311–319.
[44] B. Hirschorn, M.E. Orazem, B. Tribollet, V. Vivier, I. Frateur, M. Musiani, Determination of effective capacitance and film thickness from constant-phase-element parameters, Electrochim. Acta 55 (2010) 6218–6227.
[45] K. Deshmukh, S. Sankaran, B. Ahamed, K.K. Sadasivuni, K.S.K. Pasha, D. Ponnamma, P.S.R. Sreekanth, K. Chidambaram, Spectroscopic Methods for Nanomaterials Characterization, Elsevier, 2017, p. 237.
[46] Z. Kefallinou, S.B. Lyon, S.R. Gibbon, A bulk and localised electrochemical assessment of epoxy-phenolic coating degradation, Prog. Org. Coat. 102 (2017) 88–98.
[47] H. Hayashibara, E. Tada, A. Nishikata, Evaluation of epoxy coating for ballast tanks under thermal cycling by electrochemical impedance spectroscopy, ISIJ Int. 56 (2016) 2029–2036.

APPENDIX III

I. Šoljić, I. Šoić, L. Kostelac, S. Martinez, AC interference impact on EIS assessment of organic coatings using dummy cells, calibration foils and field exposed coated samples, Prog. Org. Coat. 165 (2022) 106767

https://doi.org/10.1016/j.porgcoat.2022.106767

Ines Šoljić: investigation, methodology, writing - original draft, review & editing.
Ivana Šoić: visualization, methodology, review & editing.
Lorena Kostelac: investigation, validation.
Sanja Martinez: conceptualization, methodology, writing- original draft, writing - review & editing.

Progress in Organic Coatings 165 (2022) 106767

Contents lists available at ScienceDirect

Progress in Organic Coatings

journal homepage: www.elsevier.com/locate/porgcoat

AC interference impact on EIS assessment of organic coatings using dummy cells, calibration foils and field exposed coated samples

Ines Šoljić, Ivana Šoić *, Lorena Kostelac, Sanja Martinez

Department of Electrochemistry, Faculty of Chemical Engineering and Technology, University of Zagreb, Marulićev trg 19, 10000 Zagreb, Croatia

ARTICLE INFO

Keywords:
EIS
Coating
Polyester
AC interferences

ABSTRACT

Field application of EIS to intact and scarcely degraded high-performance protective coatings is challenging because of ambient electromagnetic fields, which cause stochastic variations in the phase angle and, to a lesser extent, in the impedance modulus of the coating spectra. AC interferences with amplitudes between 10 and 800 mV were induced on dummy cells and calibration foils to systematically investigate the effects of interference impact on the accuracy and precision of measurements with the EIS setup intended for use on coatings in the field. For EIS signal amplitudes between 10 and 250 mV and the AC interference amplitudes ≤250 mV, the measurement accuracy and precision were limited by the synergistic influence of the AC interferences and the imprecision of the EIS instrument. For systems with impedance ≥ GΩ, the accuracy of the impedance logarithm was 97.8% at signal amplitudes ≥190 mV, and the precision increased from nearly 95% to 99% as the signal amplitude increased from 10 to 150 mV, indicating that very accurate and precise measurements can be obtained at higher signal amplitudes. An example of EIS measurements on coated samples exposed in the area of AC railway interferences is given. Although the quantitative conclusions may be instrument specific, they reflect well the declared capabilities of today's high-end EIS devices. The universal explanation is given in the context of equivalent circuit theory of the observed scatter in the EIS spectral data. The coating assessment was commented on in terms of the unique properties of the mean and relative standard deviation of impedance expressed on the logarithmic scale.

1. Introduction

Efforts are constantly being made to overcome the challenges of the field application of the Electrochemical Impedance Spectroscopy (EIS) method to protective coatings and significant advancements has been made by many researchers [1–7]. Our previous work addressed instrumental improvements aimed at increasing simplicity and speed of application [8,9], theoretical development of the equivalent circuit model that accounts for ionic space charge movement in a coating as a dielectric [10], simplification of coating assessment criteria, correlation to visual observations, and results of complementary methods [9,10]. In the present study, we focus on the effects of AC interferences of constant amplitudes, controlled under laboratory conditions, on the EIS measurements on dummy cells and calibration foils mimicking industrial coatings in intact state and in early stages of degradation.

In the laboratory and in the field, the coating impedance measurement system may be subject to electromagnetic interferences from various sources. Interferences are man-made signals [11] which are carried by electromagnetic radiation and picked up by inductive coupling between the interference source and the measurement circuit. The most common source of interference in the laboratory is the power grid and in the field are AC power lines, although many other sources are possible, including electric power tools, ignition circuits in gasoline engines, and arc-welding equipment [12]. In most cases, interferences will give a signal at the principal frequency of 50 or 60 Hz [11,13,14], but may also include some signals at multiples of the power line frequency (harmonics and subharmonics) [12,15]. While in laboratory practice AC interferences can be minimized by making measurements in a Faraday cage [4,10,12,16], experiments conducted outdoors may contain unavoidable noise in the data sets [4]. The ability to distinguish signals from noise is an important issue in the application of many measurement techniques, e.g., measuring the signal-to-noise ratio is one of the key factors in quantifying the performance of brain recording devices [17]. The quality of impedance data precisely refers to the signal-to-noise ratio [18], which is limited by the amplitude of the excitation signal [18–24].

* Corresponding author.
E-mail address: ivana.soic@fkit.hr (I. Šoić).

https://doi.org/10.1016/j.porgcoat.2022.106767
Received 13 September 2021; Received in revised form 26 January 2022; Accepted 3 February 2022
Available online 12 February 2022

On bare metal electrodes, the amplitude of the imposed signal must be as small as possible to create quasi-linear conditions and high enough to achieve an acceptable signal-to-noise ratio [15,25,26]. For EIS measurements on coatings, it is common to apply a voltage between 10 and 50 mV [6]. Although higher amplitudes may be required for samples with very high impedance [6], low amplitudes (10–20 mV) are mainly applied to protective coatings with high resistivity (10^9–10^{12} Ω cm^2) [4,16]. On the other hand, dielectric spectroscopy, which deals mostly with dry, undegraded dielectrics, uses amplitudes proportional to 1 V [27,28], much higher than those used by electrochemists. Akbarinezhad et al. [29] argue that it is possible to use a high AC signal amplitude to evaluate the performance of an intact highly resistant coating without damaging the coating. The authors offer a phenomenological explanation that for the coating of high impedance a very low AC current can flow through the circuit and this can cause some fluctuations in the measured data. The application of a high EIS input AC signal, namely 400 mV, causes a reduction of the fluctuations, while at 5 mV they are very marked. As the AC signal amplitude increases, the AC current flowing through the circuit is increased and this causes a decrease in the fluctuations.

A strong motivation for this work stems from our own experience with field measurements, as well as from a large number of studies demonstrating the scatter of EIS data of commercial coating systems obtained with low signal amplitudes [4,7,29,30]. In general, the factors responsible for poor reproducibility of EIS data can be divided into errors caused by the coating/metal system (thickness variations, defects, inhomogeneity of the metal substrate) and errors caused by the EIS device and the measurement procedure (setup of the EIS device, electrode configuration, current and voltage distribution, measurement protocol) [31,32]. Bonitz et al. [33] suggest that by using defined, homogeneous, and relatively defect-free polymer films, the sources of error in the EIS data related to the samples themselves can be reduced or eliminated. In this way, it is possible to investigate the data variability arising from the EIS measurement process, such as edge effects arising from non-uniform field and current distributions, and the importance of the impedance limit of the potentiostat.

Guided by the ideas of Akbarinezhad et al. [29] and Bonitz et al. [33], we investigated the influence of AC interference on EIS measurements of various signal amplitudes performed on 100–250 µm thick commercial polyester films and a high-impedance dummy cell constructed according to EN ISO 16773-3. Polyester films, which are very close to commercial coating systems in terms of dielectric constant [34,35] and thicknesses defined in EN ISO 12944-5, and a high impedance dummy cell, a relatively rarely applied calibration standard for potentiostats [33], have been used to mimic intact coatings or coatings in the early stages of degradation. The physical picture is drawn, explaining the observed phenomena within the framework of the equivalent circuits and the influence of the AC interferences on the accuracy and precision of measurement as well as on the coating assessment decision rule is quantified.

2. Experimental

2.1. Materials

EIS measurements were performed on a high impedance dummy cell, Xerox Never Tear, commercial polyester films with nominal thicknesses of 110, 135, 185, and 240 µm, and on samples coated with four coating systems according to EN ISO 12944-6. Measurement setups are showed in Fig. 1. The dummy cell was constructed according to EN ISO 16773-2 and 3. The circuit elements were of the order of magnitude expected for the actual coated samples. The circuit element values with measurement uncertainties determined by an accredited calibration laboratory are listed in Table 1.

The average thickness of the foils from 10 measurements done with Elcometer 945 on a flat steel substrate, is given in Table 2.

Carbon steel specimens (150 × 75 mm) were prepared according to chapter 5.11. of EN ISO 12944-5. System 1 was an alkyd system and

Table 1
Circuit element values determined by an accredited calibration laboratory.

Element	Circuit 1	Circuit 2	Circuit 3	Circuit 4
C_1/pF	152.54	151.37	101.92	10,010
R_1/MΩ	61,810	1045	1004	102.86
C_2/pF	–	472.66	20,060	9980
R_2/MΩ (+R_3/MΩ)*	–	10,074	202.78	100.65
R_{TOT}/MΩ	61,810	11,120	1206.78	203.51

* for circuit 3 of the dummy cell in Fig. 1.

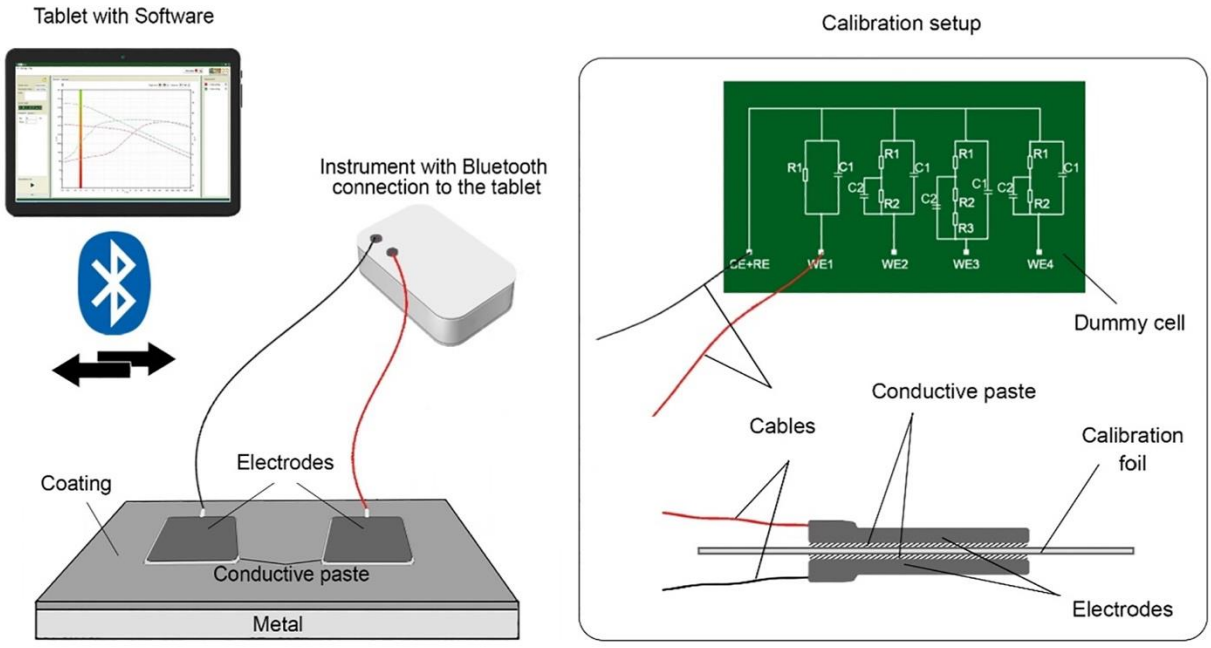

Fig. 1. Setup for coating impedance measurement and calibration measurements on a dummy cell and a calibration foil.

Table 2
Nominal and measured thickness of calibration foils.

Nominal foil thickness/µm	Average foil thickness/µm	Standard deviation/µm
110	110.0	1.8
135	131.6	1.4
185	180.0	2.0
240	234.9	2.6

systems 2 through 4 were epoxy polyurethane systems from three different paint manufacturers. The total thickness of the coating systems on the samples exposed in the field is shown in Table 3. It was measured with Elcometer 945 according to chapter 5.2 of EN ISO 2808.

Raw measurement data are accessible at DOI: 10.17632/r8wf8b64xz.1.

2.2. Methods

AC interference measurements were carried out by the ReCorr® QCQ (Quantitative Coating Quality) [8] device and ReCorr® QCQ electrically conductive paste developed in our laboratory.

Fig. 1 shows the setup for coating impedance measurement and calibration measurements on a dummy cell and a calibration foil. The setup consists of an EIS measuring instrument with shielded cables leading to the two flexible, conductive carbon- based polymer electrodes, each with an area of 25.5 cm^2, and a natural wax and carbon-based paste that allows easy and fast EIS measurements on coatings in the intact/dry state or during exposure to natural or artificial moist corrosive environments. The electrodes adhere to the flat or curved coating surfaces by the aid of the sticky paste electrolyte, after they are firmly pressed for a few seconds (against the flat surfaces) or two minutes (against the curved surfaces). During measurements on a dummy cell, the instrument's cables are connected to the terminals of one of the four circuits. For measurements on foils, the electrodes were attached to the opposite surfaces of the foils, facing one another. For measurements on coatings, the electrodes were attached to the surface of the coating. In the case of a highly insulating coating, stabilization is not required because the electrolyte is not in contact with the substrate. This is consistent with point 7.5. of the standard HR EN ISO 16773-2, which states that the open-circuit potential is not well defined for coated metal samples that are in excellent condition. The electrodes are identical so that the DC offset potential is set to zero. The frequency range used in the measurements was between 10^5 and 10^{-2} Hz with signal amplitudes from 10 to 250 mV. The amplitudes of the interference AC voltage were 0, 25, 50, 100, 250, 800 mV. The source of interference was a transformer, or more precisely the transformer coil, near which a measuring system was placed. Measurements were made at each signal amplitude outside and inside the Faraday cage to determine the influence of AC interference on the measurements.

3. Results and discussion

3.1. The influence of AC interferences on dummy cell impedance

A measurement circuit, subject to electromagnetic interference and containing a dummy cell, a calibration foil, or a coating is represented by an equivalent circuit shown in Fig. 2, where C_c is the coating capacitance, R_c is the coating resistance, and Z is the impedance, which may

Table 3
Total coating system thickness on the field exposed samples.

Sample	Average coating thickness/µm	Standard deviation/µm
System 1	148	24
System 2	147	26
System 3	209	16
System 4	238	30

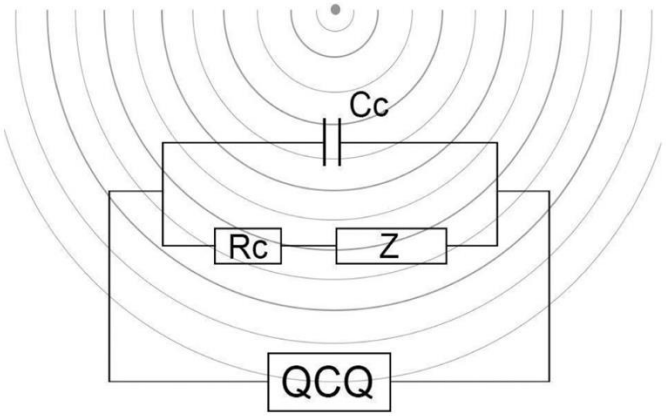

Fig. 2. Equivalent circuit of the measurement setup for measuring the impedance of a dummy cell, a calibration foil or a coating.

represent ionic space charge movement [9], active substrate area, and diffusion phenomena [36]. The elements C_c and R_c correspond to the elements C_1 and R_1 of the dummy cell.

Controlled generation of interferences was achieved by appropriate placement of the experimental setup within the magnetic field of a transformer (Iskra POBI RSO Z 76186). Many laboratory and household devices that generate an electromagnetic field can also be used for controlled interference generation. The open circuit potential, measured as a function of time between the terminals of the instrument, with any of the loads (dummy cells, foils or coating) in between, represents the interference voltage. It is shown in Figs. 3 and 4 along with the spectral intensity of the interferences in the frequency domain. The purpose of this built-in software feature is to quantify the effects of interference on the measurement system by measuring the induced voltage and to eliminate the need to use complicated methods to measure the electromagnetic field. Moreover, the interference effect depends not only on the field intensity but also on the alignment of the measurement system within the field. Therefore, in addition to increasing the measurement amplitude, interference management also includes aligning the measurement setup within the field or changing the measurement position to minimize the interference effect.

Inside the Faraday cage, a signal with a maximum of 8×10^{-5} V is typically observed (Fig. 3a) and the interference spectrum (Fig. 3b) shows no distinct main frequency. The shape of the interference voltage obtained outside the Faraday cage for all samples investigated in this study is sinusoidal and is shown in Fig. 4. The amplitude of the AC interference can be read from the graph, and represents the level of interference, that is controlled in the present study (a case of the 250 mV interference is shown in Fig. 4). A sinusoidal signal is also typically observed outside the Faraday cage (Fig. 4a). The interference spectrum in Fig. 4b shows the main frequency of 50 Hz, a subharmonic at 25 Hz and higher harmonics at 150, 250, 350, 450 and 550 Hz with much lower intensity. Under uncontrolled conditions, such as the field measurements, the sinusoidal signal may be distorted due to the specifics of the electronics causing the interference or in the presence of multiple interference sources.

While the power of the interference source and the measurement setup remained unchanged and no impressed current was present in the circuit, the respective induced AC voltage amplitudes of 280, 250, 280 and 12 mV were measured for circuits 1 to 4. Fig. 5 shows Bode spectra of the four dummy cell circuits recorded inside and outside the Faraday cage at the signal amplitudes of 10 and 250 mV. AC Interferences manifest themselves at the signal amplitude of 10 mV as pronounced stochastic variations of the phase angle and much less pronounced variations of Log Z.

The above observations and the spectra in Fig. 5 can be explained as follows:

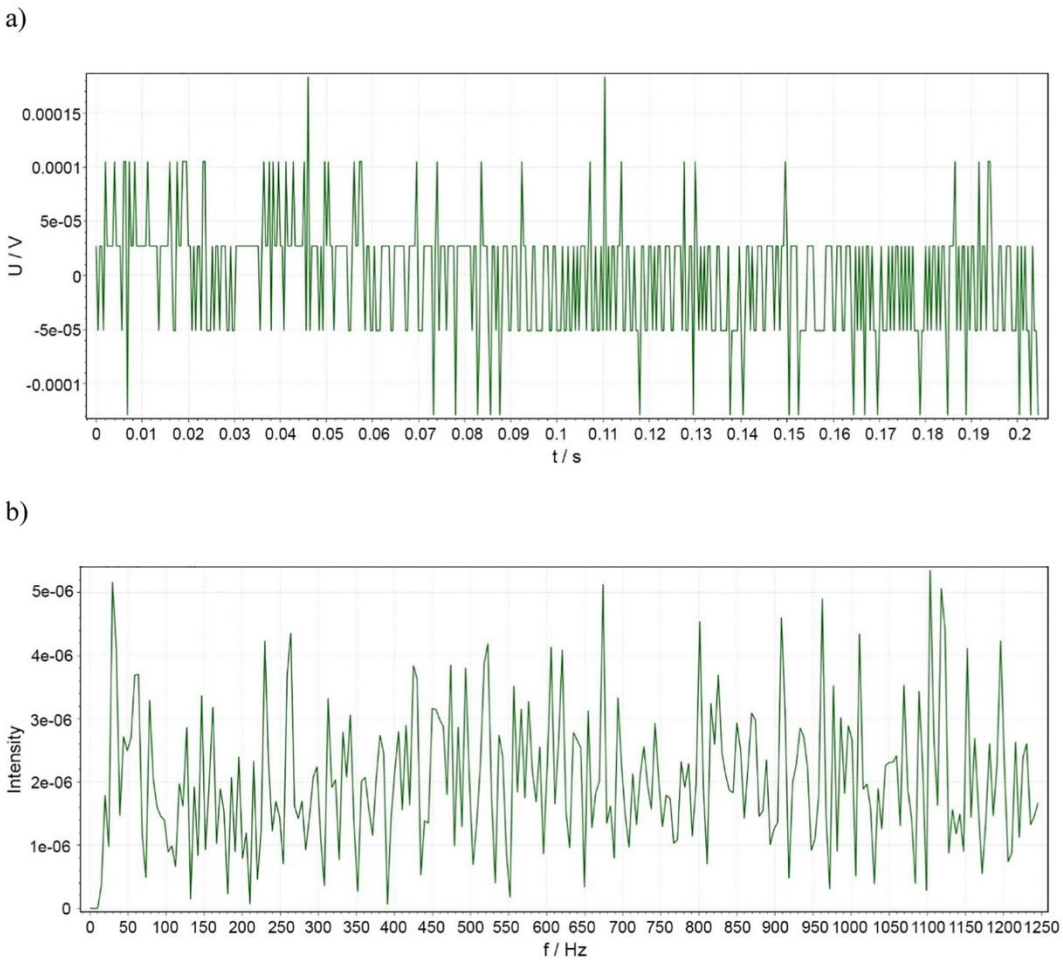

Fig. 3. Typical a) AC interference voltage inside the Faraday cage and b) the corresponding signal spectrum observed in this study.

1. A variable electromagnetic field causes a 50 Hz interference voltage difference between the terminals of a dummy cell. For an interference source of constant power and identical experimental setups, the amplitude of the induced voltage measured is similar for the circuits with comparable Z at 50 Hz (19 ± 0.27 MΩ 21.1 ± 0.02 MΩ, 28.7 ± 0.08 MΩ for circuits 1 and 2, 3) and significantly smaller for circuit 4 that has Z at 50 Hz equal to 0.325 ± MΩ.
2. During the measurement, the input signal counteracts the interference to achieve the target voltage at the terminals of a dummy cell. At high signal frequencies, the impressed current passes through the *Cc* branch of the circuit and the measurement is fast enough so that during the measurement the interference voltage variation is not significant and is easily compensated by the signal. Therefore, no noise at high frequencies is observed in the plots in Fig. 5 for all otherwise noisy spectra recorded at the signal amplitude of 10 mV.
3. For purely capacitive behaviour of the coating, as the frequency of the signal voltage decreases, the impedance increases and so does the rate of charging the capacitor, making it more difficult to counteract the interference voltage. For Circuit 1 and the signal amplitude of 10 mV (Fig. 5a), capacitive behaviour and the interference effect are observed throughout the middle and lower frequency ranges.
4. In Circuits 2 and 3 (Fig. 5b and c, respectively), a transition between capacitive and resistive behaviour occurs at intermediate frequencies, and the impressed current is distributed between *Rc* and *Cc* branches. The interference effect is observed as long as the capacitive component is present and ceases when the resistive behaviour becomes dominant. Below 0.1 Hz, the measurement is no longer significantly affected by the AC interference because the compensation of the impressed voltage is no longer limited by the charging rate of the capacitor. The impressed current flows through an ohmic resistor which has a constant resistance over the entire applied frequency range.
5. As the coating capacitance increases and the coating resistance decreases, which is characteristic of the water uptake and degradation of the coating, the influence of the AC interferences diminishes. For example, for circuit 4 no influence is observed. It can be concluded that the AC interferences will only be a problem for the intact coatings and coatings in the early stages of degradation.
6. At a signal amplitude of 250 mV, no significant data scattering is observed for all dummy cell circuits, indicating that the interference influence can be mitigated at a sufficiently high signal amplitude. This observation is commented on in the following section.

The impedance spectra from Fig. 5 were fitted to the equivalent circuits shown in Fig. 1. The spectra of circuits 1 to 3, recorded outside the Faraday cage at an amplitude of 10 mV, were not fitted because of the large dispersion of the phase angle data. The accuracy of the measurements is checked by calculating the percentage error of the fitted values of the R and C parameters with respect to the R and C values measured by independent methods in the accredited calibration laboratory.

The accuracy required by EN ISO 16773 for the R and C components of the circuit is 2% for resistors below 10^9 Ω and 5% for resistors above 10^9 Ω and the capacitors. The errors for the R and C elements in Table 4 are in most cases smaller than or slightly above the required accuracy for the elements. Moreover, the error calculated for the total ohmic

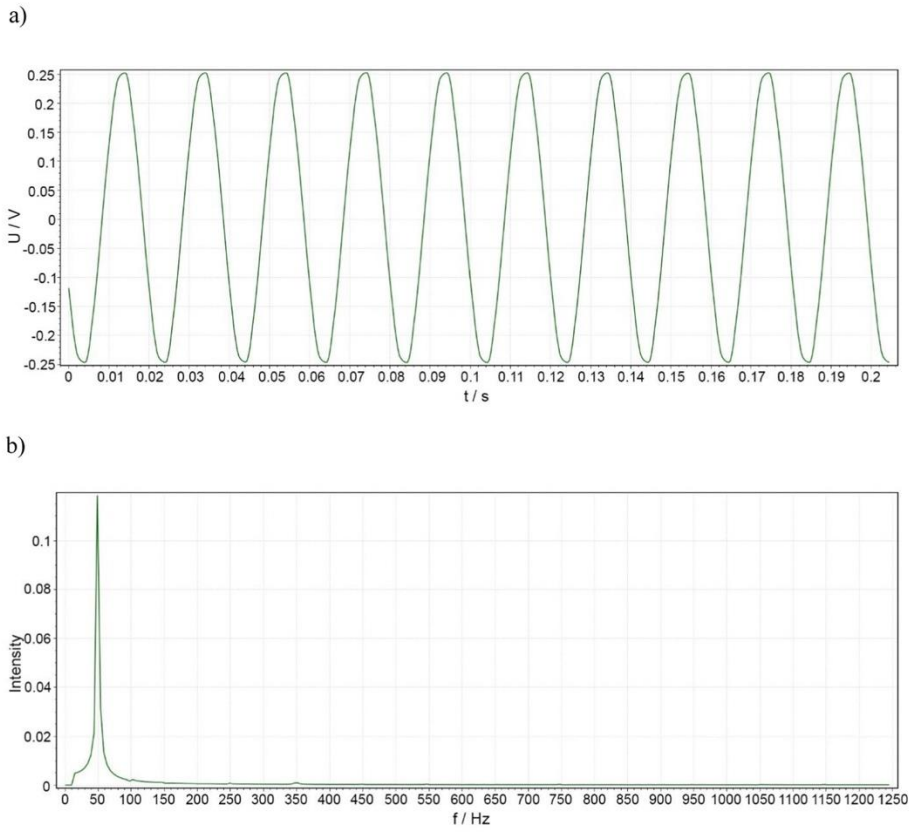

Fig. 4. Typical a) AC interference voltage outside the Faraday cage and b) the corresponding signal spectrum observed in this study.

resistance of the circuits is below 2.2% for the 10 GΩ circuit and 0.9% for the 10 < GΩ circuit, indicating a sufficiently accurate measurement of the most important parameter related to the coating quality.

The acceptable accuracy of 97.8% obtained at the maximum signal amplitude of 250 mV shows that nonlinearity does not affect the result when the measurement was performed on a dummy cell. Therefore, it can be considered that nonlinearity is not a problem for coatings in the early stages of degradation, since the active substrate area below the coating is not exposed and the main phenomena detected by EIS is water uptake by the coating, dipole and ionic space charge movement [9].

The main purpose of using the dummy cell was to demonstrate that without interference the total ohmic resistance, the most important parameter of coating barrier property, is measured with sufficient accuracy. From the overlap of the curves in Fig. 5, it is evident that the main effect of exiting the Faraday cage is related to the loss of precision. Therefore, in the remainder of the text, we have studied the effects of the various sources of uncertainty on measurement precision.

It should be noted that the further statistical analysis related to the assessment of the coating in this paper is performed in terms of the impedance modulus at 0.1 Hz on a logarithmic scale. The frequency of 0.1 Hz was chosen because it represents a compromise between the speed of the measurement and the accuracy of measuring the coating DC resistance. For intact and high-performance coatings (Log $Z_{0.1Hz}$ > 8) this value underestimates the DC resistance as these coatings behave as almost perfect capacitors i.e., perfect insulators. Nevertheless, this value is still of practical significance because, first, it indicates that the coating is an excellent barrier, and second, it is higher for thicker coatings (as demonstrated for foils in Fig. 8), indicating that a thicker, dry coating is a better barrier than the thinner one. For partially degraded industrial coatings (8 > Log $Z_{0.1Hz}$ > 6), the capacitive behaviour shifts to higher frequencies and the 0.1 Hz impedance value falls into the resistive behaviour range [37–41]. For such coatings, the 0.1 Hz impedance reflects well the DC resistance limit of the coating and its barrier effect. For highly degraded coatings (Log $Z_{0.1Hz}$ < 6) Log $Z_{0.1Hz}$ may be influenced by the polarisation resistance of the active surface beneath the coatings. However, coatings with Log $Z_{0.1Hz}$ < 6 commonly show visible damage so the purpose of the EIS testing is lost [42].

In the rest of the text, Log Z refers to Log (Z@0.1 Hz/Ω). According to the ISO/IEC Guide 98, the average value of Log Z (Z_{AVG}), standard deviation (SD), relative standard deviation (RSD), and 95% confidence intervals ($CI_{95\%}$) are calculated using the equations:

$$Log\ Z_{AVG} = \frac{1}{n}\sum_{i=1}^{n}(LogZ_i) \tag{1}$$

$$STD = \sqrt{\frac{1}{n-1}\sum_{i=1}^{n}(Log\ Z_i - Log\ Z_{AVG})^2} \tag{2a}$$

$$RSD = \frac{STD}{Z_{AVG}}100\% \tag{2b}$$

$$CI_{95\%} = \frac{STD}{\sqrt{n}}1.960 \tag{2c}$$

Fig. 6 shows Log Z, SD as error bars, RSD and $CI_{95\%}$ confidence intervals following the trend of RSD obtained for each dummy cell circuit at the signal amplitudes of 250 and 10 mV and an interference amplitude of 250 mV. SD, RSD and $CI_{95\%}$ are related to measurement uncertainty and, since the standard deviation is calculated for a set of repeated measurements, also to measurement repeatability. The increase in precision from circuit 1 to circuit 4 is due to the decrease in Z. The repeatability and precision are also higher with a higher signal amplitude.

Due to the stochastic nature of Log Z variations under the influence of AC interferences, measurement precision may also be increased by repetition and averaging, as suggested in the standard EN ISO 16773. RSD was calculated for 3, 5 and 10 repeated measurements from Fig. 6a.

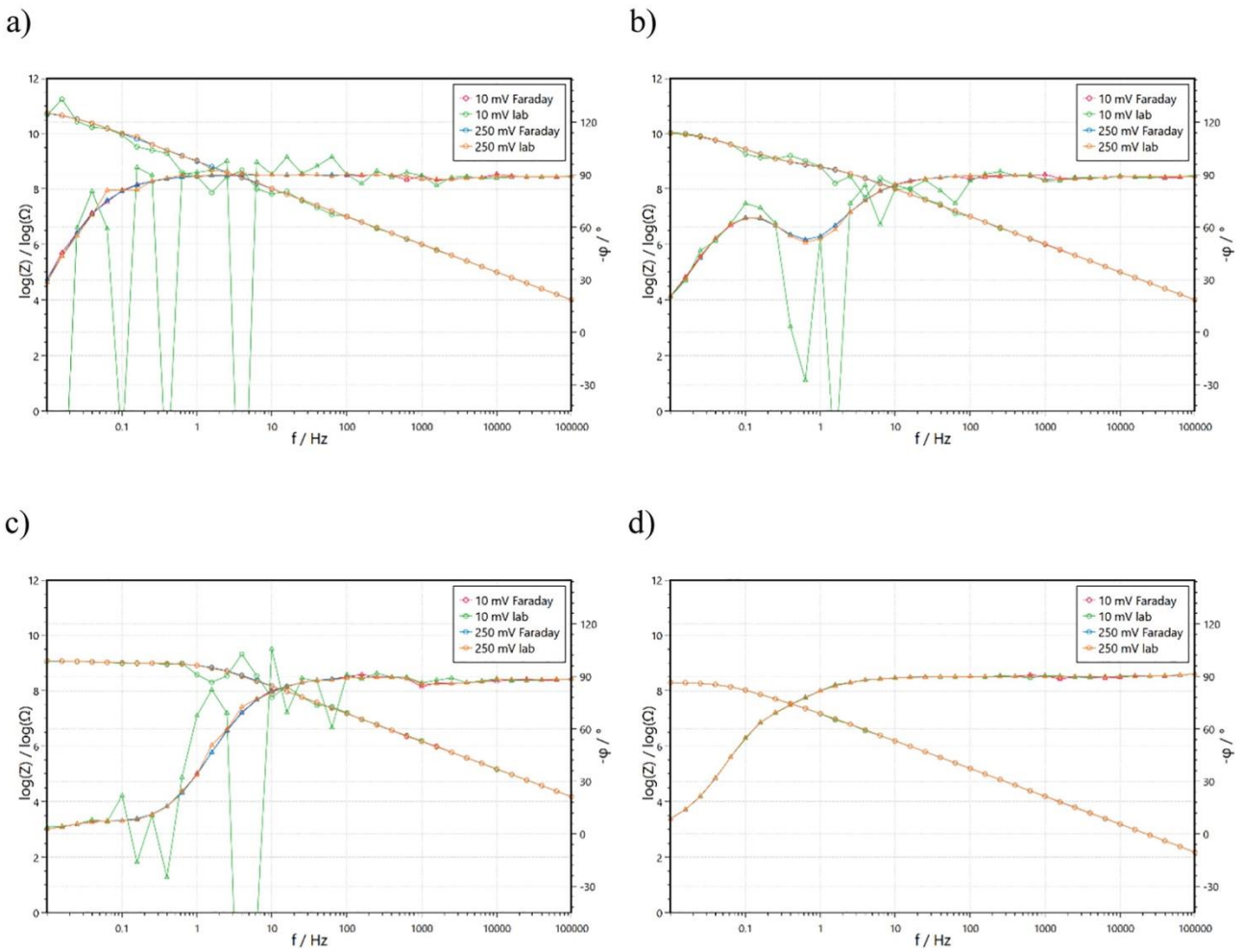

Fig. 5. Bode spectra of circuits a) 1, b) 2, c) 3 and d) 4 of the dummy cell recorded at the signal amplitudes of 10 and 250 mV in the Faraday cage and outside the Faraday cage in the presence of AC interference of 250 mV. (○ – Log *Z*; Δ – phase angle).

Fig. 7 a and b, show results for signal amplitudes of 10 and 250 mV, respectively. In both cases, only the least precise measurements appear to benefit from measurement repetition.

A parallel can be drawn between the STD, as defined by Eq. (2), and the concept of Root Mean Squared Logarithmic Error (RMSLE) [38], which is calculated according to the equation:

$$RMSLE = \sqrt{\frac{1}{n}\sum_{i=1}^{n}(Log\ (a+1) - Log\ (p+1))^2} \quad (3)$$

RMSLE is used when both the predicted value p and the true value a are large numbers. The number 1 in Eq. (3) appears because the logarithm of 0 is not defined. For $p \gg 1$ and $a \gg 1$, Eq. (4) becomes equivalent to Eq. (2a), except for the difference in the base of the logarithmic function and the factor 1/n. Nevertheless, some of the unique properties of RMSLE can be applied to STD from Eq. (2a).

Firstly, the RMSLE expresses the relative error. Therefore, in the logarithmic metric, STD indicates the relative difference of the Log *Z* values, while the scale of the difference is irrelevant. In a non-logarithmic metric, STD changes in magnitude as the scale of *Z* changes. *Z* of coatings spans over many orders of magnitude, so it is more convenient to calculate STD on a relative rather than an absolute basis.

Secondly, RMSLE is used when large numbers are compared but large errors should not be penalized [43,44]. For the same reason, RMSLE is not very sensitive to outliers. These properties are desirable in QCQ analysis because the coating quality is expected to change significantly when Log *Z* changes by an order of magnitude. In addition, STD in Log *Z* is not overly affected by the significant outliers that can occur due to AC interference.

Thirdly, logarithmic metric does not have the same tendency towards overestimates and underestimates [44]. E.g., for a 10 GΩ coating an RSD of 0.5% in Log *Z* yields an RSD of 12.1% in *Z* in the positive direction and an RSD of 10.9% in the negative direction, giving the difference between the positive and negative uncertainties of 1%. An RSD of 1% in Log *Z* yields a STD of 25.9% in *Z* in the positive direction and a STD of 20.6% in the negative direction, giving the difference between the positive and negative uncertainties of 5%. To evaluate the barrier property of the coating, the low-frequency impedance modulus is usually measured during or after exposure to the corrosive environment [45]. The values of Log (*Z*@0.1 Hz / Ω cm2) equal to 9, 8, 7 and 6 are commonly taken as lower specification limits (LSL) of excellent, good, standard and doubtful barrier performance of the coating, respectively [2]. Coatings can be rated on a logarithmic scale by taking into account the measurement uncertainty. Due to the fact that the symmetric measurement uncertainty on a logarithmic scale converts to an asymmetric measurement uncertainty on a non-logarithmic scale, coatings will be less readily pronounced to belong to the lower category if the measurement is not precise. For the precise measurements skewness of the distribution in the original space can be neglected and coating assessment can be done in the log-transformed space.

The values of RSD $< 0.35\%$ and $CI_{95\%} < 0.025\%$ for ten measurements (Fig. 7), show that precise and accurate measurements can be

Table 4
Fitted parameters of dummy cell equivalent circuits and the calculated relative errors with respect to parameter values measured by independent methods.

Element	Fitted Value	Error /%	Fitted Value	Error /%	Fitted Value at	Error /%	Fitted Value at	Error /%
Inside the Faraday cage, signal amplitude 10 mV								
	Circuit 1		Circuit 2		Circuit 3		Circuit 4	
C_1/pF	154.8	−1.49	153.7	−1.54	104.4	−2.43	10,090	−0.80
R_1/MΩ	62,730	−1.49	964.9	7.67	1009	−0.50	102.6	−1.94
C_2/pF	–	–	479.6	−1.49	20,410	−1.74	10,180	−2.00
$R_2(+R_3)$*/MΩ	–	–	10,100	−0.26	200.8	0.98	99.1	3.69
R_{TOT}/MΩ	62,730		11,065		1209.8		201.7	
R_{TOT} Error/%		−1.49		0.49		−0.25		0.91
Inside the Faraday cage, signal amplitude 250 mV								
	Circuit 1		Circuit 2		Circuit 3		Circuit 4	
C_1/pF	154.4	−1.22	153.9	−1.67	104.1	−2.14	10,050	−0.40
R_1/MΩ	62,020	−0.34	972.7	6.92	1010	−0.60	103.5	−2.83
C_2/pF	–	–	473.3	−0.14	19,670	1.94	10,080	−1.00
$R_2(+R_3)$*/MΩ	–	–	10,140	−0.66	205.1	−1.14	99.5	3.29
R_{TOT}/MΩ	62,020		11,113		1215.1		203.0	
R_{TOT} Error/%		−0.34		0.06		−0.69		0.26
Outside the Faraday cage, signal amplitude 250 mV (10 mV), interference amplitude 250 mV								
	Circuit 1		Circuit 2		Circuit 3		Circuit 4	
C_1/pF	155.0	−2.13	154.4	4.50	106.0	−1.00	10,050 (10120)	1.51 (−1.10)
R_1/MΩ	63,130	−1.60	998.0	−0.95	1014	0.29	103.9 (104.3)	−1.01 (−3.63)
C_2/pF	–	–	480.8	−1.74	20,160	−4.00	101.8 (101.1)	−1.14 (−1.30)
$R_2(+R_3)$*/MΩ	–	–	10,170	−1.72	202.2	−0.50	99.1 (98.08)	−2.00 (4.64)
R_{TOT}/MΩ	63,130		11,170		1216.2		203.0 (202.4)	
R_{TOT} Error/%		−2.13		0.44		0.28		0.24 (0.55)

* for circuit 3 of the dummy cell in Fig. 1.

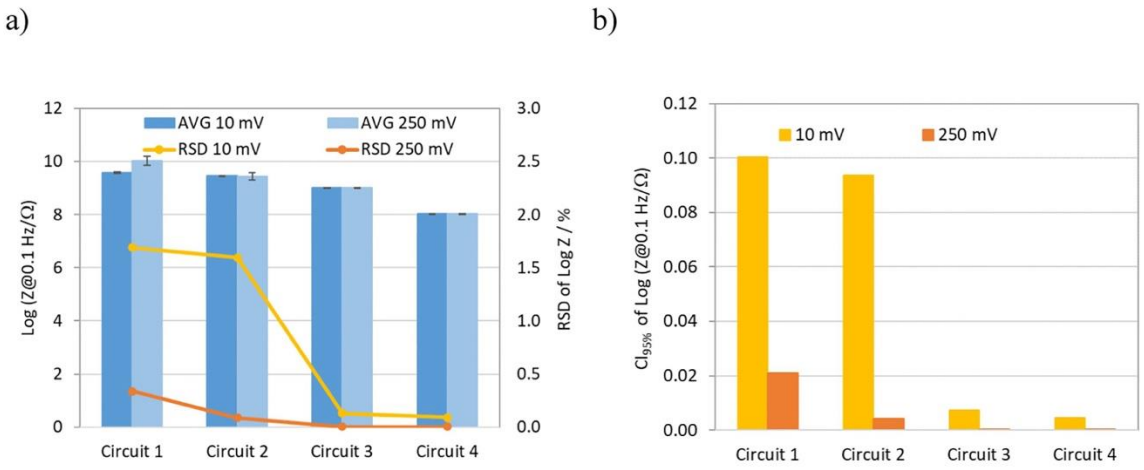

Fig. 6. Average value of Log *Z*, standard deviation as error bars, relative standard deviation and b) 95% confidence intervals obtained for each dummy cell circuit at the signal amplitudes of 250 and 10 mV and an interference amplitude of 250 mV.

made on the dummy cell mimicking high-impedance coatings outside the Faraday cage at the AC interference voltage level of 250 mV, using the maximum output signal amplitude of 250 mV.

3.2. *The influence of AC interferences on the impedance of the calibration foils*

The calibration foils were used to investigate the effects of the various sources of uncertainty that also occur in EIS measurements on coatings but cannot be simulated by a dummy cell. The uniformity of the foil thickness, on the other hand, eliminates the uncertainty due to the coating thickness variations that often occur in industrial coatings and are not inherent to the measurement system.

Fig. 8a shows the Bode impedance spectra of the 110, 135, 185, and 240 μm foils recorded inside the Faraday cage at an amplitude of 250 mV. The arithmetic mean of all *Z*@100 Hz measurements performed on different foils of the respective thicknesses during this study were used to construct the graph relating the impedance modulus *Z*@100 Hz and the foil thickness, as shown in Fig. 8b.

A linear fit of the data, forced through zero, yields a high correlation coefficient r = 0.996. The frequency of 100 Hz was chosen for the analysis based on the value of the phase angle at 100 Hz approaching

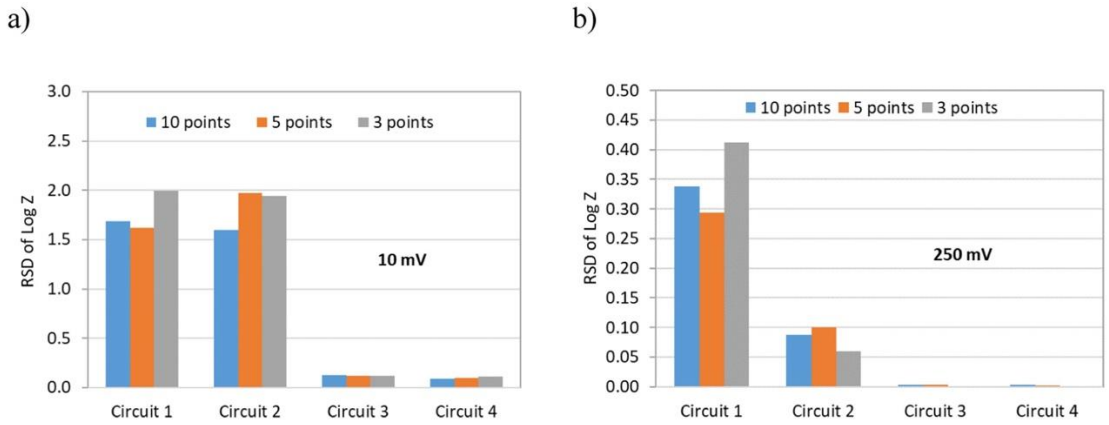

Fig. 7. RSD calculated for 3, 5 and 10 repeated measurements on circuits 1 to 4 of the dummy cell at the amplitudes of (a) 10 and (b) 250 mV and an interference amplitude of 250 mV.

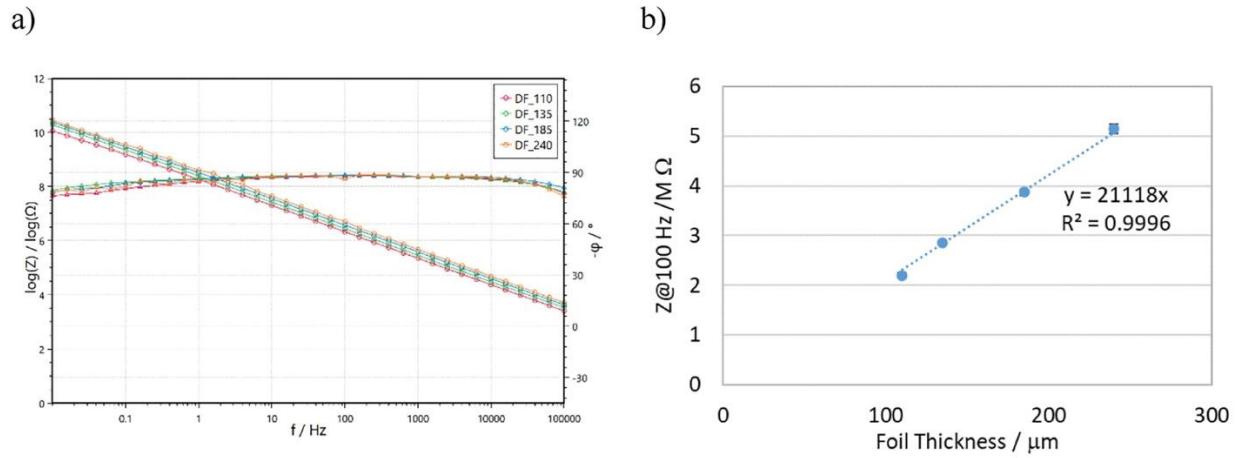

Fig. 8. a) Representative impedance spectra of the 110, 135, 185 and 240 µm foils recorded at the AC amplitude of 250 mV in the Faraday cage and b) *Z*@100 Hz, as a linear function of thickness, error bars denote standard deviation.

−90°, indicating almost pure capacitive behaviour.

The dielectric constant of the foil material can be calculated using the equations [46]:

$$\varepsilon' = \frac{-Z''}{2\pi f C_v Z^2} \quad (1)$$

$$C_v = \frac{\varepsilon_0 A}{d} \quad (2)$$

where Z is the impedance modulus, Z'' is the imaginary part of the impedance, ε_0 is the vacuum permittivity, A is the surface of the electrode and d is the coating thickness.

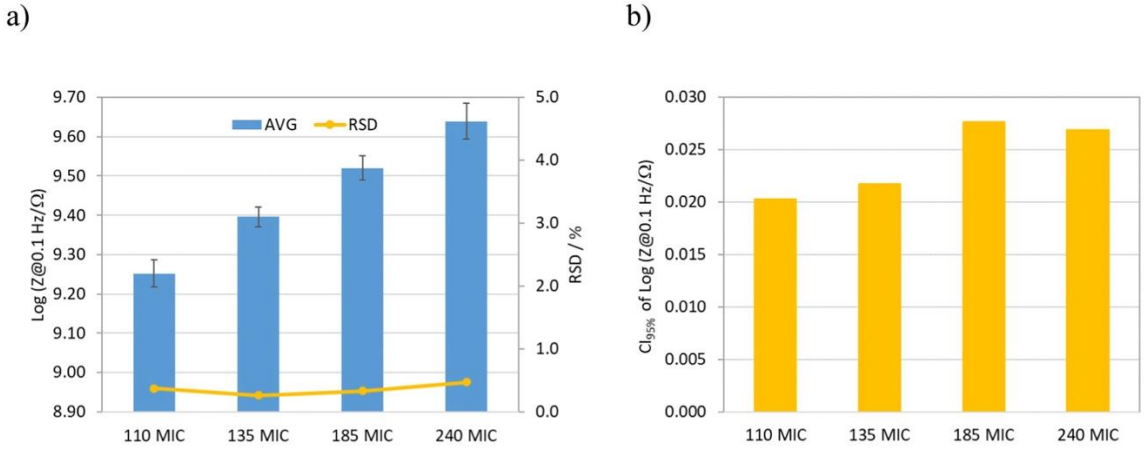

Fig. 9. Average value of Log *Z* obtained for each foil thickness. Error bars show the SD and the yellow line shows the RSD. (For interpretation of the references to color in this figure legend, the reader is referred to the web version of this article.)

A relative dielectric constant of the foils equal to 3.560 ± 0.125 corresponds to those found in the literature for polyester [34,35] and is within the range from 2 to 10 found for the protective organic coatings [47,48].

Fig. 9a shows Log *Z*, SD as error bars and RSD obtained for each foil at the signal amplitude of 250 mV. Fig. 9b shows $CI_{95\%}$ values comparable to the $CI_{95\%}$ obtained for Circuit 1 of the dummy cell from Fig. 6.

Measurements on calibration foils are more similar to measurements on coatings [33] than the measurements on dummy cell. While the accuracy and precision of the QCQ device, as well as its robustness to amplitude rise, are best tested on a high impedance dummy cell, calibration foils can serve for studying the additional contributions to measurement uncertainty, listed in Table 5.

For studying repeatability (REP), curves obtained from successive measurements without removing the electrodes between measurements were compared. To investigate reproducibility (RPD), electrodes were detached from the foil, rinsed of electrolyte paste, and dried between successive measurements on the same foil. The reproducibility for measurements on different foils (RPD_DF) of the same thickness was also investigated.

Fig. 10 a shows the RSD of Log *Z* obtained in the repeatability, reproducibility experiments for a single sample and reproducibility for different samples of the same thickness, for the 110 and 240 μm foils recorded in the Faraday cage at the amplitude of 250 mV. The results show the increase in RSD with the increase in the number of measurement uncertainty components.

The average RSD of the foil thickness is 1.23 ± 0.3%. The observed RSD of Log *Z* for different foils is smaller than the variation of foil thickness.

When the measurements are performed outside the Faraday cage, the AC interferences must be considered as an environmental component of the measurement uncertainty. Fig. 11 shows the RSD and relative error of measurements for a range of EIS signal amplitudes from 10 to 250 mV performed on the 240 μm foil inside the Faraday cage and outside the Faraday cage at different AC interference levels. The relative error was calculated for each foil from the difference between a measurement outside the Faraday cage and the average of the 10 and 250 mV measurements inside the Faraday cage.

For all interference levels, the RSD follows a similar dependence from the maximum value of about 5% for the 10 mV signals to 1% for the signals above 150 mV (Fig. 11a). The RSD inside the Faraday cage follows a similar dependence as the RSD outside the cage, but on a much smaller scale, indicating the influence of EIS device precision when measuring small currents. For the signal amplitude of 150 mV and the coating resistance of 4.36 GΩ the current can be estimated at 34 pA, while for the signal amplitude below 50 mV, the current falls into the 1 pA range. Therefore, the RSD increases and becomes more scattered, probably due to a synergistic effect of AC interferences and the imprecision of the QCQ device near and below 1 pA.

Above signal amplitudes of 150 mV, the RSD is less scattered. Nevertheless, no regularity is observed with respect to the AC interference amplitude, indicating that the main effect of increasing the signal amplitude is to avoid the inherent imprecision of the QCQ device when measuring very small currents. On the other hand, the RSD of the 800 mV interferences is 3.7 ± 1.2% and is not affected by the signal amplitude. For interference voltages equal to or less than the maximum output AC voltage of the QCQ device of 250 mV, the impressed voltage is able to counteract the induced voltage and reach the target voltage. For the induced voltages higher than 250 mV, the induced voltage not only interferes but also overrides the signal voltage, resulting in a maximum RSD of almost 6%.

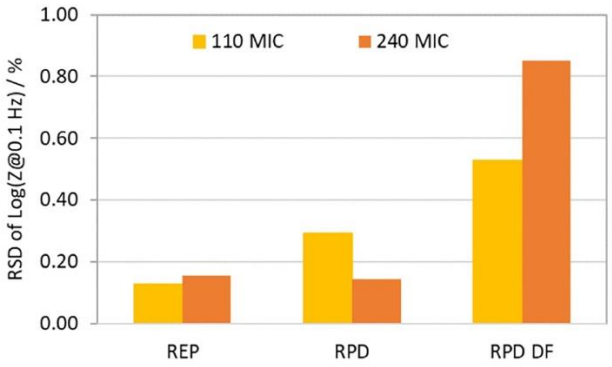

Fig. 10. Relative standard deviation of three measurements obtained under conditions of repeatability (REP), reproducibility on a single foil (RPD) and repeatability on different foils (RPD_DF) at a signal amplitude of 250 mV in a Faraday cage.

The relative error indicating accuracy is close to 0.1% for signal amplitudes of 200 mV and scatters within 2% of the mean Faraday cage value for signal amplitudes down to 20 mV. The highest scatter up to 4% is observed at the signal amplitude of 10 mV for all measurements and at the interference voltage of 800 mV in the whole range of signal amplitudes.

For measurements on coatings in the field, the only statistical tool that can be used is the RSD. Once the acceptable accuracy of the instrument is demonstrated using dummy cells as a reference, the conclusions of the present study can be applied to coatings in the reference impedance range.

3.3. Measurements on coatings in outdoor exposure

The results of the Log *Z* measurements on the four coated systems subjected to AC interferences from the nearby AC railway traction system are shown in Fig. 12. The two-electrode setup shown in Fig. 1 allowed the measurement to be performed on fully coated samples without contacting the substrate. Nogueira et al. [49] have shown, for a similar electrode geometry and coatings with a resistance of $>10^8$ Ω cm ($\sim 10^{12}$ Ω cm in the present case), that current lines tend to short-circuit through the metallic substrate. The measured impedance approaches the impedance of the coating located under the electrodes plus the interfacial impedance, which in the present case is negligible compared to the impedance of the coating. Therefore, the measured impedance for the coatings in early stages of degradation can be taken as equal to the sum of the impedances of the coating under the two electrodes, i.e., twice the impedance of the coating under a single electrode. If the connection is made to the substrate, this can be verified experimentally by measuring the impedances between individual electrodes and the substrate

Table 5
Contribution of measurement uncertainty components to the results of the REP, RPT and RPD DF experiments.

Experiment Type	Measurement device	Operator Effects	Environmental influences on the sample	Sample stability	Sample characteristics
	QCQ device precision conductive paste stability	Application of the conductive paste, positioning of the electrodes	Temperature, relative humidity	Changes in samples due to reproduction of the measurement	Variation of a sample thickness
REP	+	−	−	−	−
RPD	+	+	+	+	−
RPD_DF	+	+	+	+	+

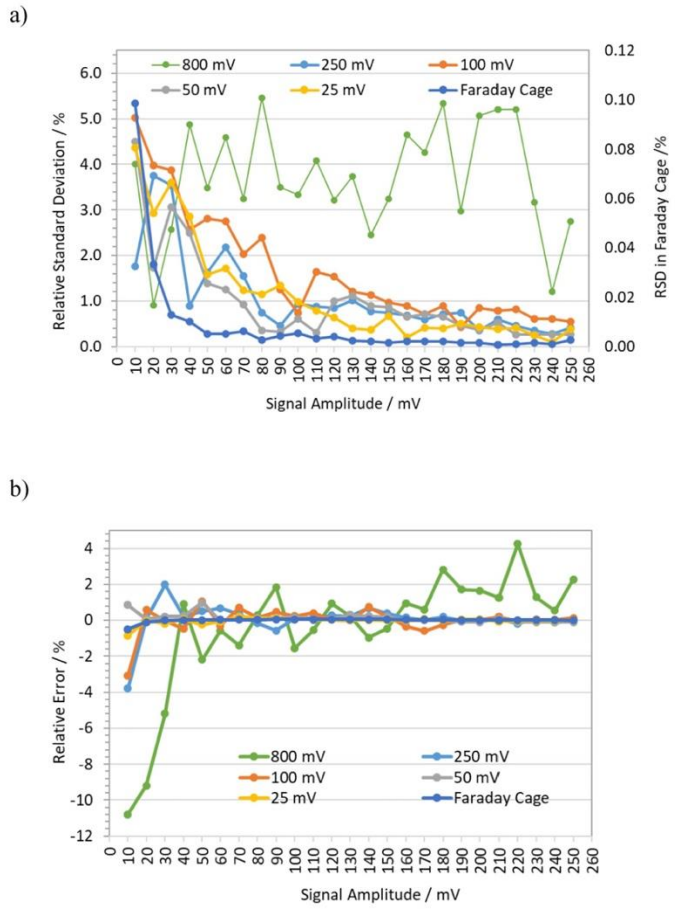

Fig. 11. a) RSD and b) relative error of measurements for a range of EIS signal amplitudes from 10 to 250 mV, recorded on the 240 µm foil inside the Faraday cage and outside the Faraday cage at different AC levels of interference.

separately and checking that they add up to the impedance measured between the same electrodes.

The minimum amplitude of the interferences obtained after favourably orienting measurement setup in the railway electromagnetic field was 50 ± 7 mV. The maximum signal amplitude of 250 mV was chosen for the measurements due to the dynamic nature of the AC railway disturbances, which are highest during train passage and peak at 3.3 V. The shape of the interferences was sinusoidal, as the one shown in Fig. 4a. The thicknesses and Log *Z* of the coatings are within the range of the calibration foils, as are the RSD values. The RSD of 10 measurements was averaged for quadruplicate samples of each coating system to obtain the average repeatability. For average reproducibility, the RSD of Log *Z* was calculated for the four samples of each coating system and is slightly higher than the RSD of repeatability. The results of the field measurements confirm the validity of the laboratory simulations and set the RSD of Log *Z* below 1%.

It should be noted that the possible destructive effects of using high signal amplitudes remain to be investigated, as well as the various situations in the field that would allow the use of lower amplitudes.

4. Conclusions

The influence of the ambient electromagnetic field on the measurement impedance of field exposed coated samples and of dummy cells and foils mimicking organic coatings in an intact or barely damaged state was measured. AC interferences cause stochastic variations of the phase angle and, to a lesser extent, of Log *Z*, which are visible in the Bode plot. The phenomenon is visible for the capacitive coating behaviour in the intermediate and low frequency range, where the compensation of the induced AC voltage by the EIS device is limited by the charging rate of the coating capacitance. It has been shown that the effects of AC interferences with the amplitude up to the maximum AC output voltage of the EIS device can be successfully mitigated by increasing the signal amplitude to 150 mV or more, giving >99% precision. Precision at lower signal amplitudes decreases (>95%) due to the synergy of the AC interference effect and the loss of EIS device precision as lower currents flow through the measurement circuit. An acceptable accuracy of 97.8% was obtained at the maximum signal amplitude of 250 mV, showing that the nonlinearity does not affect the result. For Log *Z* at 0.1 Hz equal to 8, no AC effect on dummy cell impedance was observed, suggesting that low signal amplitude can be used for coatings with poorer performance. Performing a large number of measurements with a simplified measuring cell, e.g., on different samples or coating sites, allows a statistical analysis and, taking into account the measurement uncertainty, rating of the coatings with greater confidence. In addition, rating on a logarithmic scale is less susceptible to outliers and is better suited to the case of coating impedances that start from very high values and may decrease over many orders of magnitude while the coatings are exposed to the corrosive environment.

Funding

This work was performed with the support of the Zagreb Innovation Centre, within Startup Factory BATCH 2019 Programme.

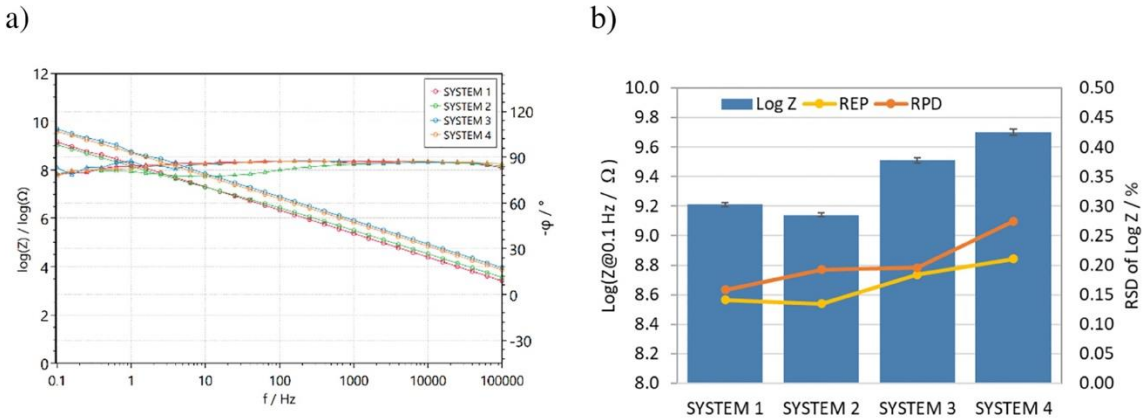

Fig. 12. a) Representative Bode plots of the four tested systems and b) average value of Log *Z* calculated for a single electrode and for each coating system. Error bars show the SD and the yellow line shows the RSD.

CRediT authorship contribution statement

Ines Šoljić: Investigation, Methodology, Writing - Original draft, Review & Editing.

Ivana Šoić: Visualization, Methodology, Review & Editing.

Lorena Kostelac: Investigation, Validation.

Sanja Martinez: Conceptualization, Methodology, Writing- Original draft, Writing - Review & Editing.

Declaration of competing interest

The authors declare that they have no known competing financial interests or personal relationships that could have appeared to influence the work reported in this paper.

References

[1] I.C.P. Margarit-Mattos, EIS and organic coatings performance: revisiting some key points, Electrochim. Acta 354 (2020), 136725, https://doi.org/10.1016/j.electacta.2020.136725.

[2] L.G.S. Gray, B.R. Appleman, EIS electrochemical impedance spectroscopy - a tool to predict remaining coating life, J. Prot. Coat. Linings 20 (2003) 66–74.

[3] K. Allahar, Q. Su, G. Bierwagen, Non-substrate EIS monitoring of organic coatings with embedded electrodes, Prog. Org. Coat. 67 (2010) 180–187, https://doi.org/10.1016/j.porgcoat.2009.10.001.

[4] B.J. Merten, U.S. Bureau, Re - Evaluating Electrochemical Impedance Spectroscopy (EIS) for the Field Inspector's Toolbox: A First Approach, 2014.

[5] B.J. Merten, Field Validation of Impedance Spectroscopy Coating Assessments, Final Report, 2020, 8540-2020-43.

[6] B.J. Merten, Electrochemical Impedance Methods to Assess Coatings for Corrosion Protection, Technical Publication, 2019, 8540-2019-03.

[7] E. Valentini, Smart electrochemical portable tools for cultural heritage analysis: a review, Sensors 19 (2019) 4303, https://doi.org/10.3390/s19194303.

[8] I. Šoić, S. Martinez, M. Dubravić, Gel-electrolyte EIS setup used for probing of IR dried/cured industrial coatings, Prog. Org. Coat. 137 (2019), https://doi.org/10.1016/j.porgcoat.2019.105331.

[9] S. Martinez, I. Šoić, V. Špada, Unified equivalent circuit of dielectric permittivity and porous coating formalisms for EIS probing of thick industrial grade coatings, Prog. Org. Coat. 153 (2021), https://doi.org/10.1016/j.porgcoat.2021.106155.

[10] M.M. Lalić, S. Martinez, A novel application of EIS for quantitative coating quality assessment during neutral salt spray testing of high-durability coatings, Acta Chim. Slov. 66 (2019) 513–522. https://doi.org/10.17344/acsi.2019.5113.

[11] D.H. Johnson , Fundamentals of electrical engineering I, (n.d.). Themes - Fundamentals of Electrical Engineering I - OpenStax CNX (accessed September 9, 2021).

[12] R. Cottis, B.C. Syrett, Electrochemical impedance and noise, in: NACE International Corros. Conf. Ser, 1999.

[13] D.D. Stupin, E.A. Kuzina, A.A. Abelit, S.V. Koniakhin, A.E. Emelyanov, Bio-Impedance Spectroscopy: Basics and Applications, 2020.

[14] A. Blidberg, Correlation between different impedance measurement methods for battery cells, in: Degree Project in Chemical Science and Engineering Second cycle Stockholm, 2012.

[15] J.J. Giner-Sanz, E.M. Ortega, V. Pérez-Herranz, Harmonic analysis based method for linearity assessment and noise quantification in electrochemical impedance spectroscopy measurements: theoretical formulation and experimental validation for tafelian systems, Electrochim. Acta 211 (2016) 1076–1091, https://doi.org/10.1016/j.electacta.2016.06.133.

[16] T.C. da Silva, S. Mallarino, S. Touzain, I.C.P. Margarit-Mattos, DMA, EIS and thermal fatigue of organic coatings, Electrochim. Acta 318 (2019) 989–999, https://doi.org/10.1016/j.electacta.2019.06.066.

[17] A. Suarez-Perez, G. Gabriel, B. Rebollo, X. Illa, A. Guimerà-Brunet, J. Hernández-Ferrer, M.T. Martínez, R. Villa, M.V. Sanchez-Vives, Quantification of signal-to-noise ratio in cerebral cortex recordings using flexible MEAs with co-localized platinum black, carbon nanotubes, and gold electrodes, Front. Neurosci. 12 (2018) 1–12, https://doi.org/10.3389/fnins.2018.00862.

[18] P. Haußmann, J. Melbert, R. Bochum, in: Impedance Spectroscopy on Lithium Ion Cells for Automotive Applications With Optimized Measurement Duration and Frequency Resolution, 2016, pp. 308–315, https://doi.org/10.5162/sensoren2016/4.4.2.

[19] F. Fasmin, R. Srinivasan, Review: nonlinear electrochemical impedance spectroscopy, J. Electrochem. Soc. 164 (2017) H443–H455, https://doi.org/10.1149/2.0391707jes.

[20] N. Meddings, M. Heinrich, J. Lee, V. Ruiz, E. Napolitano, S. Seitz, G. Hinds, R. Raccichini, M. Gaber, J. Park, in: Application of Electrochemical Impedance Spectroscopy to Commercial Li-ion Cells: A Review, 2020, p. 480, https://doi.org/10.1016/j.jpowsour.2020.228742.

[21] L. Žnidarič, G. Nusev, B. Morel, J. Mougin, Đ. Juričić, P. Boškoski, Evaluating uncertainties in electrochemical impedance spectra of solid oxide fuel cells, Appl. Energy 298 (2021), 117101, https://doi.org/10.1016/j.apenergy.2021.117101.

[22] H. Zappen, F. Ringbeck, in: Application of Time-Resolved Multi-Sine Impedance Spectroscopy for Lithium-Ion Battery Characterization, 2018, pp. 1–18, https://doi.org/10.3390/batteries4040064.

[23] E.A. Rojas-González, G.A. Niklasson, Setup for simultaneous electrochemical and color impedance measurements of electrochromic films: theory, assessment and test measurement, Rev. Sci. Instrum. 90 (2019), 085103, https://doi.org/10.1063/1.5115119.

[24] J. Harper , Non-linear system analysis: the application of electrochemical impedance spectroscopy to the study of fuel cells and batteries operated under load, (n.d.). Solartron Analytical Application Guide, (n.d.).

[25] J.J. Giner-Sanz, E.M. Ortega, V. Pérez-Herranz, Harmonic analysis based method for perturbation amplitude optimization for EIS measurements, J. Electrochem. Soc. 164 (2017) 918–924, https://doi.org/10.1149/2.1451713jes.

[26] M. Kiel, O. Bohlen, D.U. Sauer, Harmonic analysis for identification of nonlinearities in impedance spectroscopy, Electrochim. Acta 53 (2008) 7367–7374, https://doi.org/10.1016/j.electacta.2008.01.089.

[27] A. Roggero, N. Caussé, E. Dantras, L. Villareal, A. Santos, N. Pébère, Thermal activation of impedance measurements on an epoxy coating for the corrosion protection: 1. Dielectric spectroscopy response in the dry state, Electrochim. Acta 303 (2019) 239–245, https://doi.org/10.1016/j.electacta.2019.02.035.

[28] A. Roggero, N. Caussé, E. Dantras, L. Villareal, A. Santos, N. Pébère, Thermal activation of impedance measurements on an epoxy coating for the corrosion protection: 2. Electrochemical impedance spectroscopy study, Electrochim. Acta 305 (2019) 116–124, https://doi.org/10.1016/j.electacta.2019.03.007.

[29] E. Akbarinezhad, F. Rezaei, J. Neshati, Evaluation of a high resistance paint coating with EIS measurements: effect of high AC perturbations, Prog. Org. Coat. 61 (2008) 45–52, https://doi.org/10.1016/j.porgcoat.2007.09.004.

[30] E. Akbarinezhad, H.R. Faridi, Different approaches in evaluating organic paint coatings with electrochemical impedance spectroscopy, Surf. Eng. 24 (2008) 280–286, https://doi.org/10.1179/174329408X326524.

[31] W.S. Tait, Coping with errors in electrochemical impedance spectroscopy data from coated metal, J. Coat. Technol. Res. 66 (1994) 59.

[32] V.S. Bonitz, B.R. Hinderliter, G.P. Bierwagen, Random and systematic error as a function of sample area in electrochemical impedance spectroscopy data, Prog. Org. Coat. 77 (2014) 2100–2106, https://doi.org/10.1016/j.porgcoat.2014.07.008.

[33] V.S. Bonitz, B.R. Hinderliter, G.P. Bierwagen, Commercial polymer films as calibration standards for EIS measurements, Electrochim. Acta 51 (2006) 3558–3565, https://doi.org/10.1016/j.electacta.2005.10.031.

[34] E.D. Schachinger, B. Strauß, R. Braidt, A.W. Hassel, Electrochemical impedance spectroscopy on UV-aged polyester coatings: possibilities and limits of modeling water diffusion, Phys. Status Solidi Appl. Mater. Sci. 217 (2020) 1–9, https://doi.org/10.1002/pssa.201901038.

[35] G. Yilmaz, O. Kalenderli, Dielectric properties of aged polyester films, in: Conf. Electr. Insul. Dielectr. Phenom. (CEIDP), Annu. Rep 2, 1997, pp. 444–446, https://doi.org/10.1109/ceidp.1997.641107, 8540-2019-03.

[36] V.F. Lvovich, Impedance Spectroscopy, Applications to Electrochemical and Dielectric Phenomena, John Wiley & Sons, 2012.

[37] L.G.S. Gray, EIS: electrochemical impedance spectroscopy a tool to predict remaining coating life? JPCL (2003) 66–74.

[38] T. Chowdhury, N. D'Souza, N. Dahotre, Low-cost reliable corrosion sensors using ZnO-PVDF nanocomposite textiles, Sensors (Basel) 21 (12) (2021) 4147, https://doi.org/10.3390/s21124147.

[39] B.J.E. Merten, Electrochemical impedance methods to assess coatings for corrosion protection, technical publication no. 8540-2019-03. https://www.usbr.gov/tsc/techreferences/mands/mands-pdfs/ElectrochemicalImpedanceMethods_8540-2019-03_508.pdf, 2019.

[40] B.J. Merten, S. Prochaska, M. Jermyn, E. Monblatt, J. Elder, Field validation of impedance spectroscopy coating assessments, final report no. ST-2020-1884-01 8540-2020-43. https://www.usbr.gov/research/projects/index.html, 2020.

[41] A. Alizadeh Razin, B. Ramezanzadeh, H. Yari, Detecting and estimating the extent of automotive coating delamination and damage indexes after stone chipping using electrochemical impedance spectroscopy, Prog. Org. Coat. 92 (2016) 95–109, https://doi.org/10.1016/j.porgcoat.2015.11.023.

[42] B. Hudec, K. Ribičić, S. Martinez, I. Šoić, Quantitative coating quality assessment on offshore platform, Mater. Perform. 52–55 (January 2021).

[43] K.S. Kaswan, J.S. Dhatterwal, in: Big Data: An Introduction, Shashwat Publication, 2020, pp. 219–221.

[44] A. Guitart, P.P. Chen, P. Bertens, A. Perianez, Forcasting player behavioural data and simulating in-game events, in: Advances in Information and Communication Networks, Future of Information and Communication Conference (FICC) 2, 2018, pp. 274–294.

[45] T. Fu, X. Tang, Z. Cai, Y. Zuo, Y. Tang, X. Zhao, Correlation research of phase angle variation and coating performance by means of Pearson's correlation coefficient, Prog. Org. Coat. 139 (2020), 105459, https://doi.org/10.1016/j.porgcoat.2019.105459.

[46] P. Bonin, A. Roggero, N. Caussé, N. Pébère, D. Thierry, N. Le Bozec, Impedance analysis of the barrier effect of coil-coated materials: water uptake and glass transition variations, Prog. Org. Coat. 153 (2021) 1–9, https://doi.org/10.1016/j.porgcoat.2021.106163.

[47] J.A. Calderon-Gutierez, F.E. Bedoya-Lora, Barrier property determination and lifetime prediction by electrochemical impedance spectroscopy of a high performance organic coating, Dyna 81 (183) (2014) 97–106.
[48] D. Loveday, P. Peterson, B. Rodgers, Evaluation of organic coatings with electrochemical impedance spectroscopy, part 2: application of EIS to coatings, JCT Coat. Tech. (2004) 88–93.
[49] A. Nogueira, X.R. Novoa, C. Perez, On the possibility of using embedded electrodes for the measurement of dielectric properties in organic coatings, Prog. Org. Coat. 59 (2007) 186–191.

APPENDIX IV

I. Šoić, I. Šoljić, M. Eškinja, A. Mujezinović, S. Martinez, The novel paste electrolyte measuring cell for EIS testing of the commonly used surface protection on bronze, Prog. Org. Coat. 177 (2023) 107442

https://doi.org/10.1016/j.porgcoat.2023.107442

Ivana Šoić: investigation, visualization, writing
Ines Šoljić: investigation, writing
Magdalena Eškinja: investigation
Adnan Mujezinović: validation
Sanja Martinez: conceptualization, methodology, writing

Progress in Organic Coatings 177 (2023) 107442

Contents lists available at ScienceDirect

Progress in Organic Coatings

journal homepage: www.elsevier.com/locate/porgcoat

The novel paste electrolyte measuring cell for EIS testing of the commonly used surface protection on bronze

Ivana Šoić [a], Ines Šoljić [a,*], Magdalena Eškinja [a], Adnan Mujezinović [b], Sanja Martinez [a]

[a] Department of Electrochemistry, Faculty of Chemical Engineering and Technology, University of Zagreb, Marulićev trg 19, 10000 Zagreb, Croatia
[b] University of Sarajevo, Faculty of Electrical Engineering, Zmaja od Bosne bb., Sarajevo, Bosnia and Herzegovina

ARTICLE INFO

Keywords:
Paraloid B-72
Bronze
Coins
EIS
Paste electrolyte

ABSTRACT

The cell was tested on polished and patinated bronzes of different compositions, on sulfide patina/Paraloid B-72-coated bronzes with different numbers of coating layers, on protected bronze samples with different degrees of damage to the protective layers, and on uncoated and coated patinated bronzes after 24 h conditioning in the condensation chamber. A quantitative criterion of Phase Angle at 0.1 Hz was deduced and explained. The systems show two or three time constants, depending on the number and integrity of the layers. Capacitances of the high-frequency response that are attributed to the coating range from 1.8 to 31 nF/cm^2 and capacitances of the medium-frequency response attributed to the patina range from 1.1 F/cm^2 to 2.3 nF/cm^2, indicating Paraloid B-72 penetration into the pores of the patina. Log |Z| at 0.1 Hz decreases with mechanical damage to the protective layers. Damage also leads to the occurrence of the low-frequency response attributed to the Faradaic process on the substrate. The three layers of Paraloid B-72 on the sulfide patina had Log |Z| at 0.1 Hz around 8 and were insensitive to the 24-h condensation, indicating good protection. The cell was further applied to different sides of bronze coins, so no electrical contact with the substrate was required. The Kramers-Kronig test was applied to confirm the validity of the EIS results.

1. Introduction

The importance and usefulness of electrochemical impedance spectroscopy (EIS) as a tool for quantifying the protective properties of coatings exposed to natural and artificial corrosive environments has been demonstrated through decades of scientific research [1,2].

In comparison to the other electrochemical techniques, EIS is the only non-destructive method with which we can check the current state of the real specimen, but further research is needed to eliminate problems in application [3,4].

EIS has been applied not only to industrial coatings, but also to cultural heritage objects where there are greater obstacles to its application compared to industrial coating systems. Unlike industrial structures, which are usually protected by thick pigmented polymer coatings applied to abrasively cleaned substrates, art and cultural heritage objects are usually protected by thin layers of clear lacquer or wax applied either to the polished surface or to the surface covered with a porous layer of protective products [4,5], because the main requirement of the conservators is that applied protection must not modify appearance of the protected metal and all measures should avoid future deterioration and loss of material [6]. The use of thicker, permanent coatings would lead to changes in appearance and make re-conservation treatments more difficult [7–9].

Conservation coatings are temporary and serve as a protective barrier that limits the contact of moisture with metal surface [7–9]. Acrylic resins such as Paraloid are widely used as protection for cultural heritage preservation despite their inherent weaknesses, such as yellowing and low protective physical properties [3].

Barrier behavior of the temporary organic coatings for conservative purposes is limited because of their permeability to the corrosive agents which can diffuse through the pores or defects of the coating. The quality of the coating layer also depends on the application methods, and the use of EIS can provide information about the porosity and impermeability of the coatings [9] and enable assessment of the state of protection and the need for intervention [3,4,9,10].

Under the influence of gravitational sedimentation, impaction and diffusion, atmospheric aerosols of varying moisture content can be deposited on the metal surface. Consequently, even at low RH levels, liquid can condense in nanoscopic pores and crevices [11] creating a conductive path and allowing the real condition of metal substrate to be

* Corresponding author.
E-mail address: isoljic@fkit.hr (I. Šoljić).

https://doi.org/10.1016/j.porgcoat.2023.107442
Received 10 November 2022; Received in revised form 5 January 2023; Accepted 26 January 2023

measured using EIS.

Most research is concerned with estimating the corrosion rate associated with exposure, but very few of them deal with the assessment of the state of existing protection on the area of interest. There is no established method to evaluate the performance of the coating or need for recoating resulting in increased inspection costs and short intervals for recoating [7,8].

The idea and need for electrochemical cells for in situ impedance measurements on rough, curved, irregular and non-horizontal surfaces come from all electrochemical fields; industrial, cultural heritage and medical. Liquid electrolyte cells have been developed [4] using mainly artificial rain and 0.1 M Na_2SO_4 as electrolytes to mimic exposure to the atmosphere [10,12,13] and reproduce the corrosion conditions of the exposed surface [4]. Mineral water has been shown to minimize the risk of measurement-induced corrosion [14], while electrolytes containing NaCl in various combinations can be used in the laboratory on coupons to simulate a more aggressive environment, but never on real objects [4]. In addition, the selection of a suitable electrolyte solution that has sufficient conductivity but does not contain aggressive ions such as chlorides can be a problem [15,16]. Moreover, the stabilization of the cell is directly related to the reproducibility, and in the case of immersion, the stabilization time is usually longer than 10 min [14]. One of the main reasons for implementing quasi solid-state electrolytes is the ability of the electrolyte to adapt to the morphology of the surface of interest. The use of conductive gels, wet sponges, and agars for contacting the surface is reported [3,5,15–17] in an effort to find an electrolyte which is non-aggressive towards the substrate or patina, has sufficient conductivity and is stable enough to produce repeatable results [3,14].

The quality of the electrical contact with the object under investigation and the design of the measuring cell is another important consideration. Usually, a three-electrode cell is used [4,18], and in order to establish a good contact with the surface of the working electrode, it is necessary to find an area near the measurement site where it is possible to remove the patina or coating. Recently, two-electrode cells have been used in various designs [4,19,20]. One of the first attempts was the use of commercial flexible electrodes common for electrocardiograms in medicine using conductive adhesive gels and hydrogels as electrolytes [4], and while they can conform to the surface, they have lower conductivity compared to liquid electrolytes [16] and the problem of entering the pores of a substrate to obtain a correct result [5,10,21]. For these reasons, it is important to find a compromise between the consistency, conductivity and non-destructiveness of the electrolyte.

In the present study, we explore a novel cell concept that uses conductive paste electrolyte in a two-electrode system consisting of a substrate and a single counter/reference electrode to evaluate the effect of protective layers, patinas and coatings, on bronze. We have previously demonstrated the applicability of this concept for rapid in situ measurements on industrial coatings [22–24]. In this paper, the non-aggressive, quasi-solid state, paste electrolyte that contains conductive electrolyte solution, is pressed between electrode and the examined surface [25] in its original state, already balanced with the atmosphere to which it is exposed, allowing measurement of the barrier properties of the protection on substrate.

The primary advantage of the proposed cell is that flexible electrode self-adheres to surfaces of any orientation with the help of the paste electrolyte and is free of electrolyte leakage issues.

Another reported advantage of the quasi solid-state electrolytes is that they do not require stabilization of the metallic substrate because it is already in equilibrium with its environment [26]. This also allows stabilization in tens of seconds and measurement times of <3 min for a spectrum from 0.1 Hz to 10 kHz or for five repetitive measurements at a single frequency of 0.1 Hz. Simplified measurements at a single, e.g. 0.1 or 0.01 Hz, frequency are frequently chosen by researchers as a quick way to obtain information about the quality of the coating and allow quick comparison of the performance of different systems while keeping the ability to detect the differences in resistive/capacitive behavior of the coating [4,12,19,27]. This method allows measurements at multiple sites in a short time.

Further challenges encountered in measurements on bare and patinated metal and thin coatings are hereby addressed. The results of laboratory tests in various liquid electrolytes are compared with the use of paste electrolyte to evaluate their aggressiveness towards the substrate and the coating. A novel cell design is proposed to avoid short circuiting of the electrode and the substrate through the conductive paste. The sensors studied by Mascarenhas and Nandagopal [28,29], whose task is to transmit only the signal from the device to the surface with minimum interferences were the inspiration for this work.

The proposed measurement cell was first tested in a range of scenarios likely to be encountered in practice such as patinated bronze, patinated bronze protected with one, two or three-layer coating, bronze with damaged patina and coating layers, patinas on different bronze substrates and patina and coating in dry and water saturated state. The cell was then applied to a set of bronze coins which are of interest to conservators [15,30].

To our knowledge, this is the first time that the cell of the described construction and/or the paste electrolyte have been applied to investigating bronze protection as well as that the chosen multiple scenarios have been investigated systematically to assess applicability of a novel cell.

Only Bode plots are shown because they allow observing impedances spanning through many orders of magnitude and the impedance and phase angle as a function on the frequency, which provides information about capacitive and resistive behavior of the measured system [31]. The quality of the EIS results was assured by calculation of relative standard deviation of the repeated measurements and the application of Kramers-Kronig transformtions [32–34].

2. Experimental

2.1. Materials

Studies were conducted on two types of bronze samples: $CuSn_6$ (94.15 wt% Cu and 5.85 wt% Sn) and $CuSn_{12}$ (87.79 wt% Cu and 12.21 wt% Sn). Bronze plates with dimensions 5 × 5 cm were used as the metallic substrate. Samples were polished with SiC 80, 800, 1200, and 2500 grade polishing paper and repeatedly washed in ethanol using ultrasonic agitation. Twelve samples of each studied material were patinated to obtain sulfide patina. Measurements were also conducted on the seven Austro Hungarian 2 Heller coins from a private collection as an authentic sample. This specific coin was minted in the period 1895 to 1915. Various internet sources state that the alloy of these coins is composed of 95 wt% of copper, 4 wt% of tin and 1 wt% part of zinc [35].

2.2. Preparation of the sulfide patina

The sulfide patina was chemically prepared using K_2S_n in distilled water (1.25 g/50 mL) and heated to 80 °C. The hot bronze plates were immersed in the solution for a few seconds, washed off with tap water and polished with a sponge. The process was repeated until a stable patina was formed [36]. After patination, nine samples of each material were coated.

2.3. Preparation and coating application

Paraloid B72 (C.T.S.) supplied in small granules was dissolved in ethyl acetate. A solution of 15 % Paraloid B-72 in ethyl acetate was applied with a brush to the entire surface of the artificially patinated bronze to form a coating.

2.4. Coating thickness measurement

The thickness of the coating on the bronze substrate was measured by Positector 6000 thickness gauge. As coatings in conservation are applied by brush, thickness is not homogeneous. Also, the application of a layer over previous one may dissolve the underlying coating, so the thickness of a two-coat coating is not twice that of a one-coat coating. The thickness of a one coating layer was deduced from multiple measurements and amounted to 4.2 ± 1.5 μm.

2.5. EIS measurements

EIS measurements were performed in triplicate, on bare, artificially patinated, and coated bronzes. Measurements were performed using the ReCorr® QCQ (Quantitative Coating Quality) Kit [27] including setup with a single carbon-based polymer electrode, shown in Fig. 1a, acting as a counter and reference electrode and a substrate (non-patinated, patinated and coated $CuSn_6$ and $CuSn_{12}$ bronze). Comparative measurements were performed in a liquid electrolyte cell consisting of a saturated calomel electrode (RE), a platinum electrode (CE), and the bronze plate as the working electrode (WE) with 3.5 % aqueous sodium chloride solution and tap water.

The frequency range used in the measurements was between 10^5 and 10^{-1} Hz, the AC signal amplitude was 10 mV, and the DC bias potential of the EIS measurements corresponded to the value of the stabilized open circuit potential [24]. After measuring the spectra, single frequency measurement was repeated 5 times at 0.1 Hz.

In all cases, the surface of the bronze electrode was masked (Fig. 1b) with a 0.18 mm thick adhesive tape and the exposed electrode area was limited to a circular area of 1 cm^2, to which electrolyte paste was applied and covered by the counter electrode. Prior to measurements, in a cell with liquid electrolyte, 3.5 % NaCl and tap water, the working electrodes were stabilized for 1000 s. Since the samples were already in equilibrium with the environment, equilibration time of 10 s was sufficient for the working electrodes in the case of measurements with the paste. After the measurements, the paste was removed by carefully wiping the surface with a damp cloth without damaging the surface layer on bronze.

For measurements on coins, the electrodes were attached to the opposite surfaces of the coin, facing one another (Fig. 1c). The opposite, masked surfaces of the coin and the electrodes were considered identical so that the DC offset potential was set to zero. The measurement was done in the range between 10^5 and 10^{-1} Hz with signal amplitudes 10 mV and 5 points per decade. Cumulative impedance of the two surface layers (patina or patina with a one layer of coating) present on both sides of the coin is measured with this method. The final surface layer impedance is obtained by dividing the cumulative impedance by 2. The electrolyte layer resistance was found to be negligible with respect to surface layer resistances.

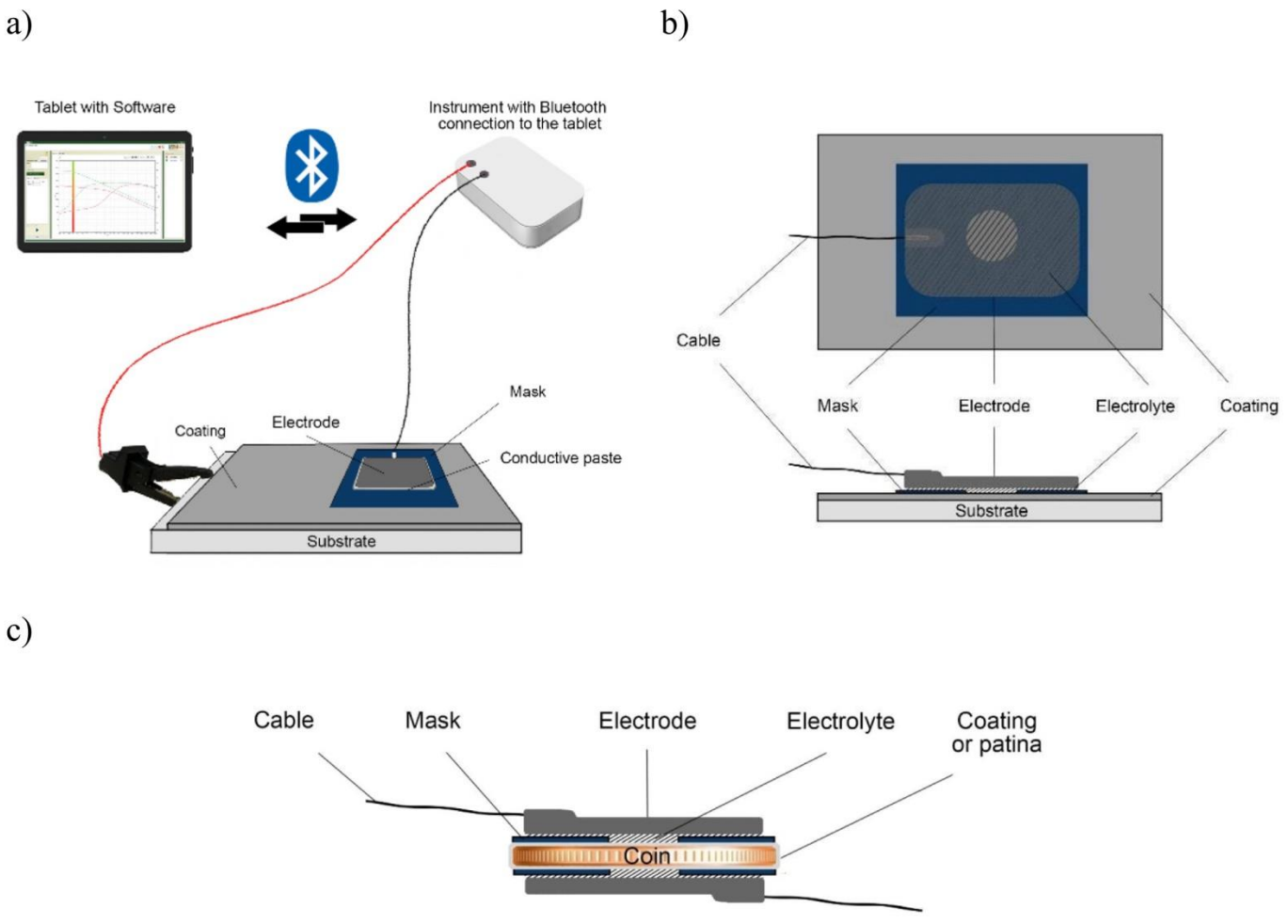

Fig. 1. Schematic diagram of a) the entire measurement setup, b) the details of the cell setup for one-electrode measurements and c) the cell setup for coins.

2.6. Condensation chamber test

Samples of $CuSn_{12}$ bronze were exposed to a condensing atmosphere in the condensation test chamber CON 300 –FL for 24 h.

3. Results and discussion

In the present study, two or three parallel CPE-R couples are used for coated bronze depending on the number and integrity of the layers, and the analysis is done in terms of characteristic frequencies to attribute a physical meaning to each time constant. It should be noted that with increasingly better barrier properties of the coating, its influence protrudes to the lower frequencies, affecting the interpretation. Also, the low frequency circuit parameters are sometimes impossible to determine [37], as significant extrapolation is required. Summary of experimental research is presented in Table 1.

The dispersion of the time constants is observed for all the circuits due to the electrochemical/potential inhomogeneity [4].

3.1. EIS tests on $CuSn_6$ bronze in various electrolytes

The results of laboratory tests on bronze in liquid electrolytes, 3.5 % NaCl solution and tap water, were compared to the measurement in the paste electrolyte to evaluate the aggressiveness of the paste towards the substrate.

Tap water and sodium chloride were selected for comparison as non-aggressive and aggressive electrolytes, according to Ramirez Barat, et al. [4].

Fig. 2 shows the fitted Bode plots and parameters of two parallel CPE-R circuits representing the behavior of $CuSn_6$ bronze in 3.5 % NaCl, tap water, and paste electrolyte. The spectra (Fig. 2a) exhibited two-time constants, which is due to the short immersion time during which a very thin oxide layer was formed [4,38]. The resistance (Fig. 2b) of the immersed samples is lower than that exposed to the paste, and it is lowest in the case of sodium chloride, where the aggressiveness of the electrolyte promotes the corrosion process. The calculated logarithm of the capacitance (Fig. 2c) shows that the values for tap water and paste electrolyte are similar and significantly lower than those measured in 3.5 % NaCl, indicating a smaller surface area that corrodes [37,39]. The characteristic frequencies (Fig. 2d) calculated as $f = 1/2\pi RC$ expressed on a logarithmic scale, appear in the middle and low frequency range, which is consistent with the adopted interpretation and indicates an oxide layer and a Faradaic process on the surface of the metal.

Interpretation of the data proved to be a challenge as a many scientists found that the same data can easily fit on multiple equivalent circuits [4,10,40] and be interpreted in different ways. Due to the surface inhomogeneities and roughness, the investigated systems do not follow the ideal capacitive behavior and the CPE (constant phase element) must be used instead of the capacitors [10,41–43]. Capacitance values have been calculated from the Q, R and α values by the equation: $C = Q^{1/\alpha}R^{(1-\alpha)/\alpha}$ [44].

According to Barat et al. [4], bare bronze in liquid electrolyte can be fitted to various equivalent electrical circuits, but most authors use a circuit with two parallel CPE-R couples, one related to the resistance of the oxide layer (R2) and its capacitance (C2) and the other (R3 and C3) related to the Faradaic reactions due to the corrosion process on the metal surface. During the exposure to the electrolyte, the third time constant appears at high frequencies [26,33] when the oxide layer reaches a certain thickness. In the present study two parallel CPE-R couples are used to fit the data obtained on bare bronze. No mechanistic conclusions are reached, since the measurements were done on freshly polished bronze surface with the main purpose of assessing corrosivity of electrolyte paste and comparing it to the corrosivity of 3.5 % NaCl and tap water.

The average values and standard deviations of electrolyte resistance R_s obtained from fitting of the equivalent circuit to the experimental data obtained in 3.5 % NaCl solution, tap water, and paste electrolyte are equal to 9.84 ± 0.03 Ω, 609.73 ± 6.37 Ω and 171.83 ± 2.31 Ω, respectively.

The resistance of about 10 Ω is frequently measured for 3.5 % NaCl solution [45]. According to the local analysis center, the measured tap water resistance ranges from 400 to 2309 Ωcm [46] and the value for the water used was 1315 Ωcm. The measured resistance of about 600 Ω is consistent with the distance of the reference electrode from the working electrode of about 0.5 cm. The resistance of the paste electrolyte in the chosen cell arrangement is about three times lower and low enough to

Table 1
Summary of experimental research.

EIS measurements on	Samples		Motivation
Bronze in various electrolytes $CuSn_6$ bronze in 3,5 % NaCl / Tap water / Paste electrolyte	$CuSn_6$ _3,5 % NaCl $CuSn_6$ _ Tap water $CuSn_6$ _ paste		Evaluate the aggressiveness of the paste towards the substrate
Two artificially patinated and coated types of bronze	Uncoated	Coated	To investigate the ability of the paste electrolyte EIS cell to discriminate between
$CuSn_6$/$CuSn_{12}$ + sulfide patina	$CuSn_6P$	$CuSn_6P\_2L$	different sulfide patinated bronze
+ 2 layers Paraloid B-72	$CuSn_{12}P$	$CuSn_{12}P\_2L$	substrates in the uncoated and coated states
Bronze with protective coating layers			To investigate the ability of the paste electrolyte EIS cell to
$CuSn_6$ bronze + sulfide patina +1 layer	$CuSn_6P\_1L$		discriminate between coatings with different number of layers
+ 2 layers	$CuSn_6P\_2L$		
+3 layers Paraloid B-72	$CuSn_6P\_3L$		
Artificially patinated coated bronze in various electrolytes	$CuSn_6P\_2L\_3{,}5\%NaCl$		To investigate the influence of electrolyte on the artificially
$CuSn_6$ bronze + sulfide patina +2 coating layers	$CuSn_6P\_2L\_tapW$		patinated and double-coated $CuSn_6$ bronze
in 3,5 % NaCl/ Tap water /Paste electrolyte	$CuSn_6P\_2L\_paste$		
Bronze with damaged protective layers $CuSn_6$ bronze + sulfide patina +1 layer Paraloid B-72 Successively mechanically damaged	$CuSn_6P\_1L$ Damage 1 Damage 2 Damage 3 Damage 4		To investigate the ability of the paste electrolyte EIS cell to resolve between the intact layers and layers damaged to various degrees
Protected bronze exposed to a condensing atmosphere $CuSn_{12}$ bronze + sulfide patina +1,2,3 L of Paraloid B-72 Before and after exposure in the condensation test chamber for 24 h	Before $CuSn_{12}P$ $CuSn_{12}P\_1L$ $CuSn_{12}P\_2L$ $CuSn_{12}P\_3L$	After $CuSn_{12}P\_W$ $CuSn_{12}P\_1L\_W$ $CuSn_{12}P\_2L\_W$ $CuSn_{12}P\_3L\_W$	To investigate the protective properties of the chosen system after exposure to constant humidity in the condensation test chamber for 24 h
Bronze coins uncoated/coated with 1 layer of Paraloid B-72	2 Heller coins 1895 1899 1900 1909 1910 1914 1915	Coated 2 Heller coins 1L_1895 1L_1899 1L_1900 1L_1909 1L_1910 1L_1914 1L_1915	To determine the reliability of the studded method for practical application to bronze heritage

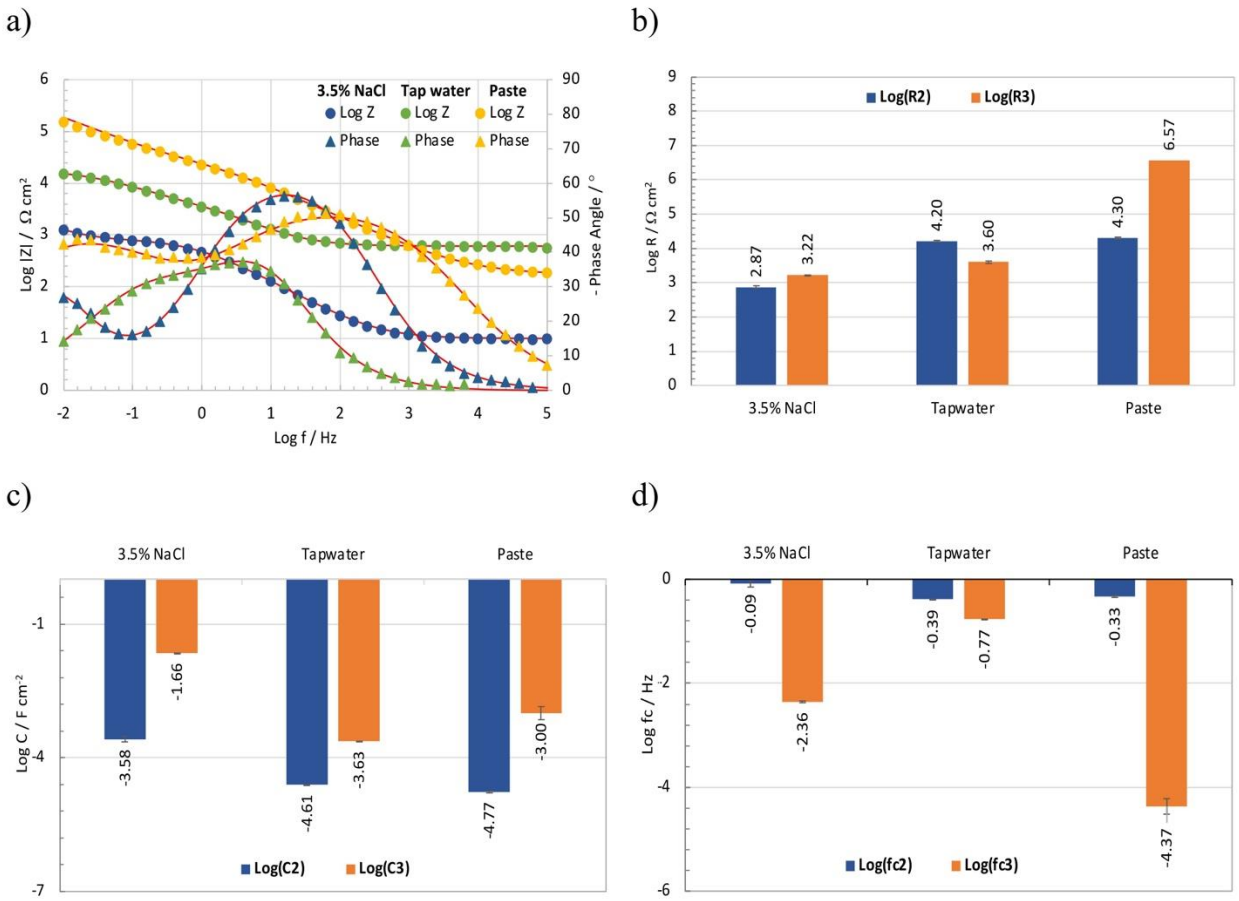

Fig. 2. a) Bode spectra measured for the $CuSn_6$ bronze in various electrolytes, logarithm of b) resistances, c) capacitances and d) characteristic frequencies of the equivalent circuit.

enable measurements of coating and polarization resistances.

Relative standard deviation (RSD) for electrolyte resistance is calculated from three measurements and it shows good repeatability and reproducibility so it will not be discussed further.

Fig. 3 shows that, after a typical EIS measurement, the surface of the bronze changed visually in aqueous solutions, while the surface remained unchanged in the electrolyte paste.

3.2. EIS tests on two artificially patinated types of bronze

To investigate the ability of the paste electrolyte EIS cell to discriminate between different sulfide patinated bronze substrates in the uncoated and coated states, the Bode spectra were measured for sulfide-patinated $CuSn_6$ and $CuSn_{12}$ bronzes without ($CuSn_6P$ and $CuSn_{12}P$) and with a two-layer coating ($CuSn_6P\_2L$ and $CuSn_{12}P\_2L$).

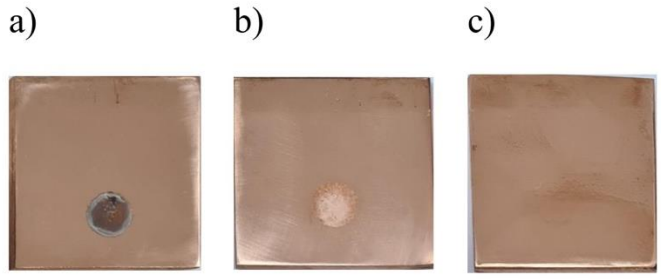

Fig. 3. The appearance of the surface of bronze with the masking tape removed after EIS measurements in a) 3.5 % aqueous sodium chloride solution, b) tap water, and c) with the paste electrolyte.

Fig. 4a and b show Bode spectra measured on the two artificially patinated bronzes and on the same patinated bronzes with two coating layers. The Log |Z| value at low frequencies is significantly higher for coated samples and also higher for $CuSn_{12}$ than for $CuSn_6$. The high-frequency phase angle is zero for $CuSn_6$, while it reaches a value of almost 60° for $CuSn_{12}$ bronze and almost 90° for the coated sample. The increase of the phase angle at high frequencies indicates an increase of the protective ability and a shift towards capacitive behavior [4].

The spectra were fitted to two CPE-R couples connected in parallel.

Studies on patinated bronze substrates with and without coating show good agreement with two-time constant equivalent circuits for coatings with good barrier properties and very compact patina, and three-time constant equivalent circuits for porous coating and patina and reactive patina [37,39,47]. In the case of two-time constant equivalent circuits, the first CPE-R couple at high frequencies is correlated with the dielectric properties of the coating or patina (R1, C1), while the second CPE-R couple at medium frequencies is attributed to the patina double layer resistance (R2) and capacitance (C2). In the case of the porous coatings and patina, the first CPE-R pair at high frequencies (10–10^3 Hz) represents the resistance (R1) of the non-reactive patina layer or pores in the coating and the appending capacitance (C1). At medium frequencies (10^{-1}-10 Hz), the reactive patina layer is described, with the second CPE-R couple providing information about the resistance (R2) of the charge transfer and the double layer capacitance (C2). The third time constant at low frequencies ($< 10^{-1}$ Hz) appears when the electrolyte finds its way through the pores to the substrates. The third CPE-R couple therefore represents the Faradaic resistance (R3) and the capacitance (C3) at the surface of the substrate [4,10,37–39,48,49]. The first CPE-R couple on high frequencies for the patinated CuSn6 bronze is not observed which implicated that the patina

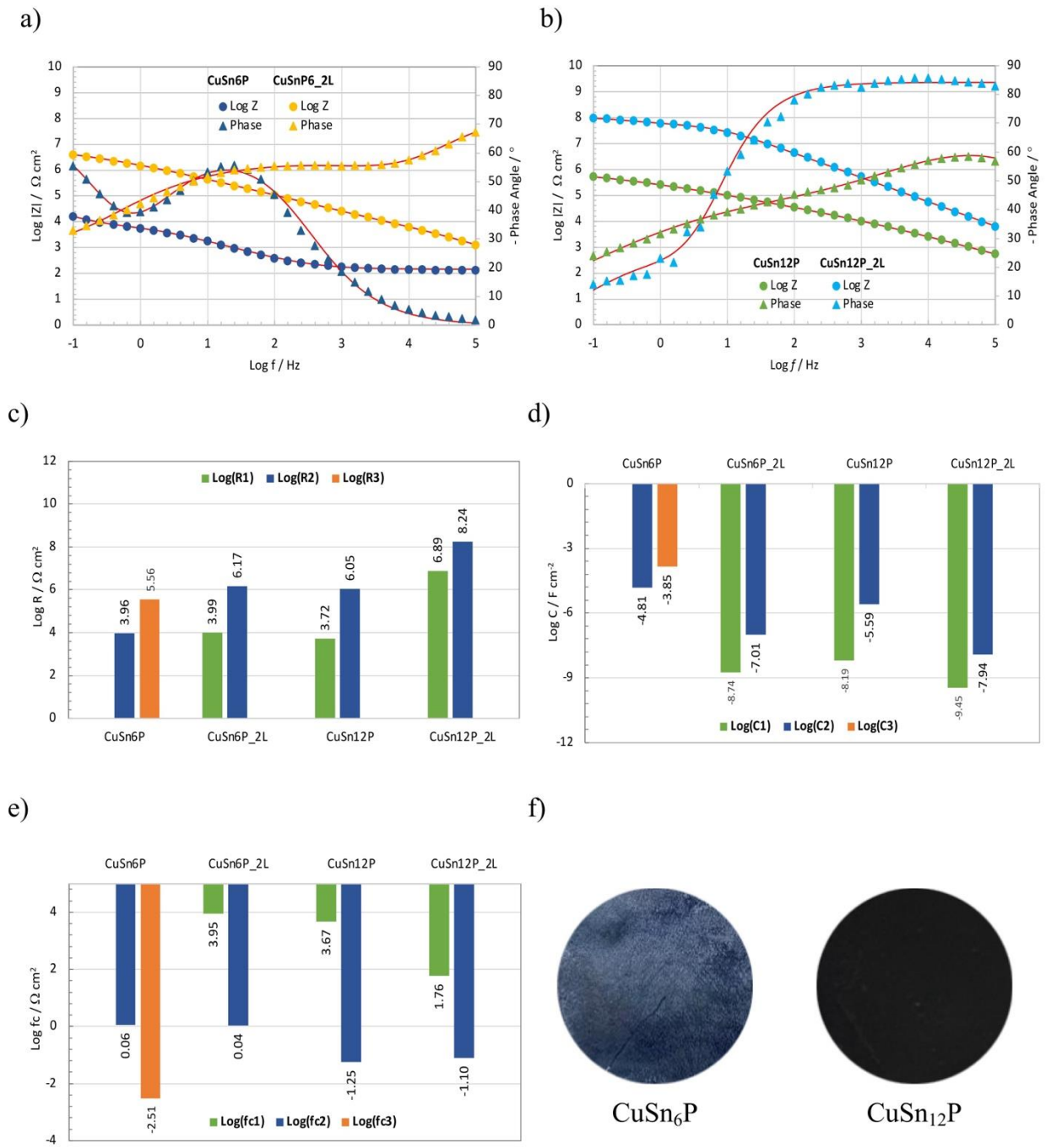

Fig. 4. Bode spectra for artificial sulfide patinas without and with two layers of coating on a) $CuSn_6$ and b) $CuSn_{12}$ bronze and logarithm of c) resistances, d) capacitances, e) characteristic frequencies of the equivalent circuit and f) visual appearance of the patinas without coating.

doesn't have non-reactive layer, only reactive.

Fig. 5a shows a schematic diagram of the paste electrolyte surfaces investigated in this study, which include polished bronze, patina, porous coating on patina, and nonporous coating on patina. The electrical equivalent circuit used to fit the part of data is shown in Fig. 5b. It consists of three parallel CPE-R circuits, where the first CPE1-R1 couple characterizes the capacitive and resistive behavior of the coating or non-reactive patina, the second CPE2-R2 couple characterizes the non-Faradaic capacitance and resistance of the active patina, and the third CPE3-R3 couple characterizes the Faradaic process on the surface of the bronze substrate.

As previously mentioned, the systems investigated in this study have two or three time constants, depending on the number and integrity of the layers and the equivalent circuit was chosen accordingly. The fitted CPE data are converted to capacitance and plotted on the graphs.

Fig. 4c shows that the resistance in the high and medium frequency ranges for the patinated bronzes increases with the application of the coating, probably due to the closing of the patina pores [43] and due to the insulating properties of the coating, respectively. The barrier properties of the protective coatings on the $CuSn_6$ sample were confirmed in Fig. 4d, where the coated $CuSn_6$ bronze has overall lower capacitance values than the uncoated $CuSn_6$ bronze. The high frequency circuit appears and the low frequency circuit is lost due to the coating. The patinated $CuSn_{12}$ bronze with the two-layer coating also shows a decrease in capacitance compared to the uncoated sample. The characteristic frequencies in Fig. 4e show that the EIS response of the

a)

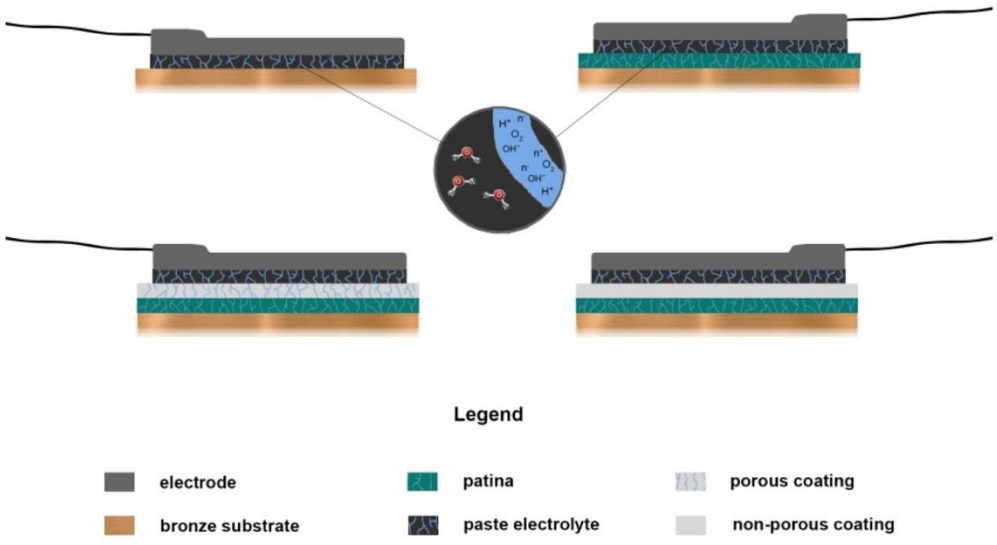

b)

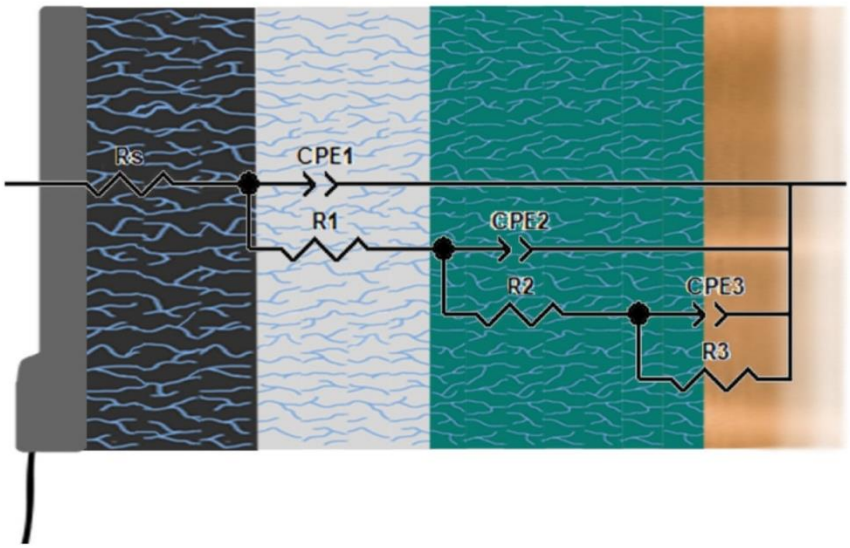

Fig. 5. a) Schematic diagram of the paste electrolyte on bronze and its protective layers and b) electric equivalent circuit used for coated samples.

patinated $CuSn_{12}$ bronze is similar to that of the coated bronze at high and medium frequencies, while the patinated $CuSn_6$ bronze shows a medium and low frequency response, indicating a Faradaic process on the metal surface [38,41]. The absence of the low frequency circuit [4,37] on $CuSn_{12}$ bronze is explained by the insulating properties of $CuSn_{12}$ patina, which is visibly more compact than $CuSn_6$ patina. Fig. 4f shows the appearance of the sulfide patina on $CuSn_6$ and $CuSn_{12}$ bronzes before the EIS test. Visually, the patina on $CuSn_6$ bronze is more porous and less compact, as confirmed by the value of Log |Z| at 0.1 Hz, which is 3.97 for $CuSn_6$ and 5.74 for $CuSn_{12}$. Resistances up to 10^4 Ω cm2 were also observed by Grassini 23 for "black patina" on bronze in 0.1 M Na_2SO_4 [23].

In conclusion, the protective ability of Paraloid-B72 depends on the type of bronze. In continuation of the experiments, the less resistant patina on $CuSn_6$ bronze was protected and subjected to intentional damage, while the more resistant sulfide patina on $CuSn_{12}$ (Fig. 4) was exposed in the condensation chamber.

3.3. EIS tests on $CuSn_6$ bronze with protective coating layers

To investigate the ability of the paste electrolyte EIS cell to discriminate between coatings with different number of layers, the Bode spectra were measured for one, two and three-layer coatings on sulfide-patinated $CuSn_6$ bronze.

Bode spectra in Fig. 6a show that Log |Z| value at low frequencies increases with the number of layers and so does the phase angle at the high frequency limit. Capacitive response becomes more pronounced with more coating layers, with the phase angle of almost 90° protruding towards lower frequencies.

Log |Z| at 0.1 Hz increases by more than one order of magnitude for the first coating layer compared to sulfide patinated $CuSn_6$ bronze (Fig. 4a and e) and by two more orders of magnitude after each of the following layers. Resistances up to 10^9 Ω cm^2 were also observed by Goidanich [3] for bronze protection by three layer coatings including Incralac and Licowax R21.

The spectra were fitted with three or two CPE-R couples connected in parallel for one layer of the coating and two and three layers, respectively. The first CPE-R couple represents the resistance and capacitance of the coating, the second CPE-R couple represents the patina behavior, and the third CPE-R couple represents the Faradaic response on the metal surface. The low frequency response is observed only for the sample with one layer of coating. Fig. 6b shows that the resistance increases with the number of applied layers. The high-frequency capacitances (Fig. 6c) are of the order of nF cm^{-2} for all samples. The medium-frequency capacitances decrease with the number of coating layers from 1.1 μF cm^{-2} to 2.3 nF cm^{-2}, which is consistent with the literature for dark green patina [48], and the low-frequency capacitance, attributed to the substrate reaction, is in the mF range. The occurrence of the third characteristic frequency for the sample with one-layer coating confirms that this layer is porous and the electrolyte can penetrate to the surface of the substrate. The characteristic frequencies for the three-layer coating show a shift to the lower values, which is typical for the high-impedance coatings with good barrier properties [50].

Repeated measurements of the entire spectrum on the sample with two coating layers with removal of the paste between the measurements give RSD of 0.14 % showing that the layer is not damaged by the cell application and the paste removal.

3.4. EIS tests on $CuSn_6$ with damaged protective coating layers

To investigate the ability of the paste electrolyte EIS cell to distinguish between intact and layers damaged to various degrees, an artificially patinated $CuSn_6$ bronze surface coated with a layer of Paraloid B-72 was gradually damaged with a scalpel, and the impedance rank was observed at each stage of damage.

Fig. 7a shows the visual appearance of the damaged layer. Fig. 7b shows Bode spectra measured for bronze with artificial sulfide patina and a one layer of coating after inflicting various degrees of damage. The data is fitted to the equivalent circuit according to the Fig. 5b.

The shape of the Log |Z| and phase angle curves in Fig. 7a changes

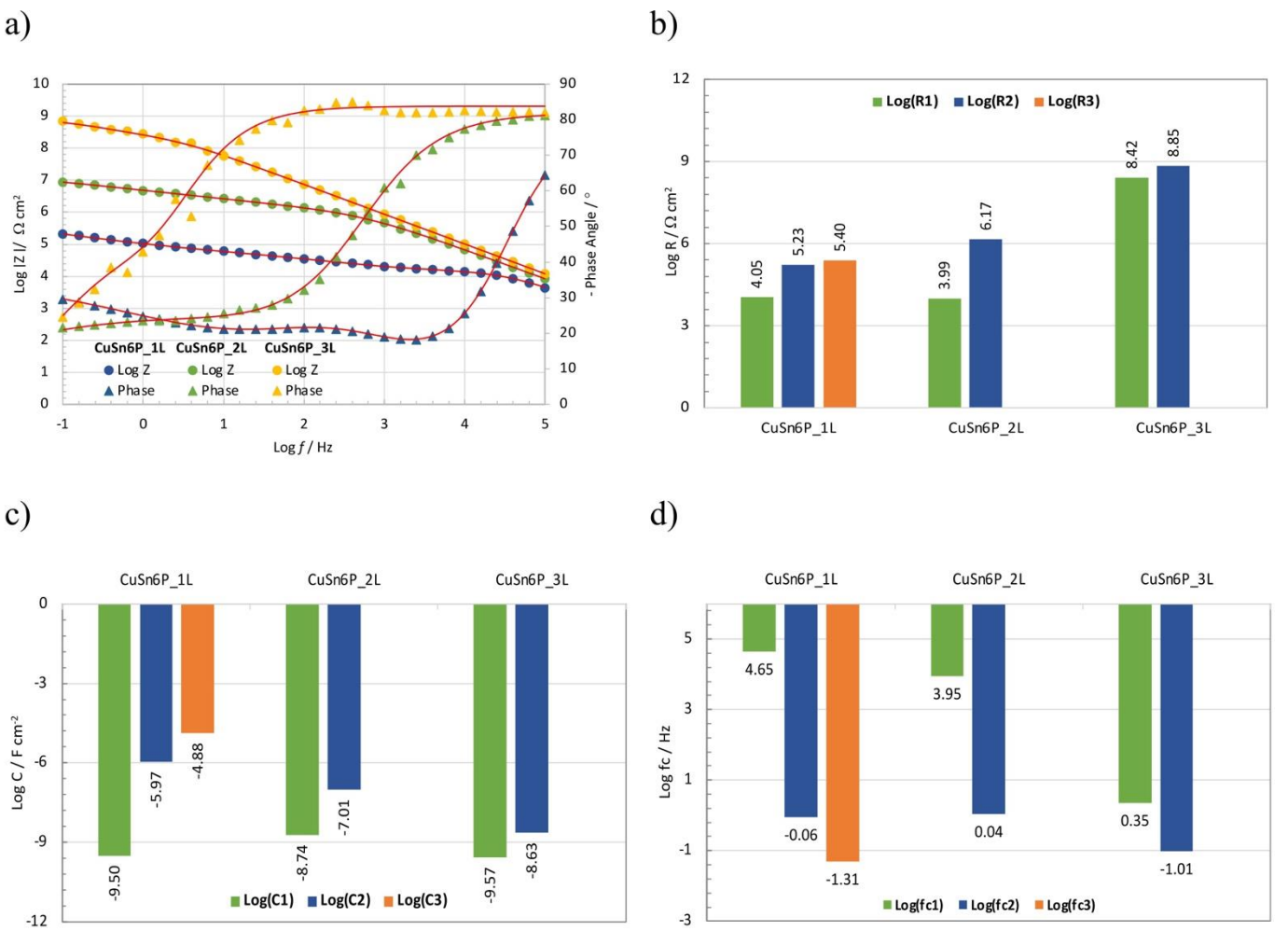

Fig. 6. a) Bode spectra measured for the sulfide patinated (P) $CuSn_6$ bronze with one (1 L), two (2 L), and three layers (3 L) of coating, logarithm of b) resistances, c) capacitances and d) characteristic frequencies of the equivalent circuit.

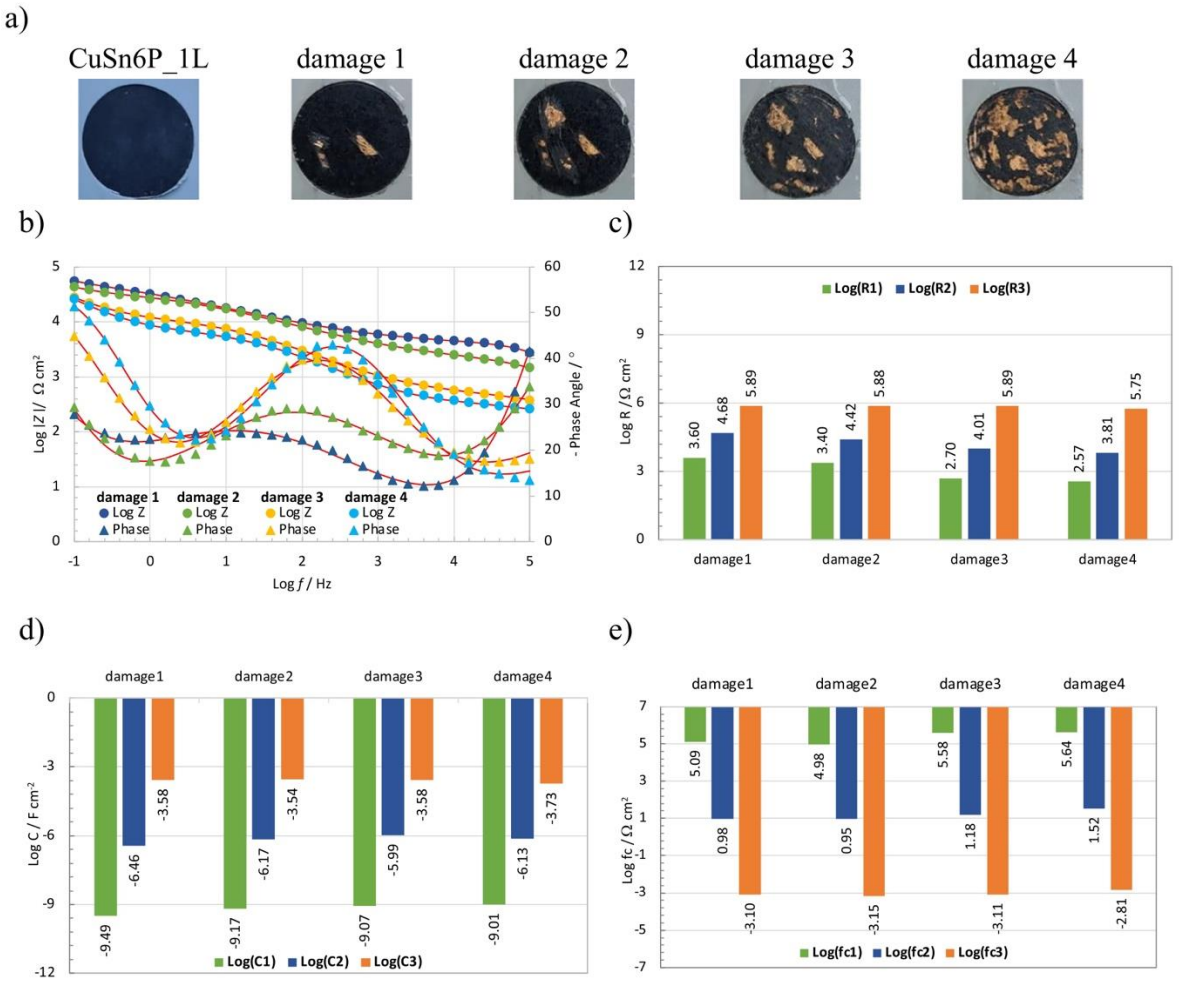

Fig. 7. a) appearance of the bronze sample covered with an artificial sulfide patina and a one-layer coating before and after being damaged to various degrees, b) Bode spectra measured for the damaged samples, logarithm of c) resistances, d) capacitances, and e) characteristic frequencies of the equivalent circuit.

from that characteristic of the sulfide patinated, bronze coated with one layer in Fig. 6a to that representative of the bronze in Fig. 4a.

The resistance values shown in Fig. 7c remain nearly unchanged at medium and low frequencies, while a decrease in coating resistance is observed at high frequencies as the surface of the specimen becomes more damaged. Damage to the protective layers on the sample exposes the Faradaic process on the substrate. The capacitance (Fig. 7c) increases with increasing damage to the protective layers, indicating an increase corrosion prone area [37,39]. The Log |Z| value in Fig. 7c decreases with mechanical damage from a value of 5.33, which characterizes the barrier effect of a one-layer coating on sulfide patina, to 4.42, which is still higher than the value of 3.97 measured for the sulfide-coated bronze.

3.5. EIS tests on artificially patinated coated bronze in various electrolytes

To investigate the influence of electrolyte on the artificially patinated and double-coated $CuSn_6$ bronze, EIS measurements were done in 3.5 % NaCl, tap water and paste electrolyte.

Two coating layers on patinated $CuSn_6$ bronze have an EIS response with two-time constants, at high and medium frequencies in all electrolytes except tap water, where a single high-frequency response is observed probably because of the very high resistance of the electrolyte which disables response from lower frequencies. The resistance is much higher and the capacitance much lower in the paste electrolyte than in 3.5 % NaCl, indicating conductive but less aggressive media (Fig. 8).

Although the corrosion process in bronze art and cultural objects most often occurs under atmospheric conditions [51], EIS measurements traditionally require immersion of the sample (or an area of the sample) in an electrolyte [52]. As pointed out by Davis G.D. et al., the presence of electrolyte can alter the temporary coating, and immersion can result in artifactual damage to the sample, even with short immersion times [52,53]. The immersion can therefore result in a drop in resistance that may not be consistent with the actual protective effect of the coating. In the case of the paste electrolyte, the barrier effect of the two-layer Paraloid B-72 on the sulfide patina is clearly evident and is around 10^7 Ω cm^2 at 0.1 Hz. The results are consistent with the impedance ranges found in the literature for acrylic layers on "black patina" [12,54].

3.6. EIS tests on protected bronze exposed to a condensing atmosphere

In order to quickly simulate the conditions to which the samples may be exposed outdoors and to investigate the protective properties of the chosen system without immersion, the set of samples was exposed to a condensing atmosphere of 100 % relative humidity in the condensation test chamber for 24 h. The barrier effect of sulfide layer on $CuSn_{12}$ bronze and of sulfide with one, two and three layers of Paraloid B-72 was investigated before and after exposure. Fig. 9a and b show Bode spectra before and after exposure, respectively.

After 24 h of the exposure, a drop in resistance is evident in all cases, as seen from the comparison of Fig. 9c and d, indicating that the surface

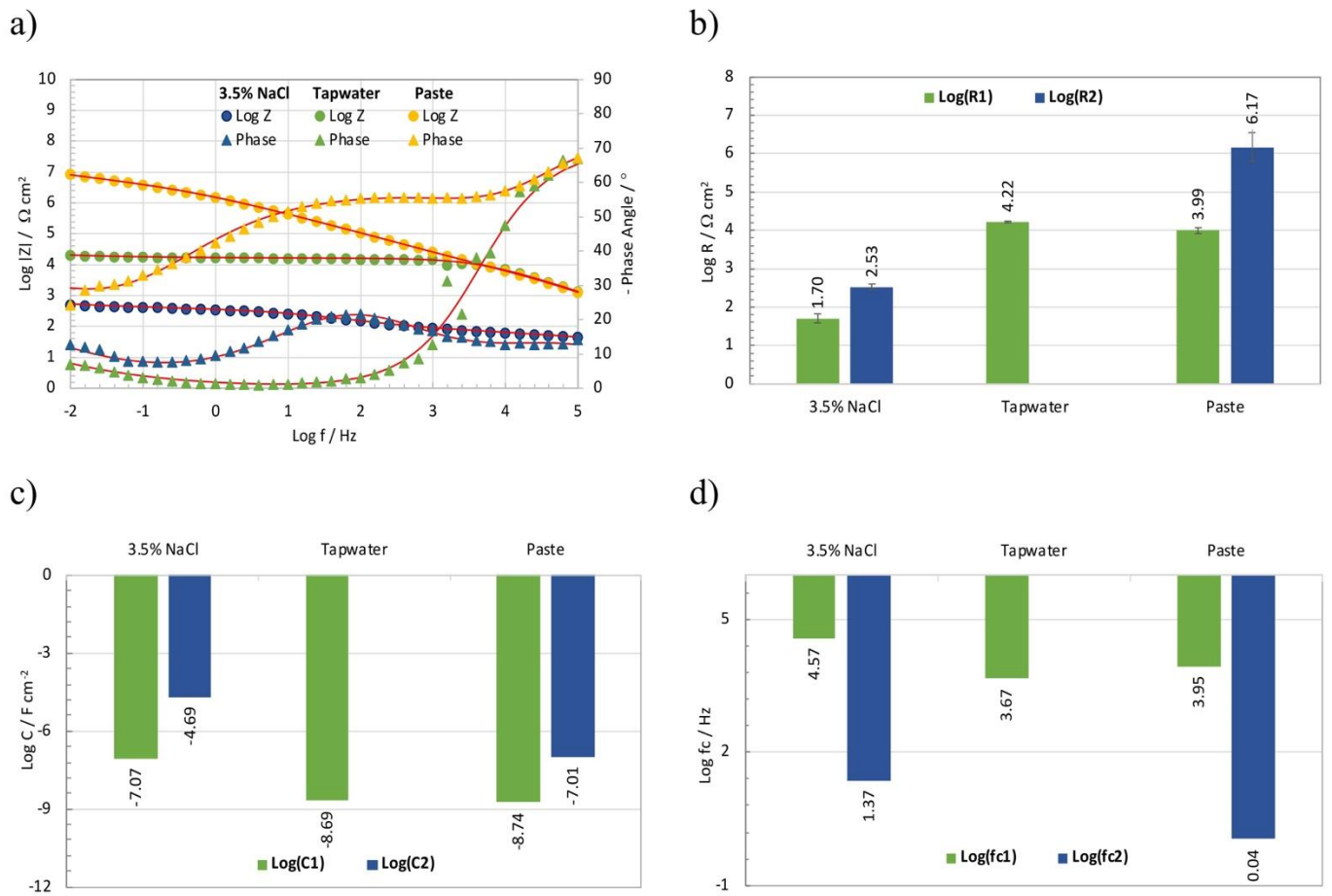

Fig. 8. a) Bode spectra measured for the sulfide patinated $CuSn_6$ bronze with two layers of coating in various electrolytes, logarithm of b) resistances, c) capacitances, and d) characteristic frequencies of the equivalent circuit.

layers are permeable to water that diffuses into the pores. The resistances of all samples are close to 10^6 Ω cm^2 after exposure, indicating that one and two layers of Paraloid B-72 do not provide a sufficient barrier under water condensation conditions. The three-layer system exhibits a resistance of about 10^8 Ω cm^2, indicating that the three layers of Paraloid B-72 provide adequate corrosion protection, even under condensation conditions. Fig. 9c and d confirm that the electrolyte does not penetrate through the three coating layers to the surface of the metal, but the protective layers maintain the high resistance values at high and medium frequencies from before exposure. The remaining samples show a response at low frequencies, indicating that the electrolyte penetrates to the surface of the metal substrate in these samples. The capacitance values increase towards lower frequencies for all samples, but the samples without and with one layer of Paraloid B-72 show a more pronounced increase in capacitance after 24 h of exposure in the condensation chamber, while the exposure has a slight and no effect on the samples with two or three layers of the coating, respectively, confirming better protection.

3.7. Measurements on bronze coins

Seven Austro Hungarian 2 Heller coins from a private collection shown in Fig. 10 were also EIS tested in their pristine state and then with one coat of Paraloid B-72. In the pristine state, the coins were covered by a thin and even layer of brown patina, with no visible signs of active corrosion or previous cleaning or coating treatments. In the further text, the coins are denoted by their mint year.

EIS measurements were performed using the experimental setup shown in Fig. 1c. The aim was to determine the reliability of the studied method for practical application to bronze heritage. Fig. 11a and b show Bode spectra of the uncoated and coated coins, respectively.

All protected coins exhibit higher impedance values and more capacitive behavior, as indicated by the phase angle at high frequencies. Unprotected coins exhibit a low-frequency resistance related to the Faradaic process on the coin surface, with a high value between 10^5 and 10^6 Ω cm^2 due to the low corrosivity of the paste electrolyte. The medium-frequency patina resistance is much lower than that of the protected coins, indicating the redox process [38]. Coated coins show resistance of coating and patina with no evidence of a Faradaic process on bronze surface. The calculated capacitances show the decrease of the surface area susceptible to corrosion of the coated samples. The characteristic frequencies confirm that the coating provides a good barrier and responds only to the high and medium frequencies, while the patina, although providing relative protection, does not prevent the corrosion of the substrate because the electrolyte can penetrate to the metal surface, causing the response in the low-frequency range.

A one layer of coating provides different protection for the similar specimens, probably due to the combination of the unevenness of the coating and the coin surface. This result justifies the common practice of applying multiple coatings to historic bronze objects.

Linearity, causality, and time invariance of the system used for EIS characterization of the coins [15,55] were tested by applying the linear Kramers-Kronig transform to all spectra in Fig. 11 [32–34]. Log |Z| was calculated from the fitted Z_{Re} and Z_{im}, and the relative error versus frequency between the measured and ideal Kramers-Kronig Log |Z| is shown in Fig. 12.

From the results given on Fig. 12a for the uncoated coins, it can be noted that residuals do not exceed ±0.2 % on the entire analyzed

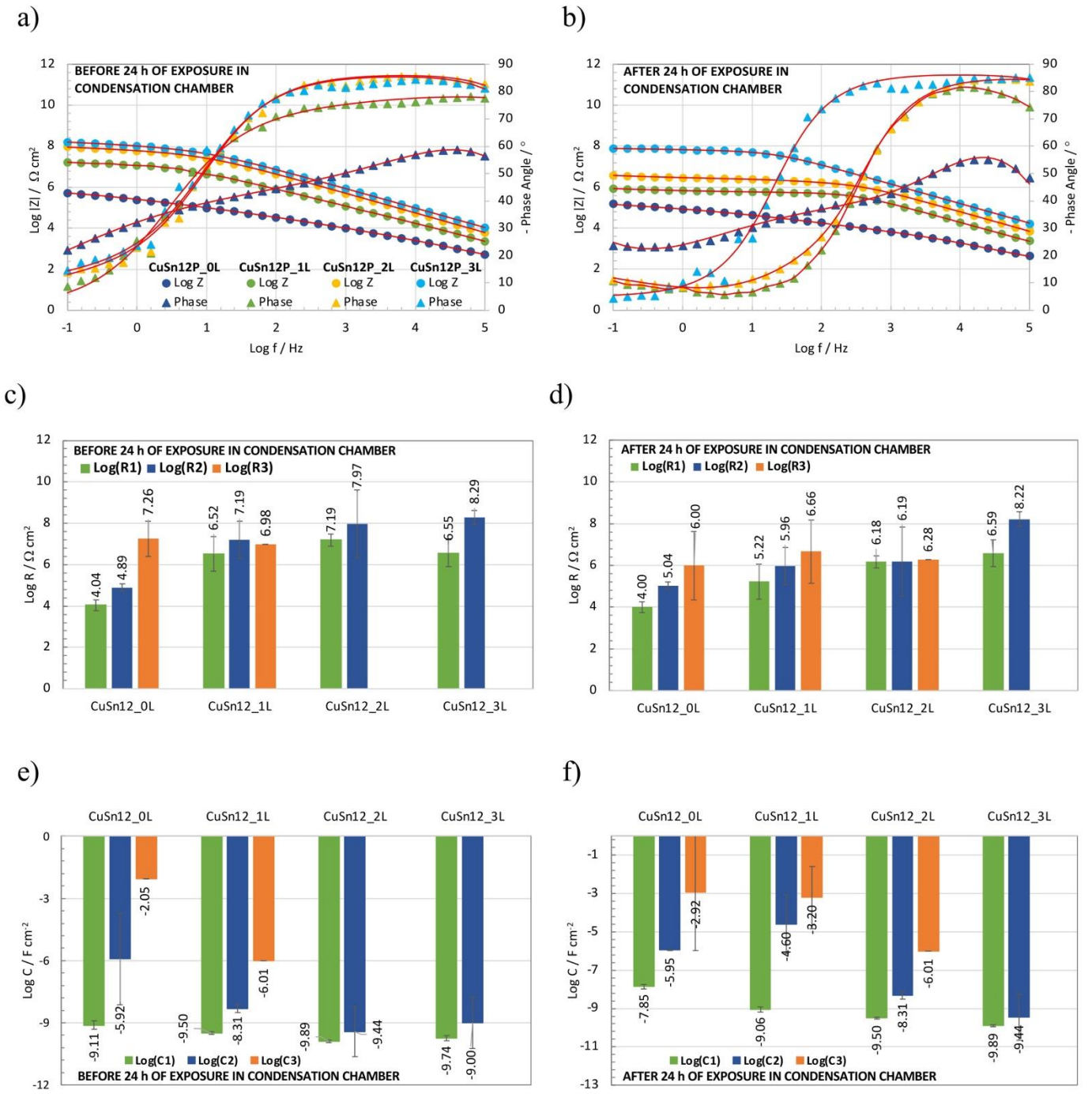

Fig. 9. Bode spectra for measurements with paste electrolyte on the sulfide patinated $CuSn_{12}$ a) before and b) after exposure in the condensation chamber for 24 h, the respective logarithm of resistances, c) and d) and the respective capacitance e) and f).

Fig. 10. Austro Hungarian 2 Heller coins from a private collection that were subjected to EIS testing in the novel cell.

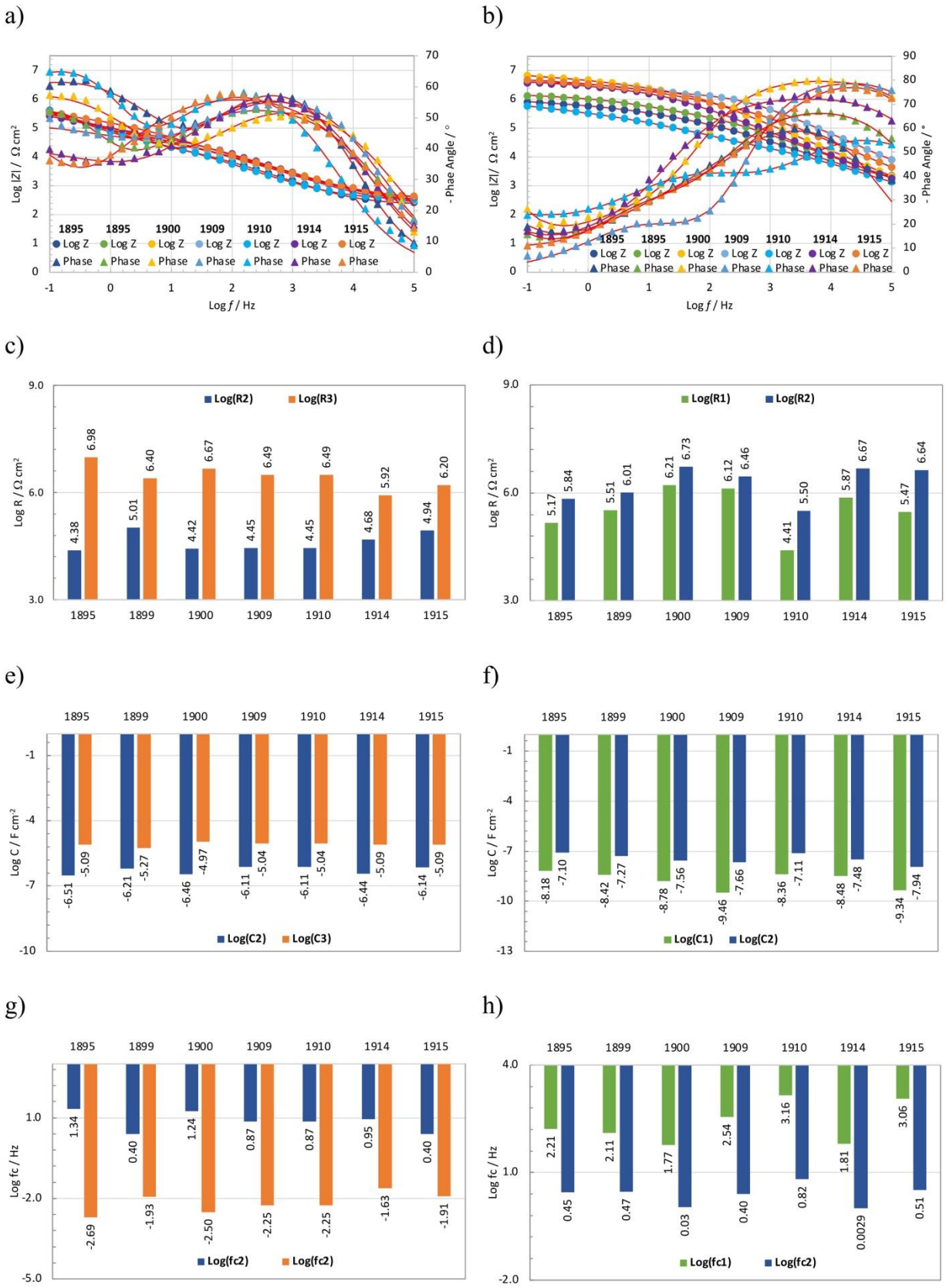

Fig. 11. Bode spectra measured on the bronze coins a) in the pristine (uncoated) state and b) with one layer of coating, the respective logarithm of c) and d) resistances, e) and f) capacitances and g) and h) characteristic frequencies of the equivalent circuit.

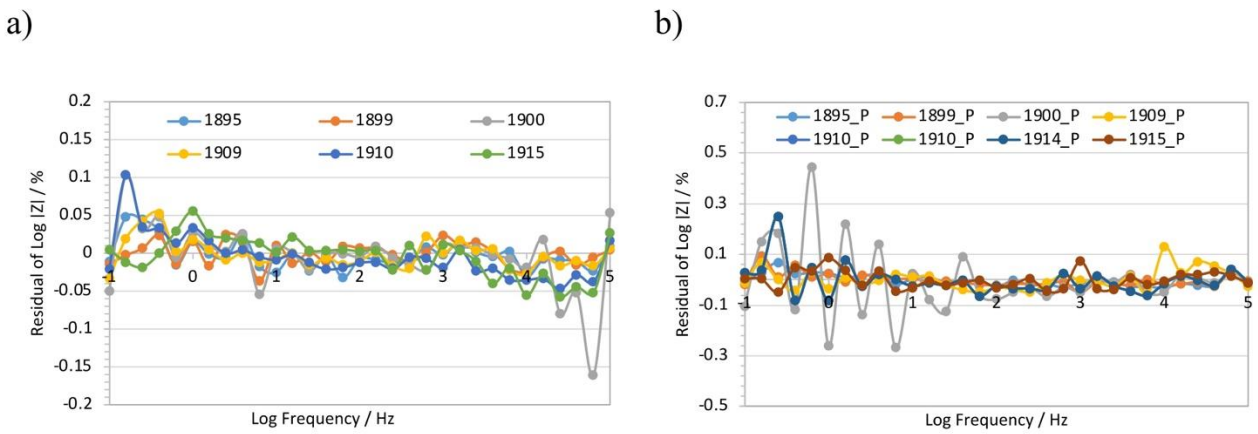

Fig. 12. Kramers-Kronig residuals of Log |Z| determined for a) unprotected coins and b) coins protected with a one layer of coating.

frequency spectrum, indicating that measured data closely match with Kramers-Kronig theoretical spectrum. In the case of coins protected by one layer given on Fig. 12b, the values of the residuals are slightly higher, but even extreme residuals do not exceed ±0.5 %. Therefore, it can be concluded that measured data agree well with Kramers-Kronig theoretical spectrum also in case of protected coins.

The residuals do not deviate from zero over the entire frequency range, indicating that the accuracy of the measurement is not affected by the measurement setup and procedure.

3.8. Log |Z| at 0.1 Hz approximation

EIS measurements allow evaluation of the effectiveness of the protection provided by the coatings. In the conservation science literature, the modulus at the low frequency is often used as a measure of corrosion resistance [4]. This simplified approach was found to be justified when the protective effect of the surface layers is comparatively evaluated [10].

Fig. 13 further explores the applicability of the Log |Z| at 0.1 Hz approximation and shows proportionality of the Log |Z| at 0.1 Hz to the sum of the high and medium-frequency resistances, $R_1 + R_2$. For most of the samples, Log |Z| at 0.1 Hz is good approximation of the cumulative resistance of the patina and coating layers with the fitted line passing through origin, having a slope of ≈1 and a coefficient of correlation R equal to 0.99.

Samples showing deviation from linearity are the pristine (uncoated) Heller coins (Fig. 10), the significantly damaged samples (damage 3 and 4 from Fig. 7a) and the sample with low-quality patina on $CuSn_6$ bronze, denoted as $CuSn_6P$ in Fig. 4f. Deviation is more obvious in Fig. 14a

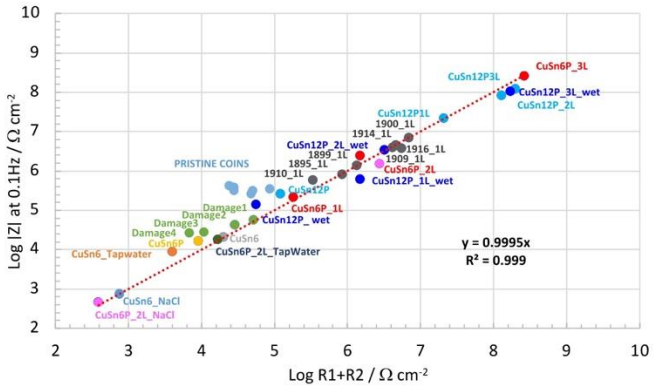

Fig. 13. Comparison of Log |Z| at 0.1 Hz and the sum of the high and medium frequency resistances resulting from fitting the equivalent circuit model to the EIS data for the measurements performed in this study.

where Log(R1 + R2) and Log |Z| at 0.1 Hz are compared.

To determine the criterion for the validity of the Log |Z| at 0.1 Hz approximation the Phase Angle at 0.1 Hz is compared to the $tan\delta = -1/\tan(-\text{PhaseAngle at 0.1Hz})$ parameter that expresses the ratio of the resistive to the capacitive current at 0.1 Hz. For $\tan\delta = 1$, capacitive (imaginary) part of the resistance equals the resistive (real) part. For $\tan\delta < 1$, the capacitive response is predominant indicating insulting characteristic of the coating.

A quantitative criterion of Phase Angle at 0.1 Hz $\leq 40°$ or $\tan\delta \geq 1.2$ for the validity of the Log |Z| at 0.1 Hz approximation of protective layers resistance can be adopted based on Fig. 14b.

Literature [14,56] shows that the unprotected surfaces of copper alloys exposed to a relatively mild environment have impedance values around 10^5 Ω cm^2 (Log |Z| = 5). Impedance values for patina on bronze are generally between 10^4 and 10^5 Ω cm^2 [12,48,57] (Log |Z| = 4–5). Surfaces with residual protective coating have impedance values around 3×10^6 Ωcm^2- 4×10^6 Ωcm^2 (Log |Z| = 6.4–6.6) and surfaces protected by wax based coatings have impedances about 10^7–10^8 Ωcm^2 (Log |Z| = 7–8) [27]. The results from Figs. 2 and 4 are in line with the above ranges.

The criteria for assessment of conservation coatings still need to be defined. Mills et al. [58] recently suggested the respective limits for good, fair and poor coatings of >10 Ω cm^2 (Log |Z| > 5), 5–0.5 Ω cm^2 (Log |Z| = 4.69–3.69) and < 0.5 Ω cm^2 (Log |Z| < 3.69) based on DC resistance measurements and electrochemical noise measurements. Much higher respective limits of Log |Z| > 8 and Log |Z| < 6, are set for good and poor industrial coatings.

4. Conclusions

The novel EIS paste electrolyte cell proved to be advantageous for the analysis of common bronze protection system i.e., sulfide patina covered by a Paraloid B72 coating.

Considering all the measurements made in this study, Log |Z| at 0.1 Hz was found to be approximately equal to the sum of the resistances of the patina and coating layers determined from modeling the EIS spectra. Log |Z| at 0.1 Hz increases from 3.9 to 9.1 ($8{\cdot}10^3$ to $1.25{\cdot}10^9$ Ω cm^2) when moving from bare and patinated bronze to bronze protected with multiple layers of Paraloid B-72. A quantitative criterion of Phase Angle at 0.1 Hz $\leq 40°$ for the validity of the Log |Z| at 0.1 Hz approximation was derived and explained in terms of the ratio of the resistive and capacitive components of the impedance, expressed by $\tan\delta \geq 1.2$. Coating the patinated bronzes of various compositions with Paraloid B-72 layers results in an increase in resistance and a decrease in capacitance.

Quantitative evaluation criteria for conservation coatings still need to be established. These may differ significantly from the criteria for

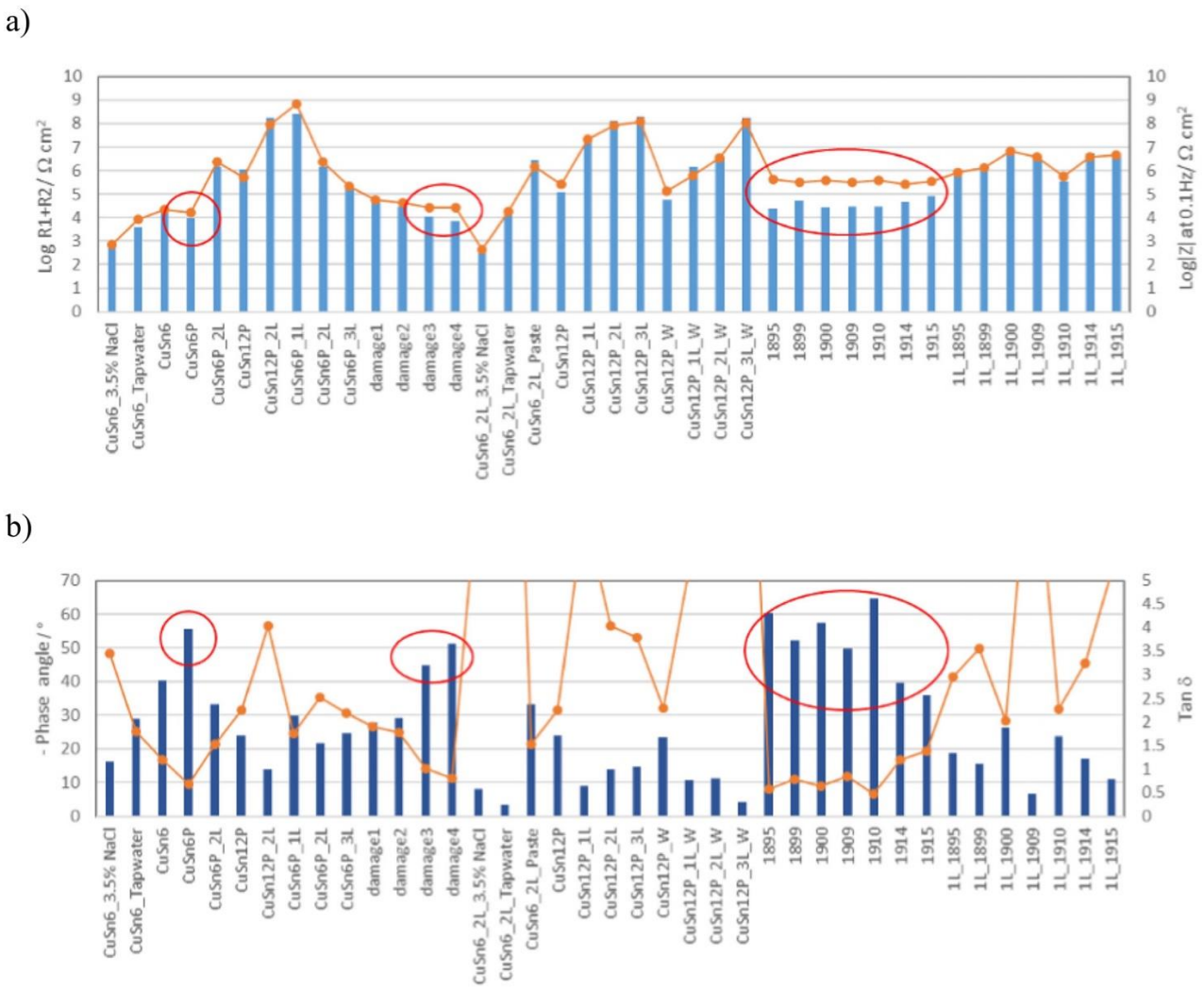

Fig. 14. Comparison of the a) Log(R1 + R2) and Log |Z| at 0.1 Hz values and b) Phase Angle at 0.1 Hz and tanδ for the measurements performed in this study.

industrial coatings, because conservation coatings are much thinner and unpigmented. In addition, the patina itself is considered protective and its morphology can influence the overall effect of the patina/coating system. This simple approach in combination with a paste electrolyte cell allows rapid measurements and the subsequent statistical analysis. Based on the data presented, it is expected that extensive application to various bronze objects, patinas of different appearance and surfaces exposed to different microclimatic conditions, unprotected or protected by conservation coatings, will reveal new behavioral patterns of the bronze objects.

Declaration

The raw/processed data have been shared and it can be access at DOI: 10.17632/ghrkj4d5kk.3

CRediT authorship contribution statement

Ivana Šoić: Investigation, Visualization, Writing.
Ines Šoljić: Investigation, Writing.
Magdalena Eškinja: Investigation.
Adnan Mujezinović: Validation.
Sanja Martinez: Conceptualization, Methodology, Writing.

Declaration of competing interest

The authors declare that they have no known competing financial interests or personal relationships that could have appeared to influence the work reported in this paper.

Data availability

The raw/processed data have been shared and it can be access at DOI: 10.17632/ghrkj4d5kk.3.

Acknowledgments

This work has been fully supported by Croatian Science Foundation under the project Development of new solutions for characterization and protection of bronze cultural heritage exposed to outdoor environment IP-2019-04-5030.

References

[1] F. Mansfeld, S.L. Jeanjaquet, M.W. Kendig, An electrochemical impedance spectroscopy study of reactions the metal/coating interface, Corros. Sci. 26 (9) (1986) 735–742, https://doi.org/10.1016/0010-938X(86)90037-5.
[2] F. Mansfeld, Electrochemical impedance spectroscopy (EIS) as a new tool for investigating methods of corrosion protection, Electrochim. Acta 35 (1990) 1533–1544, https://doi.org/10.1016/0013-4686(90)8007-B.

[3] S. Goidanich, M.A. Zappa, In Situ Non-destructive Techniques for the Study of Cleaning and Protection Methodologies for the Conservation of Bronze Artefacts, School of Industrial and Information Engineering, 2015. Master Thesis.
[4] B. Ramírez Barat, E. Cano, Advances for in-situ EIS measurements and their interpretation for the diagnostic of metallic cultural heritage, ChemElectroChem 5 (2018) 2698–2716, https://doi.org/10.1002/celc.201800844.
[5] B.Ramírez Barat, E. Cano, P. Letardi, Advances in the design of a gel-cell electrochemical sensor for corrosion measurements on metallic cultural heritage, Sensors Actuators B Chem. 261 (2018) 572–580, https://doi.org/10.1016/j.snb.2018.01.180.
[6] L.E. Sebar, L. Iannucci, C. Gori, A. Re, M. Pavis, E. Angelini, S. Grassini, In-situ multi- analytical study of ongoing corrosion processes on bronze artworks exposed outdoors, ACTA IMEKO 10 (1) (2021) 241–249, https://doi.org/10.21014/acta_imeko.v10i1.894.
[7] M.A. Jakab, G.W. Tormoen, 09509 - Measurement of CPC Performance Using EIS Based Coating Degradation Sensors, The Association for Materials Protection and Performance, NACE, 2008.
[8] M.A. Jakab, J.F. Dante, G.W. Tormoen, 08202 - Measurement of CPC Performance Using EIS Based Sensor Methods - Laboratory and Field Studies, The Association for Materials Protection and Performance, NACE, 2008.
[9] D.A. Jáuregui-Gónzalez, M. López-Arriaga, F.J. Rodríguez-Gómez, J. Contreras-Vargas, P. Roncagliolo-Barrera, Influence of the Application and Preparation of Wax Coatings Artificially Patinated Bronze Surfaces, ICOM-CC, Metal, 2016.
[10] B. Ramírez Barat, A. Crespo, E. García, S. Díaz, E. Cano, An EIS study of the conservation treatment of the bronze sphinxes at the Musei arqueologico nacional (Madrid), J. Cult. Herit. 24 (2017) 93–99, https://doi.org/10.1016/j.culher.2016.10.010.
[11] E. Schindelholz, R.G. Kelly, Wetting phenomena and time of wetness in atmospheric corrosion: a review, Corrosion Reviews 30 (2012) 135–170, https://doi.org/10.1515/corrrev-2012-0015.
[12] S. Grassini, E.Di Francia, E. Angelini, A. Elsayed, M. Parvis, J.A.Mejia Gomez, In situ EIS measurements on Columbian bronze statues, in: IMEKO International Conference on Metrology for Archaeology and Cultural Heritage, 2017, pp. 287–290.
[13] D.E. Arceo-Gómez, J. Reyes-Trujeque, G.E. Zambrano-Rengel, T. Pérez-López, R. Orozco-Cruz, Electrochemical characterization of patinas formed on a historic bell from the Cathedral Museum of Campeche- Mexico, world heritage site, Int. J. Electrochem. Sci. 11 (2016) 9379–9393, https://doi.org/10.20964/2016.11.34.
[14] C. Petiti, D. Gulotta, B. Mariani, L. Toniolo, S. Goidanich, Optimisation of the setup of LPR and EIS measurements for the onsite, non-invasive study of metallic artefacts, J. Solid State Electrochem. 24 (2020) 3257–3267, https://doi.org/10.1007/s10008-020-04822-9.
[15] F. Di Turo, Limits and perspectives of archeometric analysis of archeological metals: a focus on the electrochemistry for studying ancient bronze coins, J. Cult. Herit. 43 (2020) 271–281, https://doi.org/10.1016/j.culher.2019.10.006.
[16] G. Monrrabal, A. Bautista, F. Velasco, Use of innovative gel electrolytes for electrochemical corrosion measurements on carbon and galvanized steel surfaces, Corros. J. 75 (2019) 1502–1512, https://doi.org/10.5006/3309.
[17] E. Cano, B. Ramírez Barat, Electrochemical techniques for in situ corrosion evaluation of cultural heritage in advanced characterization techniques, diagnostic tools and evaluation methods in heritage, Science (2018) 21–32, https://doi.org/10.1007/978-3-319-75316-4_2.
[18] M.H. Nazir, Z.A. Khan, A. Saeed, A novel non- destructive sensing technology for on-site corrosion failure evaluation of coatings, IEEE Access 6 (2017) 1042–1054.
[19] S. Corbellini, M. Parvis, S. Grassini, Noninvasive solution for electrochemical impedance spectroscopy on metallic works of art, IEEE Trans. Instrum. Meas. 61 (2012) 1193–1200, https://doi.org/10.1109/TIM.2011.2175816.
[20] A. England, K. Hosbein, C. Price, M. Wylder, K. Miller, T. Clare, Assessing the protective quality of wax coating on bronze sculptures using hydrogel patches in impedance measurements, Coatings 6 (2016) 45, https://doi.org/10.3390/coatings6040045.
[21] F. di Turo, C. De Vito, F. Coletti, F. Mazzei, R. Antiochia, G. Favero, A multi-analytical approach for the validation of a jellified electrolyte: application to the study of ancient bronze patina, Microchem. J. 134 (2017) 154–163, https://doi.org/10.1016/j.microc.2017.05.015.
[22] S. Martinez, I. Šoić, V. Špada, Unified equivalent circuit of dielectric permittivity and porous coating formalisms for EIS probing of thick industrial grade coatings, Prog. Org. Coat. 153 (2021), https://doi.org/10.1016/j.porgcoat.2021.106155.
[23] I. Šoić, S. Martinez, M. Dubravić, Gel- electrolyte EIS setup used for probing of IR Dried/Cured industrial coatings, Prog. Org. Coat. 137 (2019), https://doi.org/10.1016/j.porgcoat.2019.105331.
[24] F.J.R. de Oliveira, D.C.B. Lago, L.F. Senna, L.R.M. de Miranda, E. D'Elia, Study of patina formation on bronze specimens, Mater. Chem. Phys. 115 (2009) 761–770, https://doi.org/10.1016/j.matchemphys.2009.02.035.
[25] J.N. Murray, Electrochemical test methods for evaluating organic coatings on metals: an update. Part I. Introduction and generalities regarding electrochemical testing of organic coatings, Progress in Organic Coatings (1997) 225–233, https://doi.org/10.1016/S0300-9440(96)00677-7.
[26] G.D. Davis, L.A. Krebs, C.M. Dacres, Coating evaluation and validation of accelerated test conditions using an in-situ corrosion sensor, DACCO Sci. 74 (2002) 935.
[27] B. Hudec, R. Ribičić, S. Martinez, I. Šoić, Quantitative Coating Quality Assessment on an Offshore Platform, Materials Perofrmance, 2022.
[28] A.A. Mascarenhas, Fabrication and Characterization of Flexible and Porous Biopotential Electrodes via Powder Metallurgy, Faculty of San Diego State University, 2021. Master Thesis.
[29] V. Nandagopal, Implementation of the swLORETA in a Cloud Based Service for EEG Analysis, Chalmers University of Technology, 2021. Master Thesis.
[30] F. di Turo, N. Montoya, J. Piquero-Cilla, C. De Vito, F. Coletti, G. Favero, A. Doménech-Carbó, Archaeometric analysis of Roman bronze coins from the magna mater Temple using solid state voltammetry and electrochemical impedance spectroscopy, Anal. Chim. Acta 955 (2017) 36–47, https://doi.org/10.1016/j.aca.2016.12.007.
[31] Application Note AC-1, Basics of Electrochemical Impedance Spectroscopy, Princeton Applied Research.
[32] B.A. Boukamp, A linear Kronig-Kramers transform test for immittance data validation, J. Electrochem. Soc. 142 (1995) 6.
[33] M. Schönleber, D. Klotz, E. Ivers-Tiffée, A method for improving the robustness of linear Kramers-Kronig validity tests, Electrochim. Acta 131 (2014) 20–27, https://doi.org/10.1016/j.electacta.2014.01.034.
[34] M. Schönleber, D. Klotz, E. Ivers-Tiffée, A method for improving the robustness of linear Kramers-Kronig validity tests, Electrochim. Acta 131 (2014) 20–27, https://doi.org/10.1016/j.electacta.2014.01.034.
[35] Numista, Numismatic catalogue. https://en.numista.com/catalogue/pieces2082.html, 2023 (accessed 4 Januar 2023).
[36] H. Richard, M. Rowe, The Colouring, Bronzing and Patination of Metals, Thames&Hudson, London, UK, 1991.
[37] H. Otmačić Ćurković, T. Kosec, K. Marušić, A. Legat, An electrochemical impedance study of the corrosion protection of artificially formed patinas on recent bronze, Electrochim. Acta 83 (2012) 28–39, https://doi.org/10.1016/j.electacta.2012.07.094.
[38] D. Mikić, H.Otmačić Ćurković, S. Hosseinpour, Bronze corrosion protection by long-chain phosphonic acids, Corrosion Science 205 (2022) 110445, https://doi.org/10.1016/j.corsci.2022.110445.
[39] R. Bostan, S. Varvara, L. Gaina, T. Petrisor Jr., L.M. Muresan, Prog. Org. Coat. 111 (2017) 416–427, https://doi.org/10.1016/j.porgcoat.2016.08.004.
[40] E. Cano, D. Lafuente, D.M. Bastidas, Use of EIS for the evaluation of the protective properties of coatings for metallic cultural heritage: a review, J. Solid State Electrochem. 14 (2010) 381–391, https://doi.org/10.1007/s10008-009-0902-6.
[41] C. Monticelli, F. Zanotto, V. Grassi, M. Seyedi, A. Balbo, Improving the protectiveness of 3- mercaptopropyl-trimethoxysilane coatings on bronze by addition of oxidic nano and microparticles, Coatings 10 (2020) 225, https://doi.org/10.3390/coatings10030225.
[42] T. Kosec, D. Kek Merl, I. Milošev, Impedance and XPS study of benzotriazole films formed on copper, copper-zinc alloys and zinc in chloride solution, Corros. Sci. 50 (2008) 1987–1997, https://doi.org/10.1016/j.corsci.2008.04.016.
[43] J. Sandberg, I. Odnevall Wallinder, C. Leygraf, N. Le Bozec, Corrosion induced copper runoff from naturally and pre-patinated copper in a marine environment, Corros. Sci. 48 (2006) 4316–4338, https://doi.org/10.1016/j.corsci.2006.04.004.
[44] C.H. Hsu, F. Mansfeld, Technical note: concerning the conversion of the constant phase element parameter Y0 into a capacitance, Corrosion 57 (2001) 747–748.
[45] A. Singh, Y. Lin, M.A. Quraishi, L.O. Olasunkanmi, O.E. Fayemi, Y. Sasikumar, B. Ramaganthan, I. Bahadur, I.B. Obot, A.S. Adekunle, M.M. Kabanda, E.E. Ebenso, Porphyrins as corrosion inhibitors for N80 steel in 3.5% NaCl solution: electrochemical, quantum chemical, QSAR and Monte Carlo simulations studies, Molecules 20 (8) (2015) 15122–15146, https://doi.org/10.3390/molecules200815122.
[46] Vio d.o.o, provider of public water supply and drainage services for the territory of the City of Zagreb, https://www.vio.hr/o-nama/vodoopskrba/kvaliteta-vode-za-pice/tablica-kvalitete-vode-zagreba/1852 2023 (accessed 4 Januar 2023).
[47] E. Angelini, S. Grassini, M. Parvis, Silver artefacts: plasma deposition of SiOx protective layers and tarnishing evolution assessment, Corros. Eng. Sci. Technol. 45 (5) (2010) 334–340.
[48] D.E. Arceo-Gómez, J. Reyes-Trujeque, G.E. Zambrano-Rengel, T. Pérez-López, R. Orozco-Cruz, Electrochemical characterization of patinas formed on a historic bell from the Cathedral Museum of Campeche- Mexico, world heritage site, Int. J. Electrochem. Sci. 11 (2016) 9379–9393, https://doi.org/10.20964/2016.11.34.
[49] A. Kapitanović, H. Otmačić Ćurković, The effect of corrosion conditions on aging of artificial patina on three bronzes, Coatings 12 (2022) 936.
[50] Y. Morozov, L.M. Calado, R.A. Shakoor, R. Raj, R. Kahraman, M.G. Taryba, M. F. Montemor, Epoxy coatings modified with a new cerium phosphate inhibitor for smart corrosion protection of steel, Corros. Sci. 159 (2019), 108128, https://doi.org/10.1016/j.corsci.2019.108128.
[51] L.A. Ellingson, T.J. Shedlosky, G.P. Bierwagen, E.R. de la Rie, L.B. Brostoff, The use of electrochemical impedance spectroscopy in the evaluation of coatings for outdoor bronze, Stud. Conserv. 49 (2004) 53–62, https://doi.org/10.1179/sic.2004.49.1.53.
[52] G.D. Davis, L.A. Krebs, C.M. Dacres, Coating evaluation and validation of accelerated test conditions using an in-situ corrosion sensor, J. Coat. Technol. 74 (2002) 69–74, https://doi.org/10.1007/BF02697959, 51.
[53] G.D. Davis, C.M. Dacres, L.A. Krebs, In-situ corrosion sensor for coating testing and screening, Mater. Perform. 39 (2) (2000) 46.
[54] T.J. Shedlosky, K.M. Stanek, G. Bierwagen, On-line survey results of techniques used for outdoor bronze conservation, in: AIC Objects Speciality Group Postprint 9, 2002, pp. 3–13.
[55] A. Doménech-Carbó, S. Capelo, J. Piquero, M.T. Doménech-Carbó, J. Barrion, A. Fuentes, W. Al Sekhaneh, Dating archaeological copper using electrochemical impedance spectroscopy. Comparison with voltammetry of microparticles dating, Mater. Corros. 67 (2) (2016) 120–129, https://doi.org/10.1002/maco.201408048.
[56] C. Petiti, L. Toniolo, D. Gulotta, B. Mariani, S. Goidanich, Effects of cleaning procedures on the long- term corrocion behavior of bronze artifacts of the cultural

heritage in outdoor environment, Environ. Sci. Pollut. Res. 27 (2020) 13081–13094, https://doi.org/10.1007/s11356-020-07814-4.
[57] P. Letardi, M. Albini, L. Mathys, M. Monachon, E. Joseph, EIS Measurements for Treatments Testing: The Case of a Bio-based Method Applied on Outdoor Bronze Statues in Switzerland. www.legendedautomne.ch.
[58] D.J. Mills, K. Schaefer, T. Wityk, In-situ evaluation of the protectivity of coatings applied to metal cultural artefacts using non- destructive electrochemical measurements, Corros. Mater. Degrad. 2 (2021) 120–132, https://doi.org/10.3390/cmd2010007.

Curriculum vitae

Ivana Šoić was born in 1991 in Zagreb, Croatia. She completed her undergraduate studies in 2015 and her graduate studies in Applied Chemistry in 2017 at the Department of Electrochemistry, Faculty of Chemical Engineering and Technology, University of Zagreb, under the supervision of Professor Sanja Martinez, Ph.D.

During her graduate studies, she completed a two-month professional training program at Cortec Corporation in Minnesota, USA, a company specializing in the development and production of anti-corrosion agents and coatings. While still a student, Ivana published two scientific papers related to the topics of her final and master's theses in the journals International Journal of Electrochemical Science and Građevinar.

After graduation, she was employed as an Assistant at the Department of Electrochemistry and enrolled in the Ph.D. program in Chemical Engineering and Applied Chemistry in 2018.

Together with Prof. Sanja Martinez, Ph.D., she won second place at the Zagreb Connect competition within the Startup Factory program (Batch 2019), initiating the intensive development of the innovation ReCorr® QCQ.

Ivana is a co-owner of the Faculty's spin-off company, ReCorrTech d.o.o., established in 2020, which operates successfully to this day. She is the co-author of eight scientific papers related to the innovation, five of which have been published in Q1/D1 journals in the field of Materials Science, Coatings & Films, and the remaining three in the prestigious journals *Corrosion* and *Materials Performance* (publications of AMPP).

Ivana has participated in more than 15 national and international congresses with oral presentations. She is a member of the Croatian Society for Materials Protection (HDZaM) and the international association AMPP (Association for Materials Protection and Performance).

At the Faculty of Chemical Engineering and Technology, she participates in teaching the courses Electrochemistry and several corrosion-related courses at the undergraduate and graduate levels.

She collaborates on numerous professional projects with the industry, where she conducts field corrosion measurements and prepares reports on risk assessment and the causes of material corrosive degradation. She actively participates in organizing training for the industry, including the international summer school Zagreb Corrosion Summer School (2019 and 2020), where she serves as the practical part leader. She organized a student conference in the field of electrochemistry and is a member of the faculty council.

She participated in the BroCH project (Croatian Science Foundation, IP-2019-04-5030) on the protection of bronze cultural heritage, led by Prof. Helena Otmačić Ćurković, Ph.D. (2020–2024), as well as the CeSaR – Student Career Counseling and Development Centre project (ESF, UP.03.1.1.04.0026, 2014–2020), led by Prof. Ante Jukić, Ph.D. She is currently involved in the project ReCorr® QCQ: Next-generation device for monitoring and inspection of coatings and corrosion mitigation, running from December 20, 2023, to June 20, 2026, and financed through the EU NextGenerationEU program. Ivana won the Ivan Plotnikov Award for 2024 as the best young scientist at the Faculty of Chemicall Engineering and Technology and, together with her mentor Professor Sanja Martinez, Ph.D., the University Innovation Award for 2024.

Since 2025, she has been an authorized FROSIO Inspector for coatings and surface preparation.

Publications: